Investigation of the role of microtubule dynamics in paracrine signaling and cell invasion in human cancer cells

Dissertation

for the award of the degree
"Doctor rerum naturalium"
of the Georg-August-Universität Göttingen

within the doctoral program "Molecular Biology of Cells"
of the Georg-August University School of Science (GAUSS)

submitted by
Karoline Pudelko

from Kassel, Germany

Göttingen, June 2021

Thesis Committee

Prof. Dr. Holger Bastians
Institute for Molecular Oncology
Section of Cellular Oncology
University Medical Center Göttingen

Prof. Dr. Matthias Dobbelstein
Institute for Molecular Oncology
University Medical Center Göttingen

Prof. Dr. Claudia Binder
Department of Tumor Invasion and Metastasis
University Medical Center Göttingen

Members of the Examination Board

Referee	Prof. Dr. Holger Bastians Institute for Molecular Oncology Section of Cellular Oncology University Medical Center Göttingen
2nd Referee	Prof. Dr. Matthias Dobbelstein Institute for Molecular Oncology University Medical Center Göttingen

Further members of the Examination Board

Prof. Dr. Peter Burfeind
Department of Human Genetics
University Medical Center Göttingen

Prof. Dr. Dieter Kube
Department of Hematology and Oncology
University Medical Center Göttingen

Prof. Dr. Frauke Alves
Department of Molecular Imaging in Oncology
University Medical Center Göttingen

Prof. Dr. Sigrid Hoyer-Fender
Department of Developmental Biology
GZMB Göttingen

Date of oral examination: 14.09.2021

Table of Contents

List of Figures

List of Tables

Abstract

Metastasis is a critical characteristic of aggressive human cancer, which is determined by the acquirement of increased cancer cell migration and invasion capabilities. Recent published work indicated that supernumerary centrosomes, which are frequently seen in cancer cells, induce a paracrine signaling contributing to enhanced cell invasion in breast epithelial cells. Interestingly, our lab has identified a correlation between increased microtubule plus end assembly rates in interphase cells and enhanced cell migration and invasion in colorectal cancer and melanoma cell lines suggesting that microtubule dynamics might be involved in the regulation of cancer cell migration and invasion. This Ph.D. thesis focused on the investigation of the role of supernumerary centrosomes on microtubule plus end assembly in melanoma and colorectal cancer cells and its involvement in paracrine signaling leading to increased microtubule growth rates and cell migration and invasion.

I demonstrated that colorectal cancer and melanoma cells that exhibit increased microtubule plus end growth rates in interphase show increased cell migration and invasion. Moreover, rescue experiments demonstrated a requirement of increased microtubule dynamics for migration and invasion in these cancer cells. Interestingly, these cancer-associated phenotypes were accompanied by the presence of a high proportion of cells with supernumerary centrosomes. In fact, induction of supernumerary centrosomes was sufficient to trigger increased microtubule plus end assembly rates in interphase. Intriguingly, the ability to increase microtubule plus end assembly rates could be transferred onto non-invasive cells by paracrine signaling and this was found to be mediated by shedding microvesicles in a microtubule dynamics dependent manner. Finally, evidence was obtained that microvesicle-mediated increase of microtubule dynamics might involve HER2/ERK signaling.

The data presented in this Ph.D. thesis indicate a requirement of abnormally increased microtubule dynamics for cancer cell migration and invasion and thus, for metastasis. Furthermore, the shedding of cancer-relevant microvesicles and the induction of paracrine signaling dependents on microtubule plus end assembly rates in interphase and seems to be associated with an increased activity of HER2/ERK signaling. Thus, inhibition of HER2/ERK signaling or direct suppression of microtubule dynamics, *e.g.,* by the treatment with microtubule targeting drugs including Taxol, may offer new possibilities for targeting metastasis in human cancer.

1. Introduction

1.1. The Hallmarks of Cancer

Cancer is one of the leading causes of deaths worldwide. In 2020, colorectal cancer and skin cancer (melanoma of skin) were the second and seventh most common cancer in both sexes of all ages in Europe, respectively (European Union, 2021). The development of therapy strategies in the battle against cancer shows a rising trend over the last decades. Nevertheless, it is still difficult to target and eliminate cancer cells specifically. Cancers are characterized by a mixture of specific traits (Figure 1.1) (Hanahan & Weinberg, 2011).

Figure 1.1 The hallmarks of cancer. *Cancer cells are defined by a specific set of characteristics giving them a proliferation and survival advantage compared to normal cells. Modified from (Hanahan & Weinberg, 2011).*

1.1.1. Evading growth suppression

As illustrated in Figure 1.1, an important trait of cancer cells is to evade growth suppression by inactivating crucial cell cycle checkpoint regulators that are responsible for inhibiting cell cycle progression in case of unfavorable proliferation or survival conditions. The tumor suppressor *TP53* is mutated or lost in more than 50 % of malignant tumors (Baugh et al., 2018). In normal cells that are exposed to stress conditions, such as nutrition deficiency or DNA damage, the transcription factor p53 activates a plethora of genes, among them anti-cell cycle (*e.g., CDKN1A*) and pro-apoptotic (*e.g., BAX*) genes (Fischer, 2017).

However, cells with loss of function (LOF) mutations in *TP53* progress uncontrolled through the cell cycle, even when cells are exposed to severe stress conditions, resulting in accelerated proliferation and tumor growth (Miller et al., 2016). Gain of function (GOF) mutations especially in the codons 175 and 273, so called hot spot regions, of the *TP53* gene locus result in a p53 variant that was implicated in promoting cancer progression. Mutations inhibiting the suppressive function of wildtype p53 are involved in promoting cell proliferation and foster epithelial-to-mesenchymal transition (EMT), a process that has been linked to increased cell motility (Zhang et al., 2020). The mutants p53 R175H and p53 R273H are also known to inactivate the family member and tumor suppressor p63 (Novikov et al., 2021).

Another commonly mutated or lost regulatory protein in cancer is the tumor suppressor Retinoblastoma (Rb) protein (Burkhart & Sage, 2008). Proliferating cells need to successfully surpass the G1/S restriction point to enter S phase. Cyclin dependent kinase 4 (Cdk4) and Cdk6 are activated by D-type cyclins at early G1 and phosphorylate the Rb protein. Phosphorylation of the Rb protein leads to the release of E2F1, a transcription factor for essential S phase and cell cycle regulatory genes like *MYC* and *JUN* (Bracken et al., 2004). Mutations in the *CDK4* and *CDK6* gene loci are widespread among tumors and lead to hyperactivation of the kinases. Additional mutational changes in D-type cyclins and LOF mutations in genes encoding cell cycle inhibitors (*e.g., INK4*) result in uncontrolled signaling (Malumbres & Barbacid, 2009).

1.2. Genome instability

Normal cells can faithfully segregate their chromosomes and divide to become two daughter cells, therefore ensuring proper and unperturbed cell division. Genome instability and a high rate of mutational changes are one of the hallmarks of cancer (Figure 1.1).

A tumor is composed of subpopulations of cancer cells, each equipped with different genetic and physiological properties. Tumor heterogeneity is a major hallmark of cancer (Hanahan & Weinberg, 2011) and strongly promoted through chromosomal instability (Bakhoum & Landau, 2017). Chromosomal instability (CIN) is defined as the rate by which cancer cells acquire chromosomal abnormalities. Aneuploid cells can arise through chromosomal instability and are defined by an abnormal chromosome number (Tijhuis et al., 2019). Chromosomal instability can be subdivided into two forms: structural CIN (S-CIN) or whole CIN (W-CIN). S-CIN causes structural chromosome aberrations, whereas W-CIN leads to numerical aneuploidy. Numerical changes in the composition of chromosomes are the result of chromosome missegregation during mitosis, which can be caused by different defects (Sansregret & Swanton, 2017).

Numerical changes that result from chromosome missegregation can be initiated through mutations in genes encoding members of the spindle assembly checkpoint (SAC), a machinery ensuring that every kinetochore is bound by microtubules from opposing poles before sister chromatids are separated (Lara-Gonzalez et al., 2012). W-CIN is also induced through an increased microtubule plus end assembly rate during mitosis, which leads to the formation of lagging chromosomes in anaphase (Ertych et al., 2014). Lagging chromosomes are the result of erroneous microtubule kinetochore attachments. In a normal cell, these attachments are amphitelic meaning that every centromere of a chromosomes is attached to spindles of opposing poles at the end of prometaphase (Godek et al., 2015). Monotelic attachments, where only one centromere of a chromosome is bound by microtubules, and syntelic attachments, where both centromeres of a chromosome are bound by microtubules from one pole, will not satisfy the SAC. This is associated with the initiation of the correction machinery or, if unresolvable, the induction of apoptosis and cell death (Khodjakov & Pines, 2010). Additionally, merotelic attachments are defined by the binding of microtubules from opposing poles to one centromere (Kelly & Funabiki, 2009). These erroneous attachments remain unrecognized by the microtubule-kinetochore surveillance system and lead to the formation of lagging chromosomes, an important prestage for chromosome missegregation, which leads to chromosomally instable cells and aneuploidy (Ertych et al., 2014, Ertych et al., 2016).

Chromosomes missegregation can also arise through an erroneous establishment of the mitotic spindle caused by defective or overamplified centrosomes (Cosenza et al., 2017). Supernumerary centrosomes were found to be directly linked to merotelic attachments and the formation of lagging chromosomes (Ganem et al., 2009).

Moreover, genome instability can lead to overexpression of oncogenes or loss of tumor suppressors thereby promoting tumorigenesis. For instance, overamplified growth factor receptor genes lead to an increased amount of growth factor receptors on the cell surface of cancer cells, which results in a cell proliferation and survival advantage compared to healthy cells. Overamplification of cell migration and invasion related genes results in cancer cells with enhanced invasiveness (Novikov et al., 2021). The co-occurrence of CIN and metastasis is in many cases associated with highly aggressive types of cancer characterized by low survival rates and a high probability of relapse (Bach et al., 2019; Pannu et al., 2015). Metastasizing cells are characterized by increased cell migration and invasion, essential cellular mechanisms that are explained in the next chapter.

1.3. Invasion and metastasis

Cancer cells often leave the primary tumor and form metastases in distant organs (Figure 1.1). The ability of cells to migrate and invade surrounding tissues is an important prerequisite for metastasis.

1.3.1. Metastasis

Metastasis is one of the main causes for cancer-therapy failure and cancer-associated mortality, nevertheless, the molecular mechanisms of this process remain poorly understood (Chaffer & Weinberg, 2011).
Increased cell migration and invasion are crucial prerequisites for metastasis during cancer progression. A tumor cell needs to go through a multi-step process to successfully form metastases. First, cells disseminate from the primary tumor site by invading the surrounding tissue (Zhuyan et al., 2020). Intravasation into the blood stream allows tumor cells to circulate through the body. The cells can leave the blood circulation at the location of distant organs through extravasation and start to form a pre-metastatic niche, which will develop to a micrometastasis until a stable metastatic colonization is established (Fares et al., 2020).

1.3.2. Signaling at the leading edge of the cell

Cell migration relies on the interplay between members of the cytoskeleton and the activity of cell surface receptors and is often the response to extracellular signals (Friedl & Alexander, 2011). Protrusion and retraction are the main events during cell migration. The driving force for cell protrusion is the nucleation and polymerization of actin. Filamentous actin (F-actin) build out of single globular actin (G-actin) units are orientated filaments that grow at the plus end and push at the front of the cell (Svitkina, 2018). The members of the Rho GTPase family, Ras-related C3 botulinum toxin substrate 1 (Rac1), Ras homolog family member A (RhoA) and cell division cycle 42 (Cdc42), are the main mediators of cell migration. They activate downstream effectors by exchanging guanosine diphosphate (GDP) for guanosine triphosphate (GTP). The activity of the small GTPases is regulated by guanosine exchanging factors (GEFs), Rho GDP dissociation inhibitors (GDI) or GTPase activating proteins (GAP) (Watanabe et al., 2005).
Rac1 and Cdc42 are recruited by GEFs like p21 activated protein kinase exchange factor alpha (βPIX) or T-lymphoma invasion and metastasis-inducing protein 1 (Tiam1) along microtubules to the leading edge of the cell. Rac1 will bind and activate the Wiskott-Aldrich-Syndrome family verprolin homologous NPF protein (WAVE), whereas Cdc42 binds and activates the Wiskott-Aldrich-Syndrome (WASP) protein. Both proteins activate the Arp2/3

complex, which has been described to initiate actin nucleation and polymerization (Figure 1.3) (Devreotes & Horwitz, 2015; Mayor & Etienne-Manneville, 2016).

1.3.3. Contribution of actin and actin regulators during cell migration

The actin cytoskeleton plays a crucial role in cell movement, during cytokinesis, and by strengthening the plasma membrane through its localization close to the cell cortex. F-actin is a coiled chain of identical G-actin monomers with a diameter of approximately 6 nm. F-actin is structured in a plus and a minus end, with more ATP-dependent growth at the plus end (Pollard, 2016).

During cell migration, higher organization of actin chains is achieved in filopodia and lamellipodia, where actin appears in bundles or branches, respectively (Figure 1.2). Filopodia are finger-like protrusions that interact with their surroundings through cell surface receptors, like growth factors receptors or integrins. Filopodia are characterized by parallel structured linear actin filaments. Formation and organization of filopodia is formin-dependent (Mattila & Lappalainen, 2008). Formins are regulated by Rho GTPases, like RhoA and Cdc42. They activate the Rho effectors Diaphanous related formins (Drf), such as Drf 1 and Drf 2, by binding to the N-terminal domain and removing the intramolecular autoinhibition (Maiti et al., 2013). Formins contain a formin homology 2 (FH2) domain allowing them to directly bind to actin filaments. Actin bound formins can function as capping proteins that add actin monomers to the growing strand by catching free actin dimers (Courtemanche, 2018).

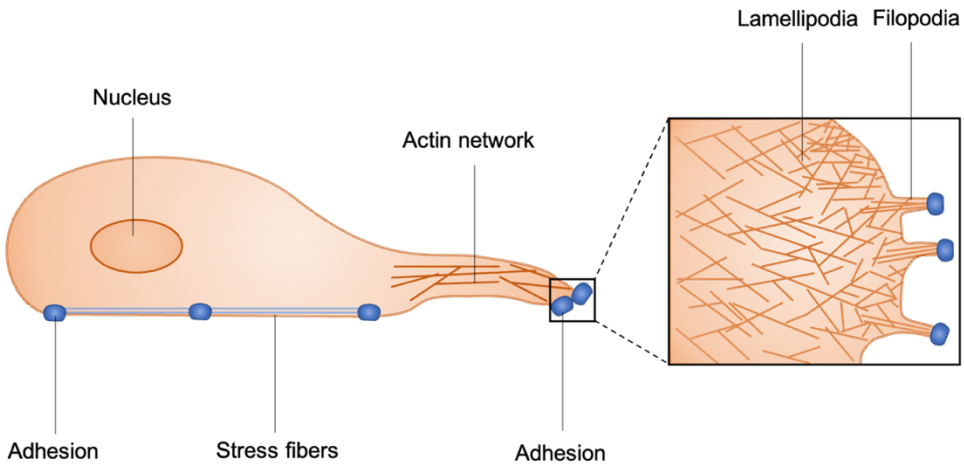

Figure 1.2 Organization of the actin network within a cell protrusion. *The actin structure in lamellipodia appears branched, whereas filopodia are formed out of parallel arranged actin bundles that establish integrin based focal adhesions to the extracellular matrix. Filopodia are constantly integrating signals from their microenvironment. Modified from (Mattila & Lappalainen, 2008).*

Lamellipodia are thin and long branched actin protrusions that adhere to the substrate (Innocenti, 2018). Since large pushing forces are required for the formation of protrusions,

branched actin filaments increase the stiffness of the actin cytoskeleton. Actin related Arp2 together with Arp3 and four other subunits form a complex that is known as the key player for branched actin filaments, the Arp2/3 complex. This complex links actin filaments in an angle of 70 °. The activation of the complex is controlled by the nucleation promotion factor (NPF), the Wiskott-Aldrich-Syndrome (WASP) protein and the small GTPase Rac and WASP family verprolin homologous NPF protein 1-3 (WAVE 1-3) (Figure 1.3) (Molinie & Gautreau, 2018). Since actin polymerization is a dynamic process, debranching can be achieved by conformational changes of the filaments, thereby reducing the affinity for the Arp2/3 complex. The actin depolymerizing factors (ADF) cofilin 1 and cofilin 2 belong to the ADF/cofilin family (Maiti et al., 2013). The ADF/cofilin complex preferentially binds to ADP bound F-actin and leads to the depolymerization of the filament, thereby enhancing the turn-over of actin monomers at the plus end. Free G-actin monomers are released and used for actin polymerization at other locations (Bravo-Cordero et al., 2013; Tanaka et al., 2018).

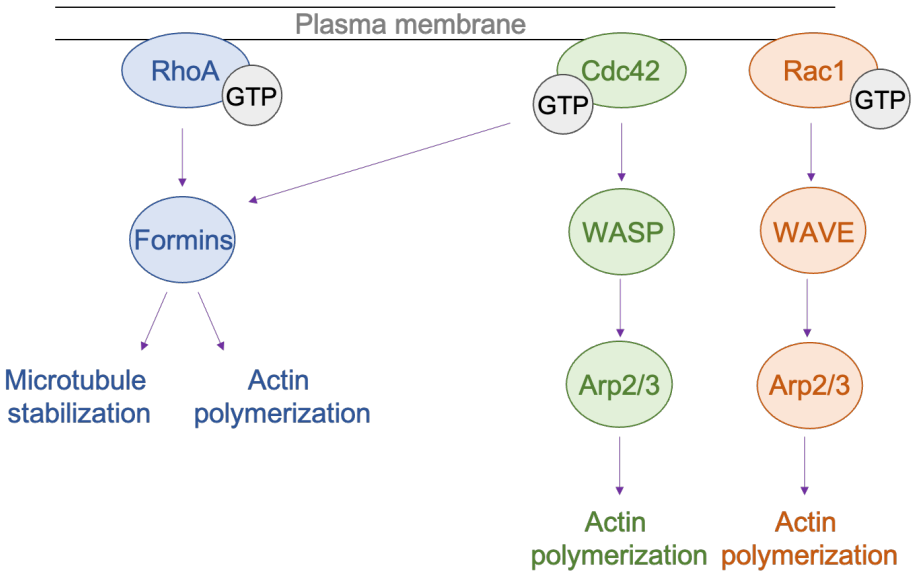

Figure 1.3 Signaling downstream of Rho GTPases. *RhoA, Cdc42 and Rac1 are located at the plasma membrane and remain in an activate state when they are bound to guanosine triphosphate (GTP). RhoA and Cdc42 activate formins, such as Drf1 and Drf2, which will contribute to actin polymerization and microtubule stabilization. Cdc42 will bind and activate the Wiskott-Aldrich-Syndrome (WASP) protein, which is known to induce actin polymerization. Rac1 functions through the Wiskott-Aldrich-Syndrome (WASP) family verprolin homologous NPF protein (WAVE) in activating actin polymerization. Modified from* (Møller et al., 2019).

1.3.4. Invadopodia

A cancer cell needs to invade the surrounding extracellular matrix (ECM) to escape from the primary tumor and successfully metastasize to distant organs. Growth factor induced formation of invadopodia is essential for the invasion to the ECM and can be structured into three phases (Figure 1.4). The initiation of invadopodia is associated with the Arp2/3

complex dependent nucleation and polymerization of actin. Initial integrin-based connections to the extracellular matrix are established (Murphy & Courtneidge, 2011). After initialization, actin filaments crosslink mainly mediated by the activity of WASP and cortactin during the stabilization phase (Augoff et al., 2020). Moreover, integrins connect to cortical actin bundles via adaptor proteins, become locally enriched, start to cluster, and develop focal contacts. This region of the invadopodium is also referred to as the outer adhesive ring, which was shown to be essential for secretion of proteinases (Branch et al., 2012). Different subclasses of integrins bind different parts of the extracellular matrix, *e.g.,* $\alpha 2\beta 1$ integrins bind collagen fibers and $\alpha 5\beta 1$ integrins bind fibronectin. The adaptor protein tyrosine kinase substrate 5 (Tsk5) localizes specifically to invadopodia and additionally anchors crosslinked actin filaments to the membrane, creating a stable 3D structure, which is also known as the actin rich core (Seals et al., 2005).

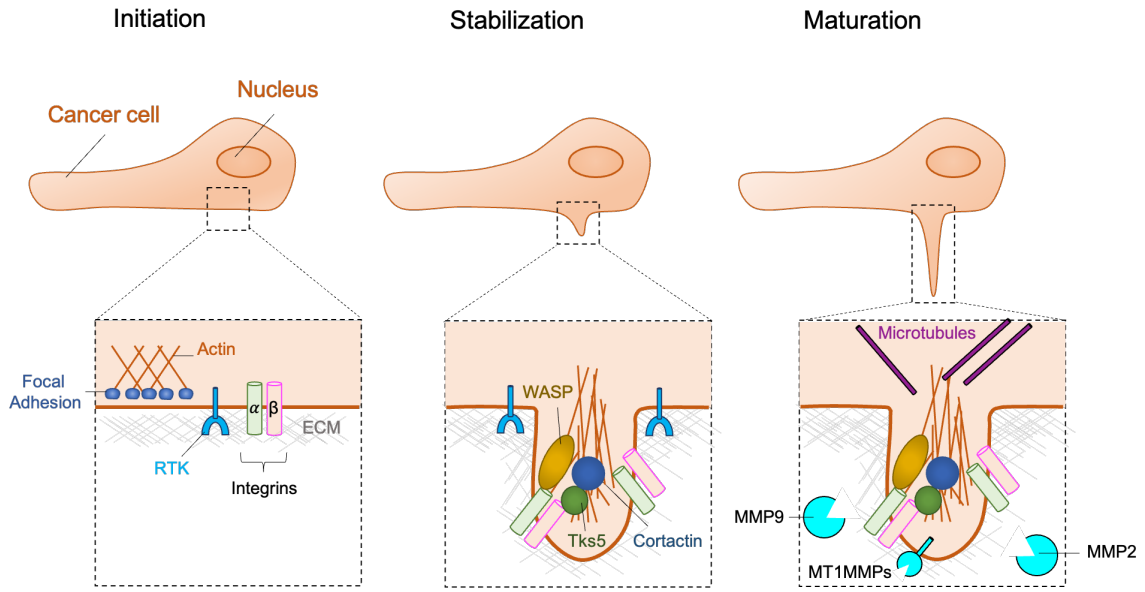

Figure 1.4 Steps of invadopodia formation. *Invadopodia are formed in response to growth factor stimulation, which is detected through receptor tyrosine kinases (RTK) anchored in the plasma membrane. During initiation, actin nucleation and polymerization is initialized and integrins, consisting of an α- and β-subunit, establish connections to the extracellular matrix (ECM). During the stabilization phase, WASP and cortactin initialize actin filament crosslinking. Integrins connect to the actin cytoskeleton through adaptor proteins, like tyrosine kinase substrate 5 (Tks5), and enhance the stability of the invadopodium. The maturation phase is characterized by the recruitment and microtubule dependent delivery of proteinases to degrade the ECM. Modified from (Murphy & Courtneidge, 2011).*

Maturation is the last step of invadopodia formation and is characterized by the elevated recruitment of surface proteinases, mainly matrix metalloproteinases (MMPs). MMPs mediate degradation of protein components of the ECM allowing the invasion of the tumor cells into the extracellular space (Friedl & Wolf, 2003). MMPs are zinc-dependent endopeptidases that are expressed cell type specifically and are specialized for the different

components of the ECM, *e.g.,* collagenases and gelatinases cleave and denature collagens, fibronectins, or gelatins (Cathcart et al., 2015). MMPs from different families exhibit a conserved structure consisting of a signal peptide at the N-terminal end, which is crucial for the localization of the proteinases, a propeptide and a catalytic domain. Additional modulations of the structure in form of hemopexins at the C-terminal end or fibronectin-like domains are specific for each family of MMPs. MMPs are either linked to the plasma membrane with a transmembrane anchor and an extracellular domain (*e.g.,* membrane type 1 matrix metalloproteinases (MT1MMP)) or are secreted (*e.g.,* MMP2 and MMP9) (Figure 1.4) (Cathcart et al., 2015; Conlon & Murray, 2019). Many melanoma cell lines are characterized by overexpression of MMPs explaining their highly invasive behavior connected with a poor prognosis for patients (Hofmann et al., 1999, Hofmann et al., 2000).

1.3.5. The epithelial-to-mesenchymal transition

The epithelial-to-mesenchymal transition (EMT) is an essential and initial process for tumor cells to invade the surrounding tissue and escape from the primary tumor. Epithelial cells are well-organized in monolayers, have an apical to basal polarity, are mainly immotile, and are characterized by tight cell-cell junctions to neighboring cells (Figure 1.5). These characteristic features are established through a specific gene expression profile, including increased expression of *CDH1* (*Epithelial cadherin*), *KRT18* (*Cytokeratin-18*) and *LAMB1* (*Laminin-1*) (Yang et al., 2020).

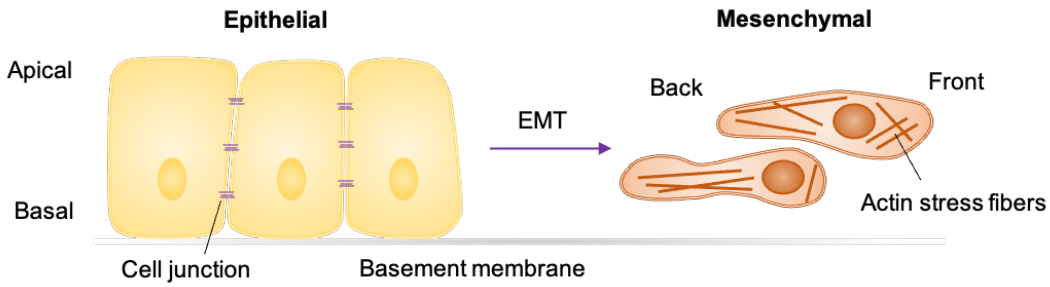

Figure 1.5 The process of epithelial-to-mesenchymal transition. *Epithelial cells characterized by an apical to basal polarity and established cell-cell junctions undergo step-by-step the transition to the mesenchymal state by changing their gene expression profile and losing connection to the basement membrane and neighboring cells. Modified from (Dongre & Weinberg, 2019).*

Mesenchymal cells are spindle-shaped, less organized, due to missing connectivity to adjacent cells more motile, and characterized by expression of mesenchymal genes, like *CDH2* (*Neuronal cadherin*) and *VIM* (*Vimentin*) (Figure 1.5). These genes are upregulated by a specific elevated expression of master transcription factors, like *SNAI1* (*Snail*), *SNAI 2* (*Slug*), and *TWIST1* (*Twist1*), which repress the epithelial state and induce the mesenchymal state (Dongre & Weinberg, 2019). Usually, tumor cells remain in a part-epithelial,

part-mesenchymal state with a mixed gene expression profile and do not undergo a full transition (Dongre & Weinberg, 2019).

1.3.6. The role of the microtubule cytoskeleton for cell migration and invasion

Microtubules are, like actin filaments, constituents of the cytoskeleton. They organize the transport of cargo and influence the orientation and organization of organelles within the cytoplasm of cells (Furey et al., 2020). They are key to the mitotic spindle that segregates chromosomes during mitosis (Meunier & Vernos, 2012). Furthermore, microtubules actively contribute to mechanisms involved during cell movement (Garcin & Straube, 2019). In the complex process of cell migration, the organization of the microtubule network changes significantly (Figure 1.6).

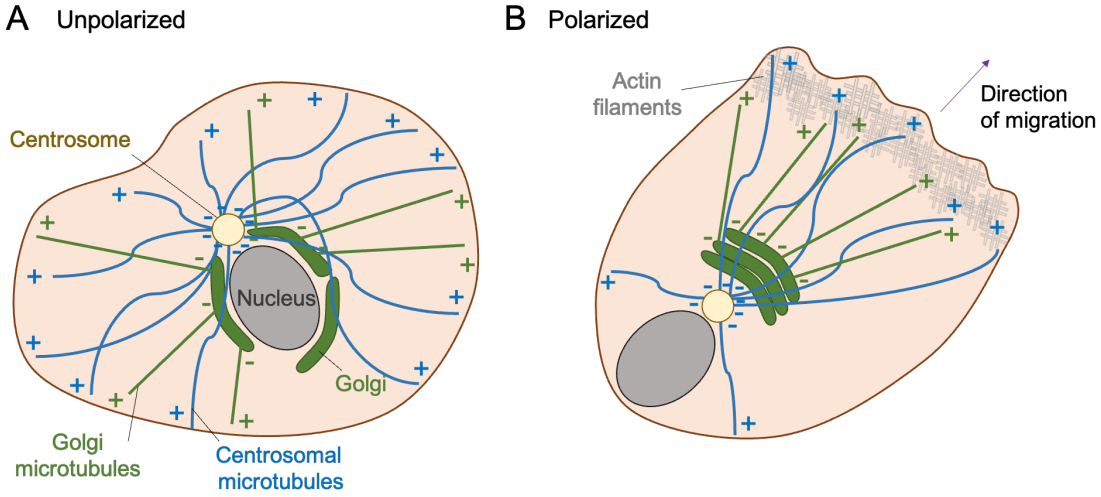

Figure 1.6 Changes in the microtubule network before cell migration. *A) The majority of microtubules in an unpolarized cell have their origin at the centrally positioned centrosome. Their distribution is radial and the microtubule plus ends are directed towards the cell cortex. B) The localization of the centrosome changes and microtubules are orientated towards the direction of cell migration. Modified from* (Meiring et al., 2020).

Interphase microtubules are mainly anchored at the centrosome. In an unpolarized cell, the centrosome is located in the cell center and microtubules are radially orientated with the microtubule plus ends directed towards the cell cortex. In preparation for cell migration, the centrosome relocates to the front of the cell nucleus, ensures the proper organization of the golgi complex, which functions as a non-centrosomal microtubule organizing center (Hao et al., 2020), and microtubules establish cell polarization by orientating their plus ends in the direction of cell migration (Meiring et al., 2020).

Microtubules contribute to cell migration and invasion (Liao et al., 1995; Watanabe et al., 2005) by mediating the transport of functional components to the protruding cell edge or by recycling adhesion molecules, such as integrins (Garcin & Straube, 2019; Kaverina &

Straube, 2011). The overexpression of integrin linked kinase (ILK), an essential kinase and adaptor protein localized to invadopodia, was associated with microtubule depolymerization (Lim et al., 2013). The formins Drf1 and Drf2, activated by the small GTPases RhoA and Cdc42 (Figure 1.3), not only regulate actin nucleation and polymerization, but also function as microtubule regulators that cap and stabilize growing microtubule plus ends (Bartolini et al., 2008). The p21 activated kinase (PAK), a downstream effector of both small GTPases Rac1 and Cdc42, phosphorylates Stathmin (oncoprotein 18), which is usually known for its role in destabilizing microtubules. However, the phosphorylation of serine 16 was shown to disable the activity of Stathmin leading to increased stabilization of growing microtubules (Watanabe et al., 2005). Growing microtubules transport and enrich GEFs and therefore increase the concentration of cortical Rac1 at the position where lamellipodia are about to be established. In turn, activated Rac1 influences microtubule growth by regulating microtubule associated proteins (MAPs), such as Stathmin (oncoprotein 18), CLIP associated proteins (CLASPs), and the cytoplasmic linker protein 170 (CLIP-170). CLASPs are microtubule stabilizing factors that suppress microtubule dynamics and CLIP-170 is a plus end interacting protein (Trogden & Rogers, 2015).

1.4. Chromosomal instability and metastasis

The state of aneuploidy, arising through chromosomal instability, changes the gene dosage of cells, thereby leading to dysregulated expression of oncogenes and tumor suppressor genes (Kojima & Cimini, 2019). A plethora of genes regulating diverse cellular mechanisms can be affected. For instance, the gene expression landscape during the epithelial-to-mesenchymal transition (EMT), a driver for metastasizing cells, is undergoing a variety of modifications. Chromosomally instable epithelial cells were shown to induce an invasive phenotype through the loss of essential intercellular junction proteins (Gao et al., 2016). A recent study analyzed the effect of single chromosome gains in the colorectal cancer cell line HCT116 and the outcome on invasive behavior. Gains of six different chromosomes were included in the study, from which the gain of chromosome 5 was shown to increase the invasiveness through inducing partial EMT and upregulation of matrix metalloproteases (Vasudevan et al., 2020).

A frequent pre-stage of chromosomal instability is the formation of lagging chromosomes during anaphase, which arise through merotelic attachments. Lagging chromosomes are exposed to torsional stress due to pulling forces emanating from opposing spindle poles. The torsional stress can lead to DNA damage or breakage, resulting in chromosome fragments. These fragments are not included in the main nucleus and are often found in so called micronuclei (Thompson & Compton, 2011). Bakhoum and colleagues published

intriguing results demonstrating that micronuclei containing chromosome fragments are prone to rupture and can release DNA into the cytosol of cells. In consequence, the intrinsic DNA sensing machinery is activated. Cyclic GMP-AMP synthase (cGAS) acts as a DNA receptor and forms dimers by directly binding to cytosolic DNA. In this process, dimerized cGAS produces the endogenous cyclic dinucleotide second messenger molecule – cGAMP, which activates the endoplasmic reticulum bound, transmembrane protein stimulator of interferon genes (STING). Downstream effects of STING activation include the activation of the canonical nuclear factor κ-light-chain enhancer (NF-κB) and mitogen activated protein kinase (MAPK) signaling pathway and the activation of type I interferons, like interferon regulatory factor 3 (IRF3), usually leading to an innate immune response. Strikingly, tumor cells can suppress the immune response and upregulate only the non-canonical NF-κB signaling to establish a pro-tumorigenic microenvironment (Bakhoum et al., 2018; Hopfner & Hornung, 2020). The activation of the non-canonical NF-κB signaling pathway is linked to increased nuclear localization of the transcription factor Rel-like domain-containing protein B (RelB) and the enhanced transcription of EMT promoting factors leading to the initialization of an invasive phenotype (Kendellen et al., 2014; Lee et al., 2013).

1.5. The microtubule cytoskeleton

Since the microtubule cytoskeleton fulfills ubiquitous functions within the cell, the structure, associated proteins, and the contribution of microtubules to genome instability will be explained in detail.

1.5.1. Structure and function of microtubules

α/β-tubulin heterodimers form protofilaments in a head-to-tail manner, with α-tubulin present at the minus end and β-tubulin exposed at the plus end. The minus end is orientated towards the centrosome, where α-tubulin directly binds to the γ-tubulin ring complex (γ-TuRC). Microtubules are formed out of thirteen parallelly orientated protofilaments appearing in a straw-like shape with a diameter of 25 nm, offering a large surface for molecular motor proteins to attach and transport cargo directionally along microtubules (Muroyama & Lechler, 2017). Microtubules are known for their dynamic instability, which describes phases of growth and shrinkage where guanosine triphosphate (GTP) bound heterodimers are added rapidly to the plus end leading to growth of the microtubule in one direction. GTP hydrolysis of incorporated tubulin leads to controlled catastrophe events and microtubule shrinkage, happening preferentially near the cell cortex (Figure 1.7) (Roostalu & Surrey, 2017). The measurement of the rate by which microtubules grow using

fluorescence labelled end binding (EB) proteins, like EB1 or EB3, in combination with a live cell microscope offers insights into essential cellular processes (Zwetsloot et al., 2018).

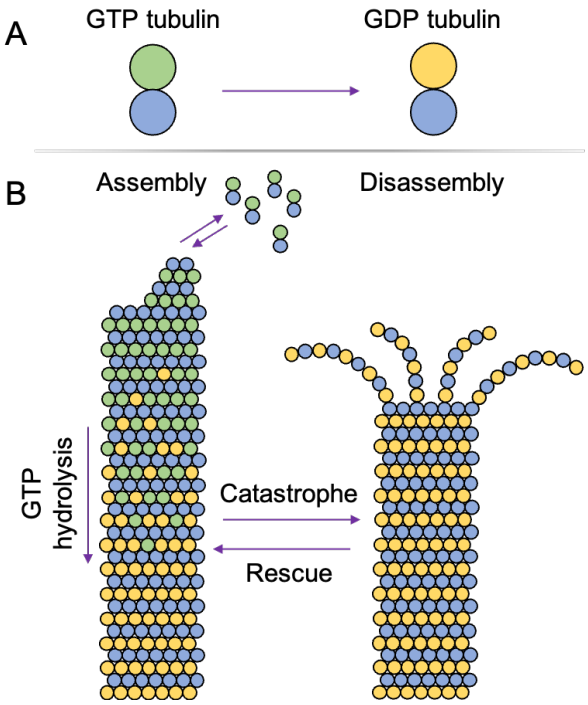

Figure 1.7 Dynamic instability of microtubules. *A) Guanosine triphosphate (GTP) bound α/β-tubulin heterodimers and the subsequent hydrolysis of GTP to guanosine diphosphate (GDP). B) Microtubule protofilaments and plus end associated incorporation of GTP bound heterodimers (assembly), followed by GTP hydrolysis and induced catastrophe (disassembly). Modified from (Al-Bassam & Chang, 2011).*

1.5.2. Microtubule plus end assembly affects chromosomal instability in cancer cells

Our lab has identified a key mechanism leading to the formation of lagging chromosomes, a frequent pre-stage for chromosome missegregation, and chromosomal instability in human cancer. Interestingly, increased microtubule polymerization rates within the mitotic spindle were found to cause transient spindle mispositioning, thereby fostering kinetochore mal-attachments and chromosome missegregation (Ertych et al., 2014). Intriguingly, the lab found cancer-related upstream regulators that mediate an increased microtubule plus end assembly rate in mitotic cells. For instance, loss of the tumor suppressor Brca1 or loss of its positive regulator Chk2 is sufficient to trigger abnormal microtubule assembly rates resulting in lagging chromosomes, chromosome missegregation, and numerical aneuploidy. Furthermore, overexpression of the kinase *AURKA,* which is known to negatively regulate Brca1, also triggered chromosomal instability by inducing deregulated microtubule dynamics (Ertych et al., 2016; Stolz et al., 2010).

1.5.3. Function of microtubule associated proteins

Microtubule associated proteins (MAPs) are known to bind to microtubules and affect their dynamics. Microtubule-associated motor proteins can transform chemical, ATP-based energy into mechanical energy resulting in their movement. Most of these motor proteins belong to the kinesin superfamily and are plus end directed (Hirokawa et al., 2009). Especially during cell movement, secretory vesicles and mRNAs encoding the actin regulator profilin or components of the Arp2/3 complex are transported from the center to the cell periphery where they are required at the leading edge. On the other hand, motor proteins are also essential for recycling adhesion molecules, like integrins, used during cell migration and invasion (Garcin & Straube, 2019). Other essential motor proteins, like the kinesin Eg5, function during mitosis to establish the mitotic spindle (Wordeman, 2010).
Additional members of the family of MAPs are proteins of the Xenopus microtubule associated protein 215 (XMAP215) and CLIP associated protein (CLASP) family that are characterized by N-terminal tumor overexpressed genes (TOG) domains. Each TOG domain contains six structural HEAT repeat motifs and exhibits a high affinity to tubulin dimers (Byrnes & Slep, 2017). XMAP215, in humans also referred to as colonic and hepatic tumor overexpressed gene (chTOG) protein (gene name: *CKAP5* - *Cytoskeleton associated protein 5*), is composed of five TOG arrays and affects interphase and mitotic microtubules by directly binding to the plus end and promoting the incorporation of tubulin dimers to the growing strand (Brouhard et al., 2008; Herman et al., 2020). As a cell proceeds through mitosis, chTOG together with the transforming acidic coiled-coiled protein 3 (TACC3) and clathrin is responsible for stabilizing microtubules at the kinetochore, therefore ensuring proper chromosome segregation and preventing chromosomal instability (Booth et al., 2011). Furthermore, chTOG was found to cooperate with the γ-tubulin ring complex during *de novo* microtubule nucleation at the centrosome (Thawani et al., 2018). The centrosome is the main organizing unit for microtubules and is also known as the microtubule organizing center (MTOC) of the cell.

1.6. The Centrosome – the microtubule organizing center of the cell

A normal cell in G1 phase of the cell cycle has one centrosome consisting of a mother centriole, also known as the basal body, and a daughter centriole. Before centriole duplication starts during S phase, the two centrioles disengage to become two independent mother centrioles that can act as a template for the formation of new daughter centrioles. After recruitment of microtubule nucleation factors to the centrosome during G2 phase, to ensure proper establishment of the mitotic spindle, the centrosomes start to move apart

and assemble the spindle during early mitosis. During cell division, every daughter cell will be equipped with one centrosome (Buchwalter et al., 2016; Conduit et al., 2015).

1.6.1. Microtubule nucleation at the centrosome

De novo microtubule nucleation takes place at the centrosome and depends on the γ-tubulin ring complex (γ-TuRC). The formation of new microtubules is a kinetically unfavorable process, in which a large energy barrier must be overcome. γ-tubulin is the main microtubule nucleator and forms together with γ-tubulin complex proteins (GCP) a centrosome linked docking station for α/β-tubulin heterodimers (Roostalu & Surrey, 2017). The microtubule polymerase chTOG interacts through its C-terminal domain with γ-tubulin and 'catches' with its N-terminal TOG-domains free α/β-heterodimers from the cytoplasm, therefore cooperating with γ-tubulin, enabling the nucleation of microtubules and the establishment of the mitotic spindle (Thawani et al., 2018).

1.6.2. Centrosomes as actin regulators

The centrosome is not just known for its role in organizing microtubules, but also offers a nucleation platform for actin filaments. Studies demonstrated that actin regulatory proteins, like the Arp2/3 complex, cofilin, and the WASP and SCAR homologue (WASH), are enriched around the centrosome (Farina et al., 2016). The activity of the Arp2/3 complex close to the centrosome was shown to be essential to link the centrosome to the nucleus in interphase (LoMastro & Holland, 2019).
Actin filaments can control and regulate microtubules at multiple levels, including altering the rates of growth or shrinkage and directing branching or alignment. Profilin 1, a major actin regulator that induces actin polymerization, is localized at the centrosome and negatively regulates microtubule nucleation (Nejedlá et al., 2020). In reverse, microtubule plus end binding proteins, like EB1, were shown to actively modulate F-actin levels (Juanes et al., 2020). Considering these insights, the interactions between actin filaments and microtubules are not only projected to the cell periphery, but happen also at the centrosome, especially right before and during mitosis (Farina et al., 2016, Farina et al., 2019).

1.6.3. Centrosome duplication

Centrosome duplication occurs during S phase. Cdk2-cyclin A and Cdk2-cyclin E activity is mandatory for successful entry into S phase and thus, for centrosome duplication (Gönczy, 2015). Centrioles within one centrosome separate from each other to become two independent mother centrioles, able to function as a template for new procentrioles (Figure 1.8A). Essential factors for proper centrosome duplication are the serine-threonine

protein kinase polo like kinase 4 (Plk4) as well as the proteins SCL/TAL interrupting locus (Stil) and spindle assembly abnormal protein 6 homolog (Sas-6).

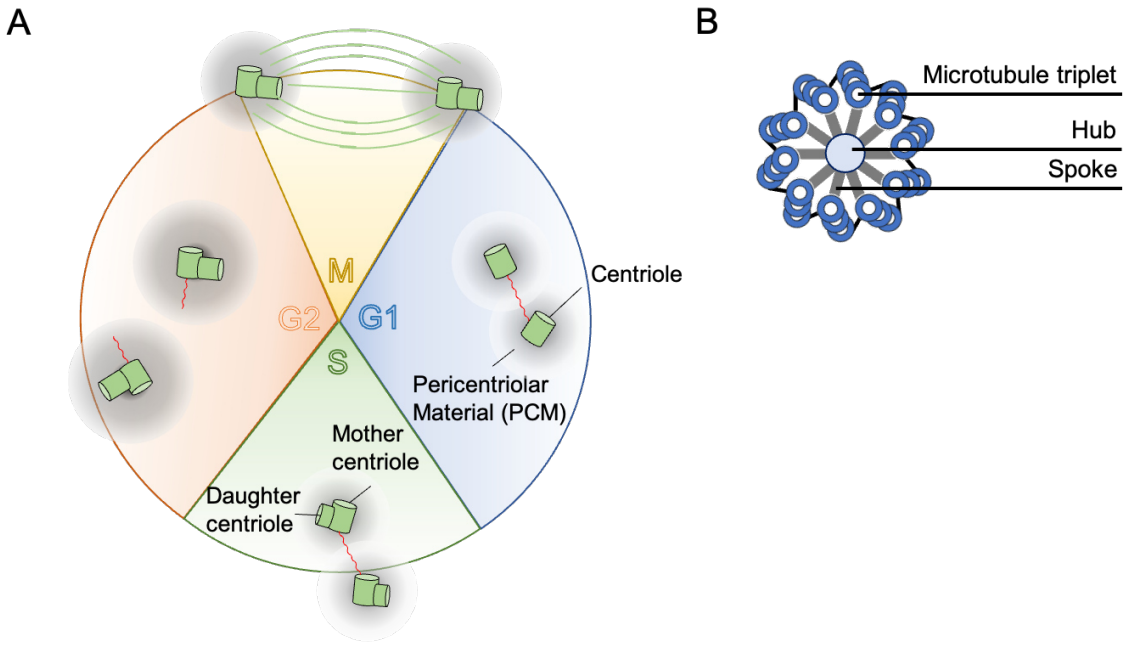

Figure 1.8 Centrosomal changes during cell cycle progression and the structure of the cartwheel during procentriole formation. *A) Cells start in G1 phase with one centrosome consisting of two centrioles and the surrounding pericentriolar material (PCM). During S phase, the two centrioles separate and each act as a template for the formation of a new daughter centriole. During G2 phase, PCM matures and accumulates γ-tubulin ring complexes to ensure proper spindle assembly. During early mitosis, centrosomes start to move apart and assembly the spindle for the upcoming chromosome segregation. Each daughter cell receives a centrosome, which in G1 phase again consists of one mother and one daughter centriole, ready for progression through the cell cycle. Modified from* (Conduit et al., 2015)*. B) The central hub is surrounded by nine radial spokes, each connected to a microtubule triplet. Modified from (Azimzadeh & Marshall, 2010).*

The assembly of procentrioles is initialized by the Stil-dependent recruitment of Sas-6 to the mother centrioles. Sas-6 homodimers together with centromere protein J (Cenpj) and centrosomal protein 135 (Cep135) serve as the backbone of the cartwheel, a central hub with nine radial spokes (Figure 1.8B). Plk4 mediated phosphorylation of Sas-6 establishes the link between the procentriole cartwheel and the microtubule wall (Moyer & Holland, 2019; Vulprecht et al., 2012). After procentriole initiation, procentrioles elongate during late S and early G2 phase and the pericentriolar material (PCM) starts to mature by increasing its size and recruiting a plethora of factors necessary for the establishment of the mitotic spindle. The cleavage of pericentrin leads to centriole disengagement in late G2 phase. Polo like kinase 1 (Plk1), cyclin dependent kinase 1 (Cdk1), and Aurora kinase A are essential factors during centriole disengagement. Cdk1 in complex with G2/M cyclins activates the serine/threonine kinase Aurora A, which in turn stimulates Plk1, thereby inducing centriole/procentriole separation (Gönczy, 2015). The PCM is the microtubule anchoring matrix that surrounds the centrioles. The key regulator during the maturation process is

Plk1 that phosphorylates pericentriolar proteins. This leads to the accelerated recruitment of Cep192, Cep215, pericentrin, and γ-tubulin from the cytosol to the centrosome to allow proper assembly of the spindle apparatus, ensure correct chromosome segregation and maintenance of chromosome stability (Buchwalter et al., 2016; Conduit et al., 2015; Mennella et al., 2014).

1.7. Supernumerary centrosomes in cancer

Centrosomes organize microtubules and contribute to the establishment of the mitotic spindle, cell polarity, cell morphology, and cell motility (Mittal et al., 2020). Dysregulation of these processes can have fatal consequences and are associated with the development of a variety of tumors and the progression of cancer (Chan, 2011). The main reason for the formation of supernumerary centrosomes is the deregulation of factors that participate in the duplication cycle of centrosomes, such as Plk4 and Sas-6 (Godinho & Pellman, 2014). In normal cells, Plk4 kinase activity underlies a strict regulation to prevent possibly fatal errors during centriole duplication. Nevertheless, the *PLK4* gene locus is mutated and overexpressed in a variety of cancers, such as colorectal and breast cancer (Kazazian et al., 2017; Liao et al., 2019; Shinmura et al., 2014; Zhang et al., 2021). Ectopic *PLK4* overexpression was shown to induce supernumerary centrosomes, chromosome missegregation, and tumor formation in mice (Levine et al., 2017). Overexpression of *PLK4* accompanied by p53 deficiency was associated with the increased formation of skin tumors in mice (Serçin et al., 2016). Furthermore, over-elongation of centrioles during G2 phase is associated with fragmented centrosomes or ectopic procentriole formation leading to abnormal centrosome amplifications (Marteil et al., 2018). Apart from being overduplicated, supernumerary centrosomes can also arise through aborted cell division or cell fusion (Nigg, 2002).

Besides its defined role during centriole duplication, *PLK4* overexpression is also associated with enhanced cell migration and invasion *in vitro.* For instance, the activation of Plk4 by the Cep85-Stil complex is essential for centriole duplication while also mediating the phosphorylation of the Arp2/3 complex subunit Arp2 at the leading edge of invasive cells (Kazazian et al., 2017; Liu et al., 2020).

1.7.1. Supernumerary centrosomes and chromosomal instability

Since persistent multipolar spindles arising from an abnormal number of centrosomes would lead to massive chromosome missegregation and chromosomal instability (CIN), cancer cells found a way to cope with an abnormal number of centrosomes (Ganem et al., 2009). During interphase, multiple centrosomes are clustered close to the nucleus and

start to move apart at the beginning of prophase by surrounding the nucleus. After the nuclear envelope breakdown (NEB), centrosomes first form a multipolar spindle intermediate, which is followed by the establishment of a nearly perfect bipolar spindle, the so called pseudo-bipolar spindle (Ganem et al., 2009; Mittal et al., 2020). The non-essential kinesin motor protein Kifc1, a minus end directed kinesin 14 motor protein, plays an essential role during the clustering process (Venuto et al., 2020). Kifc1 was shown to be overexpressed in breast, ovarian, and hepatocellular carcinoma to ensure proper clustering of centrosomes and survival of tumor cells. Inhibition of Kifc1 leads to a multipolar spindle and cell death, making it a potent target for cancer therapy (Fan et al., 2021; Krämer et al., 2011). Other motor proteins, like dynein and HSET, cooperate with nuclear mitotic apparatus (NuMA) protein to link and bundle the minus ends of microtubules resulting in clustered poles (Kwon, 2016). Furthermore, signal transducer and activator of transcription 3 (Stat3) contributes to centrosome clustering in mammary tumor cells (Morris et al., 2017). However, even if cancer cells manage to establish a nearly perfect bipolar spindle, the multipolar spindle intermediate was shown to trigger the formation of merotelic attachments and lagging chromosomes, a frequent pre-stages of chromosome missegregation leading to chromosomally instable cells (Mittal et al., 2020).

1.7.2. Supernumerary centrosomes and cancer cell invasion

An excess of centrosomes in cancer cells was shown to be associated with chromosomal instability and metastasis (Ganem et al., 2009). Centrosomes and emanating microtubules are essential for intracellular trafficking and regulate the spatial organization of organelles during interphase. Centrosome positioning dictates the position of the golgi apparatus and therefore regulates the route of secretory pathways within the cell (Gönczy, 2015). Centrosomes with an abnormal size are characterized by a higher microtubule nucleation capacity, which leads to the formation of compact microtubule bundles that are favoring cell migration by promoting cell polarization (Mittal et al., 2020).

Pellman and colleagues published an intriguing link between supernumerary centrosomes and the induction of invasiveness in human mammary epithelial cells. The study used a doxycycline inducible *PLK4* overexpression system in MCF-10A cells leading to the induction of supernumerary centrosomes. Cells with an abnormal number of centrosomes formed more invasive protrusions when they were embedded in a 3D matrix. Interestingly, increased Rac1 activity further promoted invasiveness in cells with supernumerary centrosomes (Godinho et al., 2014). Moreover, the Godinho lab showed that cells with an abnormal number of centrosomes induce invasiveness in neighboring cells through a paracrine signaling (Figure 1.9). In fact, conditioned medium from cells with supernumerary

centrosomes was able to induce invasive protrusions in recipient cells. Cells with supernumerary centrosomes were shown to exhibit a changed protein secretion profile compared to cells with a normal number of centrosomes.

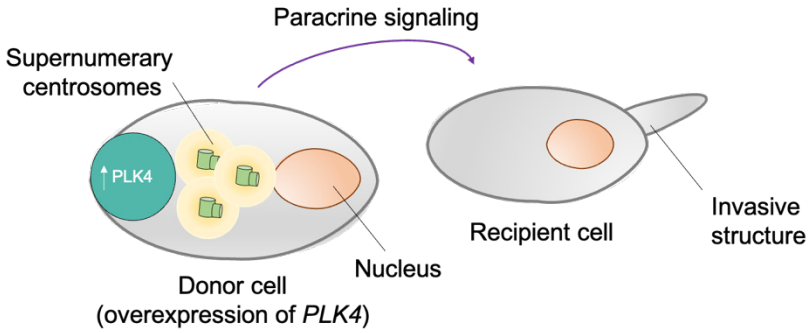

Figure 1.9 Paracrine signaling triggers formation of invasive protrusions in recipient cells. *Donor cells with a doxycycline inducible overexpression of PLK4 were shown to exhibit supernumerary centrosomes leading to the secretion of factors that will lead in recipient cells to the formation of invasive structures* (Arnandis et al., 2018).

Of particular interest was the elevated secretion of interleukin 8 (IL8), growth/differentiation factor 15 (GDF-15), and angiopoietin like 4 (ANGPTL4), since treatment of mammary organoids with the combination of the three factors led to the induction of invasive protrusion. Furthermore, the group showed that the induction of supernumerary centrosomes in MCF-10A cells led to an early stress response, detected by elevated levels of reactive oxygen species (ROS), which was shown to be directly linked to the secretion of the mentioned factors (Arnandis et al., 2018). Finally, it was demonstrated that the invasion triggering activity was dependent on the activity of the human epidermal growth factor receptor 2 (HER2).

1.8. Cell-cell communication

Based on the observation that supernumerary centrosomes induce enhanced paracrine signaling, the Godinho lab showed in a recent publication that pancreatic cells with supernumerary centrosomes secrete elevated levels of small extracellular vesicles. The induction of high levels of ROS in cells with more centrosomes (Arnandis et al., 2018) leads to defective lysosomes, which is associated with the enhanced fusion of multivesicular bodies with the plasma membrane and thus, with an elevated release of small extracellular vesicles. The vesicles were shown to modulate the tumor microenvironment by activating pancreatic stellate cells, indicating an increased communication between different cell types.

1.8.1. Ways of cell-cell communication

Communication between cells is essential and happens permanently. Cells can communicate either through direct cell-cell contact or via secretion of soluble factors, which bind to surface receptors of the same or neighboring cells to trigger a response by activating signaling pathways downstream of the receptor. Signaling affecting the same cell is referred to as autocrine signaling. If additional cells are involved, it is possible to distinguish between nearby signaling (juxtracrine), short distance (paracrine), and long distance (endocrine) signaling (Brücher & Jamall, 2014).

Normal cells, as well as tumor cells, can secrete various factors into the surrounding microenvironment, which will not only modulate the behavior and abilities of the same or adjacent cells, but also modifies the microenvironment. It is well known that cytokines, chemokines, and hormones can be secreted directly by the cells and reach the same or adjacent cells in closer proximity by binding to appropriate receptors on the cell surface. Among different types of receptors, G protein coupled receptors (GPCR) and receptor tyrosine kinases (RTK) are most relevant in this regard (Gavi et al., 2006).

1.8.2. Extracellular vesicles

Cells do not only communicate through cell-cell contact or secreted soluble factors, but can also secrete membrane-based, actin rich extracellular vesicles that can transport cargo safely over longer distances (Menck et al., 2020). These vesicles can contain cytokines, chemokines, and other signaling proteins, nucleic acids (*e.g.,* DNA, RNA, microRNA), DNA bound histones, lipids, and receptors anchored in the membrane of the vesicles (Al-Nedawi et al., 2008; Mannavola et al., 2020; O'Brien et al., 2020; Schiera et al., 2016). Transmembrane receptors can be transported to adjacent cells and can be incorporated into the cell membrane of the target cell. Using this mechanism, cells can transmit tumorigenic features, like invasiveness, to neighboring cells (Arnandis et al., 2018). However, the exact mechanism by which vesicles are formed and secreted is not completely understood.

It is possible to distinguish between different types of vesicles based on their size, the speed by which they can be sedimented, the cargo they transport, and their location of synthesis. Based on the latter, it is possible to distinguish between ectosomes and exosomes. Exosomes with 50-150 nm are the smallest type of extracellular vesicles, which can be sedimented only at very high centrifugation accelerations of > 100000 x g. They originate from invagination of the plasma membrane. The fusion with other vesicles inside the cell will lead to the formation of multivesicular bodies (MVB), which can fuse again with the plasma membrane to release their content (Kalluri & LeBleu, 2020). The exact function

of exosomes remains to be identified, but it has been shown that cells can store cellular waste inside of exosomes and remove it through secretion (Rashed et al., 2017). In contrast, ectosomes are vesicles of medium and large size. Vesicles of medium size (100-1000 nm) are so called microvesicles and sediment at 10000 to 20000 x g. Large oncosomes have a size of 1000-10000 nm and already sediment at 2000 x g.

1.8.3. Ectosome shedding

The ATP-dependent mechanism by which microvesicles are secreted is called plasma membrane budding. It is based on the relocation and exposure of phosphatidylserines (PS) to the outer membrane. Additionally, membrane regions where microvesicle budding occurs are characterized by a specific composition of lipids, mainly cholesterol, and are referred to as lipid rafts (Hurley et al., 2010; Muralidharan-Chari et al., 2010).
The small GTPases Adenosine diphosphate-ribosylation factor 1 and 6 (Arf1, Arf6) and other members of the Rho and Ras related in brain (Rab) small GTPase family are essential for inducing actin rearrangements, recruitment of cargo to ectosomes, and shedding of ectosomes (Casalou et al., 2020). Ectosome shedding is based on the ATP-dependent interplay between the actin and myosin cytoskeleton. Arf6 activates its downstream effector, the extracellular signal-regulated kinase (ERK), which activates the myosin light chain kinase (MLCK) at the location of membrane budding. MLCK phosphorylates the myosin light chain (MLC) leading to the activation of the contractile machinery (Tricarico et al., 2017). Additionally, ERK activity simultaneously leads to the stimulation of RhoA, which also activates MLC through the Rho associated protein kinase (ROCK) pathway (Tong et al., 2016).

1.9. The HER2 signaling

Conditioned medium from cells with supernumerary centrosomes induces the formation of invasive protrusions in target cells. Interestingly, this function was shown to involve human epidermal growth factor receptor 2 (HER2) signaling and the activation of the mitogen-activated protein kinase (MAPK) signaling pathway in recipient cells (Arnandis et al., 2018). HER2 and MAPK signaling are major oncogenic pathways with various functions.

1.9.1. The oncogenic role of HER2 signaling

The human epidermal growth factor receptor 2 (HER2) belongs to a family of four oncogenic receptor tyrosine kinases – HER1, HER2, HER3, and HER4, also called ErbB1, ErbB2, ErbB3, and ErbB4, respectively. The receptors consist of an extracellular binding domain, multiple transmembrane regions, and intracellular domains with tyrosine kinase

activity (Iqbal & Iqbal, 2014). In mammalian cells, ligands for the receptors are members of the epidermal growth factor (EGF) family. Receptors of the HER family appear as monomers. After ligand binding, receptors undergo dimerization and phosphorylate each other at their intracellular domain (Yarden & Sliwkowski, 2001). The phosphorylated tyrosine residues recruit signaling molecules to the plasma membrane and activate downstream signaling pathways, such as the mitogen activated protein kinase (MAPK) signlaing pathway, the protein kinase C (PKC) and phosphatidylinositol-4,5-biphosphate 3-kinase (PI3K) pathway. HER2 is an incomplete receptor molecule. It lacks ligand binding activity and is mainly known for its role as a dimerization partner (Jeong et al., 2017; Moasser, 2007). Signaling downstream of the receptor is initiated through recruitment of SH2 domain containing proteins, like src kinases, to the phosphorylated tyrosine residues of the receptors. Src kinases activate PI3K/AKT leading to the establishment of tumorigenic features, like increased proliferation, enhanced survival, upregulated metabolism, and invasiveness. Upregulated PI3K/AKT signaling can also lead to the deregulation of the G1/S restriction point by affecting D-type cyclins and p27 (Moasser, 2007).

HER2 was shown to be overexpressed in 15 to 30 % of invasive breast and ovarian cancers with protein levels up to 40- to 100-fold higher in cancer cells compared to normal cells (Oh & Bang, 2020). Alternatively, HER2 mutations can lead to hyperactivation of the receptor dimerization and constitutively activated downstream signaling (Shi et al., 2021). HER2 activation has been shown to disrupt cell polarity and cell adhesion, resulting in increased cell motility, and triggering EMT (Gupta & Srivastava, 2014; Ingthorsson et al., 2016). Accordingly, hyperactivated HER2 is associated with shorter disease free and overall survival of cancer patients. Monoclonal antibodies and small molecule inhibitors targeting HER2 show high effectiveness in the treatment of HER2 positive breast cancer cases. The monoclonal antibody trastuzumab binds to the extracellular domain of HER2. Antibody binding has several effects, like inhibition of dimerization, receptor degradation, and cellular cytotoxicity, resulting in decreased activation of the downstream signaling pathways PI3K/AKT and MAPK (Iqbal & Iqbal, 2014; Oh & Bang, 2020).

1.10. The MAPK pathway downstream of HER2 activation

The treatment of cells with conditioned medium from cells with supernumerary centrosomes induced increased phosphorylation of extracellular signal-regulated kinases 1 and 2 (ERK1 and ERK2) downstream of HER2 signaling, which was rescued using the selective MEK1/2 inhibitor PD98059 (Arnandis et al., 2018). The kinases ERK1 and ERK2 are known to alter cell proliferation, cell motility, and cell metabolism. Both kinases phosphorylate serine-threonine residues of target proteins and belong to a family of structurally

related kinases, the mitogen-activated protein kinases (MAPK) (Guo et al., 2020). The signaling cascade is activated in response to growth factor binding to cell surface receptors, like HER2. GTP bound Ras located at the plasma membrane in proximity to the receptor is activated and translocates rapidly accelerated fibrosarcoma (Raf) kinases to the plasma membrane leading to dimerization of the Raf kinase domain. Raf activates MEK by phosphorylation of its activation domain. At last, MEK phosphorylates ERK1 and ERK2 (Figure 1.10) (Braicu et al., 2019; Guo et al., 2020; Lavoie et al., 2020).

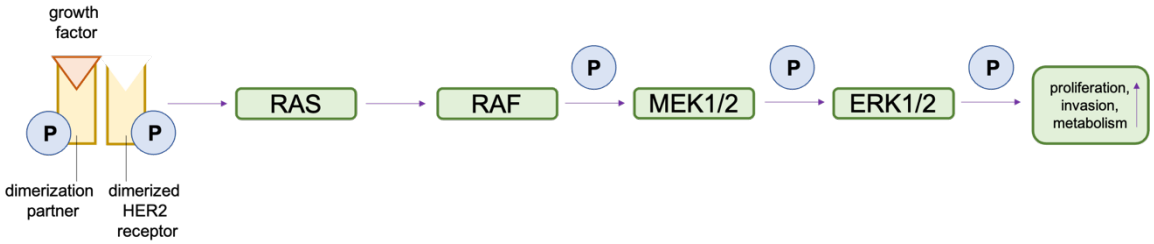

Figure 1.10 Mitogen activated protein kinase signaling pathway downstream of HER2. *The binding of growth factors to HER2 dimerization partners leads to the dimerization and autophosphorylation of the receptors. Autophosphorylated receptors activate Ras, which will lead to the recruitment of Raf to the plasma membrane. Raf will phosphorylate and activate MEK, which will in turn activate ERK. ERK fulfills a plethora of different functions by activating the transcription of essential cell cycle regulators and factors for cell growth and proliferation, cell migration and invasion and cell metabolism. Modified from* (Braicu et al., 2019).

Activated ERK is known to regulate a plethora of genes, like *JUN*, *FOS*, *MYC*, *EGF*, and *CREB* (*cAMP response element binding protein*) (Braicu et al., 2019; Lavoie et al., 2020). Furthermore, ERK is known to phosphorylate and activate key components of the migration and invasion machinery. Among them are members of the family of small GTPases, like RhoA, known to activate formins and leading to the elongation of actin filaments (Tong et al., 2016). Moreover, ERK phosphorylates members of the WAVE complex, which is known to activate the Arp2/3 complex, essential for actin polymerization (Lavoie et al., 2020).

Scope of the study

The loss of *TP53* and *TP73* triggered both, abnormal microtubule dynamics and CIN suggesting that p53 and p73 collaborate in mitosis to regulate microtubule assembly and chromosome segregation. Moreover, it was demonstrated that a direct consequence of p53/p73 deficiency is the loss of the Cdk inhibitor $p21^{Cip1}$ leading to accelerated activity of Cdk1. Unleashed Cdk1 activity causes abnormal microtubule plus end growth rates and chromosome missegregation, resulting in aneuploidy and whole chromosomal instability (Berger, 2016; Schmidt et al., 2021). Interestingly, the loss of *TP53* and *TP73* not only led to an increase in microtubule plus end growth rates during mitosis, but also changed microtubule plus end growth rates in interphase cells. Astonishingly, this abnormal microtubule regulation was associated with an increase in cell migration and invasion in HCT116 cells (Berger, 2016), indicating a connection between increased microtubule plus end assembly rates and enhanced cell migration and invasion.

This present study focuses on the link between increased microtubule plus end assembly rates in interphase and enhanced cell migration and invasion. Based on the published findings (Adams et al., 2021; Arnandis et al., 2018; Godinho et al., 2014), the study focuses on the question if increased microtubule plus end assembly is linked to aberrant centrosome biogenesis and cell invasion, and if a microtubule growth rate dependent paracrine signaling pathway is involved in transferring cancer-relevant factors onto target cells leading to the deregulation of microtubule dynamics in interphase.

2. Material and Methods

2.1. Material

All standard materials used in the cell culture and daily laboratory work including falcon tubes, pipettes and filter tips, cell culture dishes and reaction tubes were purchased from

- Greiner BioOne (Frickenhausen, Germany)
- Sarstedt (Numbrecht, Germany)
- Starlab (Hamburg, Germany)
- Ibidi (Martinsried, Germany).

2.2. Equipment

Standard equipment and devices used for the research project are listed in Table 2.1.

Table 2.1 Equipment

Equipment	Model	Company
Biological Safety Cabinet	HERAsafe™ M	Thermo Fisher Scientific, Karlsruhe, Germany
Centrifuge, cooling	Multifuge X3R	Thermo Fisher Scientific, Karlsruhe, Germany
Centrifuge, small	Heraeus Pico 17 Centrifuge	Thermo Fisher Scientific, Karlsruhe, Germany
Centrifuge, small cooling	Heraeus Fresco 21 Centrifuge	Thermo Fisher Scientific, Karlsruhe, Germany
Chemiluminescence Imaging	Fusion-SL-3500.WL	VWR International, Radnor, PA, USA
Chemiluminescence Imaging	Fusion FX	Vilber Lourmat, Collégien, France
Electroporation Device	GenePulser Xcell©	BioRad Laboratories, München, Germany
Electrophoresis Power Supply	EV231	Peqlab, Erlangen, Germany
Heating Block	TDB-120 Dry Block Thermostat	Biosan, Riga, Latvia
Incubator	HERAcell 240 CO_2 Incubator	Thermo Fisher Scientific, Karlsruhe, Germany

Incucyte	Incucyte® S3 Live Cell Analysis System	Essen BioScience Inc., Ann Arbor, MI, USA
Laboratory Scale	Sartorius Research R200D	Sartorius, Göttingen, Germany
Magnetic Mixer	IKAMAG© IKA	Labortechnik, Stauffen, Germany
Mass Spectrometer	Q Exactive HF mass spectrometer	Thermo Fisher Scientific, Karlsruhe, Germany
Matrigel™ Invasion Chamber	BioCat Matrigel™ Invasion Chamber 24-well	Corning, New York, NY, USA
Microscope (1)	Delta Vision Elite©	Applied Precision, Chalfont St. Giles, UK
Microscope (2)	Leica DMI6000B	Leica, Wetzlar, Germany
Microscope (3)	Leica DM IL LED	Leica, Wetzlar, Germany
Microscope Camera (1)	sCMOS camera	GE Healthcare, Chalfront St. Giles, UK
Microscope Camera (2)	Leica DFC369 FX	Leica, Wetzlar, Germany
Microscope Camera (3)	Leica EC3 12110026601	Leica, Wetzlar, Germany
Migration Chamber	ThinCerts, 24 well, 8 µm pore size	Greiner BioOne, Frickenhausen, Germany
Multilabel Plate Reader	Victor© X3	PerkinElmer, Rodgau, Germany
Counting chamber	Neubauer improved counting chamber, 0.1 mm depth	Superior Marienfeld, Lauda-Königshofen, Germany
Pipettes	Pipetman	Gilson International, Limburg Offheim, Germany
Pipettor	Pipetboy 2	INTEGRA Biosciences, Zizers, Switzerland
Semi-dry Blotting System	Perfect Blue©	Peqlab, Erlangen, Germany
Spectrophotometer	NanoDrop 2000	Thermo Fisher Scientific, Karlsruhe, Germany
Thermomixer	Thermomixer Comfort	Eppendorf, Hamburg, Germany
Vertical Electrophoresis System		Own manufacturing
Vortex Mixer	VORTEX-GENIE©2	Scientific Industries Inc., Bohemia, NY, USA

Wet Blotting System	Mini Trans-Blot®Cell	BioRad Laboratories, München, Germany
Wet Blotting System		Own manufacturing

2.3. Chemicals and inhibitors

Inhibitors and other chemicals applied in this study are listed in Table 2.2.

Table 2.2 Chemicals and inhibitors

Chemical	Applied concentration	Effect	Company
Adriamycin (Doxorubicin hydrochloride)	600 nM	Intercalates with the DNA backbone and induces DNA damage	Santa Cruz, Dallas, TX, USA
Canertinib	1 µM	Irreversible inhibitor of EGFR and ErbB2	Selleck Chemicals, Houston, TX, USA
CVT313	100 nM	Inhibitor of Cdk2	Santa Cruz, Dallas, TX, USA
Collagen I, rat tail	2 mg/ml	Extracellular matrix for 3D spheroid assay	Enzo Life Science, Farmingdale, NY, USA
Dimethylenastron (DME)	2 µM	Inhibitor of kinesin Eg5	Calbiochem, La Jolla, CA, USA
Matrigel™	8-12 mg/ml	Extracellular matrix for 3D spheroid assay	Corning, New York, NY, USA
Mounting medium		Coating of immunofluorescence staining's	Vector Laboratories, Inc., Peterborough, UK
Nitrocellulose membrane		Membrane for western blotting	GE Healthcare, Chalfront St., Giles, UK
PD0332991 (Isethionate)	75 nM	Inhibitor of Cdk4	Sigma-Aldrich, Taufkirchen, Germany
PD98059	20 µM	Inhibitor of MEK1 and MEK2	Tocris Bioscience, Bristol, UK
RO3306	1 µM	Inhibitor of Cdk1	Santa Cruz, Dallas, TX, USA
SCH-527123	100 nM	Antagonist of the IL8 receptor CXCR1/2	MedChemExpress, Monmouth Junction, NJ, USA
Taxol	0.2 nM (HCT116), 0.5 nM (melanoma)	Microtubule stabilizing drug	Sigma-Aldrich, Taufkirchen, Germany

Trastuzumab	40 µM	Neutralizing monoclonal antibody for HER2	Kindly provided by Prof. Gerald Wulf (Göttingen, Germany)

2.4. Software

Software used to analyze and visualize the data is listed in Table 2.3.

Table 2.3 Software

Software	Company
Graph Pad Prism 6.0	GraphPad Software, San Diego, CA, USA
Incucyte® Base Software	Essen BioScience Inc., Ann Arbor, MI, USA
ImageJ	NIH Image, Bethesda, MD, USA
Leica Application Suite 2.7.3.9723	Leica, Wetzlar, Germany
Leica LAS EZ	Leica, Wetzlar, Germany
Soft Worx 6.0 Software Suite and Soft Worx Explorer 1.3.0	Applied Precision Inc., Issaquah, WA, USA

2.5. Primary Antibodies

Table 2.4 shows primary antibodies with information about the host, clonality, and dilutions for indicated methods.

Table 2.4 Primary antibodies

Antigen	Host	Clonality	Used for	Dilution	Catalog number	Company
α-Tubulin (B-5-1-2)	mouse	monoclonal	WB, IF	1:700 (IF) 1:1000 (WB)	#sc-23948	Santa Cruz, Dallas, TX, USA
α-Tubulin	rabbit	polyclonal	IF	1:700 (IF)	#ab18251	Abcam, Cambridge, UK
β-actin (AC-15)	mouse	monoclonal	WB	1:6000	#A5441	Sigma Aldrich, Taufkirchen, Germany
γ-Tubulin (GTU88)	mouse	monoclonal	WB, IF	1:1000 (IF) 1:500 (WB)	#T6557	Sigma Aldrich, Taufkirchen, Germany

Cep192	rabbit	polyclonal	WB	1:500	#A302324A	Bethyl Laboratories, Montgomery, TX, USA
chTOG (H-4)	mouse	monoclonal	WB	1:400	#sc-374394	Santa Cruz, Dallas, TX, USA
Cyclin D1 (HD11)	mouse	monoclonal	WB	1:400	#sc-246	Santa Cruz, Dallas, TX, USA
E2F1 (KH95)	mouse	monoclonal	WB	1:400	#sc-251	Santa Cruz, Dallas, TX, USA
GFP (GF28R)	mouse	monoclonal	WB	1:2000	#MA515256	Thermo Fisher Scientific, Karlsruhe, Germany
$p21^{CIP1}$ (DCS60)	mouse	monoclonal	WB	1:1000	#2946	Cell Signaling, Danvers, MA, USA
p53 (DO-1)	mouse	monoclonal	WB	1:500	#sc-126	Santa Cruz, Dallas, TX, USA
p73 (EP436Y)	rabbit	monoclonal	WB	1:1000	#ab40658	Abcam, Cambridge, UK
Plk4 (6H5)	mouse	monoclonal	WB	1:400	#MABC544	Merck Millipore, Darmstadt, Germany
Rb (IF-8)	mouse	monoclonal	WB	1:400	#sc-102	Santa Cruz, Dallas, TX, USA
Stil	rabbit	polyclonal	WB	1:5000	#A302442A	Bethyl Laboratories, Montgomery, TX, USA

2.6. Secondary Antibodies

Table 2.5 shows secondary antibodies.

Table 2.5 Secondary antibodies

Antibody	Host	Clonality	Used for	Dilution	Company
Anti-Mouse Alexa-Fluor 594	goat	polyclonal	IF	1:1000	Invitrogen, Carlsbad, CA, USA
Anti-Rabbit Alexa-Fluor 488	goat	polyclonal	IF	1:1000	Invitrogen, Carlsbad, CA, USA
Anti-Mouse Horseradish Peroxidase (HRP)	goat	polyclonal	WB	1:10000	Dianova, Hamburg, Germany
Anti-Rabbit Horseradish Peroxidase (HRP)	goat	polyclonal	WB	1:10000	Dianova, Hamburg, Germany

2.7. siRNA

Table 2.6 shows applied siRNAs with sequence information and reference publications.

Table 2.6 siRNAs

Target gene	Sequence	Reference
CCND1	5´-GUAGGACUCUCAUUCGGGA-3´	Peer *et al.,* 2012
CEP192	5`-AGCAGCUAUUGUUUAUGUUGAAAA-3´	Gomez-Ferreria *et al.,* 2007
CKAP5	5`-GAGCCCAGAGTGGTCCAAA-3´	De Luca *et al*., 2008
E2F1	5´-AAGUCACGCUAUGAGACCUCA-3´	Taura *et al.,* 2010
LUCIFERASE	5´-CUUACGCUGAGUACUUCGAUU-3´	Elbashir *et al.,* 2001
RB	5´-AAGUUUCAUCUGUGGAUGGAG-3´	Guo *et al.,* 2011
TUBG1	5´-AGGAGGACAUGUUCAAGGA-3´	Choi *et al.,* 2010

2.8. Plasmids

Table 2.7 shows used plasmids, their purpose, and reference publications.

Table 2.7 Plasmids

Vector	Purpose	Reference
pcDNA3.1	CMV-promoter driven expression of inserted sequence. Used as a control plasmid.	Invitrogen, Carlsbad, CA, USA

pEGFP-C1	CMV-promoter driven expression of inserted sequence. Used as a control plasmid.	Clontech, Saint-Germain-en-Laye, France
pCR-*CEP192*-GFP	Expression of GFP-tagged *CEP192* to induce microtubule nucleation.	Kindly provided by Prof. David Sharp (London, UK)
pEGFP-*CKAP5*	Expression of GFP-tagged *CKAP5* to induce microtubule dynamics.	Kindly provided by Prof. Linda Wordeman (Seattle, WA, USA)
pEGFP-*EB3*	Expression of GFP-tagged *EB3* to analyze microtubule dynamics.	Kindly provided by Prof. Linda Wordeman (Seattle, WA, USA)
pEGFP-mCherry-*EB3*	Expression of mCherry-tagged *EB3* to analyze microtubule dynamics.	Kindly provided by Prof. Linda Wordeman (Seattle, WA, USA)
pCMV-*PLK4*	Expression of FLAG-tagged *PLK4* to induce supernumerary centrosomes.	Kindly provided by Prof. Ingrid Hoffman (Heidelberg, Germany)
pEGFP-*STIL*	Expression of GFP-tagged *STIL* to induce supernumerary centrosomes.	Kindly provided by Prof. Alwin Krämer (Heidelberg, Germany)
pmCitrine-*TUBG1*	Expression of YFP-tagged *TUBG1* to induce microtubule nucleation.	Addgene, Watertown, MA, USA

2.9. Human cell lines

All parental human cell lines and generated cell lines, which were used for this study are listed in Table 2.8 and 2.9.

Table 2.8 Parental human cell lines

Cell line	Origin	Reference
HCT116	colon carcinoma	Obtained from ATCC, USA
HCT116 + scrambled shRNA	colon carcinoma	(Schmidt et al., 2021)
HCT116 + *TP73* shRNA	colon carcinoma	(Schmidt et al., 2021)
HCT116 + *TP53*$^{-/-}$ + scrambled shRNA	colon carcinoma	(Schmidt et al., 2021)
HCT116 + *TP53*$^{-/-}$ + *TP73* shRNA	colon carcinoma	(Schmidt et al., 2021)

SK-Mel-19	melanoma	Carey *et al.* 1976 Kindly provided by Dr. Maria S. Soengas (Madrid, Spain)
SK-Mel-173	melanoma	Real et al., 1985 Kindly provided by Dr. Maria S. Soengas (Madrid, Spain)
SK-Mel-103	melanoma	Gruis *et al.* 1995 Kindly provided by Dr. Maria S. Soengas (Madrid, Spain)
SK-Mel-147	melanoma	Gruis *et al.* 1995 Kindly provided by Dr. Maria S. Soengas (Madrid, Spain)

2.10. Generated cell lines

Table 2.9 Generated cell lines

Cell line	Parental cell line	Plasmid	Selection marker
SK-Mel-103 + scrambled shRNA	SK-Mel-103	pLKO.1-scrambled shRNA	Blasticidine
SK-Mel-103 + *CKAP5* shRNA	SK-Mel-103	pLKO.1-*CKAP5* shRNA	Blasticidine
clone 17.2 + *LUCIFERASE*	HCT116 + *TP53*$^{-/-}$ + *TP73* shRNA	pcDNA3.1-*LUCIFERASE*	Zeocin
clone 17.2 + *LUCIFERASE* + scrambled shRNA	clone 17.2 + *LUCIFERASE*	pLKO.1-scrambled shRNA	Zeocin, Blasticidine
clone 17.2 + *LUCIFERASE* + *CKAP5* shRNA	clone 17.2 + *LUCIFERASE*	pLKO.1-*CKAP5* shRNA	Zeocin, Blasticidine

2.11. Cell culture

2.11.1. Cultivation of human cells

Cultivation of all cell lines was carried out in a HERAcell 240 CO_2 incubator with constant 37 °C, 5 % CO_2 and saturated humidity. Sterile handling of cells was conducted in a HERAsafe™ M safety cabinet.

All cell lines were cultured in RPMI1640 (PAN-Biotech GmbH, Aidenbach, Germany) supplemented with 10 % (v/v) FCS (Corning, New York, USA) and 1 % (v/v) penicillin-streptomycin (100 µg/ml streptomycin, 100 units/ml penicillin, Anprotec, Bruckberg, Germany). Culture medium for cultivation of stable cell lines contained appropriate antibiotics for selection. Cells were passaged every 48 to 72 h. For that, cells were washed with phosphate buffered saline (PBS) followed by detachment using trypsin/EDTA 1x in PBS without calcium, magnesium, or phenol red (#AC-EZ-0009 Anprotec, Bruckberg, Germany). Proportions of the cell suspension were cultured on new 10 cm plates with fresh culture medium. Cell lines were transferred to liquid nitrogen for long-term storage. Cells were harvested, centrifuged for 5 min at 491 x g and resuspended in RPMI1640 supplemented with 20 % (v/v) FCS, 1 % (v/v) penicillin-streptomycin and 10 % (v/v) DMSO. Cryovials were stored at -80 °C for 24 h before they were transferred to liquid nitrogen for long-term storage.

2.11.2. Conditioned media and isolation of microvesicles

Cells were grown in a 6-well plate to a confluency of 80 %, washed once with PBS before 1 ml RPMI1640 without phenol red (PAN-Biotech GmbH, Aidenbach, Germany) containing 1 % (v/v) penicillin-streptomycin was added. After 24 h at 37 °C, medium was collected and centrifuged at 2000 x g for 10 min to remove cell debris. Supernatant containing microvesicles was transferred to a new tube and was added to cells mixed with fresh complete medium in a ratio of 60:40. Microvesicles were isolated from supernatant from cells grown in 10 cm plates. Microvesicles were pelleted by additional centrifugation for 35 min at 14000 x g. The pellet containing microvesicles was resuspended in 200 µl PBS or fresh culture medium and transferred in a ratio of 60:40 with fresh complete medium onto target cells.

2.11.3. Analysis of microvesicles by mass spectrometry

To analyze the constituents of microvesicles, I performed mass spectrometry analyses in collaboration with Angela Wieland and Dr. Markus Räschle (Technical University of Kaiserlautern). Cells were grown to a confluency of 80 to 90 %, washed twice with PBS followed by an incubation for 3 h at 37 °C with plain growth medium. After incubation, cells were washed once with PBS and were again incubated with plain growth medium for 24 h at 37 °C. On the next day, the medium was collected and centrifuged for 10 min at 2000 x g to remove dead cells and debris. The supernatant was transferred into a new falcon and centrifuged for 35 min at 14000 x g to sediment microvesicles. The microvesicle pellet was resuspended in PBS, transferred to a 1.5 ml tube, and centrifuged for 35 min at 14000 x g. The supernatant was removed, microvesicle pellets were snap frozen and stored at -20

°C until mass spectrometry analysis. Microvesicles collected from ten 10 cm plates were used for one experiment. To analyze microvesicles derived from cells with an overexpression of *PLK4*, cells were transfected with a plasmid for *PLK4* overexpression, followed by an incubation for 24 h at 37 °C. After 24 h, the experiment was proceeded as described above. Mass spectrometry (MS) was performed by Angela Wieland and Dr. Markus Räschle. Microvesicles were resuspended in 30 µl lysis buffer (6 M guanidinium chloride, 10 mM TCEP, 40 mM CAA, 100 mM Tris pH 8.5) and incubated 10 minutes at 96°C. After sonication, lysates were centrifuged at 15700 x g. 25 µg protein was diluted 1:10 in LT-digestion buffer (10 % ACN, 25 mM Tris pH 8.5) and digested with LysC (1:150) and trypsin (1:50) overnight at 37°C. Trypsin (1:100) was added and lysates were incubated for 30 min at 37 °C. After digestion, samples were acidified (1 % TFA final), centrifuged and soluble peptides desalted by stage tipping using three layers of SDB-RPS (Rappsilber et al., 2007). Samples were vacuum dried and resolubilized in 10.8 µl buffer A (0.1 % formic acid in MS grade water) and 1.2 µl buffer A* (0.1 % formic acid, 0.1% TFA in MS grade water). 4 µl of the tryptic peptides were separated by nano-high pressure liquid chromatography (nano-HPLC) on an Easy nLC 1200 chromatography system and sprayed directly into a Q Exactive HF mass spectrometer (Thermo Fisher Scientific, Karlsruhe, Germany). Reversed-phase columns (40 cm with a 75 µm inner diameter, New Objective, Woburn, MA, USA) were packed in-house with ReproSil Pur 120 C18 AQ (Dr. Maisch, Ammerbuch-Entringen, Germany). For chromatography, buffer A (0.1% formic acid) and buffer B (80 % acetonitrile, 0.1 % formic acid) were used as mobile phases and a 180 min gradient (5 % to 95 % buffer B) was used for peptide elution. All MS data was recorded with a data-dependent acquisition method. In each scan cycle, fragmentation spectra of the fifteen most intense peptide precursors in the survey scan were acquired in the higher-energy collisional dissociation (HCD) mode. Raw data were processed using the MaxQuant software environment (Cox & Mann, 2008) and peak lists were searched with Andromeda (Cox et al., 2011) against the Uniprot database as well as a list of commonly observed contaminants. The minimal required peptide length was set to seven amino acids and both protein and peptide identifications were accepted at a false discovery rate (FDR) of 1 %. MS data was processed with Perseus (Tyanova et al., 2016). Data was filtered to contain 4421 proteins. Differentially regulated proteins were identified by a modified t-test using an S0=0.1 and an FDR of 5 %. Gene set enrichment analysis of the differentially regulated proteins was carried out using the web-based toolkit WebGestalt (Zhang et al., 2005). 1D pathway enrichment analysis was carried out in Perseus with an FDR cut-off of 5 %.

2.12. Transfection of cells

2.12.1. Transfection of cells with siRNA

Cells were transfected with siRNAs using ScreenFect® siRNA. siRNA was diluted in 30 µl dilution buffer to a final concentration of 80 pmol. Separately, 4 µl ScreenFect® siRNA (#S-4001, ScreenFect®, Eggenstein-Leopoldshafen, Germany) reagent was diluted in 30 µl dilution buffer. Both components were mixed and incubated for 20 min at room temperature (RT) to allow complex formation. Cells grown in a 6-well plate to a confluency of 70 to 80 % were washed with PBS and overlaid with 1.5 ml RPMI1640 supplemented with 10 % (v/v) FCS. After 20 min, the siRNA mix was added dropwise to the cells. Cells were incubated overnight with a medium change on the next day. After 48 h, cells were harvested for further experiments.

2.12.2. Transfection of cells with plasmids

2.12.2.1. Electroporation

Electroporation was conducted using a BioRad Genepulser Xcell™. Cells grown on a 10 cm plate were washed with PBS and detached using trypsin/EDTA. After centrifugation at 491 x g for 5 min at RT, the cell pellet was resuspended in 400 µl fresh medium. 10 to 15 µg plasmid were added and mixed. The plasmid/cell mixture was transferred to an 0.4 cm electroporation cuvette (BioRad, Hercules, CA, USA) and pulsed at the following settings: HCT116 (500 µF, 300 V, ∞Ω, 4mm), SK-Mel cell lines (950 µF, 220 V, ∞Ω, 4mm). Transfected cells were transferred to a 6-well plate with 2 ml fresh medium.

2.12.2.2. ScreenFect® A

Cells were grown in a 6-well plate to a confluency of 70 to 80 % at the timepoint of transfection. In tube A, 30 µl dilution buffer were mixed with 6 µl ScreenFect® A (#S-3001, ScreenFect®, Eggenstein-Leopoldshafen, Germany) transfection reagent. In tube B, 30 µl dilution buffer and 1.5 µg/µl plasmid were added. Solution A and B were mixed and incubated for 20 min at RT. Cells were washed with PBS and 1.5 ml RPMI1640 supplemented with 10 % (v/v) FCS were added. After incubation, the transfection mix was added dropwise to the cells. Medium was changed the next day. Further, experiments were conducted after 48 h.

2.12.2.3. Lipofectamine 3000

Plasmids were diluted in 125 µl Opti-MEM™ medium (Gibco™ by Thermo Fisher, Karlsruhe) to a final concentration of 2.5 µg/µl. 5 µl P3000™ reagent were added to the mix. In

a second reaction tube, 6.25 µl Lipofectamine™ 3000 reagent (Invitrogen™ by Thermo Fisher, Karlsruhe, Germany) was diluted in 125 µl Opti-MEM™ medium. Both tubes were mixed and incubated for 15 min at RT. Cells with a confluency of 70 to 80 % in a 6-well plate were washed with PBS and overlaid with 1.5 ml fresh medium without penicillin-streptomycin. The plasmid mix was added dropwise. After 4 h the medium was changed. Transfected cells were used for experiments after 48 h.

2.12.3. Stable cell lines

In reaction tube A, 2 µg/µl plasmid DNA were diluted in 100 µl PBS. In tube B, 6 µl Metafectene® Pro (Biontex Laboratories GmbH, München, Germany) were diluted in 100 µl PBS. Both parts were mixed separately and slowly. Solution B was transferred to tube A, again slowly mixed and incubated for 15 min at RT. Cells cultured in a 6-well plate with a confluency of 70 to 80 % were washed once with PBS and 1.8 ml fresh medium without penicillin-streptomycin were added. After the incubation, the transfection mix was added dropwise to the cells. Cells were incubated overnight at 37 °C and 5 % CO_2 with a medium change on the next day. For stable transfections, selection medium containing appropriate antibiotics was added after 48 h.
48 h after transfection, cells were seeded in different dilutions to grow single cell clones. Therefore, dilutions of 1:1000, 1:500, 1:250, and 1:100 were seeded in 10 cm plates with medium containing the appropriate antibiotic for selection. Single cell clones were grown for up to two weeks with medium changes every 48 to 72 h. Colonies were transferred to 24-well plates, cultured, and further characterized.

2.13. Immunofluorescence microscopy

10 x 10 mm coverslips (Thermo Fisher Scientific, Karlsruhe, Germany) were placed in a 24-well plate and washed once with PBS. 500 µl fresh medium were added and cells were grown onto then for 24 to 48 h. Cells were fixed with 2 % paraformaldehyde (PFA) for 5 min at RT. Immediately after fixation, cells were permeabilized with pre-cold -20 °C methanol for 5 min at -20 °C. Cells were washed twice with PBS and stored at 4 °C or proceeded further. Blocking solution (5 % (v/v) FCS in PBS) was added for 30 min at RT. Cells were washed with PBS and incubated over night at 4 °C with primary antibodies diluted in 2 % (v/v) FCS in PBS. Cells were washed three times with PBS and were incubated for 1.5 h at RT with secondary antibodies diluted in 2 % (v/v) FCS in PBS. Immediately after incubation, cell nuclei were stained for 5 min at RT with Hoechst33342 (Thermo Fisher Scientific, Karlsruhe, Germany) diluted 1:15000 in PBS. Cells were washed three times with PBS and coverslips were placed on Whatman paper to dry. Cells were covered with

VECTASHIELD® (Vector Laboratories, Inc., Burlingame, CA, USA), sealed with nail polish, and stored at 4 °C until imaging.

2.13.1. Microtubule plus end growth rate measurements

The growth rate of microtubules was determined by tracking GFP- or mCherry-tagged end binding protein 3 (EB3). For this purpose, cells were transfected by electroporation using 10 or 15 µg GFP- or mCherry-tagged EB3 plasmid, respectively.
After 48 h, living interphase cells were imaged for measurement of microtubule plus end growth rates at 37 °C and 5 % CO_2. Cells were treated with 2 µM DME 1 h before measuring mitotic microtubules. Images of growing plus ends decorated by EB3-GFP/mCherry were acquired every two seconds for 30 seconds in total with an optical z-stack distance of 0.4 µm using a Delta Vision Elite© live cell microscope. Analysis of deconvolved and projected images was done measuring the distance one plus end covered in two seconds. 20 microtubules of 10 different cells were analyzed per experiment.

2.14. Analyzing cell migration and invasion *in vitro*

2.14.1. *In vitro* Migration Transwell Assay

Prior to seeding cells in migration transwell inserts (Greiner BioOne, Frickenhausen, Germany), cells were starved overnight in RPMI1640 containing 0.5 % (v/v) FCS and 1 % (v/v) penicillin-streptomycin. Cells were washed with PBS, detached, and counted using a Neubauer improved counting chamber with 0.1 mm depth (#0640010, Superior Marienfeld, Lauda-Königshofen, Germany). The inserts were placed in a 24-well plate with 500 µl fresh complete medium. 2 x 10^5 cells were resuspended in 200 µl starvation medium and seeded to the insert. After 24 h, cells were removed and inserts were incubated in 500 µl trypsin/EDTA for 10 min at 37 °C. All wells were rinsed and cells were collected in a reaction tube, centrifuged, resuspended in 100 µl PBS, and counted.

2.14.2. *In vitro* Invasion Transwell Assay

Prior to starting the invasion assay, inserts covered with Matrigel™ (Corning, New York, USA) were rehydrated to restore dried Matrigel™. For this, inserts were filled with 500 µl medium and placed in a 24-well plate with 500 µl medium for 2 h. Cells that were starved overnight in medium containing 0.5 % (v/v) FCS, were washed with PBS, detached, and counted. Inserts were transferred into a new 24-well plate with 750 µl fresh complete medium. 2 x 10^5 cells in 500 µl starvation medium were transferred into the transwell insert. Inserts were incubated for 48 h at 37 °C and 5 % CO_2. Afterwards, cells were removed,

and inserts were incubated for 10 min in 500 µl trypsin/EDTA. Inserts were rinsed with trypsin/EDTA. Medium and trypsin/EDTA were transferred to a reaction tube and centrifuged at 491 x g for 5 min at RT. Pellets were resuspended in 100 µl PBS and invaded cells were counted.

2.14.3. Invasion Wound Healing Assay

To measure the speed of wound closure through a extracellular matrix, the Incucyte S3 Live Cell Analysis System was used (in cooperation with Dr. Oliver Hahn, University Medical Center in Göttingen).
5 x 10^4 cells were seeded one day prior to starting the assay in flat bottom 96-well plates (Essen BioScience Inc., Ann Arbor, MI, USA) that were coated with 25 µl collagen mixed with 10 x PBS, 1 M NaOH and fresh culture medium. On the next day, before making the scratch, cells were washed two times with fresh medium. The WoundMaker™ (Essen BioScience Inc., Ann Arbor, MI, USA) was disinfected for 5 min in 70 % (v/v) ethanol and washed for 5 min in H_2O. After positioning the WoundMaker™ on the 96-well plate, wounds were made simultaneously by a single controlled, directional movement. Afterwards, cells were washed three times with medium to remove detached, floating cells. 50 µl collagen mixture were added and plates were incubated for 15 min at 37 °C. 100 µl medium were added and invasive wound closure was imaged using the Incucyte system (Essen BioScience Inc., Ann Arbor, MI, USA), kindly provided by Dr. Oliver Hahn from the University Medical Center in Göttingen. Images were taken every hour for a total of 46 h. Data were analyzed using the Incucyte software (Incucyte® Base Software, Essen BioScience Inc., Ann Arbor, MI, USA).

2.14.4. Spheroid formation

Spheroid assays enable the assessment of invasive cell behavior in a 3D matrix based on Matrigel™. 500 cells were seeded into low attachment, U-shaped 96-well plates and centrifuged at 874 x g for 20 min at RT. Spheroid formation was completed after an incubation of 48 to 72 h at 37 °C. 8-well slides were precoated with Matrigel™ diluted with fresh complete medium in a ratio of 70 to 30 % to avoid attachment of the spheroids to the bottom of the slide. After solidification at 37 °C for 20 min, spheroids were collected, resuspended in Matrigel™ diluted with fresh medium and seeded on top of the precoated Matrigel™ (Figure 2.1). After another solidification step at 37 °C for 30 min, the gel matrix was overlayed with fresh complete medium, optionally containing inhibitors. Images were taken every 24 h. Inhibitor treatments were already started during spheroid formation, 24 h prior to embedding spheroids in extracellular matrix.

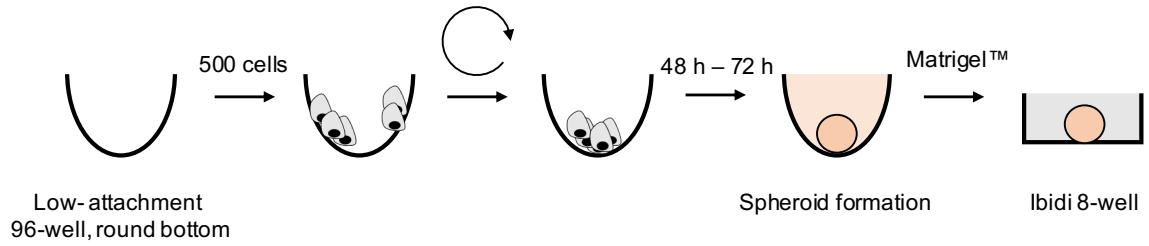

Figure 2.1 Schematic depiction of spheroid formation. *500 cells were seeded in low attachment, round bottom 96-well plates. After centrifugation, spheroids were forming for 48 to 72 h at 37 °C with 5 % CO_2. Spheroids were transferred to Matrigel™ in 8-well slides.*

2.14.5. Determination of 3D invasion by using spheroids

3D spheroids were grown in Matrigel™ for 48 h until images were taken. The area of growth and invasion was measured using the threshold tool in the ImageJ software. Images were converted to 8-bit. After background subtraction, application of the threshold tool covered the spheroid area in black (Figure 2.2). Determination of the black area using the analysis measurement tool of ImageJ resulted in the area covered by the outgrowth of the spheroid. Treated spheroids were normalized to control spheroids for every experiment by setting the size of control spheroids as 100 % and calculating the reduction of outgrowth of every treated spheroid.

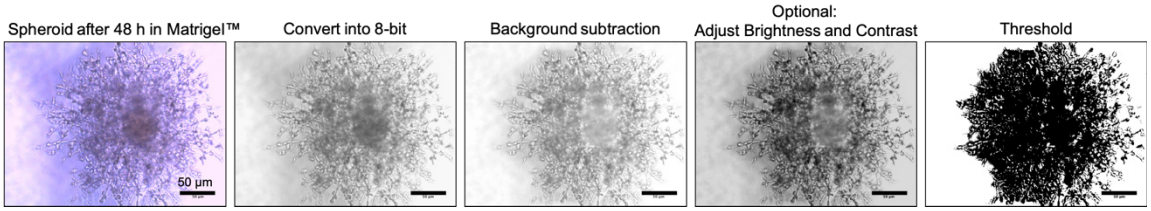

Figure 2.2 Measurement of the spheroid area in 3D. *Images were converted to 8-bit. After background subtraction, brightness, and contrast were adjusted and the threshold tool was applied. Scale bar, 50 µm.*

2.15. Protein biochemistry

2.15.1. Generation of whole cell lysates for SDS PAGE

Cells in 6-well plates were washed once with PBS. For detachment, cells were incubated with 500 µl PBS/ EDTA (0.5 mM) for 5 min at RT. Cells were centrifuged at 491 x g for 5 min at RT to remove dead cells and debris, followed by an incubation with 40 to 60 µl lysis buffer (50 mM Tris HCl pH 7.4, 150 mM NaCl, 5 mM EGTA pH 8.0, 5 mM EDTA pH 8.0, 1 % (v/v) NP40, 0.1 % (w/v) SDS, 0.1 % (w/v) sodium desoxycholate, phosphatase inhibitor cocktail (25 mM β-glycerophosphate, 50 mM NaF, 5 mM Na_2MoO_4, 0.2 mM Na_3VO_4, 5 mM EDTA, 0.5 µM microcystin), cOmplete™ EDTA free protease inhibitor cocktail (Roche, Basel, Switzerland)) dependent on the size of the cell pellet for 10 min on ice. Lysed cells

were centrifuged at 21100 x g for 10 min at 4 °C. The protein concentration of the supernatant was determined and 25 to 50 µg of protein was mixed with 5x SDS loading buffer (15 % (w/v) SDS, 15 % (v/v) β-mercaptoethanol, 50 % (v/v) glycerol, 0.25 % (w/v) bromophenol blue) and incubated for 5 min at 95 °C. Samples were stored at -20 °C or immediately loaded onto the SDS-polyacrylamide gel.

2.15.2. Determination of the protein concentration

Increasing concentrations of 1 % (v/v) bovine serum albumin (BSA) diluted in H_2O used for a protein standard curve were added to the first row of a flat bottom 96-well plate. Lysates were added in duplicates 1:10 diluted in water. 25 µl of protein assay reagent A (#500-0113, BioRad, Hercules, CA, USA) 1:40 mixed with reagent S (#500-0115, BioRad) were added to each well. 200 µl of reagent B (#500-0114, BioRad) were added and plates were incubated at RT for 10 min. Protein concentrations were measured using a plate reader (Victor© X3 microplate reader) at a wavelength of 750 nm.

2.15.3. Sodium dodecylsulfate polyacrylamide gel electrophoresis (SDS PAGE)

To separate proteins based on their molecular weight, the SDS polyacrylamide gel (SDS PAGE) was used. The resolving gel with acrylamide percentages ranging from 6 to 13 %, dependent on the molecular weight of the proteins of interest, was prepared. 17 ml gel mix containing resolving gel buffer (375 mM Tris-HCl pH 8.8, 0.1 % (w/v) SDS) and 6 to 13 % (v/v) acrylamide were mixed with ammonium persulfate (APS) and TEMED (Carl Roth GmbH & Co. KG, Karlsruhe, Germany) to start polymerization. The mixture was poured between two glass plates separated by spacers. 7 ml stacking gel mix containing stacking gel buffer (157 mM Tris-HCl pH 6.8, 0.1 % (v/v) SDS) and 5 % (v/v) acrylamide were added on top. Polymerized gels were stored at 4 °C or used immediately. Protein samples were loaded onto the gel and proteins were separated based on their molecular weight for up to 3 h in two steps: 1 h at 26 mA and 150 W, 2 h at 42 mA and 150 W.

2.15.4. Coomassie staining

After electrophoresis, gels were fixed for 60 min in 40 % (v/v) ethanol and 10 % (v/v) acetic acid diluted in water on a rocking table at RT. Afterwards, gels were washed twice with water for 10 min. Gels were stained in coomassie solution (0.1 % (w/v) Coomassie Brilliant Blue G250, 5 % (w/v) aluminum sulfate-(14-18)-hydrate, 10 % (v/v) methanol, 2 % (w/v) ortho-phosphoric acid) overnight. After three additional 10 min washing steps, gels were scanned for documentation.

2.15.5. Western Blotting

After SDS PAGE was completed, proteins were transferred onto nitrocellulose membranes. Smaller proteins with a molecular weight of up to 100 kDa were transferred using semi-dry western blotting, whereas bigger proteins were transferred by wet blotting.

2.15.5.1. Semi-dry blotting

Blotting of smaller proteins was conducted using the semi-dry technique. For this, gels were placed onto nitrocellulose membranes (GE Healthcare, Chalfront St., Giles, UK) and put between two Whatman® paper on each side. Blotting buffer (24.8 mM Tris-HCl pH 8.0, 170 mM glycine, 0.0025 % (w/v) SDS, 15 % (v/v) methanol pH 8.0) was added to the semi-dry blotting chamber. Blotting was performed for 1 ½ h at 200 mA per gel with 150 W.

2.15.5.2. Wet blotting

Proteins with higher molecular weight were blotted using the wet blot technique. The gel was positioned on a nitrocellulose membrane between three Whatman® paper and one sponge on each side. The wet blot chamber was filled with blotting buffer (24.8 mM Tris-HCl pH 8.0, 170 mM glycine, 0.0025 % (w/v) SDS, 15 % (v/v) methanol pH 8.0) and settings were set to 3 h at 450 mA and 150 W.

2.15.6. Protein detection on nitrocellulose membranes

After western blotting, nitrocellulose membranes were blocked in 5 % (w/v) milk powder dissolved in TBS (50 mM Tris/HCl, 0.9 % (w/v) NaCl, pH 7.2) for 60 min. Nitrocellulose membranes were washed twice with water and kept in TBS until primary antibodies diluted in 3 % (w/v) BSA in TBS were prepared. Nitrocellulose membranes were incubated overnight in primary antibodies on a rocking table at 4 °C. On the next day, nitrocellulose membranes were washed twice in TBS-T (+0.1 % (v/v) Tween 20) and once in TBS before secondary antibodies diluted in 3 % (w/v) milk powder were added. Nitrocellulose membranes were incubated for 1 h at RT and afterwards washed three times for 10 min in TBS-T. For protein detection, nitrocellulose membranes were incubated with chemiluminescence solution (0.1 M Tris-HCl pH 8.5, 2.5 mM luminol (AppliChem, Darmstadt Germany), 0.4 mM p-coumaric acid, 0.06 % (v/v) H_2O_2) for 1 min. Membranes were imaged using the Fusion-SL-3500. WL (VWR International, Radnor, PA, USA) or the Fusion FX (Vilber Lourmat, Collégien, France) imaging system. After imaging, membranes were washed with TBS-T and stored at 4 °C or incubated with another primary antibody solution.

2.16. Molecular biology

2.16.1. *E. coli*

All transformations were carried out in the *E. coli* strain DH5αF^{-}Φ80*lacZ*ΔM15 Δ(*lacZYA-argF*) U169 *deoR recA1 hsdR*17 (r_k^-, m_k^+) *phoA sup*E44 *thi*-1 *gyr*A96 relA1λ^-.

2.16.2. Transformation of DH5-α cells

50 µl chemical competent DH5-α cells were slowly thawed on ice. 1 µl of plasmids was added and incubated for 30 min on ice. Bacteria were heat shocked for 45 sec at 42 °C and were immediately put back on ice. Afterwards, 600 µl LB medium was added and bacteria were incubated for 30 min at 37 °C shaking at 300 rpm. Bacteria were transferred to an Erlenmeyer flask with 200 ml LB medium supplemented with appropriate antibiotics for selection (either 100 mg/ml ampicillin or 50 mg/l kanamycin). Flasks were incubated while shaking at 120 rpm at 37 °C overnight. On the next day, bacteria were harvested by centrifugation at 1365 x g for 20 min at RT. Pellets were stored at -20 °C or plasmids were immediately isolated using a DNA plasmid purification kit.

2.16.3. Plasmid Isolation

Plasmid isolation was conducted by using the DNA plasmid purification kit – NucleoBond Xtra Midi and as described in the manufactures protocol (Macherey-Nagel, Düren, Germany). In brief, pellets were dissolved in 10 ml resuspension buffer. 10 ml lysis buffer were added, tubes were inverted and incubated for 5 min. Column filters were equilibrated with 12 ml equilibration buffer. After incubation, 10 ml neutralization buffer were added, tubes were inverted, and lysates were loaded onto column filters. After washing the filters with 5 ml equilibration buffer, filters were discarded. Columns were washed once and plasmids were eluted with 5 ml elution buffer. 3.5 ml Isopropanol were added, tubes were vortexed and centrifuged at 15000 g for 30 min at 4 °C. DNA pellets were washed with 70 % (v/v) ethanol and again centrifuged at 15000 x g for 5 min at RT. Pellets were dried and were dissolved in dH_2O dependent on the excepted plasmid concentration. DNA concentrations were determined using a spectrophotometer.

2.17. Statistics

Statistical analysis of all data was performed using an unpaired t-test. The indicated p-values are defined as followed: **** = $p \leq 0.0001$, *** = $p \leq 0.001$, ** = $p \leq 0.01$, * = $p \leq 0.05$ and non-significant (ns) = $p > 0.05$. Statistics for wound healing assays with several

timepoints for every measurement was performed using a two-way ANOVA. The p-values were defined as mentioned above.

3. Results

Previous results of our lab showed that an induction of microtubule plus end growth rates during mitosis leads to transient spindle mispositioning and the formation of lagging chromosomes during anaphase. A direct consequence of lagging chromosomes is chromosome missegregation resulting in aneuploid cells (Ertych et al., 2014; Stolz et al., 2010). A trigger for increased microtubule plus end growth rates during mitosis is the concomitant loss of the transcription factors *TP53* and *TP73* (Schmidt et al., 2021). Interestingly, increased microtubule plus end assembly after loss of *TP53* and *TP73* were also detected in interphase cells accompanied by enhanced cell migration and invasion (Berger, 2016).

3.1. Increased microtubule plus end growth rates in interphase contribute to cell migration and invasion in melanoma and colorectal cancer cells

3.1.1. HCT116 cells with a concomitant loss of *TP53* and *TP73* show increased microtubule plus end growth rates in interphase cells that correlate with an invasive phenotype

The set of cells for the initial experiments was generated based on the knockout cell line HCT116 + *TP53*$^{-/-}$ (Schmidt et al., 2021) and included scrambled shRNA (scrshRNA) transfected HCT116 cells, which were used as control cells, cells with the knockout of *TP53* alone, cells with a shRNA mediated knockdown of *TP73* and cells with the concomitant loss of both transcription factors, where two independent cell clones were analyzed: HCT116 + *TP73*shRNA/*TP53*$^{-/-}$ clone 10.2 and HCT116 + *TP73*shRNA/*TP53*$^{-/-}$ clone 17.2 (further referred to as clone 10.2 and clone 17.2). To measure microtubule plus end growth rates in interphase, cells were transfected with GFP- or mCherry-tagged EB3, which decorates growing microtubule plus ends. After 48 h, asynchronous growing cells were analyzed using a Delta Vision Elite© live cell microscope.

3.1.1.1. Analysis of HCT116 cells with a concomitant loss of TP53 and TP73

The stable shRNA mediated knockdown of *TP73* and the knockout of *TP53* in HCT116 cells were verified by western blot (Figure 3.1A). Prior to cell lysis, cells were treated with Adriamycin to induce DNA damage, which leads to the upregulation of p53 and p73 and enables a better examination of the knockdown and knockout efficiency. As expected, the knockout of *TP53* led to a complete loss of p53 protein. The expression of *TP73* was low compared to control cells. The expression of *CDKN1* (p21^{Cip1}), a relevant target gene of

p53 and p73 (Schmidt et al., 2021), was reduced in HCT116 + *TP53*$^{-/-}$ cells. Interestingly, the expression of *CDKN1* was even more reduced in cells with the concomitant loss of both transcription factors.

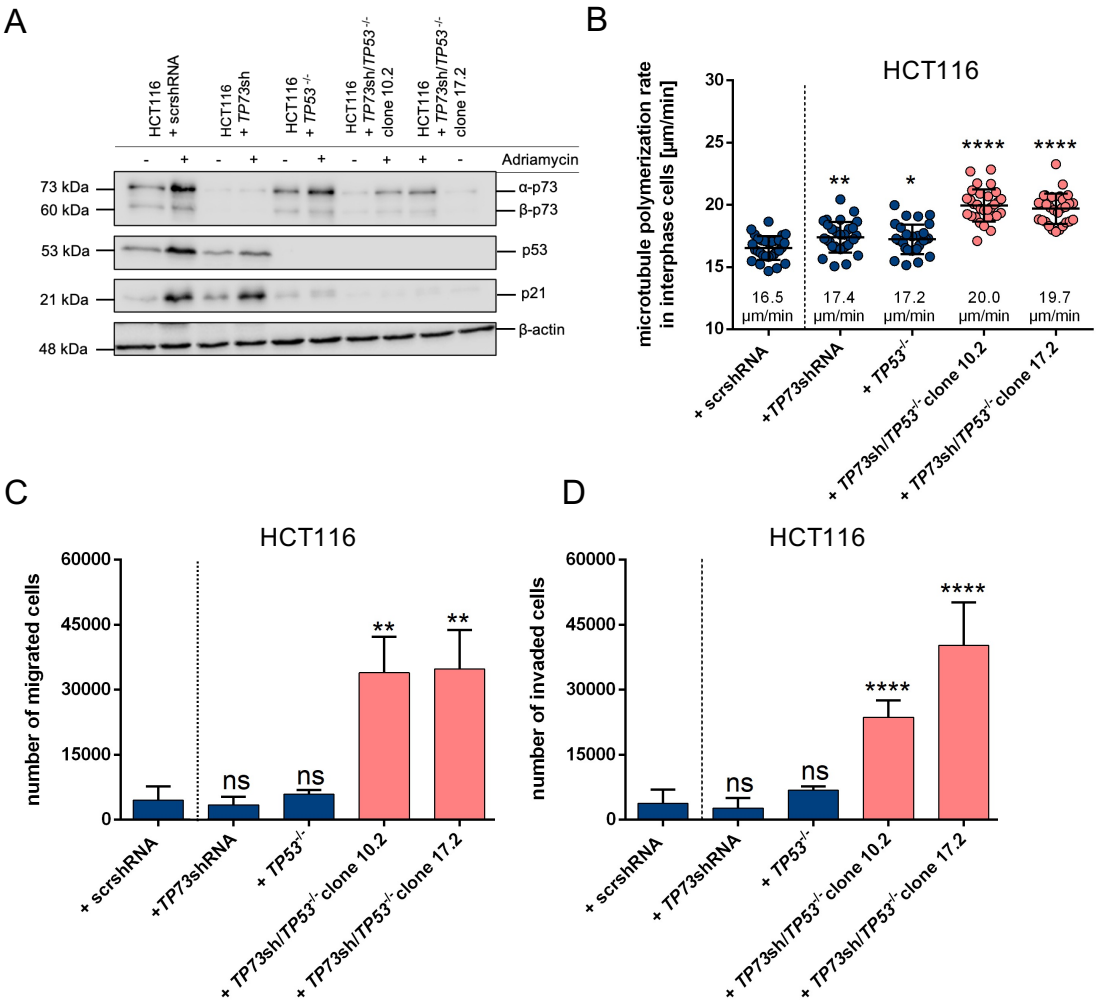

Figure 3.1 Increased interphase microtubule growth rates in HCT116 with concomitant loss of TP53 and TP73 correlate with enhanced cell migration and invasion. *A) Representative western blots of cells transfected with scrambled shRNA (scrshRNA), cells with a shRNA mediated knockdown of TP73 or knockout of TP53 and cells with a concomitant loss of TP73/TP53. Cells were treated with 600 nM of Adriamycin or DMSO as a control. Protein levels of p73 (EP436Y, mouse, monoclonal antibody (mAb)), p53 (DO-1, mouse, mAb) and p21 (DCS60, mouse, mAb) were detected. β-actin (AC-15, mouse, mAb) was used as the loading control. B) Measurements of interphase microtubule polymerization rates in cells transfected with scrambled shRNA (scrshRNA), TP73 shRNA or TP53*$^{-/-}$ *cells, and in cells with a concomitant loss of both transcription factors, represented with two independent cell clones (clone 10.2 and clone 17.2). Scatter dot plots are presented with mean values ± SD of 30 cells. Depicted are the results of three independent experiments with measurements of 20 microtubules per cell. C) and D) Determination of cell migration and invasion of cells transfected with scramble shRNA (scrshRNA), TP73 shRNA or TP53*$^{-/-}$ *cells, and cells with a concomitant loss of both factors. Mean values ± SD of three or five (five experiments were done with HCT116 + TP73shRNA/TP53*$^{-/-}$ *clone 17.2 cells in the transwell invasion assay) independent experiments. All experiments were statistically analyzed using an unpaired t-test. Indicated stars are defined as: **** = p ≤ 0.0001, ** = p ≤ 0.01, * = p ≤ 0.05 and non-significant (ns) = p > 0.05. Significances refer to control cells. Control cells within one graph are separated from the other conditions by a dotted line.*

Comparable to the effects during mitosis (Schmidt et al., 2021), the loss of *TP53* and *TP73* led to the significant increase of microtubule plus end growth rates during interphase with average microtubule polymerization rates of 20.0 µm/min for clone 10.2 and 19.7 µm/min for clone 17.2 compared to control cells with an average growth rate of 16.5 µm/min (Figure 3.1B). The cells with either *TP73* or *TP53* loss showed just slightly increased growth rates with 17.4 µm/min and 17.2 µm/min, respectively. To measure cell migration and invasion, 2 x 10^5 serum-starved cells were seeded into transwell migration or invasion inserts and migrated or invaded cells were counted after 24 or 48 h, respectively, using a Neubauer improved cell counting chamber. Intriguingly, cells with an increased interphase microtubule plus end growth rates also showed enhanced cell migration and invasion in transwell migration and invasion assays compared to control cells or cells with the loss of one transcription factor (Figure 3.1C and D). HCT116 cells with the loss of both transcription factors migrated approximately six times more and were seven times more invasive compared to their non-invasive counterparts.

3.1.1.2. Are increased interphase microtubule plus end assembly rates required for enhanced cell migration and invasion?

Since increased microtubule rates and enhanced cell migration and invasion correlated in HCT116 + *TP73*shRNA/*TP53*$^{-/-}$ cells, I hypothesized that microtubule plus end assembly functions upstream of cell migration and invasion. To test for that, normal microtubule plus end assembly rates were restored in p53/p73 deficient cells and cell migration and invasion was determined.

The processive microtubule polymerase chTOG enhances incorporation of α/β-heterodimers into the growing microtubule strand (Brouhard et al., 2008). In fact, it was previously shown that the transient knockdown of *CKAP5* rescues increased microtubule plus end growth rates in mitosis by slowing down α/β-heterodimers incorporation (Ertych et al., 2014). Additionally, increased growth rates can be rescued using sub-nanomolar doses of the microtubule stabilizing drug Taxol (0.2 – 0.5 nM) (Ertych et al., 2014; Stolz et al., 2015). In my hands, treatment with 0.2 nM of Taxol rescued the increased microtubule growth rates in interphase cells with a concomitant loss of both transcription factors from 20.0 to 17.1 µm/min for clone 10.2 and from 19.7 to 17.2 µm/min for clone 17.2, without effecting microtubule growth rates of control cells (Figure 3.2A). Interestingly, increased cell migration and invasion of clone 17.2 was partially rescued by treatment with 0.2 nM of Taxol. Migration as well as invasion of clone 17.2 were approximately 25 % reduced compared to DMSO treated cells, whereas the treatment with Taxol showed no significant effect on

clone 10.2 (Figure 3.2B and C). It is unclear why clone 10.2 does not recapitulate the results seen in clone 17.2.

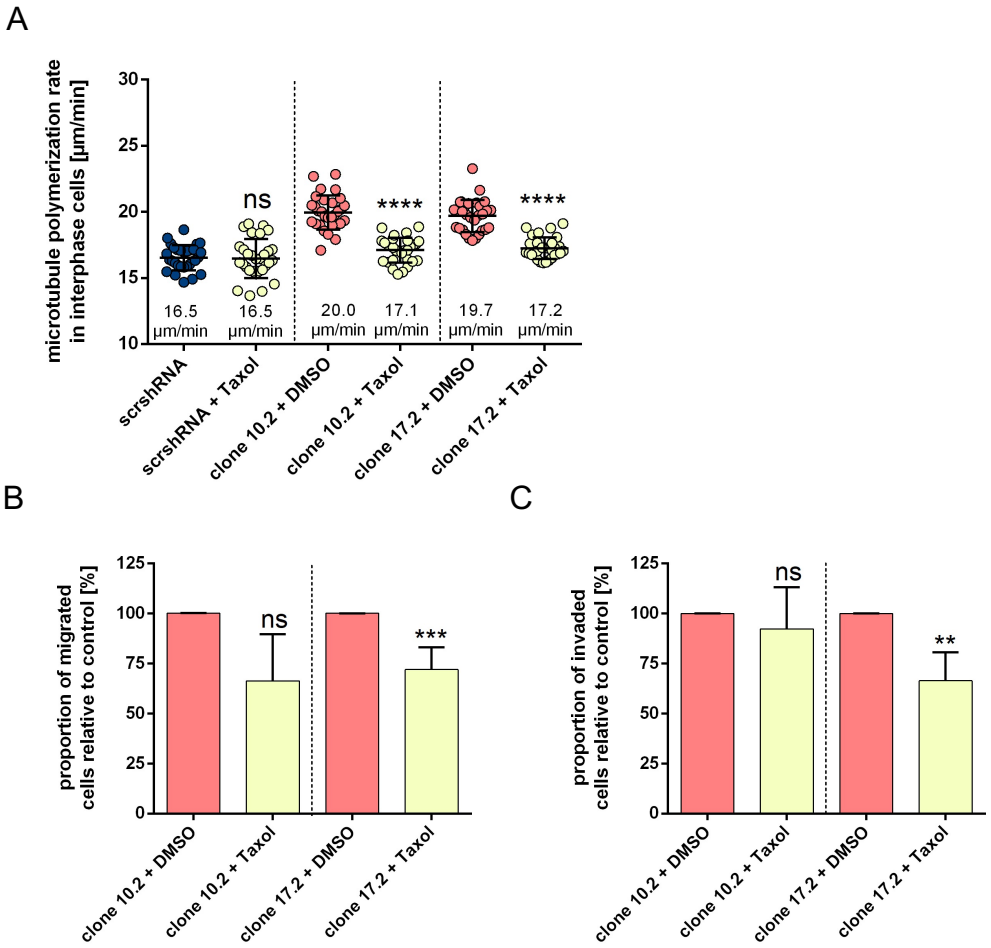

Figure 3.2 Rescue of increased interphase microtubule polymerization rates using Taxol leads to partially rescued cell migration and invasion of HCT116 + TP73shRNA/TP53$^{-/-}$ clone 17.2 cells. *A) Measurements of interphase microtubule plus end growth rates in cells transfected with scrambled shRNA (scrshRNA) and cells with a concomitant loss of TP73/TP53 represented with two independent clones (clone 10.2 and clone 17.2) after treatment with DMSO or 0.2 nM of Taxol. Scatter dot plots show the mean values ± SD, n=30, 20 microtubules were measured per cell, t-test. B) Determination of cell migration of HCT116 + TP73shRNA/TP53$^{-/-}$ clone 10.2 and clone 17.2 cells after treatment with DMSO or 0.2 nM of Taxol. Migration assays were analyzed after 24 h. Bar graphs show the mean values ± SD of three or five (five experiments were done with HCT116 + TP73shRNA/TP53$^{-/-}$ clone 17.2 cells in the transwell migration assays with Taxol treatment) independent experiments. C) Determination of cell invasion of HCT116 + TP73shRNA/TP53$^{-/-}$ clone 10.2 and clone 17.2 cells after treatment with DMSO or 0.2 nM of Taxol. Invasion assays were analyzed after 48 h. Bar graphs show the mean values ± SD of three or four (four experiments were done with HCT116 + TP73shRNA/TP53$^{-/-}$ clone 17.2 cells in the transwell invasion assays with Taxol treatment) independent experiments. All experiments were analyzed using a t-test. Indicated stars are defined as: **** = p ≤ 0.0001, *** = p ≤ 0.001, ** = p ≤ 0.01, * = p ≤ 0.05 and non-significant (ns) = p > 0.05. Different cell lines within one graph are separated by a dotted line. Significances refer to corresponding DMSO treated control cells.*

However, more robust results were obtained with cells with a transient knockdown of *CKAP5*. The siRNA mediated transient as well as the shRNA mediated stable knockdown of *CKAP5* were verified by western blot (Figure 3.3A).

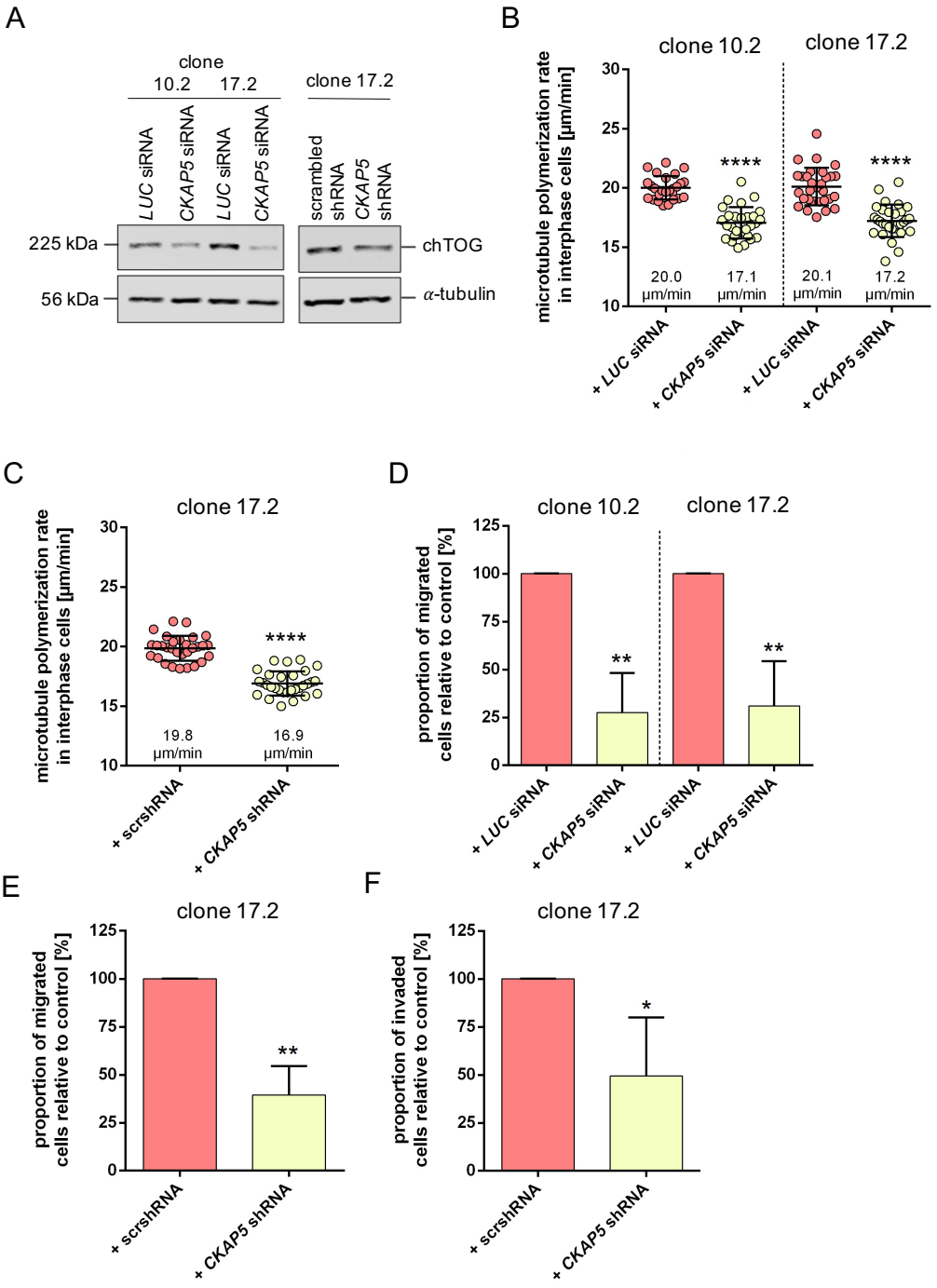

Figure 3.3 Rescue of increased interphase microtubule polymerization rates using CKAP5 knockdown leads to partially rescued cell migration and invasion of both clones. *A) Representative westernblots showing reduced protein levels of chTOG upon siRNA or shRNA meditated knockdown in HCT116 + TP73shRNA/TP53$^{-/-}$ clone 10.2 and clone 17.2 cells. Protein levels of chTOG (H-4, mouse, monoclonal antibody (mAb)) were detected. α-tubulin (B-5-1-2, mouse, mAb) served as a loading control. B) Measurements of interphase microtubule plus end growth rates in HCT116 + TP73shRNA/TP53$^{-/-}$ clone 10.2 and clone 17.2 cells after the siRNA mediated knockdown of CKAP5 or LUCIFERASE (LUC) as a control. Data for the measurements of interphase microtubule growth rates are the results of three independent experiments with 30 cells. 20 microtubules from 10 different cells were measured per experiment. Scatter dot plots show the mean values ± SD. C) Measurements of interphase microtubule plus end assembly in HCT116 + TP73shRNA/TP53$^{-/-}$ clone 17.2 cells with a stable shRNA mediated knockdown of CKAP5. D) Determination of cell migration of HCT116 + TP73shRNA/TP53$^{-/-}$ clone 10.2 and clone 17.2 cells after siRNA mediated knockdown of CKAP5. Migration was analyzed after 24 h. E) Determination of cell*

*migration of HCT116 + TP73shRNA/TP53$^{-/-}$ clone 17.2 cells stably transfected with shRNA targeting CKAP5. Migration was analyzed after 24 h. F) Determination of cell invasion of HCT116 + TP73shRNA/TP53$^{-/-}$ clone 17.2 cells stably transfected with shRNA targeting CKAP5. Cell invasion was analyzed after 48 h. Depicted bar graphs show the mean values ± SD for three independent experiments. All experiments were analyzed using a t-test. Indicated stars are defined as: **** = p ≤ 0.0001, *** = p ≤ 0.001, ** = p ≤ 0.01, * = p ≤ 0.05 and non-significant (ns) = p > 0.05. The indicated significances refer to LUC transfected control cells. Different cell lines within one graph are separated by a dotted line.*

48 h after transfection, cells with the transient or stable knockdown of *CKAP5* exhibited rescued microtubule plus end growth rates for clone 10.2 and clone 17.2 compared to control cells transfected with *LUCIFERASE (LUC)* siRNA or scrambled (scr) shRNA (Figure 3.3B and C). For the transwell migration assay, cells were transfected with *LUCIFERASE (LUC*) or *CKAP5* siRNA. After 24 h, cells were starved with serum-reduced medium overnight and seeded into transwell migration inserts. Cell migration upon siRNA mediated loss of *CKAP5* was reduced by 70 % compared to control cells (Figure 3.3D). Cell migration and invasion of cells with a shRNA mediated stable knockdown of *CKAP5* in p53/p73 deficient cells was reduced to approximately 45 % (Figure 3.3E and F).

3.1.2. Invasive melanoma cell lines exhibit enhanced microtubule plus end growth rates in interphase

3.1.2.1. Analysis of non-invasive vs. invasive melanoma cell lines

The HCT116 cell system with loss of *TP73* and *TP53* suggested a possible link between increased microtubule polymerization rates and the regulation of cell migration and invasion. To analyze this possibility further, melanoma cell lines were used for subsequent experiments. Several melanoma cell lines are well defined for their non-invasive or invasive behavior (García-Fernández et al., 2016; Rebecca et al., 2020). Among them, the melanoma cell lines SK-Mel-19 and SK-Mel-173 are representatives for non-invasive cell lines, and the cell lines SK-Mel-103 and SK-Mel-147 are defined as invasive cell lines (Carey et al., 1976; Gruis et al., 1995; Real et al., 1985). First, the status of migration and invasiveness of the melanoma cell lines was verified. SK-Mel-19 and SK-Mel-173 cells showed little migration or invasion in transwell assays compared to the invasive cell lines, SK-Mel-103 and SK-Mel-147 that are characterized by at least 25-fold more cell migration or invasion (Figure 3.4A and B). To further confirm the invasiveness of the cell lines, invasion wound healing experiments using the Incucyte S3 Live Cell Analysis System (kindly provided by Dr. Oliver Hahn, University Medical Center in Göttingen) were performed. After creating the wound, collagen embedded cells closed the wound by invading the extracellular matrix and were imaged for 46 h in total with images taken every hour.

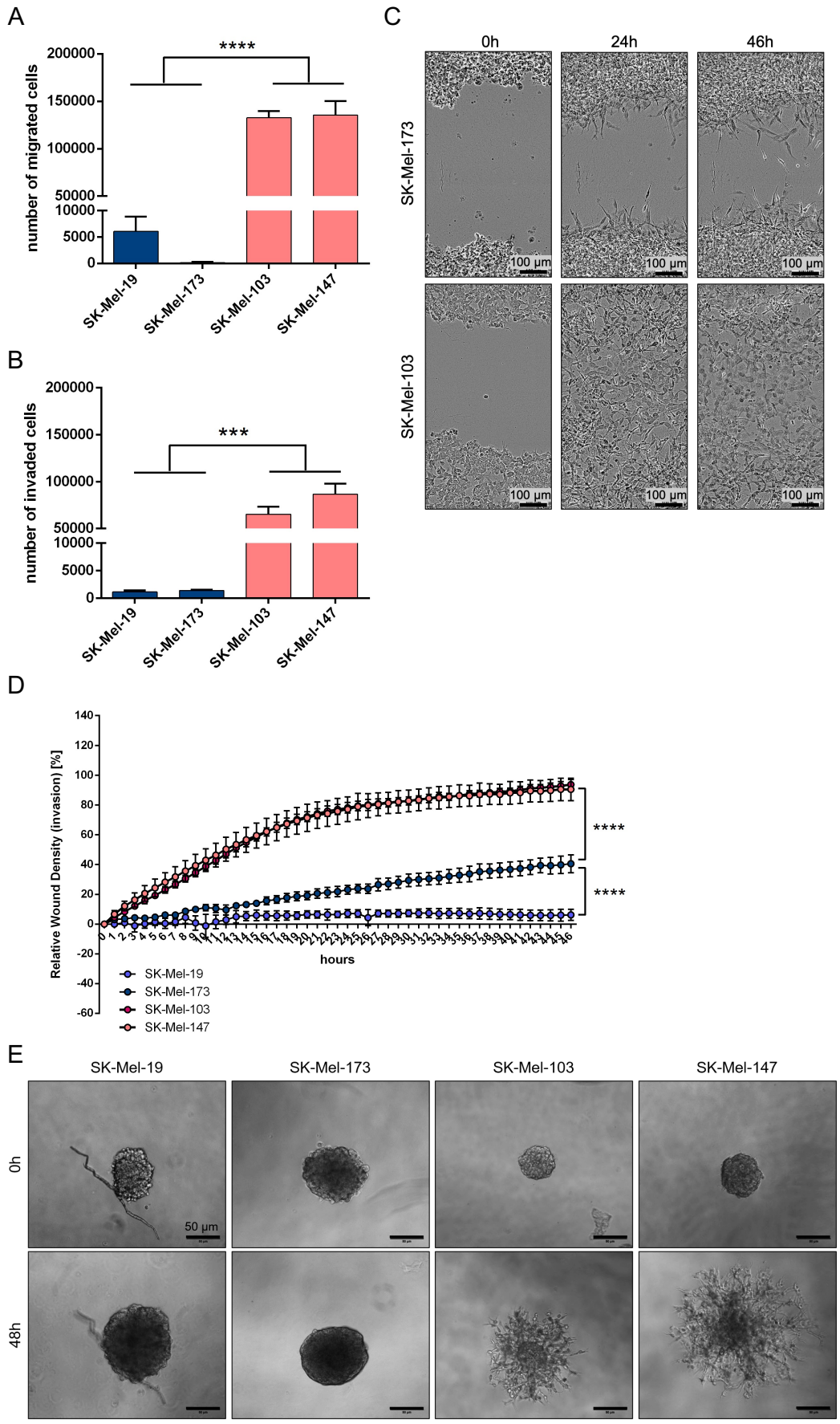

Figure 3.4 Characterization of non-invasive and invasive melanoma cell lines. *A) and B) Determination of cell migration and invasion of non-invasive SK-Mel-19 and SK-Mel-173 cells, as well*

*as invasive SK-Mel-103 and SK-Mel-147 cells. 2 x 10^5 serum-starved cells were seeded into transwell inserts and cells migrated or invaded through an 8 µm porous membrane were counted after 24 or 48 h, respectively. Bar graphs show mean values ± SD, n=3, t-test. C) Representative images of invasion wound healing assays using the Incucyte S3 Live Cell Analysis System. Presented are images of cells from the non-invasive cell line SK-Mel-173 and the invasive cell line SK-Mel-103 0, 24 and 46 h after creating the wound. Scale bar, 100 µm. D) Measurements of invasive wound closure over time of the melanoma cell lines SK-Mel-19, SK-Mel-173, SK-Mel-103 and SK-Mel-147. Cells were seeded into collagen precoated wells of a 96-well plate, wounds were created, and images of invasive wound closure were taken every hour for 46 h in total. Depicted graphs show the mean values ± SD, n=3. Data were analyzed using a two-way ANOVA test. E) Exemplary images of the invasiveness of spheroids derived from the cell lines SK-Mel-19, SK-Mel-173, SK-Mel-103 and SK-Mel-147 in Matrigel™ after 48 h. Cells were seeded into 96-well plates, spheroids were formed for 48 h, and were transferred to Matrigel™. Scale bar, 50 µm. Indicated p-values are defined as. **** = p ≤ 0.0001, *** = p ≤ 0.001. Significances refer to non-invasive control cells.*

Representative images of wound closure of the non-invasive cell line SK-Mel-173 and the invasive cell line SK-Mel-103 after 0, 24 and 46 h are shown in Figure 3.4C. The relative wound density of all cell lines dependent on the time is shown in Figure 3.4D. Both invasive cell lines were able to close the wound to approximately 80 % after 24 h, whereas the non-invasive cell lines SK-Mel-19 and SK-Mel-173 were at 6.5 % and 21.8 % of wound closure after 24 h, respectively. The invasive cell lines reached a plateau of wound closure within 46 h of observation. Additional Matrigel™ based 3D assays confirmed the invasiveness of spheroids derived from SK-Mel-103 and SK-Mel-147 cells. For this, 500 cells of each cell line were transferred to low attachment, U-shaped 96-well plates and incubated for 48 h to enable spheroid formation. Spheroids were transferred to Matrigel™ and imaged every 24 h. Clearly, spheroids derived from the cell lines SK-Mel-103 and SK-Mel-147 showed more invasion into the extracellular matrix after 48 h compared to spheroids derived from non-invasive cells (Figure 3.4E).

3.1.2.2. Increased microtubule growth rates are required for increased cell migration and invasion in human melanoma cell lines

Due to a possible association between increased microtubule plus end growth rates and increased invasiveness, microtubule plus end growth rates in non-invasive and invasive melanoma cell lines were measured in asynchronous growing cells.

Interestingly, the invasive melanoma cell lines SK-Mel-103 and SK-Mel-147 exhibited higher microtubule plus end growth rates compared to the non-invasive cell lines SK-Mel-19 and SK-Mel-173. SK-Mel-103 and SK-Mel-147 cells showed microtubule polymerization rates of 23.3 µm/min and 23.9 µm/min, whereas the non-invasive cell lines SK-Mel-19 and SK-Mel-173 exhibited microtubule growth rates of 19.2 µm/min and 19.0 µm/min, respectively (Figure 3.5A). To restore normal microtubule plus end assembly rates in invasive melanoma cell lines, cells were treated with sub-nanomolar concentrations of Taxol.

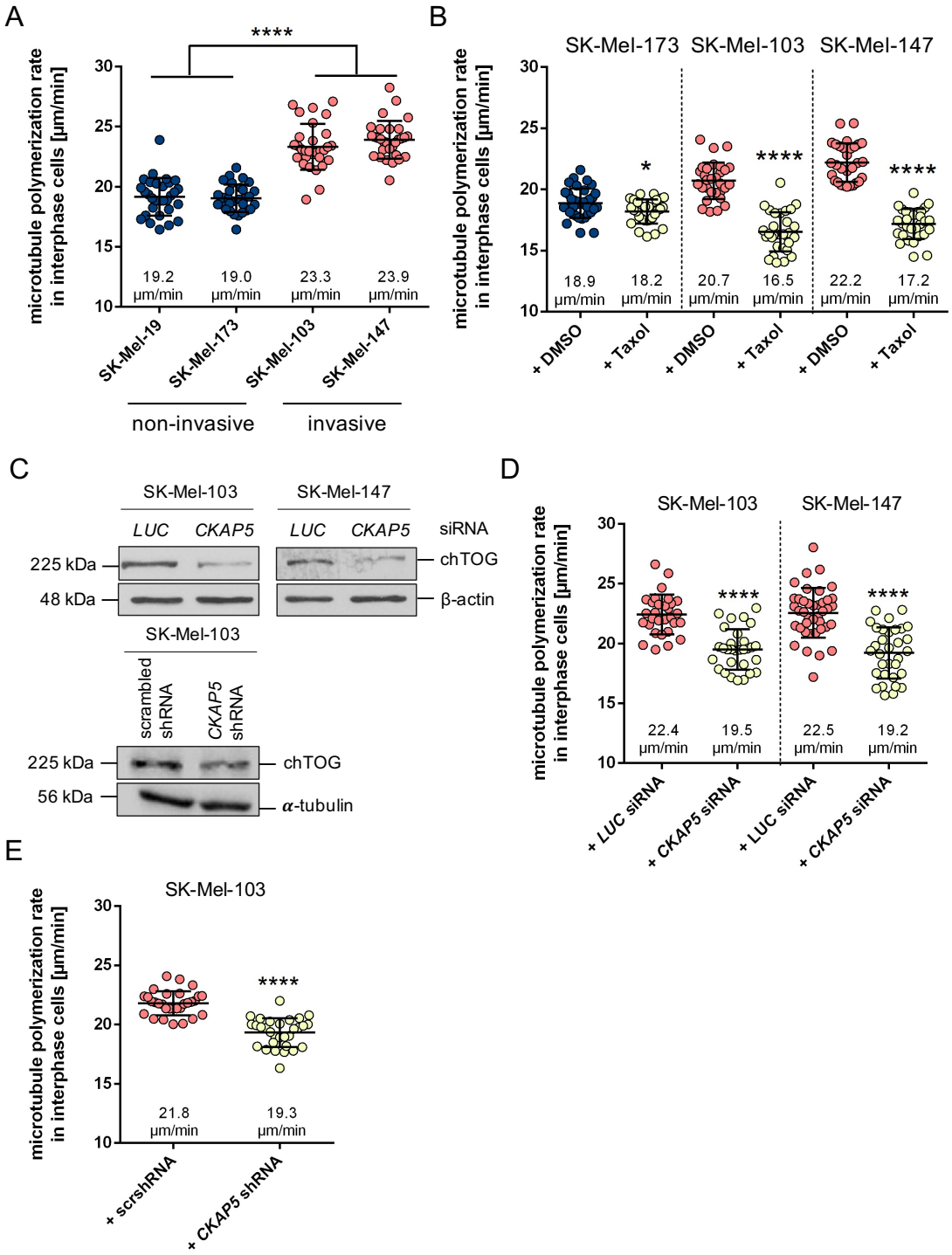

Figure 3.5 Increased microtubule plus end assembly rates during interphase are restored after Taxol treatment or siRNA mediated knockdown of CKAP5. *A) Measurements of interphase microtubule growth rates in non-invasive SK-Mel-19 and SK-Mel-173 cells and in invasive SK-Mel-103 and SK-Mel-147 cells. B) Measurements of interphase microtubule growth rates in SK-Mel-173 cells and SK-Mel-103 and SK-Mel-147 cells after treatment with 0.5 nM of Taxol or DMSO as a control. C) Representative western blots showing the transient knockdown of CKAP5 in the melanoma cell lines SK-Mel-103 and SK-Mel-147 and the stable shRNA mediated knockdown of CKAP5 in SK-Mel-103 cells. Protein levels of chTOG (H-4, mouse, monoclonal antibody (mAb)) were detected. β-actin (AC-15, mouse, mAb) and α-tubulin (B-5-1-2, mouse, mAb) served as loading controls. D) Measurements of interphase microtubule plus end assembly in melanoma cell lines upon CKAP5 knockdown. E) Measurements of microtubule plus end assembly rates in SK-Mel-103 interphase cells upon stable shRNA mediated knockdown of CKAP5. Scatter dot plots show mean*

*values ± SD, n=30, 20 microtubules were measured per cell. Data were analyzed using a t-test. Significances are defined as: **** = p ≤ 0.0001, ** = p ≤ 0.01, * = p ≤ 0.05. Significances refer to corresponding control cells. Different cell lines within one graph are separated with a dotted line.*

Indeed, treatment of melanoma cell lines with Taxol rescued increased microtubule plus end growth rates in the invasive melanoma cell lines SK-Mel-103 and SK-Mel-147 from 20.7 to 16.5 µm/min and from 22.2 to 17.2 µm/min, respectively, with no effect on the non-invasive control cell line (Figure 3.5B). Further, increased microtubule polymerization rates were rescued using a siRNA mediated transient or shRNA mediated stable knockdown of *CKAP5*. The successful transient or stable knockdown of *CKAP5* was verified by western blot (Figure 3.5C). As expected, enhanced microtubule plus end growth rates of the invasive cell lines SK-Mel-103 and SK-Mel-147 were reduced to control cell level from 22.4 to 19.5 µm/min and 22.5 to 19.2 µm/min upon knockdown of *CKAP5*, respectively (Figure 3.5D). SK-Mel-103 cells with a stable shRNA mediated knockdown of *CKAP5* also exhibited restored normal microtubule plus end growth rates (Figure 3.5E).

To investigate if interphase microtubule plus end dynamics is required for increased cell migration and invasion in melanoma cell lines, cells were treated with 0.5 nM of the microtubule stabilizing drug Taxol to restore normal microtubule polymerization rates. Cell migration and invasion were subsequently measured. Taxol treatment of invasive cell lines before and during transwell migration and invasion assays led to an approximately 30 % reduction of cell migration and invasion (Figure 3.6A and B). After knockdown of *CKAP5*, cell migration and invasion were reduced by 35 % compared to *LUC* siRNA transfected cells (Figure 3.6C and D). SK-Mel-103 cells stably transfected with shRNA targeting *CKAP5* migrated approximately 50 % less than control transfected cells (Figure 3.6E).

Matrigel™ based 3D spheroid assays where spheroids are embedded in a 3D matrix and outgrowth of invasive structures can be observed in real time resemble the actual *in vivo* situation better. Therefore, spheroids of invasive melanoma cell lines were generated and treated with DMSO or 0.5 nM of Taxol. Additionally, SK-Mel-103 cells with a stable shRNA mediated knockdown of *CKAP5* were used for spheroid formation. Cells stably transfected with scrambled shRNA (scrshRNA) were used as control cells. Images of the spheroids were taken after 48 h and the area of spheroid outgrowth relative to control spheroids was measured. Figure 3.7A and B show representative images of spheroids derived from the invasive cell lines SK-Mel-103 and SK-Mel-147 after Taxol treatment for 48 h and invasiveness of spheroids derived from SK-Mel-103 cells with a stable knockdown of *CKAP5*.

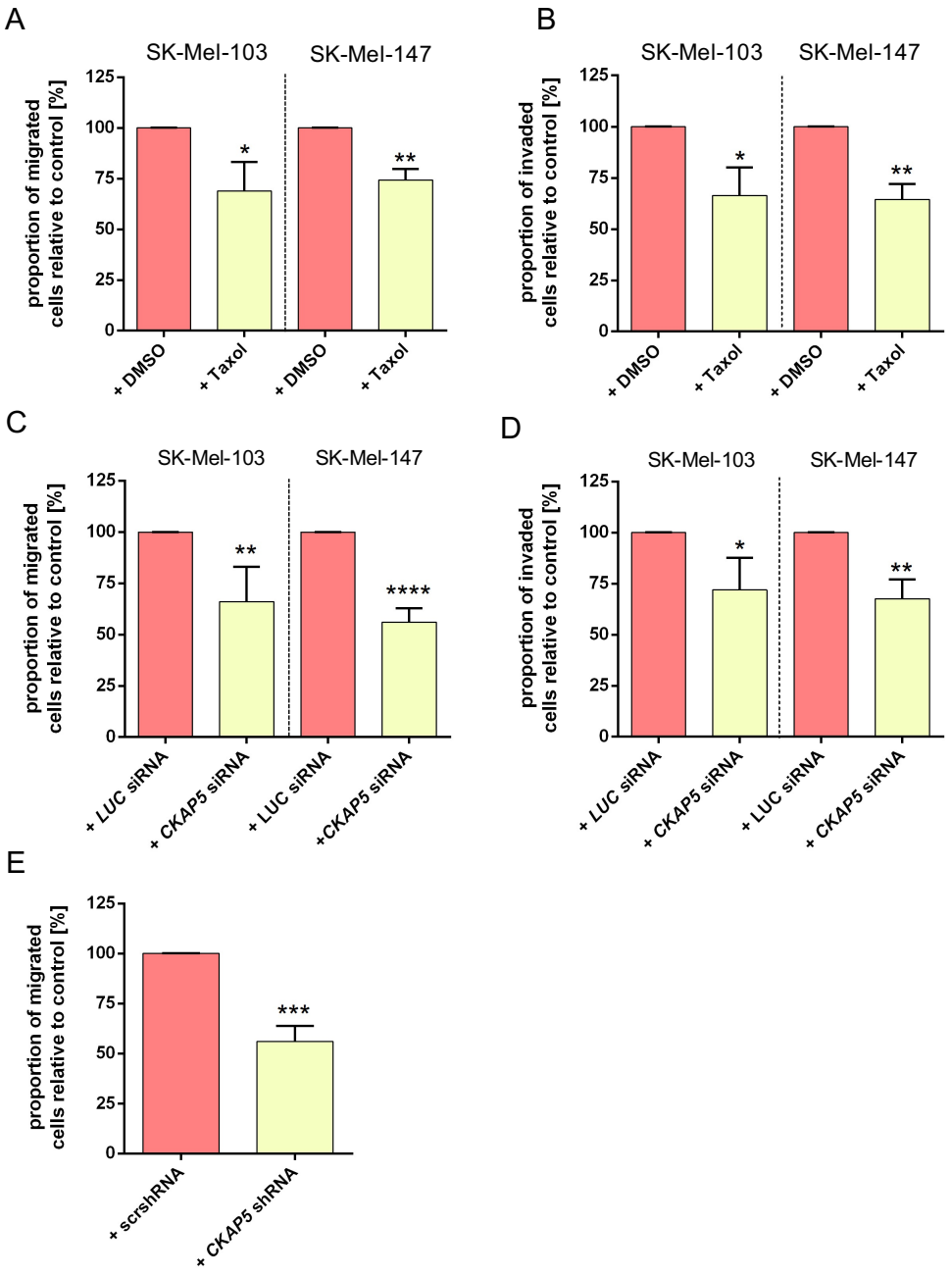

Figure 3.6 Increased cell migration and invasion are suppressed upon restoration of normal microtubule growth rates in interphase. *A) and B) Determination of cell migration and invasion of invasive cell lines after restoration of normal microtubule plus end assembly rates. Cells were treated before and during transwell migration and invasion assays with 0.5 nM of Taxol or DMSO as a control. 2 x 10^5 serum-starved cells were seeded into inserts and migrated or invaded cells were counted after 24 h (migration) or 48 h (invasion). The proportion of migrated or invaded cells was calculated relative to control cells. C) Determination of cell migration of invasive melanoma cell lines after partial depletion of chTOG. Migration was analyzed after 24 h. Depicted are mean values ± SD, n=4. D) Determination of cell invasion of melanoma cell lines upon partial depletion of chTOG. Invaded cells were counted after 48 h. E) Determination of cell migration after stable knockdown of CKAP5 in SK-Mel-103 cells. Bar graphs with mean values ± SD, n=3. All experiments were statistically analyzed using a t-test. Indicated p-values are defined as: **** = p ≤ 0.0001, *** = p ≤ 0.001, ** = p ≤ 0.01, * = p ≤ 0.05. Significances refer to control cells. Different cell lines within one graph are separated through a dotted line.*

Intriguingly, spheroids of both cell lines treated with Taxol showed an approximately 60 % reduction of spheroid outgrowth compared to DMSO treated spheroids (Figure 3.7C). The stable shRNA mediated knockdown of *CKAP5*, which restored proper interphase microtubule growth rates, also suppressed spheroid outgrowth. The outgrowth area was reduced by 40 % compared to control transfected cells (Figure 3.7D).

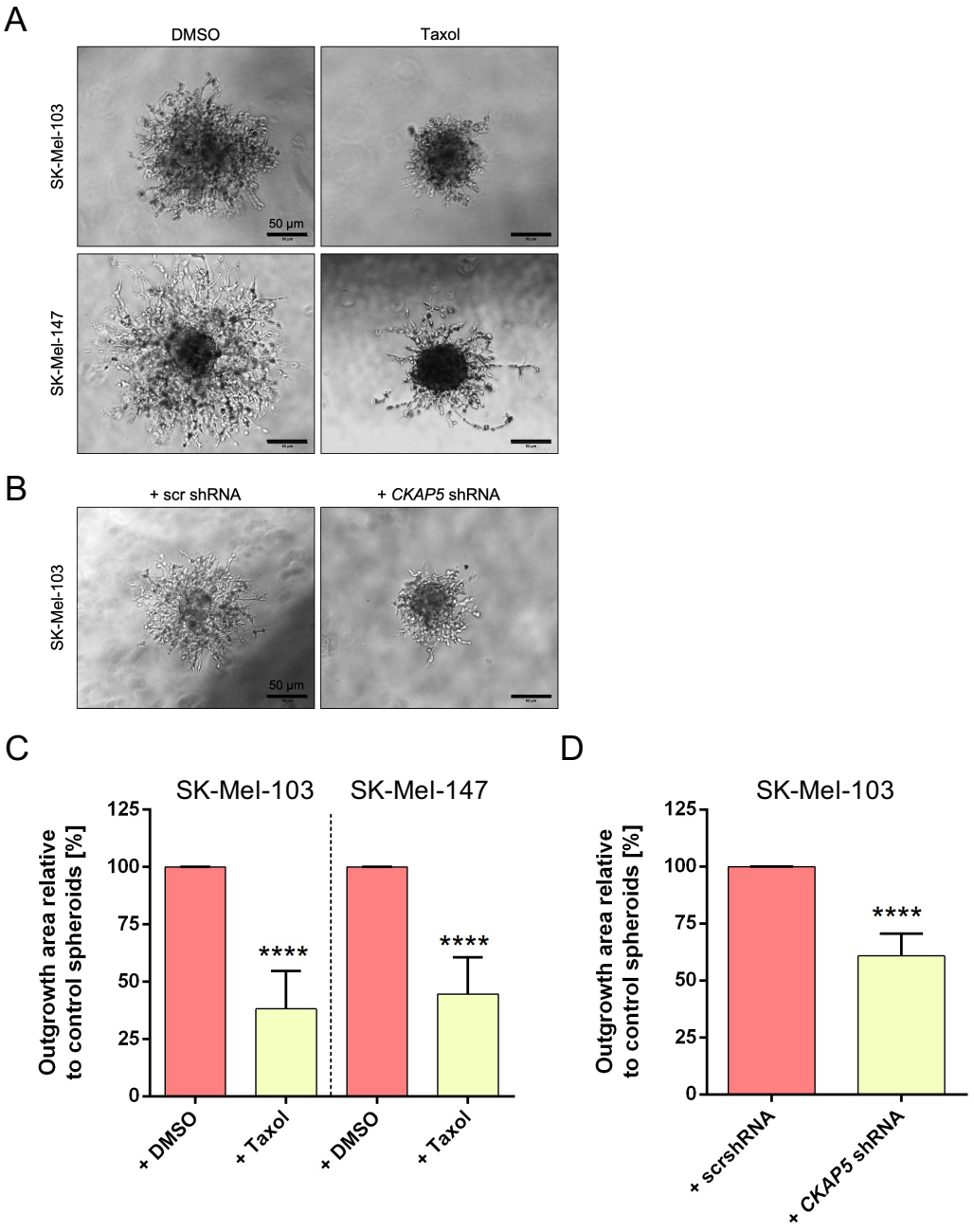

Figure 3.7 Reduction of spheroid outgrowth after rescue of increased microtubule plus end growth rates using Taxol or CKAP5 knockdown. *A) Representative images of the outgrowth of spheroids derived from invasive cells after treatment with DMSO or 0.5 nM of Taxol. 500 cells were seeded into low-attachment 96-well plates and spheroid formation lasted for 48 h. Spheroid treatment with DMSO or Taxol started 24 h before transferring the spheroids to Matrigel™. Images were taken after 48 h. Scale bar, 50 µm. B) Representative images of spheroids derived from SK-Mel-103 cells stably transfected with scrambled or CKAP5 shRNA. Scale bar, 50 µm. C) Quantitative analysis of the outgrowth area of spheroids derived from SK-Mel-103 and SK-Mel-147 cells after*

*48 h. n=20 (SK-Mel-103 spheroids) or n=26 (SK-Mel-147 spheroids) were analyzed for spheroid outgrowth after treatment with Taxol or DMSO as a control. The area of outgrowth was calculated relative to control cells. D) Quantitative analysis of spheroid outgrowth of SK-Mel-103 cells with a stable knockdown of CKAP5 or corresponding control cells. 25 spheroids were analyzed. Bar graphs show mean values ± SD, n=3, t-test. Indicated stars are defined as followed: **** = p ≤ 0.0001. The indicated significances refer to control cells.*

3.1.2.3. Induction of increased microtubule plus end growth rates in non-invasive melanoma cell lines does not lead to increased invasiveness

The knockdown of *CKAP5* and the treatment with Taxol led to a restoration of normal microtubule growth rates in invasive melanoma cell lines. Importantly, this was associated with decreased cell migration and invasion, indicating that increased microtubules plus end assembly rates are required for regulating cell motility.

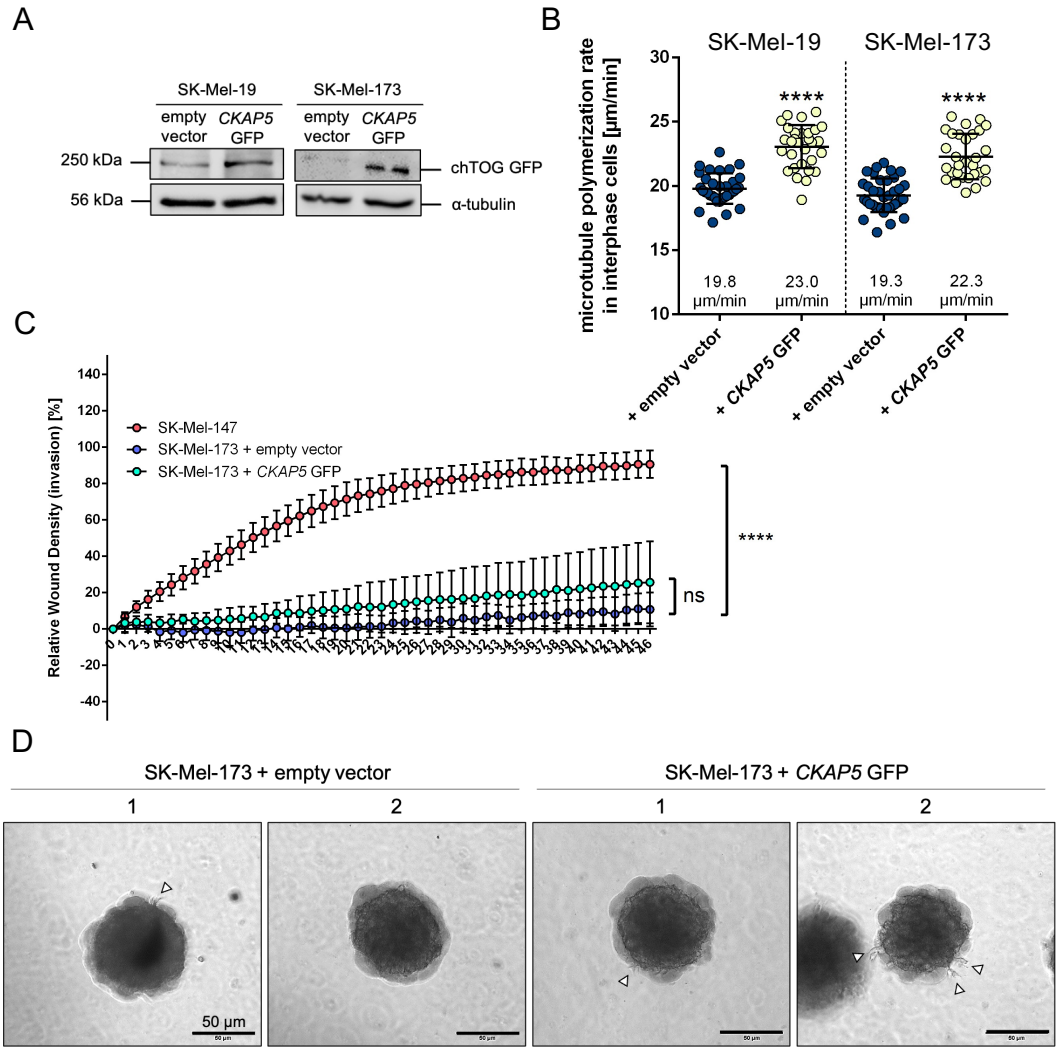

Figure 3.8 Induction of increased interphase microtubule plus end growth rates upon overexpression of CKAP5 does not affect cellular invasion. *A) Representative western blots showing CKAP5 overexpression in the non-invasive cell lines SK-Mel-19 and SK-Mel-173. GFP (GF28R, mouse, monoclonal antibody (mAb)) was detected. α-tubulin (B-5-1-2, mouse, mAb) served as the loading control. B) Measurements of interphase microtubule plus end assembly rates upon CKAP5*

*overexpression. Scatter dot plot shows mean values ± SD, n=30. 20 microtubules were measured per cell. C) Measurements of invasive wound closure over time of the melanoma cell line SK-Mel-173 transfected with a CKAP5 overexpressing plasmid. Images were taken every hour for 46 h in total. Data for the invasive wound closure of SK-Mel-147 were already shown in Figure 3.4 and are shown here as a positive control. Graphs show mean values ± SD, n=3, two-way ANOVA test. D) Exemplary images of two spheroids derived from SK-Mel-173 cells with a transient overexpression of CKAP5. Images were taken after four days. White triangles mark invasive structures. Scale bar, 50 µm. Indicated stars are defined as: **** = p ≤ 0.0001. The significances refer to corresponding control cells. Dotted lines separate different cell lines depicted in one graph.*

Further, it was analyzed whether induction of increased microtubule plus end assembly is sufficient to increase cell migration and invasion. Since the overexpression of chTOG was shown before to increase microtubule plus end assembly in mitotic cells (Ertych et al., 2014), *CKAP5* was overexpressed in the non-invasive cell lines SK-Mel-19 and SK-Mel-173 and microtubule plus end assembly rates were measured in interphase. The overexpression of *CKAP5* was verified by western blot (Figure 3.8A). *CKAP5* overexpression was associated with accelerated microtubule growth rates from 19.8 to 23.0 µm/min for SK-Mel-19 cells and from 19.3 to 22.3 µm/min for SK-Mel-173 cells (Figure 3.8B). However, despite the induction of increased microtubule plus end growth rates, non-invasive SK-Mel-173 cells transfected with a *CKAP5* overexpressing plasmid did not show enhanced invasive wound healing closure (Figure 3.8C). Furthermore, non-invasive SK-Mel-173 spheroids in Matrigel™ with a transient overexpression of *CKAP5* did not show increased formation of invasive structures after four days (Figure 3.8D).

Taken together, the obtained data show a correlation of microtubule plus end dynamics with cell migration and invasion in colorectal and melanoma cell lines. Restoration of normal interphase microtubule growth rates in invasive cells caused a partial reduction of cell migration and invasion. However, the induction of enhanced microtubule plus end assembly *per se* was not sufficient to trigger increased cell migration and invasion. These results suggest that microtubule dynamics is required, but not sufficient to trigger increased migration and invasion in human cancer cells.

3.1.3. Signaling upstream of enhanced microtubule plus end growth rates in interphase cells

Previous results of our lab showed that the concomitant loss of *TP53* and *TP73* in HCT116 cells leads to the loss of the Cdk inhibitor $p21^{Cip1}$. Loss of $p21^{Cip1}$ unleashes the activity of Cdk1 resulting in increased microtubule plus end growth rates during mitosis, formation of lagging chromosomes during anaphase, chromosomal instability, and aneuploidy (Schmidt et al., 2021). To search for potential factors triggering increased microtubule plus end growth rates in interphase cells that would lead to enhanced cell motility, different cell

cycle regulators in melanoma cell lines known to regulate the cytoskeleton and therefore potentially influencing microtubule plus end dynamics and cell movement were analyzed.

3.1.3.1. *Inhibition of Cdk1 activity restores normal microtubule plus end growth rates in invasive melanoma cell lines and reduces cell migration and invasion*

Cdk1 is well described for its function as a mitotic kinase (Malumbres & Barbacid, 2009; Satyanarayana & Kaldis, 2009). Since accelerated Cdk1 activity was associated with chromosomal instability in HCT116 cells, the effect of Cdk1 inhibition on interphase microtubule plus end growth rates and cell migration and invasion in melanoma cell lines was analyzed.

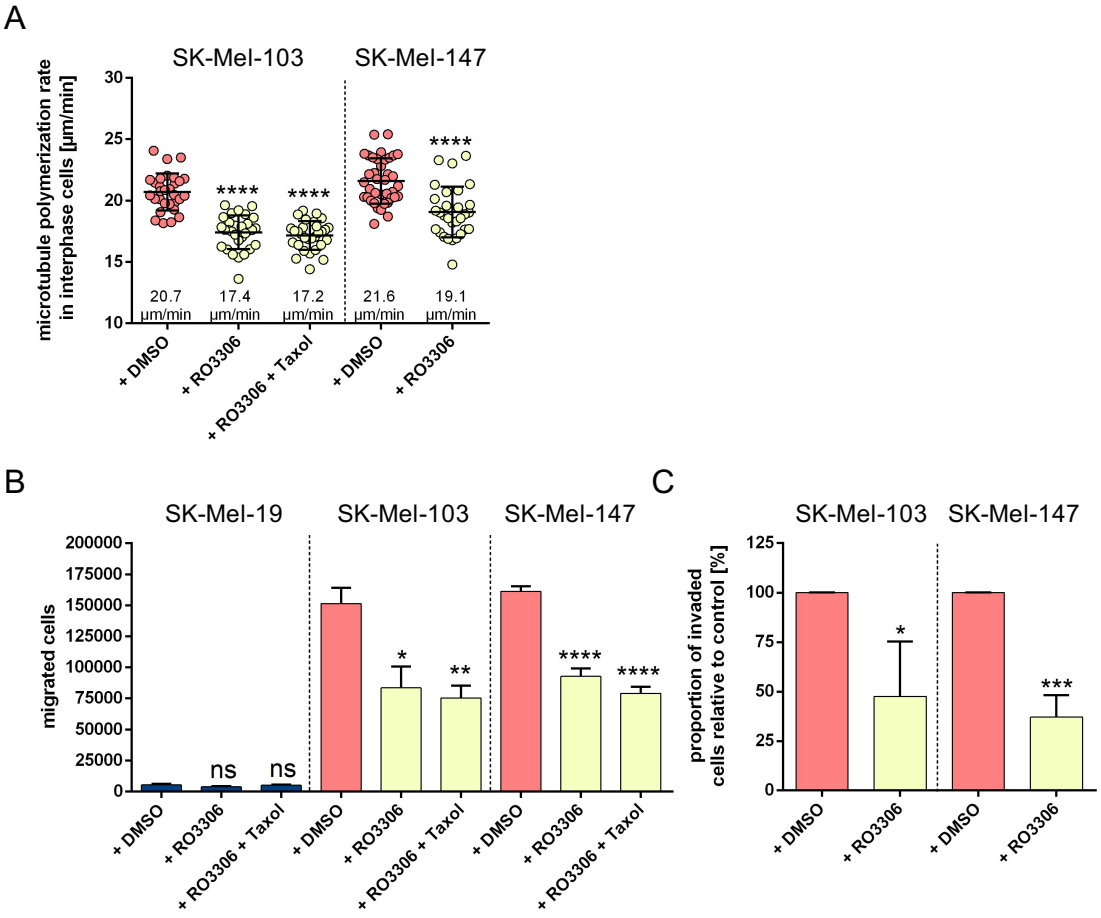

Figure 3.9 Inhibition of Cdk1 activity rescues increased interphase microtubule plus end growth rates and enhanced cell migration and invasion in invasive melanoma cell lines. *A) Measurements of interphase microtubule plus end growth rates in invasive melanoma cell lines upon RO3306 treatment. SK-Mel-103 and SK-Mel-147 cells were treated with 1 µM of the Cdk1 inhibitor RO3306 or DMSO as a control. SK-Mel-103 cells were treated simultaneously with 0.5 nM of Taxol and 1 µM of the Cdk1 inhibitor. Scatter dot plot shows mean values ± SD, n=30, 20 microtubules were measured per cell, t-test. B) Determination of cell migration of SK-Mel-19, SK-Mel-103 and SK-Mel-147 cells after treatment with the Cdk1 inhibitor RO3306. Cells were treated with 1 µM of RO3306 and 1 µM of RO3306 together with 0.5 nM of Taxol. DMSO treatment served as a control. Migration was analyzed after 24 h. Bar graphs show mean values ± SD from three or five (five experiments were done with SK-Mel-147 cells in transwell migration assays upon RO3306 treatment) independent experiments, t-test. C) Determination of cell invasion of melanoma cell lines*

*upon treatment with the Cdk1 inhibitor RO3306. Cells were treated with 1 µM of the Cdk1 inhibitor RO3306 or DMSO as a control. Cell invasion was analyzed after 48 h. Bar graphs with mean values ± SD, n=3, t-test. p-values are defined as followed: **** = p ≤ 0.0001, *** = p ≤ 0.001, ** = p ≤ 0.01, * = p ≤ 0.05 and non-significant (ns) = p > 0.05. Significances refer to corresponding control cells. Different cell lines within one graph are separated by a dotted line.*

Interestingly, treatment of the invasive cell lines SK-Mel-103 and SK-Mel-147 with 1 µM of the selective Cdk1 inhibitor RO3306 reduced the microtubule plus end growth rates from 20.7 to 17.4 µm/min for SK-Mel-103 cells and from 21.6 to 19.1 µm/min for SK-Mel-147 cells (Figure 3.9A). Simultaneous treatment of SK-Mel-103 cells with the Cdk1 inhibitor and 0.5 nM of the microtubule stabilizing drug Taxol did not lead to further reduction of the microtubule growth rates, hence, excluding an additive effect of Taxol and Cdk1 inhibitor treatment and indicating that both signalings might share the same pathway. For migration and invasion transwell assays SK-Mel-103 and SK-Mel-147 cells were treated with 1 µM of the Cdk1 inhibitor or DMSO as a control. Cdk1 inhibitor treated cells displayed at least 50 % reduced cell migration and invasion compared to control cells (Figure 3.9B and C). The simultaneous treatment with the Cdk1 inhibitor and Taxol showed again no additive effect.

3.1.3.2. Hyperactive E2F1 might be a potential trigger for increased interphase microtubule plus end dynamics

The G1/S restriction point is a cell cycle checkpoint to regulate entry into S phase. Essential factors for regulating the transcription of important S phase regulators are the Retinoblastoma (Rb) protein and the transcription factor E2F1. Cdk4 in complex with D-type cyclins phosphorylates Rb at the G1/S restriction point, which leads to its dissociation from E2F1 and the immediate binding of the activated transcription factor to its target genes (Bracken et al., 2004). Since E2F1 is often found to be upregulated in cancer (Burkhart & Sage, 2008), I hypothesized that increased activity of the transcription factor E2F1 leads to elevated interphase microtubule polymerization rates and hence, to increased cell migration and invasion. The transient siRNA mediated knockdown of *RB* or the overexpression of *E2F1* were verified by western blot (Figure 3.10A) and resulted in increased microtubule polymerization rates in the non-invasive cell line SK-Mel-173 with enhanced growth rates from 19.3 to 22.5 µm/min and from 18.9 to 22.1 µm/min, respectively (Figure 3.10B). Transfection of the invasive cell line SK-Mel-103 with a siRNA targeting *E2F1*, the representative western blot is shown in Figure 3.10A, resulted in the reduction of microtubule plus end growth rates from 22.9 to 19.7 µm/min and approximately 30 % reduced cell migration (Figure 3.10C and D).

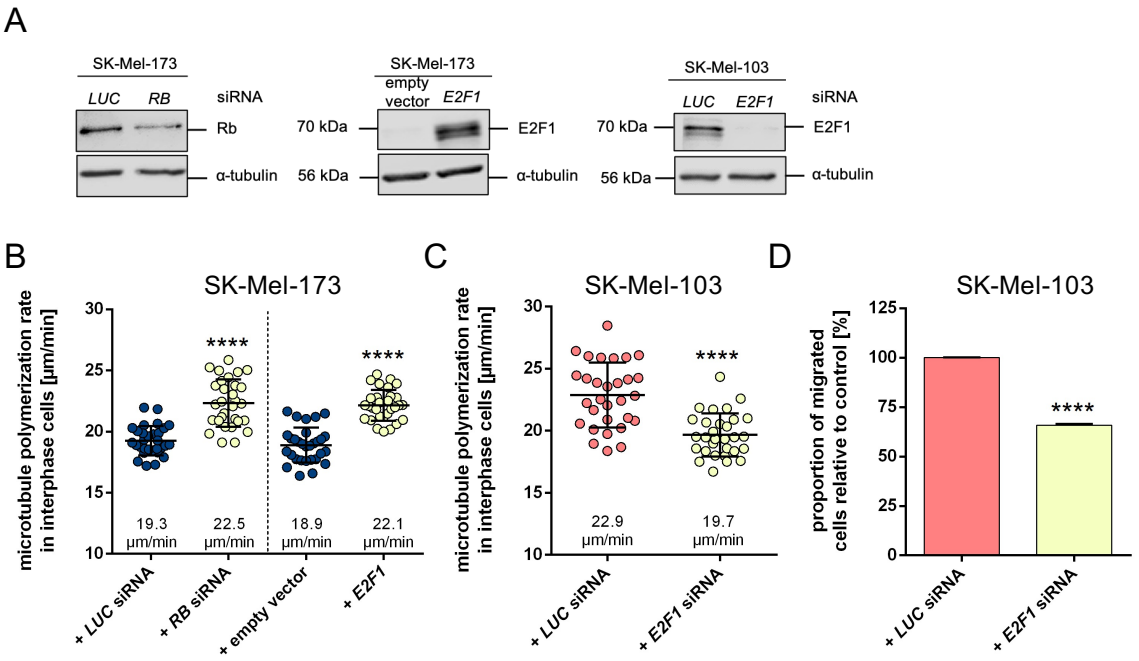

Figure 3.10 E2F1 activity participates in the regulation of interphase microtubule plus end growth rates and cell migration in melanoma cell lines. *A) Representative western blots showing the siRNA mediated knockdown of RB or E2F1 overexpression in the non-invasive cell line SK-Mel-173, and E2F1 knockdown in the invasive cell line SK-Mel-103. E2F1 (KH95, mouse, monoclonal antibody (mAb)) and Rb (IF-8, mouse, mAb) were detected. β-actin (AC-15, mouse, mAb) and α-tubulin (B-5-1-2, mouse, mAb) served as the loading controls. B) Measurements of interphase microtubule plus end assembly rates in the non-invasive cell line SK-Mel-173 after the siRNA mediated knockdown of RB or transient overexpression of E2F1. C) Measurements of interphase microtubule plus end growth rates in SK-Mel-103 cells upon siRNA mediated knockdown of E2F1. Scatter dot plots in B) and C) show mean values ± SD, n=30, 20 microtubules were measured per cell, t-test. D) Determination of cell migration of SK-Mel-103 cells after siRNA mediated knockdown of E2F1. Migration was analyzed after 24 h. Bar graphs show mean values ± SD, n=3, t-test. Stars are defined as: **** = p ≤ 0.0001. The indicated significances refer to control cells that were marked by dotted lines. Different transfections within one graph were separated by a dotted line.*

After the initial experiments were indicating a potential contribution of E2F1 activity in the regulation of microtubule plus end growth rates in interphase, further upstream regulators of E2F1 activity were analyzed for their effect on interphase microtubule plus end assembly. Since the binding of Cdk2 to E-type cyclins and Cdk4 to D-type cyclins is also known to phosphorylate the Rb protein (Martínez-Alonso & Malumbres, 2020), the effects of Cdk4 and Cdk2 inhibitors on microtubule plus end dynamics in interphase cells and on cell migration and invasion were analyzed. Cells from the invasive cell line SK-Mel-103 were treated with 75 nM of Cdk4 inhibitor (PD0332991) or 100 nM of Cdk2 inhibitor (CVT313) before cells were analyzed for microtubule plus end growth rates in interphase. The measurements for inhibitor treated cells showed no significant reduction of microtubule growth rates after treatment with the Cdk4 inhibitor and just a slight reduction for the treatment with the Cdk2 inhibitor (Figure 3.11A). The invasive cell line SK-Mel-103 was treated prior and during transwell cell migration and invasion assays with Cdk4 or Cdk2 inhibitors. All measurements showed a reduction by at least 40 % of cell migration or invasion

(Figure 3.11B and C). However, it is unclear why the transwell invasion assays with SK-Mel-103 cells upon Cdk2 inhibitor treatment did not show a significant reduction of cell invasion.

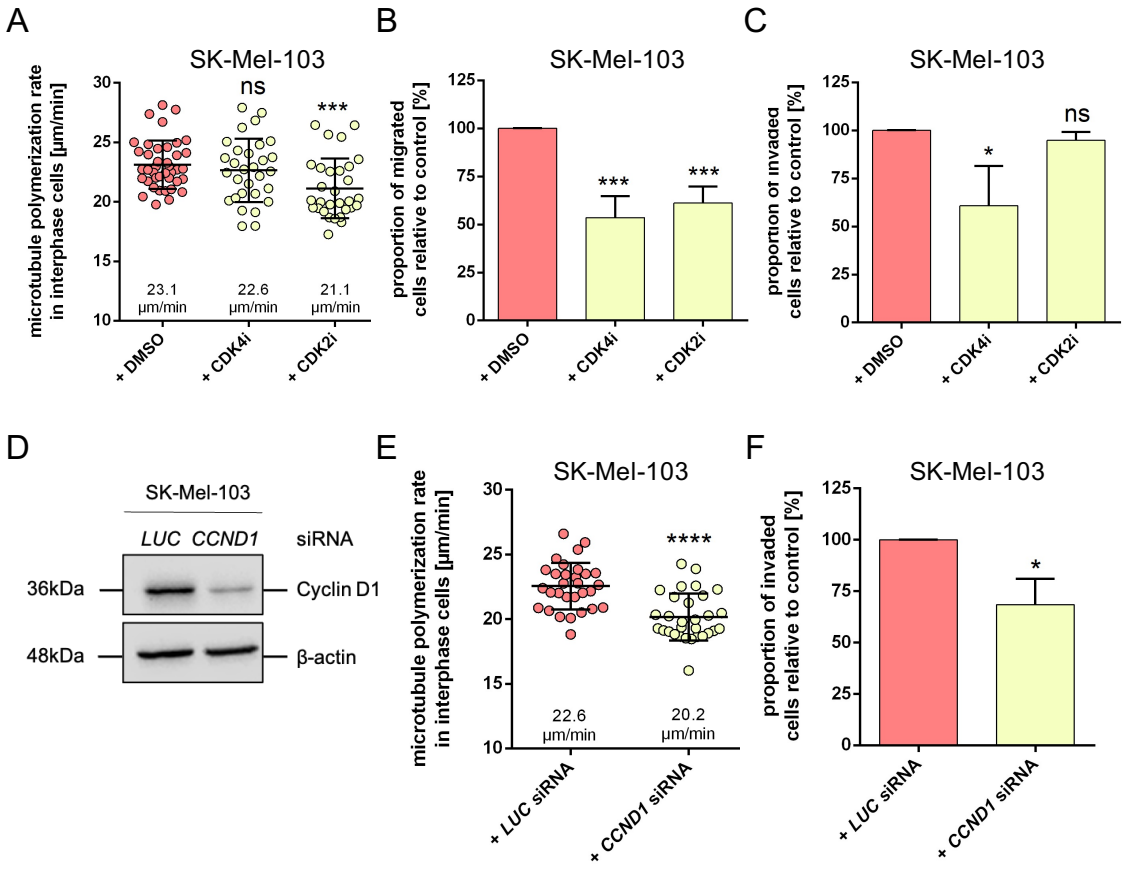

Figure 3.11 Upstream regulators of E2F1 signaling affect microtubule plus end growth rates and cell migration and invasion in melanoma cell lines. *A) Measurements of interphase microtubule plus end assembly in SK-Mel-103 cells upon treatment with inhibitors for Cdk2 (CVT313) and Cdk4 (PD0332991). Cells were treated with 75 nM of Cdk4 and 100 nM of Cdk2 inhibitor. DMSO treated cells were used as control cells. B) and C) Determination of cell migration and invasion of the melanoma cell line SK-Mel-103 upon treatment with inhibitors for Cdk2 (CVT313) and Cdk4 (PD0332991). Migrated or invaded cells were counted after 24 h or 48 h, respectively. D) Representative western blot showing the partial depletion of cyclin D1 in SK-Mel-103 cells. Cyclin D1 (HD11, mouse, monoclonal antibody (mAb)) was detected. β-actin (AC-15, mouse, mAb) was used as a loading control. E) Measurements of interphase microtubule plus end growth rates after the transient knockdown of CCND1 in SK-Mel-103 cells. Cells transfected with LUCIFERASE (LUC) siRNA were used as control cells. F) Determination of cell invasion of cells with a transient knockdown of CCND1. Analyzed after 48 h. Scatter dot plots show mean values ± SD, n=30, 20 microtubules were measured per cell, t-test. Bar graphs present mean values ± SD, n=3, t-test. Definition of the p-values: **** = p ≤ 0.0001, *** = p ≤ 0.001, ** = p ≤ 0.01, * = p ≤ 0.05 and non-significant (ns) = p > 0.05. The indicated significances refer to corresponding control cells. Dotted lines separate different cell lines within one graph.*

To analyze the contribution of D-type cyclins on regulating microtubule plus end dynamics and cell migration and invasion, a siRNA mediated transient knockdown of *CCDN1* in SK-Mel-103 cells was performed and the effects on microtubule plus end assembly rates and cell invasion were analyzed. Western blot verification of the partial depletion of cyclin D1

in SK-Mel-103 cells is shown in Figure 3.11D. Microtubule polymerization rate measurements showed reduced growth rates from 22.6 to 20.2 µm/min (Figure 3.11E). The siRNA mediated knockdown of *CCND1* led to a reduction of cell invasion by at least 25 % (Figure 3.11F).

Taken together, to find upstream regulators that trigger an enhanced microtubule plus end assembly in melanoma cell lines and subsequently an increased cell migration and invasion, a screen with essential regulators at the G1/S restriction point of the cell cycle was performed. These factors are already linked to promote cell migration and invasion in various types of cancer (Roworth et al., 2015). A hyperactivated E2F1 transcription factor in melanoma cell lines might be one of many triggers for enhanced microtubule plus end growth rates and elevated cell migration and invasion. Decreased E2F1 activity restored normal microtubule dynamics and partially reduced cell migration and invasion. However, not all data showed significant results. Further analyses are needed.

3.2. Paracrine signaling regulates increased microtubule growth rates in invasive melanoma cell lines

A recent study from the Godinho lab demonstrated that human breast epithelial cells (MCF-10A) with an abnormal number of centrosomes induce an invasive phenotype in surrounding cells by secretion of extracellular vesicles. The paracrine signaling involved the secretion of three factors, interleukin 8 (IL8), growth/differentiation factor 15 (GDF-15) and angiopoietin like 4 (ANGPTL4) (Arnandis et al., 2018). Since the centrosome is the microtubule organizing center of the cell, I investigated if the regulation of microtubule plus end assembly rates is linked to centrosome amplification. Moreover, I analyzed if a paracrine signaling can contribute to deregulation of microtubule plus end growth rates in melanoma cells.

3.2.1. Invasive melanoma and colorectal cancer cell lines with elevated microtubule plus end growth rates exhibit a higher proportion of cells with supernumerary centrosomes

To investigate centrosome numbers in melanoma and colorectal cancer cells, cells were analyzed for γ-tubulin foci by immunofluorescence microscopy. Representative images of supernumerary centrosomes of the invasive cell lines SK-Mel-103 and SK-Mel-147 compared to the non-invasive cell line SK-Mel-173 are shown in Figure 3.12A. The statistical analysis of 600 (melanoma) or 400 (HCT116) interphase cells showed that invasive melanoma cell lines (Figure 3.12B) as well as invasive HCT116 + *TP73*shRNA/*TP53*$^{-/-}$ cells (Figure 3.12C) exhibited a higher proportion of cells with more than two centrosomes.

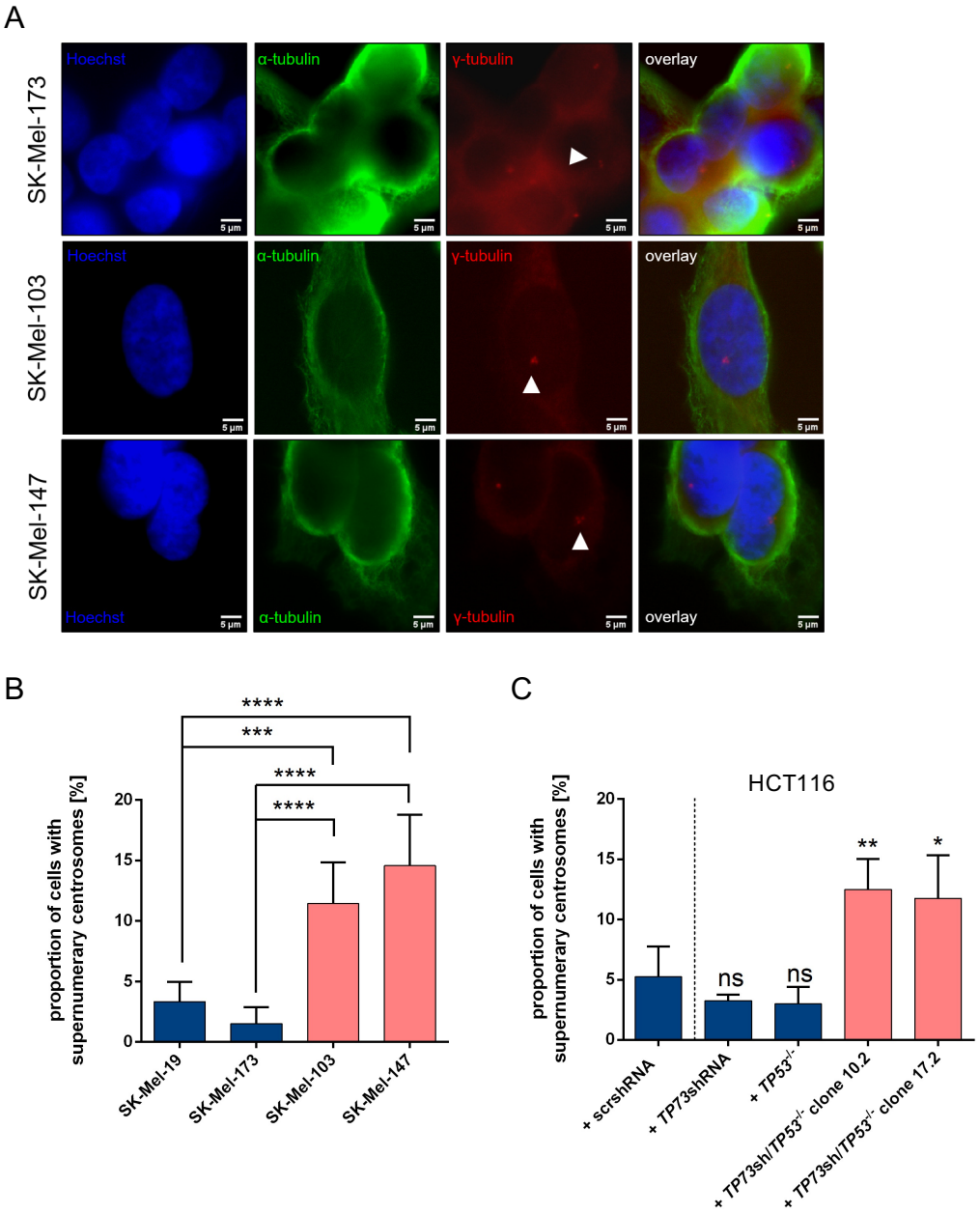

Figure 3.12 Quantification of supernumerary centrosomes in melanoma and colorectal cancer cells. *A) Representative images of interphase melanoma cells stained for centrosomes (red) and microtubules (green) using γ-tubulin (GTU88, mouse, monoclonal antibody (mAb)) and α-tubulin (rabbit, polyclonal antibody) antibodies. DNA was stained using Hoechst33342 (blue). Depicted are images of SK-Mel-173 cells with two centrosomes and SK-Mel-103 and SK-Mel-147 cells with each cell line presenting cells with three centrosomes. White triangles mark exemplary centrosomes. Scale bar, 5 µm. B) Proportion of cells with supernumerary centrosomes in SK-Mel-19, SK-Mel-173, SK-Mel-103 and SK-Mel-147 cell lines. 600 interphase cells were analyzed. Every cell with more than two centrosomes was defined as a cell with supernumerary centrosomes. C) Proportion of HCT116 cells with supernumerary centrosomes transfected with scrambled shRNA, TP73shRNA, with a knockout of TP53 or with a concomitant loss of TP73/TP53 (clone 10.2 and clone 17.2). 400 cells per cell line were analyzed. Bar graphs show mean values ± SD of four or six (six experiments were done with the melanoma cell lines) independent experiments. All experiments were statistically analyzed using a t-test. The indicated p-values are defined as: **** = p ≤ 0.0001, *** = p ≤ 0.001, ** = p ≤ 0.01, * = p ≤ 0.05 and non-significant (ns) = p > 0.05. The indicated significances refer to non-invasive control cells. Control cells for the HCT116 cell line are separated by a dotted line.*

SK-Mel-103 and SK-Mel-147 cell lines exhibited 11.4 and 14.6 % cells with supernumerary centrosomes, compared to the non-invasive cell lines SK-Mel-19 and SK-Mel-173 with 3.3 and 1.5 %. HCT116 + *TP73*shRNA/*TP53*$^{-/-}$ clone 10.2 and clone 17.2 cells exhibited 12.5 and 11.8 % cells with an abnormal centrosome number, compared to control cells, cells with the single shRNA mediated knockdown of *TP73* or a knockout of *TP53* with 5.3, 3.3 and 3 %, respectively. This is in line with data from the literature, where cell lines cultured *in vitro* exhibit usually not more than 15 % of cells with supernumerary centrosomes (Difilippantonio et al., 2009; Mittal et al., 2017).

3.2.2. Overexpression of the centriole duplication regulators Plk4 and Stil leads to a higher proportion of cells with supernumerary centrosomes and to increased interphase microtubule plus end growth rates

To establish a correlation between supernumerary centrosomes and increased microtubule plus end assembly rates, the centriole duplication regulators Plk4 and Stil were overexpressed in non-invasive melanoma cell lines that exhibit no supernumerary centrosomes and the effect on microtubule polymerization rates in interphase was analyzed. The successful overexpression of *PLK4* and *STIL* was verified by western blots (Figure 3.13A). As expected, the overexpression of *PLK4* and *STIL* led in both non-invasive cell lines to a higher proportion of cells with supernumerary centrosomes (Figure 3.13B) with 2.7 % in SK-Mel-19 control transfected cells and 7.3 % and 13.3 % for cells transfected with a *STIL* or *PLK4* overexpressing plasmid, respectively. SK-Mel-173 control transfected cells exhibited 2.2 % of cells with supernumerary centrosomes, whereas the overexpression of *STIL* or *PLK4* resulted in 6 or 9 % of cells with an abnormal number of centrosomes. Interestingly, *PLK4* as well as *STIL* overexpression led to a significant increase of interphase microtubule polymerization rates in SK-Mel-19 and SK-Mel-173 cells. SK-Mel-19 cells exhibited microtubule growth rates from 19.8 to 23.8 µm/min for *PLK4* and from 19.8 to 23.6 µm/min for *STIL* overexpression. In SK-Mel-173 cells microtubule growth rates were elevated from 19.2 to 22.2 µm/min for *PLK4* and from 19.3 to 22.6 µm/min for *STIL* overexpression (Figure 3.13C and D). This might indicate a link between the centrosome number and microtubule plus end assembly. Since HCT116 + *TP73*shRNA/*TP53*$^{-/-}$ cells showed a similar higher proportion of cells with supernumerary centrosome compared to control cells, HCT116 cells were used for the overexpression of *PLK4* and *STIL*. Representative western blots of the overexpression are shown Figure 3.14A.

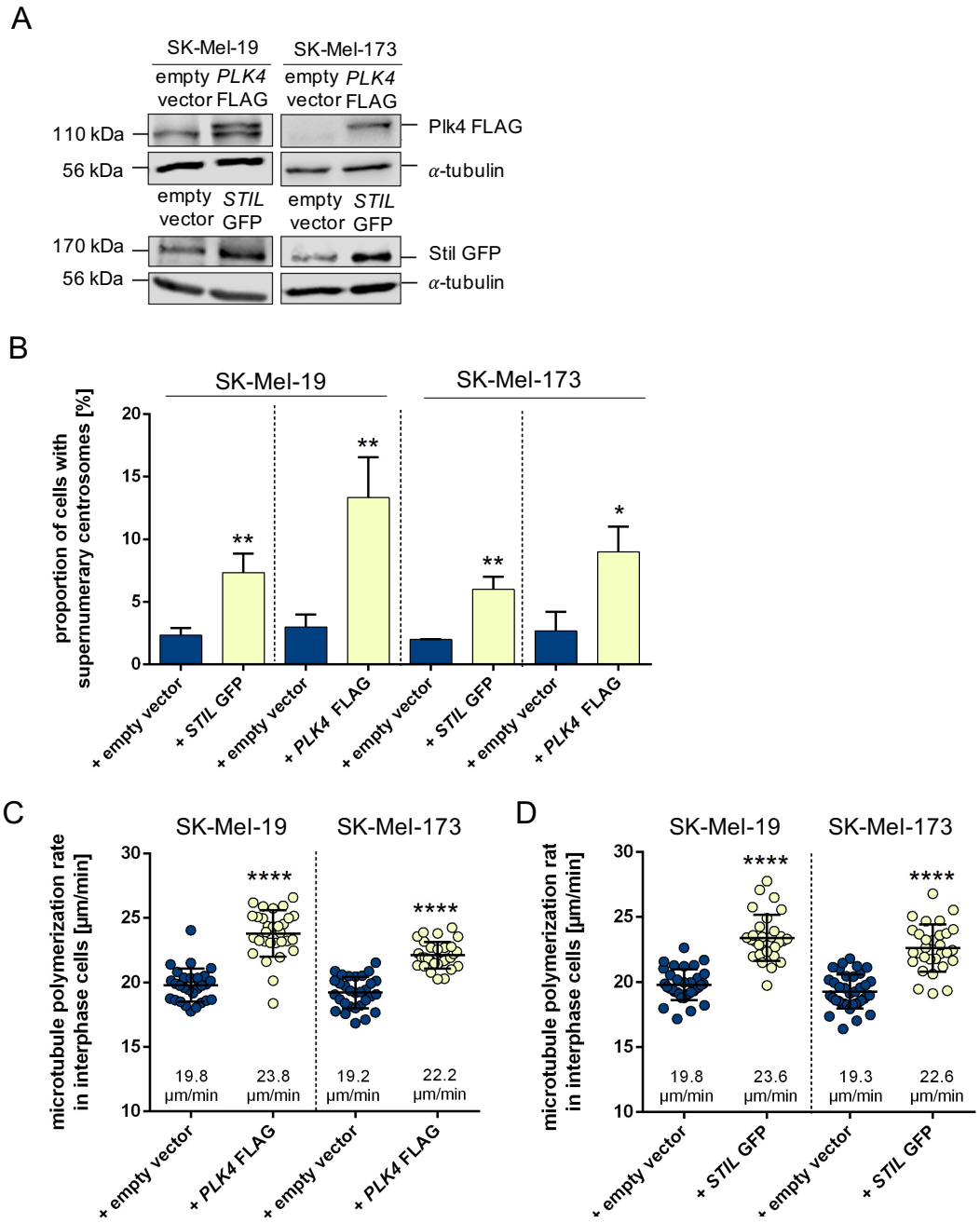

Figure 3.13 PLK4 and STIL overexpression increases the centrosome number and accelerates microtubule plus end growth rates in non-invasive melanoma cells. *A) Representative western blots showing PLK4 or STIL overexpression in the non-invasive melanoma cell lines SK-Mel-19 and SK-Mel-173. Protein levels of Plk4 (6H5, mouse, monoclonal antibody (mAb)) and GFP (GF28R, mouse, mAb) were detected. α-tubulin (B-5-1-2, mouse, mAb) served as a loading control. B) Proportion of cells with supernumerary centrosomes exhibiting a transient overexpression of PLK4 or STIL. C) Measurements of interphase microtubule plus end assembly rates in the non-invasive cell lines SK-Mel-19 and SK-Mel-173 with a transient overexpression of PLK4. D) Measurements of interphase microtubule plus end assembly rates in non-invasive cell lines upon transient overexpression of STIL. Scatter dot plots, mean values ± SD, n=30, 20 microtubules were measured per cell, t-test. Bar graphs, mean values ± SD, n=300, t-test. The p-values are defined as: **** = p ≤ 0.0001, ** = p ≤ 0.01, * = p ≤ 0.05. Significances refer to corresponding control cells. Dotted lines separate different cell lines or transfections within one graph.*

Similar to melanoma cells, the overexpression of *PLK4* and *STIL* led to a higher proportion of cells with supernumerary centrosomes with 4.3 to 15.5 % and 3.2 to 10.3 %, respectively (Figure 3.14B). HCT116 cells with *PLK4* or *STIL* overexpression exhibited increased microtubule plus end growth rates up to 20.0 and 20.1 µm/min, respectively (Figure 3.14C and D). Interestingly, *PLK4* overexpression was not sufficient to induce microtubule growth rates during mitosis, suggesting a specificity of aberrant centrosome amplification and microtubule plus end growth rates in interphase (Figure 3.14C).

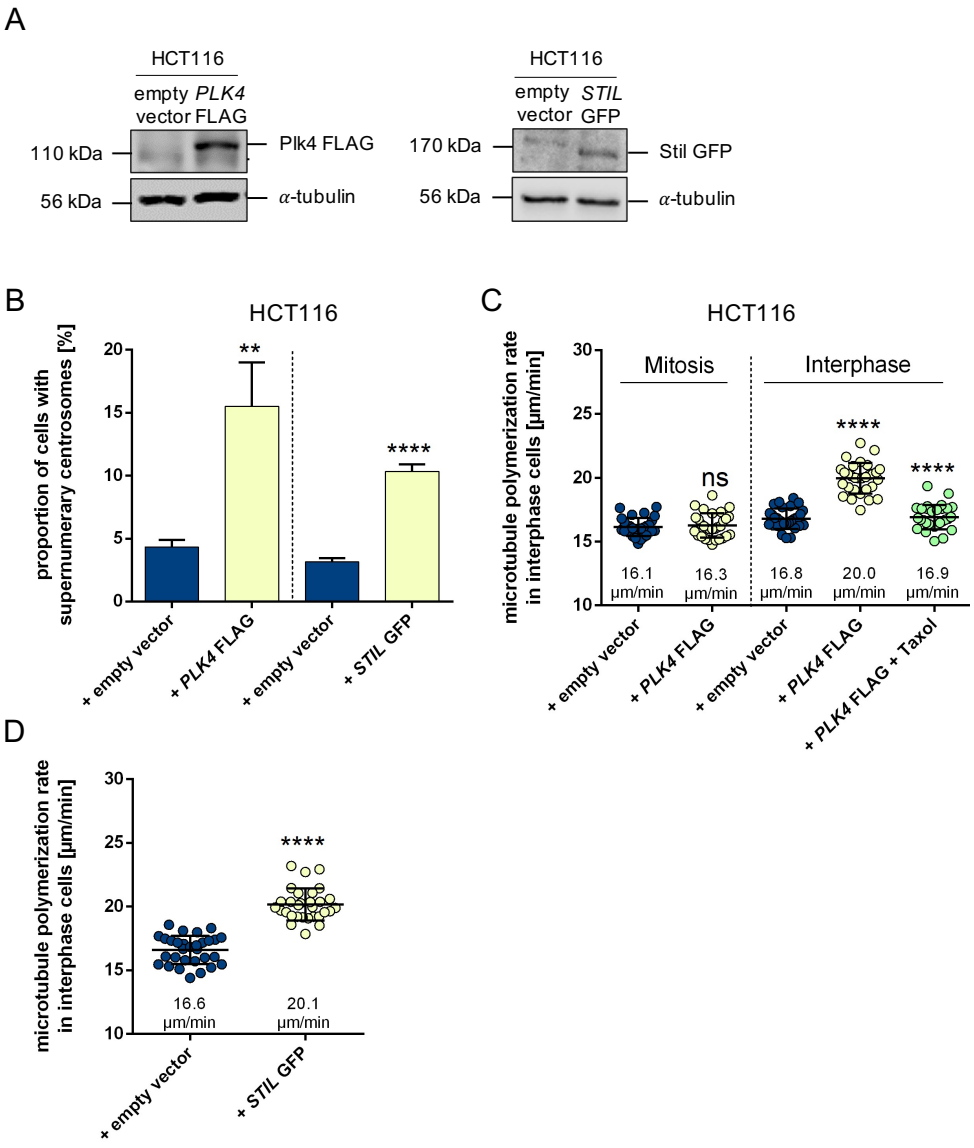

Figure 3.14 PLK4 and STIL overexpression induces supernumerary centrosomes and accelerates microtubule plus end growth rates in HCT116 cells. *A) Representative images of western blots showing protein levels of Plk4 (6H5, mouse, monoclonal antibody (mAb)) and GFP (GF28R, mouse, mAb) in HCT116 cells. α-tubulin (B-5-1-2, mouse, mAb) was used as a loading control. B) Quantification of the proportion of cells with supernumerary centrosomes after overexpression of PLK4 or STIL. Cells were stained for γ-tubulin (GTU88, mouse, mAb) to detect interphase centrosomes. C) Measurements of interphase microtubule plus end assembly rates in control cells transfected with a PLK4 overexpressing plasmid. Growth rates of mitotic and interphase cells were measured. To analyze mitotic cells, cells were treated one hour before live cell measurements with 2 µM DME. For the rescue of increased growth rates, cells were treated 2 h before and during*

*microtubule growth rate measurements with 0.2 nM of Taxol. D) Measurements of interphase microtubule plus end assembly rates in control cells transfected with a plasmid for the overexpression of STIL. Scatter dot plots show mean values ± SD, n=30. Every experiment includes 10 cells with 20 microtubules were measured per cell. Bar graphs show mean values ± SD, n=300. The statistically analysis was done using an unpaired t-test. The indicated p-values are defined as followed: **** = p ≤ 0.0001, ** = p ≤ 0.01. Significances refer to control cells. Dotted lines separate different transfections or cell cycle phases within one graph.*

3.2.3. The co-cultivation of invasive cells with non-invasive cells leads to an increase of microtubule plus end growth rates in non-invasive interphase cells

Based on the findings of the Godinho lab in 2018, I analyzed if the co-cultivation of invasive cell lines characterized by an increased microtubule plus end dynamic and a higher proportion of cells with supernumerary centrosomes with non-invasive cells would affect the microtubule plus end growth rates in non-invasive cell lines.

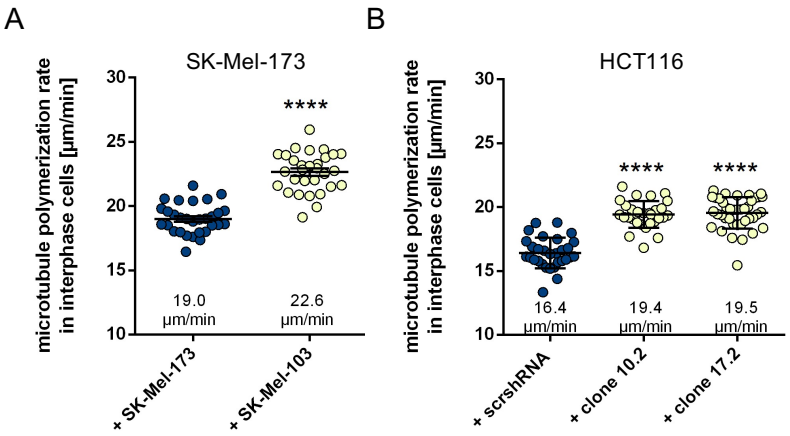

Figure 3.15 Microtubule plus end assembly rates in non-invasive cells are increased upon co-cultivation with invasive cell lines. *A) Measurements of interphase microtubule plus end assembly rates in SK-Mel-173 cells that were co-cultivated with the invasive cell line SK-Mel-103 (1:1). Cells were co-cultured for 24 h before measuring microtubule plus end assembly rates. SK-Mel-173 cells were co-cultivated with non-invasive SK-Mel-173 cells as a control. B) Measurements of interphase microtubule plus end assembly rates in non-invasive HCT116 cells co-cultivated with the invasive cell lines HCT116 + TP73shRNA/TP53$^{-/-}$ clone 10.2 and clone 17.2 (1:1). Scatter dot plots show mean values ± SD, n=30. 20 microtubules were measured per cell. The statistically analysis was done using an unpaired t-test. The indicated p-values are defined as: **** = p ≤ 0.0001. The significances refer to corresponding control cells.*

Therefore, the non-invasive cell line SK-Mel-173 expressing GFP-tagged EB3 was co-cultivated with the invasive cell line SK-Mel-103 in a ratio of 1:1 and microtubule polymerization rates in SK-Mel-173 cells were measured. Interestingly, SK-Mel-173 cells co-cultivated with the invasive cell line showed increased microtubule polymerization rates from 19.0 to 22.6 µm/min (Figure 3.15A). The co-cultivation of GFP-tagged EB3 expressing HCT116 control cells with invasive HCT116 + *TP73*shRNA/*TP53*$^{-/-}$ clone 10.2 or clone 17.2 cells resulted also in an increase of microtubule plus end growth rates in control cells (Figure 3.15B).

3.2.4. Paracrine regulation of microtubule plus end growth rates

The co-cultivation of invasive cell lines characterized by a high proportion of cells with supernumerary centrosomes and elevated microtubule polymerization rates with control cell lines resulted in the induction of microtubule plus end growth rates in control cells,

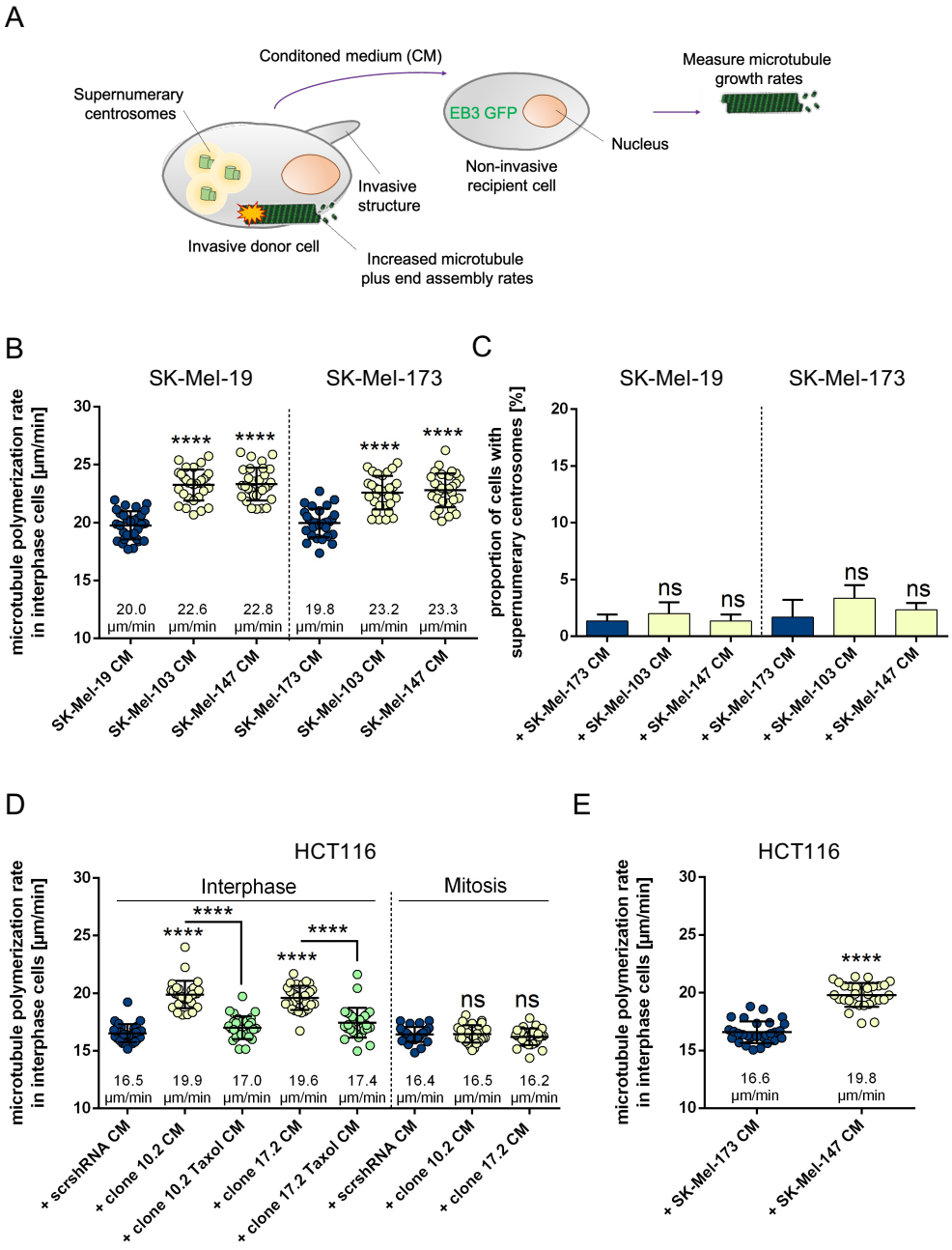

Figure 3.16 Conditioned medium from invasive cell lines is sufficient to induce microtubule plus end growth rates in non-invasive cell lines. *A) Scheme of the experimental set up. B) Measurements of interphase microtubule plus end assembly rates in non-invasive melanoma cell lines treated with invasive conditioned medium (CM). C) Proportion of cells with supernumerary centrosomes in the non-invasive cell lines SK-Mel-19 and SK-Mel-173 after treatment with conditioned medium from invasive cells. Cells were treated with conditioned medium for 48 h before fixation. Conditioned medium derived from the non-invasive cell line SK-Mel-173 was used as a control. D) Measurements of interphase microtubule plus end assembly rates in non-invasive HCT116 cells treated with conditioned medium derived from invasive cells. Increased growth rates during*

*interphase were rescued with 0.2 nM of Taxol. Mitotic microtubule growth rates were measured by adding 2 µM DME to the cells one hour before starting measurements. E) Measurements of interphase microtubule plus end assembly rates in non-invasive colorectal cancer cell lines treated with conditioned medium from invasive melanoma cells. Scatter dot plots show mean values ± SD, n=30, 20 microtubules were measured per cell, t-test. Bar graphs show mean values ± SD, n=300, t-test. The indicated p-values are defined as: **** = p ≤ 0.0001, non-significant (ns) = p > 0.05. The indicated significances refer to control cells. Different cell lines or cell cycle stages presented in one graph are separated through a dotted line.*

suggesting the possibility for paracrine regulation of microtubule plus end growth rates. To analyze this, the non-invasive cell lines SK-Mel-19 and SK-Mel-173 (recipient cells) were incubated with conditioned media (CM) derived from the invasive cell lines SK-Mel-103 and SK-Mel-147 (donor cells). Microtubule polymerization rates and centrosome number specifically in the EB3-GFP transfected recipient cells were determined in interphase cells (Figure 3.16A).

Intriguingly, treatment of non-invasive cells with conditioned medium derived from invasive cells was sufficient to accelerate microtubule plus end growth rates in the recipient cell lines (Figure 3.16B). Microtubule growth rates were increased from control cell level of 20.0 µm/min to 22.6 and 22.8 µm/min in SK-Mel-19 cells and from 19.8 µm/min to 23.2 and 23.3 µm/min in SK-Mel-173 cells when treated with conditioned medium from SK-Mel-103 or SK-Mel-147 cells, respectively. Importantly, the treatment of non-invasive melanoma cell lines with conditioned medium from invasive cells did not change the proportion of cells with supernumerary centrosomes (Figure 3.16C), indicating that an induction of centrosome amplification does not account for the observed increase in microtubule plus end growth rates. Microtubule plus end growth rates in interphase were also increased in HCT116 control cells treated with conditioned medium from invasive HCT116 + *TP73*shRNA/*TP53*$^{-/-}$ cells (Figure 3.16D). Interestingly, conditioned medium from invasive cells did not accelerate the growth rates of microtubules in mitotic cells. The conditioned medium from invasive melanoma cell lines was also active enough to induce microtubule polymerization rates in HCT116 cells (Figure 3.16E), excluding a cell type specific effect.

3.2.5. Paracrine signaling from cells with *PLK4* or *STIL* overexpression is sufficient to induce microtubule polymerization rates in non-invasive cell lines without affecting the number of centrosomes

The conditioned medium from invasive colorectal or melanoma cell lines was sufficient to induce microtubule polymerization rates in non-invasive cell lines otherwise exhibiting normal microtubule growth rates. For the following experiments, conditioned medium from non-invasive cell lines with a transient overexpression of *PLK4* or *STIL*, which was shown to induce supernumerary centrosomes and microtubule growth rates in donor cells, was

collected and microtubule growth rates in non-invasive recipient cells were measured after incubation with the conditioned medium (Figure 3.17A).

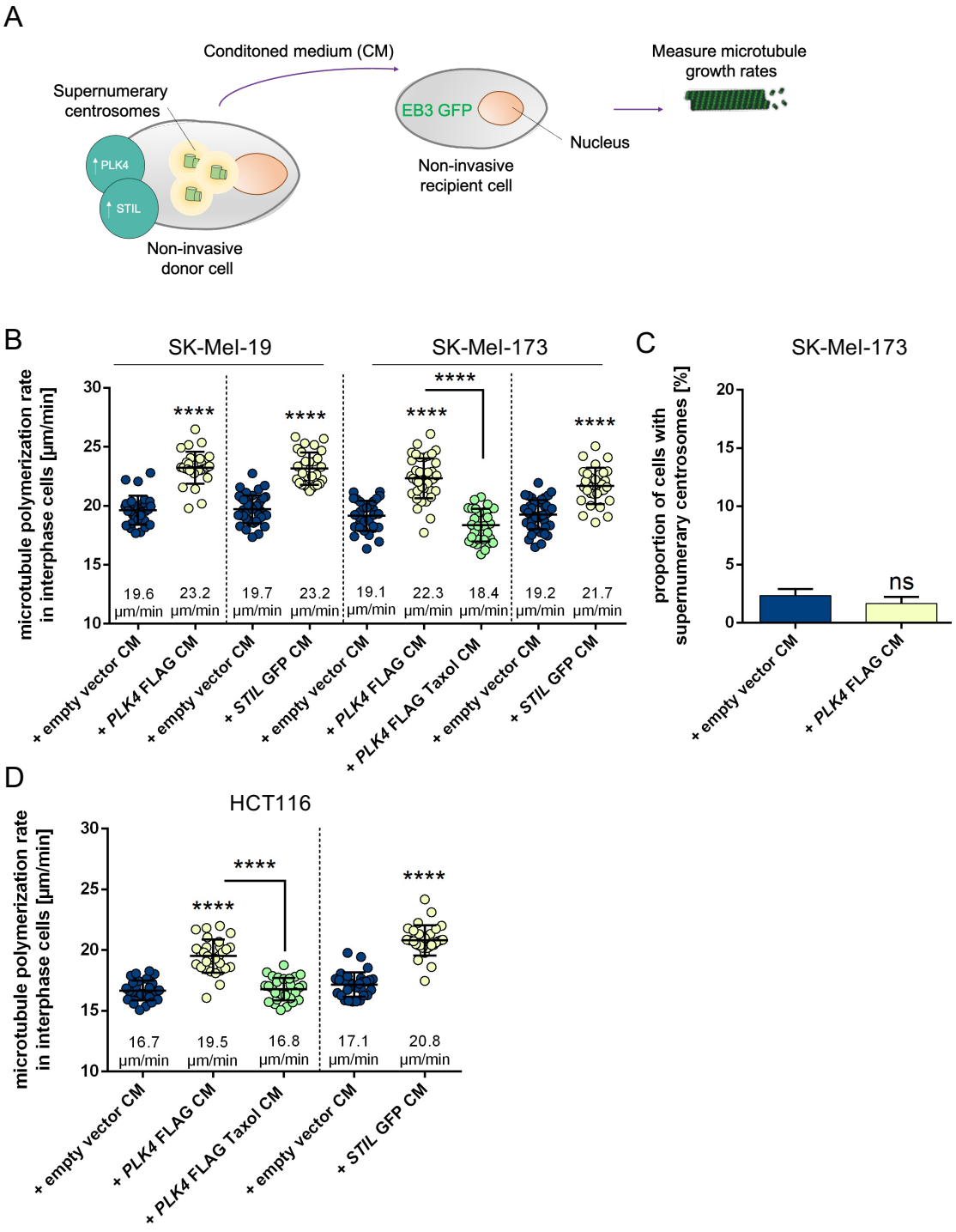

Figure 3.17 Paracrine signaling from colorectal cancer or melanoma cells overexpressing PLK4 or STIL is sufficient to induce microtubule plus end assembly rates. *A) Scheme of the experimental set up. B) Measurements of interphase microtubule plus end assembly rates in melanoma cells treated with conditioned medium (CM) derived from cells overexpressing PLK4 or STIL. Where indicated, 0.2 nM of Taxol was added to conditioned medium before cells were incubated and analyzed. C) Quantification of the proportion of SK-Mel-173 cells with an abnormal number of centrosomes after treatment with conditioned medium from cells with a transient overexpression of PLK4. Cells were stained for γ-tubulin (GTU88, mouse, monoclonal antibody) and cells with more than two centrosomes were defined as cells with supernumerary centrosomes. D)*

*Measurements of interphase microtubule plus end assembly rates in colorectal cancer cells treated with conditioned medium from HCT116 cells overexpressing PLK4 or STIL. 0.2 nM of Taxol was added to conditioned medium to restore normal microtubule plus end assembly rates. Scatter dot plots present the mean values ± SD, n=30. 20 microtubules were measured per cell. Bar graphs show the mean values ± SD, n=300. All experiments were statistically analyzed using an unpaired t-test. The indicated p-values are defined as followed: **** = p ≤ 0.0001. The indicated significances refer to corresponding control cells. Dotted lines separate different experimental conditions within one graph.*

To obtain conditioned medium from transfected cells, cells were washed 24 h after transfection and incubated for 24 h with serum-free medium. Non-invasive cells transfected with GFP-tagged EB3 were incubated with the conditioned medium. Conditioned medium from *PLK4* as well as *STIL* overexpressing cells was sufficient to accelerate microtubule growth rates in non-invasive recipient melanoma cell lines (Figure 3.17B). SK-Mel-19 cells treated with conditioned medium derived from control cells exhibited a growth rate of 19.6/19.7 µm/min, which was induced to 23.2 µm/min when treated with conditioned medium from melanoma cells with a transient overexpression of *PLK4* or *STIL*. SK-Mel-173 cells exhibited a control growth rate of 19.1/19.2 µm/min, which was accelerated to 22.3 or 21.7 µm/min when treated with conditioned medium derived from melanoma cells with a transient overexpression of *PLK4* or *STIL*. The inductive effect of conditioned medium from cells transiently overexpressing *PLK4* was rescued to 18.4 µm/min using sub-nanomolar concentrations of Taxol. However, treatment of the non-invasive cell line SK-Mel-173 with conditioned medium from cells overexpressing *PLK4* was not affecting the proportion of cells with supernumerary centrosomes (Figure 3.17C), indicating that the paracrine signaling is not dependent on supernumerary centrosomes.

The same set up with colorectal cancer cells showed that the conditioned medium from *PLK4* or *STIL* overexpressing HCT116 cells was also sufficient to induce interphase microtubule plus end growth rates in parental HCT116 cells (Figure 3.17D), excluding a cell type specific effect.

3.2.6. Conditioned medium from cells with *CKAP5* overexpression is sufficient to induce microtubule polymerization rates in non-invasive cell lines independent from centrosome amplification

PLK4 overexpression in donor cells led to accelerated microtubule growth rates and induced supernumerary centrosomes. Treating non-invasive recipient cells with conditioned medium from these *PLK4* overexpressing cells resulted in induced microtubule plus end assembly without affecting the number of centrosomes in recipient cells (Figure 3.17). To distinguish between a paracrine signaling that was induced through accelerated microtubule growth rates or through the abnormal number of centrosomes, I overexpressed the microtubule polymerase chTOG in non-invasive cell lines.

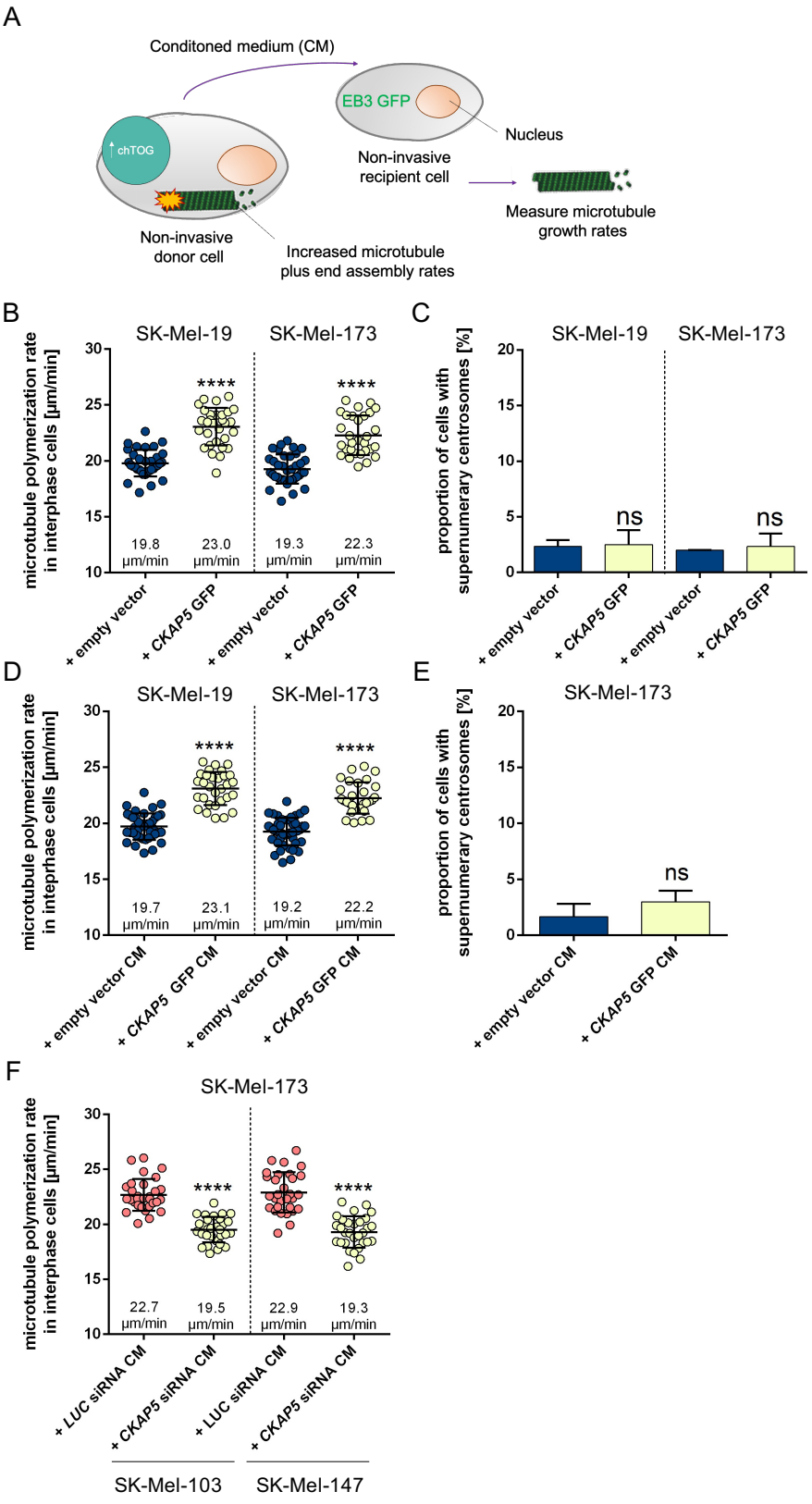

Figure 3.18 Conditioned medium derived from cells overexpressing CKAP5 is sufficient to induce microtubule plus end growth rates. *A) Scheme of the experimental set up. B) Measurements of interphase microtubule plus end assembly rates in non-invasive melanoma cell lines with overexpression of CKAP5. The data from this graph were already shown in Figure 3.8. C) Proportion of cells with supernumerary centrosomes after CKAP5 overexpression. Cells were stained for γ-tubulin (GTU88, mouse, monoclonal antibody) to detect centrosomes. D) Measurements of*

*interphase microtubule plus end assembly rates in non-invasive melanoma cell lines treated with conditioned medium (CM) from cells with an overexpression of CKAP5. E) Proportion of cells with supernumerary centrosomes after treatment with conditioned medium derived from cells overexpressing CKAP5. Cells were stained with an antibody against γ-tubulin to detect centrosomes. F) Measurements of interphase microtubule plus end assembly rates in non-invasive melanoma cell lines treated with conditioned medium from SK-Mel-103 and SK-Mel-147 cells with a transient knockdown of CKAP5. LUCIFERASE (LUC) transfected cells were used as a control. Scatter dot plots show the mean values ± SD, n=30, 20 microtubules were measured per cells, t-test. Bar graphs show the mean values ± SD, n=300, t-test. The indicated p-values are defined as: **** = p ≤ 0.0001 and non-significant (ns) = p > 0.05. The significances refer to corresponding control cells. Different cell lines within one graph are separated through dotted lines.*

CKAP5 overexpression induced increased microtubule growth rates (Figure 3.18B). However, the overexpression of *CKAP5* did not change the proportion of cells with supernumerary centrosomes (Figure 3.18C), indicating that *CKAP5* overexpression provides the possibility to distinguish between paracrine signaling that is induced through supernumerary centrosomes or increased microtubule plus end assembly rates in interphase.

In the next step, non-invasive recipient cells were incubated 2 h before microtubule polymerization rate measurements with conditioned medium (CM) derived from *CKAP5* overexpressing cells (Figure 3.18A). Interestingly, microtubule growth rates of non-invasive recipient cells were accelerated when treated with conditioned medium from *CKAP5* overexpressing donor cells (Figure 3.18D). The non-invasive cell line SK-Mel-19 exhibited an accelerated interphase microtubule growth rate from 19.7 to 23.1 µm/min and the non-invasive cell line SK-Mel-173 showed an enhanced microtubule polymerization rate from 19.2 to 22.2 µm/min (Figure 3.18D). However, treatment of recipient cells with conditioned medium from cells with a transient overexpression of *CKAP5* did not change the proportion of cells with supernumerary centrosomes in non-invasive recipient cells (Figure 3.18E). To prove further that accelerated microtubule growth rates in donor cells are responsible for the effects in recipient cells, a transient siRNA mediated knockdown of *CKAP5* was used to restore normal microtubule plus end assembly rates in invasive cell lines. Conditioned medium from these cells was collected and non-invasive recipient cells were incubated 2 h before measuring interphase microtubule growth rates. Indeed, SK-Mel-173 cells treated with conditioned medium from invasive cells with a transient knockdown of *CKAP5* did no longer show accelerated microtubule growth rates compared to invasive conditioned medium from *LUC* transfected cells (Figure 3.18F).

The same effects were seen in the colorectal cancer cell line HCT116. HCT116 cells with a transient overexpression of *CKAP5* (Figure 3.19A) showed accelerated microtubule growth rates (Figure 3.19B) without inducing supernumerary centrosomes (Figure 3.19C).

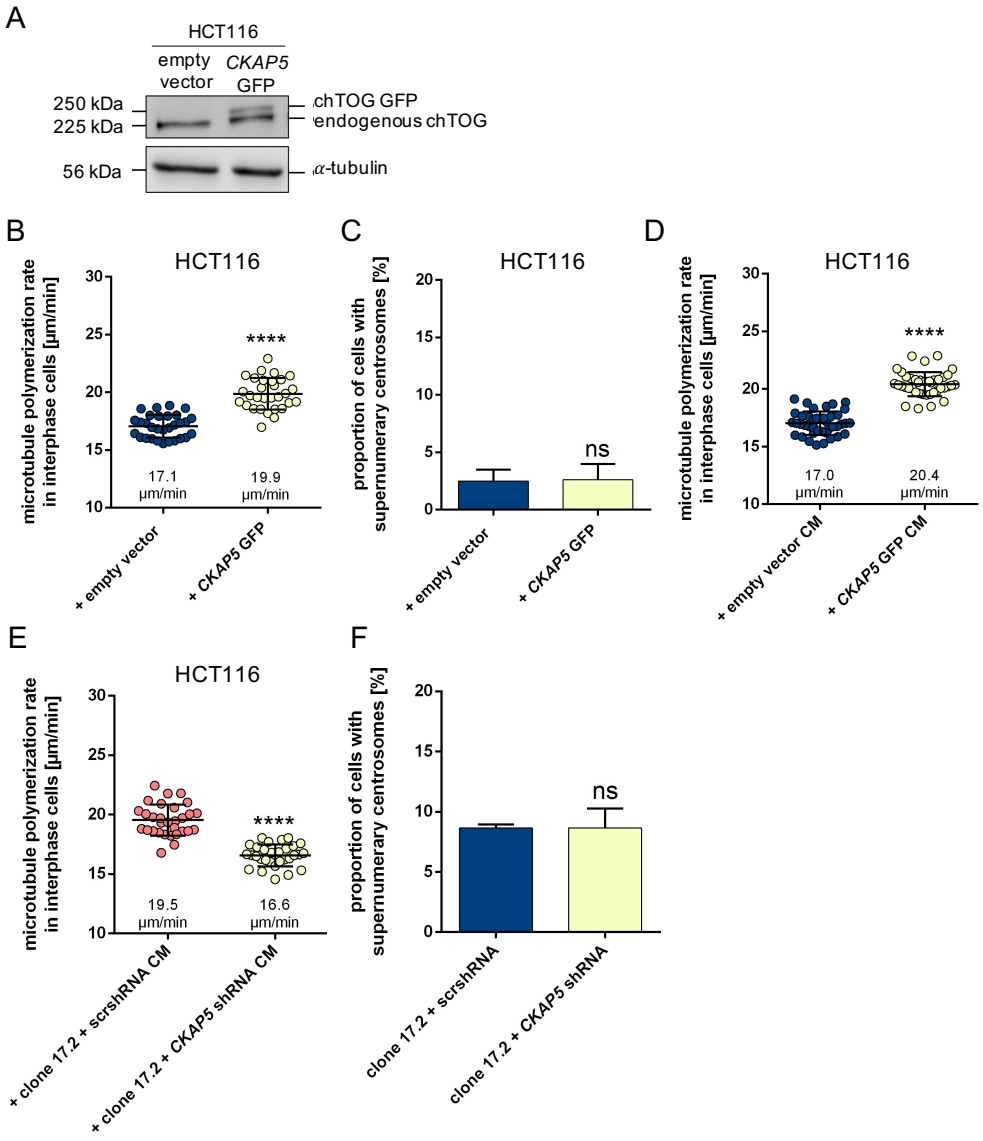

Figure 3.19 Conditioned medium from HCT116 cells with a transient overexpression of CKAP5 induces microtubule plus end growth rates in recipient HCT116 cells. *A) Representative western blots showing the overexpression of CKAP5 in HCT116 cells. Protein levels of GFP (GF28R, mouse, monoclonal antibody (mAb)) and chTOG (H-4, mouse, mAb) were detected. α-tubulin (B-5-1-2, mouse, mAb) served as the loading control. B) Measurements of interphase microtubule plus end assembly in HCT116 cells after overexpression of CKAP5. C) Quantification of the proportion of cells with supernumerary centrosomes after CKAP5 overexpression. Centrosomes were detected using an antibody against γ-tubulin (GTU88, mouse, mAb). D) Measurements of microtubule plus end growth rates in interphase cells upon treatment with conditioned medium (CM) from cells with a transient overexpression of CKAP5. E) Measurements of microtubule plus end growth rates in interphase cells upon treatment with conditioned medium from HCT116 + TP73shRNA/TP53$^{-/-}$ (clone 17.2) cells with a stable shRNA-mediated knockdown of CKAP5. F) Proportion of cells with supernumerary centrosomes in HCT116 + TP73shRNA/TP53$^{-/-}$ clone 17.2 cells with a stable knockdown of CKAP5. Scatter dot plots show the mean values ± SD, n=30, 20 microtubules were measured per cell, t-test. Bar graphs show the mean values ± SD, n=3, 300 cells in total, t-test. The indicated p-values are defined as: **** = p ≤ 0.0001 and non-significant (ns) = p > 0.05. The indicated significances refer to corresponding control cells.*

HCT116 cells treated with conditioned medium from *CKAP5* overexpressing cells exhibited increased microtubule growth rates from 17.0 to 20.4 µm/min (Figure 3.19D), while

conditioned medium collected from HCT116 + *TP73*shRNA/*TP53*$^{-/-}$ clone 17.2 cells with a stable knockdown of *CKAP5* was no longer able to induce microtubule growth rates (Figure 3.19E). Again, the stable knockdown of *CKAP5* did not affect the increased proportion of cells with supernumerary centrosomes seen in HCT116 + *TP73*shRNA/*TP53*$^{-/-}$ cells (Figure 3.19F). Taken together, the data imply that the trigger for secretion of microtubule growth rate inducing factors might be the accelerated microtubule plus end growth rates in donor cells rather than the increased number of centrosomes.

3.2.7. Increased microtubule plus end growth rates in invasive melanoma cells are regulated by centrosome-associated microtubule nucleation factors

The outgrowth of microtubules from the centrosomes requires their nucleation and polymerization (Roostalu & Surrey, 2017). Important nucleation factors are γ-tubulin, the main component of the γ-tubulin ring complex and the anchor of microtubules to the centrosome, and the centrosomal protein 192 (Cep192), an important component of the pericentriolar material and a crucial factor for further recruitment of microtubule nucleation promoting factors (Roostalu & Surrey, 2017).

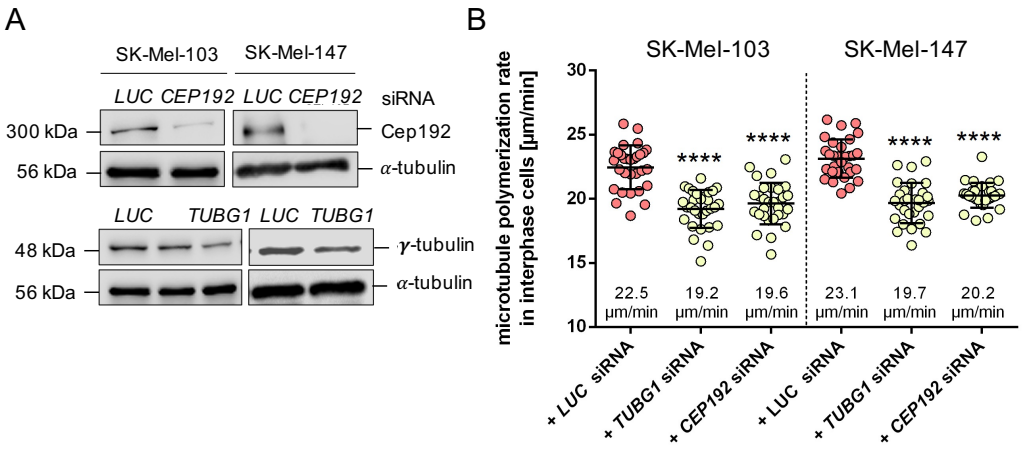

Figure 3.20 Partial depletion of the microtubule nucleators γ-tubulin and Cep192 suppresses microtubule plus end growth rates in invasive melanoma cells. *A) Representative western blots showing the siRNA mediated knockdown of TUBG1 and CEP192 in the invasive cell lines SK-Mel-103 and SK-Mel-147. Protein levels of Cep192 (rabbit, polyclonal antibody) and γ-tubulin (GTU88, mouse, monoclonal antibody (mAb)) were detected. α-tubulin (B-5-1-2, mouse, mAb) was used as a loading control. B) Measurements of interphase microtubule plus end assembly rates in invasive cell lines with a transient knockdown of TUBG1 and CEP192. Scatter dot plots, mean values ± SD, n=30, 20 microtubule were measured per cell, t-test. The indicated p-values are defined as followed: **** = p ≤ 0.0001. The indicated significances refer to corresponding control cells. Different cell lines within one graph are separated by a dotted line.*

To analyze if nucleation factors might affect microtubule plus end assembly, I knocked down *TUBG1* and *CEP192* by using siRNAs in invasive melanoma cell lines (Figure 3.20A) and measured microtubule plus end growth rates. Interestingly, cells with a knockdown of

TUBG1 and *CEP192* exhibited reduced microtubule plus end growth rates (Figure 3.20B), indicating that the nucleation factors γ-tubulin and Cep192 are affecting microtubule plus end assembly rates in interphase. Vice versa, overexpression of *TUBG1* and *CEP192* in the non-invasive cell line SK-Mel-173 (Figure 3.21A) was sufficient to increase microtubule plus end growth rates from 19.4 µm/min to about 22 µm/min (Figure 3.21B), while not affecting the number of centrosomes (Figure 3.21C). Intriguingly, conditioned medium collected from *TUBG1* or *CEP192* overexpressing cells was sufficient to induce microtubule plus end assembly in non-invasive cells (Figure 3.21D).

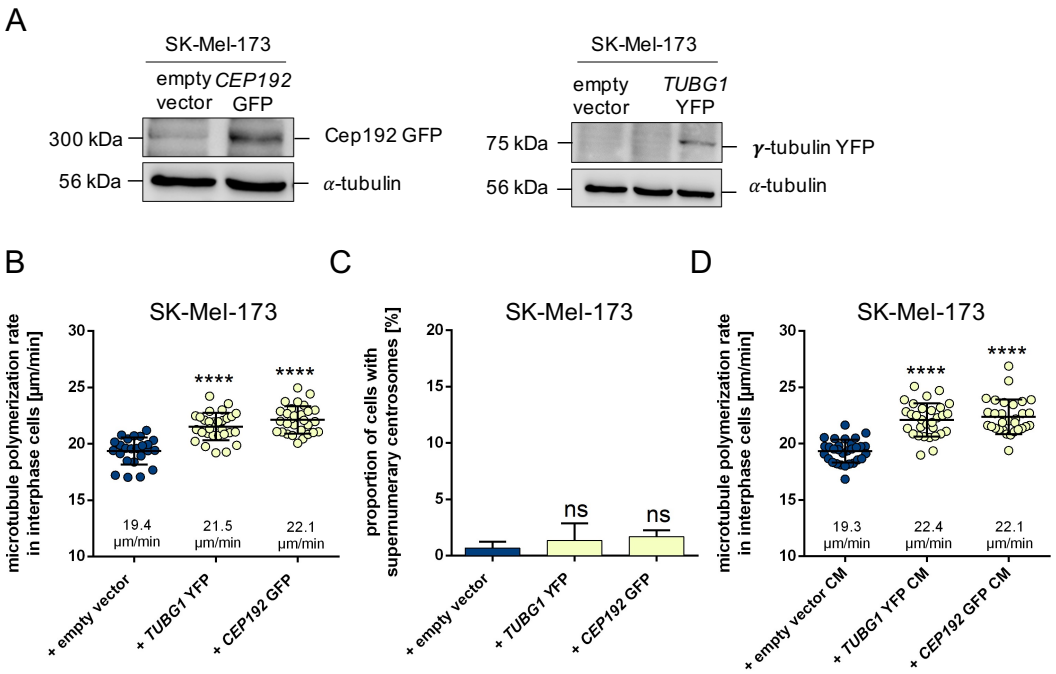

Figure 3.21 Overexpression of TUBG1 and CEP192 and conditioned medium from cells with a TUBG1 or CEP192 overexpression induce enhanced microtubule growth rates. *A) Representative western blots showing the transient overexpression CEP192 or TUBG1 in SK-Mel-173 cells. Protein levels of Cep192 (rabbit, polyclonal antibody) and γ-tubulin (GTU88, mouse, monoclonal antibody (mAb)) were detected. α-tubulin (B-5-1-2, mouse, mAb) was used as the loading control. B) Measurements of interphase microtubule plus end growth rates in SK-Mel-173 cells after the transient overexpression of TUBG1 or CEP192. C) Quantification of the proportion of cells with supernumerary centrosomes after the transient overexpression of TUBG1 or CEP192. Cells were defined as cells with supernumerary centrosomes when more than two centrosomes were counted. D) Measurements of interphase microtubule plus end growth rates in SK-Mel-173 cells after treatment with conditioned medium (CM) from cells with a transient overexpression TUBG1 or CEP192. Scatter dot plots show mean values ± SD, n=30, 20 microtubules were measured per cell, t-test. Bar graphs show mean values ± SD, n=300, t-test. The indicated p-values are defined as: **** = p ≤ 0.0001 and non-significant (ns) = p > 0.05. The significances refer to control cells.*

3.2.8. The induction of microtubule plus end growth rates upon centrosome amplification is dependent on the microtubule nucleation factors γ-tubulin and Cep192

Since the knockdown or overexpression of microtubule nucleation factors affected microtubule plus end assembly rates in melanoma cells, I investigated whether these

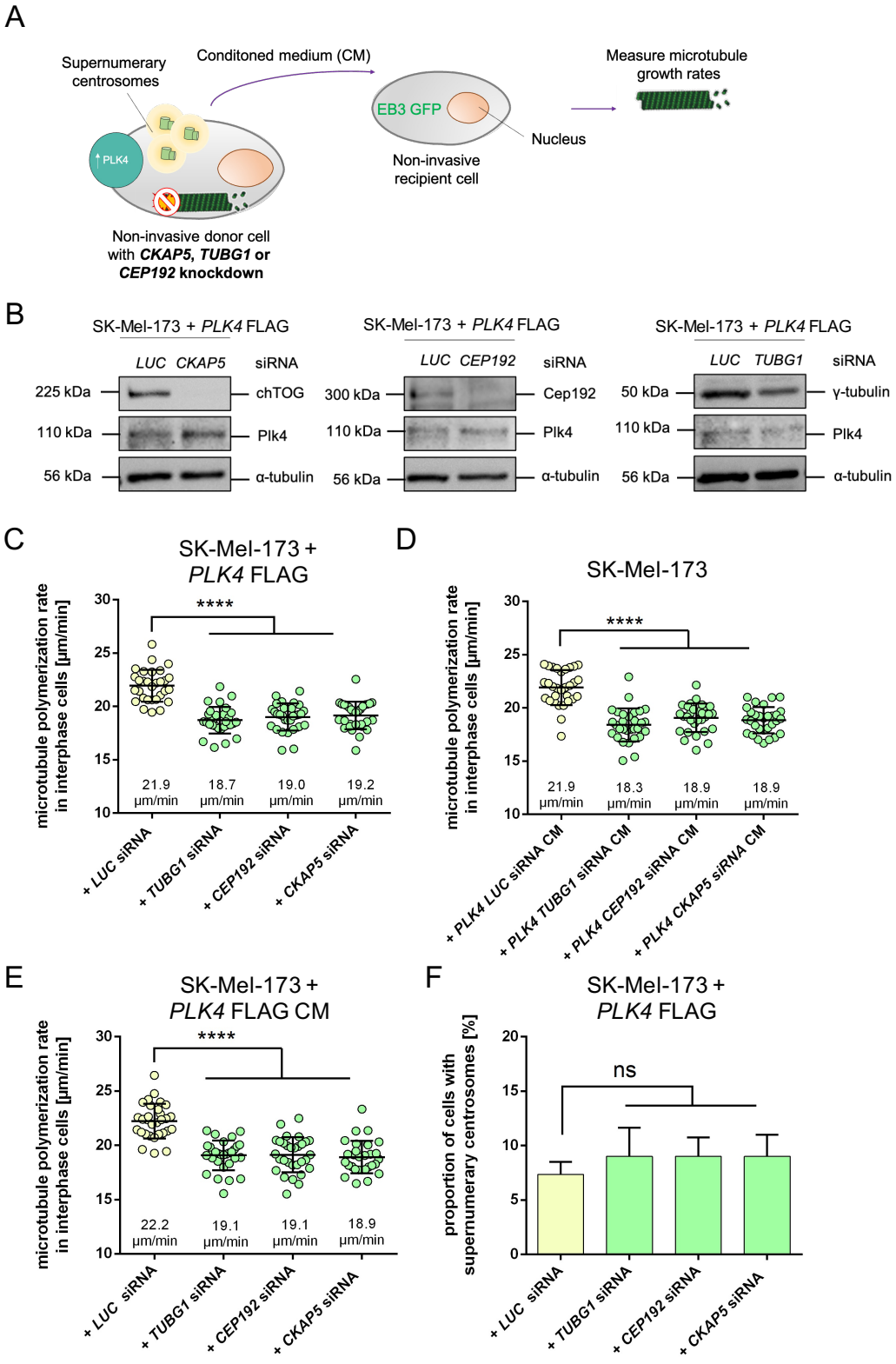

Figure 3.22 Centrosome-induced microtubule growth rates are dependent on the microtubule nucleators γ-tubulin and Cep192 in melanoma cells. *A) Scheme of the experimental set up. B) Representative western blots showing the overexpression of PLK4 and the simultaneous knockdown of CKAP5, TUBG1 or CEP192 in SK-Mel-173 cells. Protein levels of Plk4 (6H5, mouse, monoclonal antibody (mAb)), chTOG (H-4, mouse, mAb), Cep192 (rabbit, polyclonal antibody) and γ-tubulin (GTU88, mouse, mAb) were detected. α-tubulin (B-5-1-2, mouse, mAb) was used as a loading control. C) Measurements of interphase microtubule plus end growth rates in SK-Mel-173*

*cells transfected with a PLK4 overexpressing plasmid and a siRNA targeting CKAP5, TUBG1 or CEP192. D) Measurements of interphase microtubule plus end growth rates in SK-Mel-173 cells transfected with a PLK4 overexpressing plasmid and treated with conditioned medium (CM) derived from cells with a transient knockdown of CKAP5, TUBG1 or CEP192. E) Measurements of interphase microtubule plus end growth rates in SK-Mel-173 cells transfected with a siRNA targeting CKAP5, TUBG1 or CEP192 and treated with conditioned medium from cells overexpressing PLK4. F) Quantification of the proportion of cells with an abnormal number of centrosomes after overexpression of PLK4 and knockdown of CKAP5, TUBG1 or CEP192. Cells with more than two centrosomes were defined as cells with supernumerary centrosomes. Scatter dot plots show mean values ± SD, n=30, 20 microtubules were measured per cell, t-test. Bar graphs show mean values ± SD, n=300, t-test. The indicated p-values are defined as followed: **** = p ≤ 0.0001 and non-significant (ns) = p > 0.05. The significances refer to corresponding control cells.*

nucleation factors are required for centrosome-induced microtubule dynamics. For this, microtubule plus end assembly rates were measured in cells with an overexpression of *PLK4* and knockdown of *TUBG1* and *CEP192*, the knockdown of *CKAP5* served as a control (Figure 3.22A). In total, I used three different approaches: first the effect of the overexpression of *PLK4* and the knockdown of *CKAP5, TUBG1* and *CEP192* on microtubule growth rates in interphase was analyzed. Second, the effect of conditioned medium collected from these cells on recipient cells was determined. And third, the effect of conditioned medium from cells with a transient *PLK4* overexpression on recipient cells with a transient knockdown of *CKAP5, TUBG1* and *CEP192* was analyzed.

The knockdown of *CKAP5, TUBG1* and *CEP192* and the overexpression of *PLK4* was verified by western blot (Figure 3.22B). Non-invasive SK-Mel-173 cells with an overexpression of *PLK4* showed elevated levels of microtubule growth rates of 21.9 µm/min as shown before (Figure 3.13C). The siRNA mediated knockdown of *TUBG1*, *CEP192* or *CKAP5* resulted in the rescue of high microtubule growth rates (Figure 3.22C). Very similar results were obtained when conditioned medium from non-invasive cells with a concomitant overexpression of *PLK4* and a knockdown of *TUBG1*, *CEP192* or *CKAP5* was used (Figure 3.22D). Lastly, non-invasive cells with a knockdown of *TUBG1*, *CEP192* and *CKAP5* were treated with conditioned medium from *PLK4* overexpressing cells. *LUC* control cells treated with conditioned medium from *PLK4* overexpressing cells showed an average high growth rate of 22.2 µm/min. Conditioned medium from cells overexpressing *PLK4* was not able to induce increased microtubule growth rates in non-invasive cells with a knockdown of *TUBG1*, *CEP192* or *CKAP5* (Figure 3.22E). The knockdown of *TUBG1*, *CEP192* and *CKAP5* in *PLK4* overexpressing cells did not change the high proportion of cells with supernumerary centrosomes detected after overexpression of *PLK4* (Figure 3.22F). Thus, the secretion of factors that led to the induction of microtubule growth rates in recipient and the regulation of microtubule growth rates in donor cells is dependent on key regulators of microtubule nucleation and polymerization.

Confirming results were obtained using HCT116 cells. The knockdown of *TUBG1*, *CEP192* and *CKAP5* and the overexpression of *PLK4* in HCT116 cells were verified by western

blotting (Figure 3.23A). HCT116 cells with an overexpression of *PLK4* and the concomitant loss of *TUBG1*, *CEP192* and *CKAP5* were analyzed for changes in microtubule plus end growth rates. Control cells with *PLK4* overexpression showed accelerated growth rates, whereas the additional knockdown of *TUBG1*, *CEP192* or *CKAP5* rescued this defect (Figure 3.23B). The treatment of recipient cells with conditioned medium collected from cells with *PLK4* overexpression was not sufficient to induce growth rates in *TUBG1*, *CEP192* and *CKAP5* siRNA transfected cells (Figure 3.23C). The knockdown of nucleation and polymerization factors in *PLK4* overexpressing cells did not change the number of cells with an abnormal number of centrosomes (Figure 3.23D).

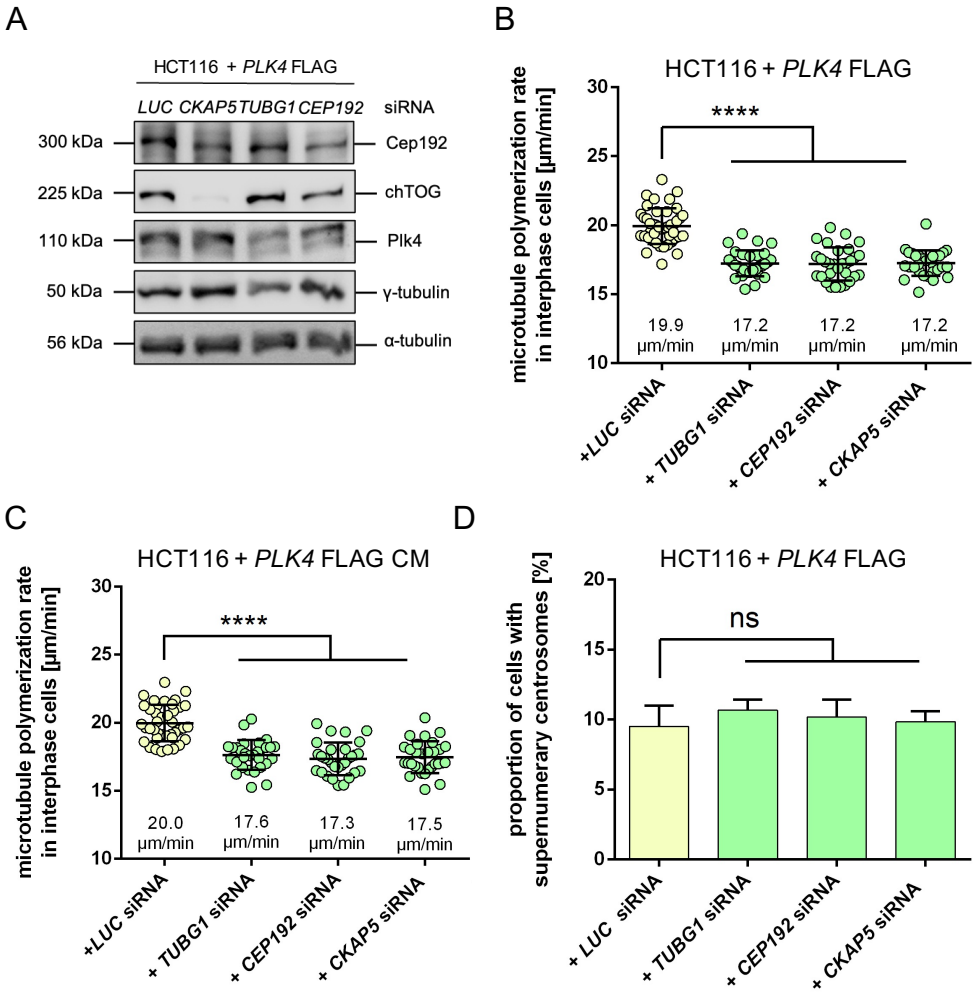

Figure 3.23 Centrosome-induced microtubule growth rates are dependent on the microtubule nucleators γ-tubulin and Cep192 in colorectal cancer cells. *A) Representative western blots from HCT116 cells with an overexpression of PLK4 and simultaneous knockdown of CKAP5, TUBG1 or CEP192. Protein levels of Plk4 (6H5, mouse, monoclonal antibody (mAb)), chTOG (H-4, mouse, mAb), Cep192 (rabbit, polyclonal antibody) and γ-tubulin (GTU88, mouse, mAb) were detected. α-tubulin (B-5-1-2, mouse, mAb) was used as a loading control. B) Measurements of microtubule growth rates in HCT116 cells with overexpression of PLK4 and knockdown of CKAP5, TUBG1 or CEP192. C) Measurements of interphase microtubule growth rates in HCT116 cells transfected with a siRNA targeting CKAP5, TUBG1 or CEP192 and treated with conditioned medium (CM) from PLK4 overexpressing HCT116 cells. D) Quantification of the proportion of cells with*

*supernumerary centrosomes after overexpression of PLK4 and knockdown of CKAP5, TUBG1 or CEP192. Cells were fixed, permeabilized and stained for γ-tubulin to detect centrosomes. Cells with more than two centrosomes were defined as cell with supernumerary centrosomes. Scatter dot plots show mean values ± SD, n=30, 20 microtubules were measured per cell, t-test. Bar graphs show mean values ± SD, n=300, t-test. The indicated p-values are defined as: **** = p ≤ 0.0001 and non-significant (ns) = p > 0.05. The significances refer to control cells.*

3.2.9. HER2 – ERK signaling is part of the paracrine signaling leading to the induction of increased microtubule plus end assembly

Published work showed that paracrine signaling from cells with supernumerary centrosomes is able to induce an invasive phenotype in recipient cells (Arnandis et al., 2018). It was shown that Interleukin-8 (IL8), HER2 and ERK contribute to this effect. To test if these factors are also involved in the paracrine signaling leading to increased microtubule plus end assembly rates, HER2 (Trastuzumab) and ERK (PD98059) inhibitors, as well as an antagonist of the IL8 receptor (SCH-527123) were used.

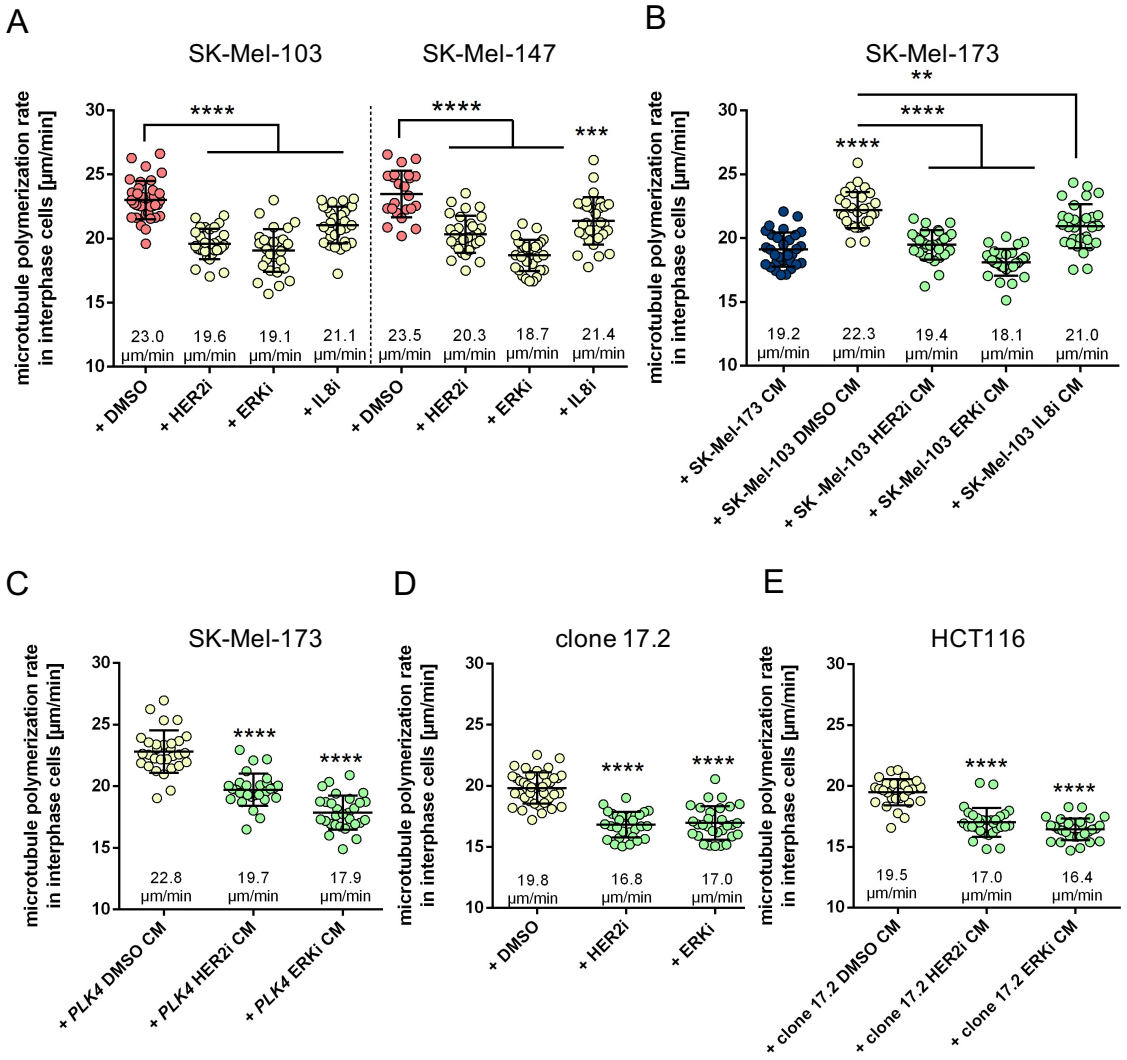

Figure 3.24 The HER2/MAPK pathway mediates the paracrine signaling leading to the induction of microtubule plus end assembly rates in melanoma and colorectal cancer cells. *A) Measurements of interphase microtubule plus end assembly in invasive melanoma cell lines in*

*response to HER2, ERK, or IL8 inhibition. Cells were treated with 40 µM HER2i (Trastuzumab), 20 µM ERKi (PD98059) or 100 nM IL8 inhibitor (SCH-527123). DMSO treatment served as a control. B) Measurements of microtubule growth rates in a non-invasive melanoma cell line after treatment with conditioned medium (CM) derived from invasive cells supplemented with inhibitors. Conditioned media were supplemented with 40 µM HER2i (Trastuzumab), 20 µM ERKi (PD98059) or 100 nM IL8 inhibitor (SCH-527123). C) Measurements of interphase microtubule plus end assembly rates in SK-Mel-173 cells after incubation with conditioned medium from PLK4 overexpressing cells supplemented with inhibitors. Conditioned media were supplemented with 40 µM HER2i (Trastuzumab) or 20 µM ERKi (PD98059). D) Measurements of interphase microtubule plus end assembly rates in HCT116 + TP73shRNA/TP53$^{-/-}$ clone 17.2 cells in response to inhibitor treatment. Cells were treated with 40 µM HER2i (Trastuzumab) or 20 µM ERKi (PD98059). DMSO treatment served as a control. E) Measurements of interphase microtubule plus end assembly rates in HCT116 cells after incubation with conditioned medium from HCT116 + TP73shRNA/TP53$^{-/-}$ clone 17.2 cells supplemented with inhibitors. Conditioned media were supplemented with 40 µM HER2i (Trastuzumab) or 20 µM ERKi (PD98059). Scatter dot plots show mean values ± SD, n=3. Every experiment includes data from 30 cells and 20 microtubules were measured per cell. All experiments were statistically analyzed using an unpaired t-test. The indicated p-values are defined as: **** = p ≤ 0.0001 and ** = p ≤ 0.01. The indicated significances refer to corresponding control cells. The dotted line separates different cell lines within one graph.*

First, the invasive cell lines SK-Mel-103 and SK-Mel-147 were treated with inhibitors for HER2, ERK and IL8 signaling. DMSO treated control cells showed high growth rates with 23.0 µm/min for SK-Mel-103 cells and 23.5 µm/min for SK-Mel-147 cells. The treatment with HER2 (Trastuzumab) and ERK (PD98059) inhibitors rescued the accelerated microtubule growth rates to 19.6 and 19.1 µm/min for SK-Mel-103 cells and 20.3 and 18.7 µm/min for SK-Mel-147 cells, respectively. The antagonist for the IL8 receptor (SCH-527123) showed only a partial rescue of microtubule growth rates in SK-Mel-103 and SK-Mel-147 cells with 21.1 and 21.4 µm/min, respectively (Figure 3.24A). Interestingly, the supplementation of conditioned medium (CM) from invasive cells with the HER2 and ERK inhibitor suppressed the induction of high microtubule growth rates in recipient cells (Figure 3.24B). Addition of conditioned medium from SK-Mel-103 cells to the non-invasive cell line SK-Mel-173 induced growth rates to 22.3 µm/min compared to conditioned medium derived from control cells. Conditioned medium derived from invasive cells supplemented with the HER2 or ERK inhibitor rescued the high growth rates to control cell level.

The supplementation of the conditioned medium with the IL8 antagonist was again only partially rescuing high microtubule plus end growth rates to 21.0 µm/min and was therefore not included in further experiments. Further, conditioned medium from *PLK4* overexpressing cells supplemented with the HER2 and ERK inhibitor was not able to induce high microtubule growth rates in recipient cells (Figure 3.24C), indicating the contribution of HER2/ERK in paracrine signaling mediated induction of microtubule plus end growth rates. Confirming results were obtained with colorectal cancer cell lines. HCT116 + *TP73*shRNA/*TP53*$^{-/-}$ clone 17.2 cells treated with HER2 and ERK inhibitors showed rescued microtubule growth rates of 16.8 or 17.0 µm/min, respectively, compared to DMSO treated cells with 19.8 µm/min (Figure 3.24D). The supplementation of conditioned

medium derived from HCT116 + *TP73*shRNA/*TP53*$^{-/-}$ clone 17.2 cells with HER2 and ERK inhibitors and the incubation of non-invasive recipient cells with the collected conditioned medium was not sufficient to induce microtubule plus end growth rates compared to conditioned medium that was supplemented with DMSO (Figure 3.24E).

3.2.10. Extracellular vesicles mediate paracrine regulation of microtubule plus end dynamics

It is well established that extracellular vesicles can contribute to paracrine signaling in human cancer cells (Menck et al., 2020). To test if extracellular vesicles are involved in paracrine regulation of microtubule plus end assembly rates, collected conditioned medium was centrifuged at 14000 x g to sediment large extracellular vesicles. In addition, the conditioned medium was incubated for 30 min at 56 °C to denature proteins.

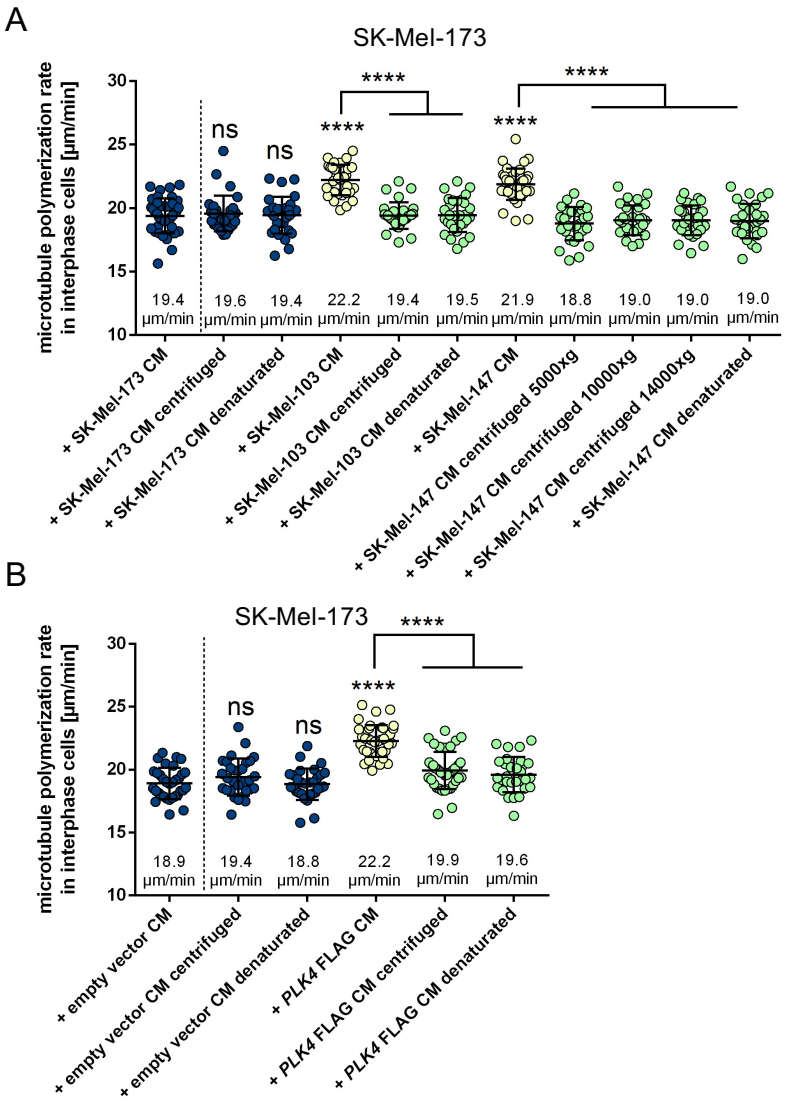

Figure 3.25 Extracellular vesicles mediate paracrine signaling to regulate microtubule growth rates. *A) Measurements of interphase microtubule plus end growth rates in SK-Mel-173 cells after treatment with conditioned medium from invasive cells. Conditioned medium derived from*

*invasive cells was either left untreated, was centrifuged at 5000 x g, 10000 x g, or 14000 x g for 35 min (centrifuged) or was incubated for 30 min at 56 °C (denaturated). B) Measurements of microtubule growth rates in the non-invasive cell line SK-Mel-173 after incubation with conditioned medium from PLK4 overexpressing cells that was either centrifuged or incubated at 56 °C (denaturated). Scatter dot plots show mean values ± SD, n=30, 20 microtubules were measured per cell, t-test. The p-values are defined as: **** = p ≤ 0.0001 and non-significant (ns) = p > 0.05. The indicated significances refer to control cells.*

Both, centrifugation and denaturation eliminated the activity to increase microtubule plus end growth rates (Figure 3.25A). The same was true for conditioned medium derived from cells with a transient overexpression of *PLK4* (Figure 3.25B). Interestingly, conditioned medium from SK-Mel-147 cells was centrifuged at different speed (5000, 10000, 14000 x g) and 5000 x g already eliminated the inductive effect on microtubule plus end assembly rates (Figure 3.25A), indicating that extracellular vesicles of bigger size might contribute to the paracrine signaling. A signaling mediated through exosomes that are sedimented at higher speed (> 100000 x g) was therefore excluded.

3.2.11. Microvesicles induce microtubule polymerization rates in non-invasive melanoma cells possibly in a HER2-dependent manner

Microvesicles are typical 100 to 1000 nm in size and are sedimented at 14000 x g. To enrich microvesicles, conditioned medium from invasive SK-Mel-103 and SK-Mel-147 cells was centrifuged and the microvesicle pellet was resuspended in PBS. The non-invasive cell line SK-Mel-173 was incubated with concentrated microvesicles before measurements of microtubule polymerization rates. Non-invasive cells treated with microvesicles from the invasive cell lines SK-Mel-103 and SK-Mel-147 showed increased microtubule plus end assembly rates with 22.2 and 23.2 µm/min (Figure 3.26B).

Since treatment of donor or recipient cells with the monoclonal antibody against HER2 (Trastuzumab) resulted in rescued microtubule growth rates (Figure 3.24) and microvesicles are known to transport receptors anchored in their plasma membrane to other cells (Nanou et al., 2020), I speculated that invasive cell lines are shedding microvesicles with incorporated HER2. To analyze if the transport of HER2 in the membrane of microvesicles is responsible for increased microtubule plus end growth rates in recipient cells, the isolated microvesicles were pre-incubated for 2 h with 1 µM of an irreversible EGFR/HER2 inhibitor (Canertinib). Subsequently, microvesicles were washed to remove unbound inhibitor (Figure 3.26A). To make sure that the washing steps after the incubation were sufficient to remove the unbound inhibitor, microvesicles were also incubated with the reversible HER2 inhibitor (Trastuzumab). The preincubation of the microvesicles with the irreversible EGFR/HER2 inhibitor abolished the inductive effect of microvesicles. Microtubule growth rates were rescued from 22.2 to 19.8 µm/min after treatment with microvesicles derived from SK-Mel-103 cells and from 23.2 to 20.2 µm/min after incubation with

microvesicles derived from SK-Mel-147 cells. However, the preincubation of microvesicles from SK-Mel-147 cells with the reversible HER2 inhibitor (Trastuzumab) had no effect on increased microtubule plus end growth rates (Figure 3.26B). I also analyzed the activity of microvesicles isolated from cells overexpressing *PLK4*. In fact, Plk4-induced microvesicles increased microtubule plus end growth rates in the non-invasive cell line SK-Mel-173 (Figure 3.26C), indicating that microvesicles from invasive melanoma cells and from cells overexpressing *PLK4* exhibit potentially overlapping factors that contribute to the induction of microtubule plus end assembly rates in interphase.

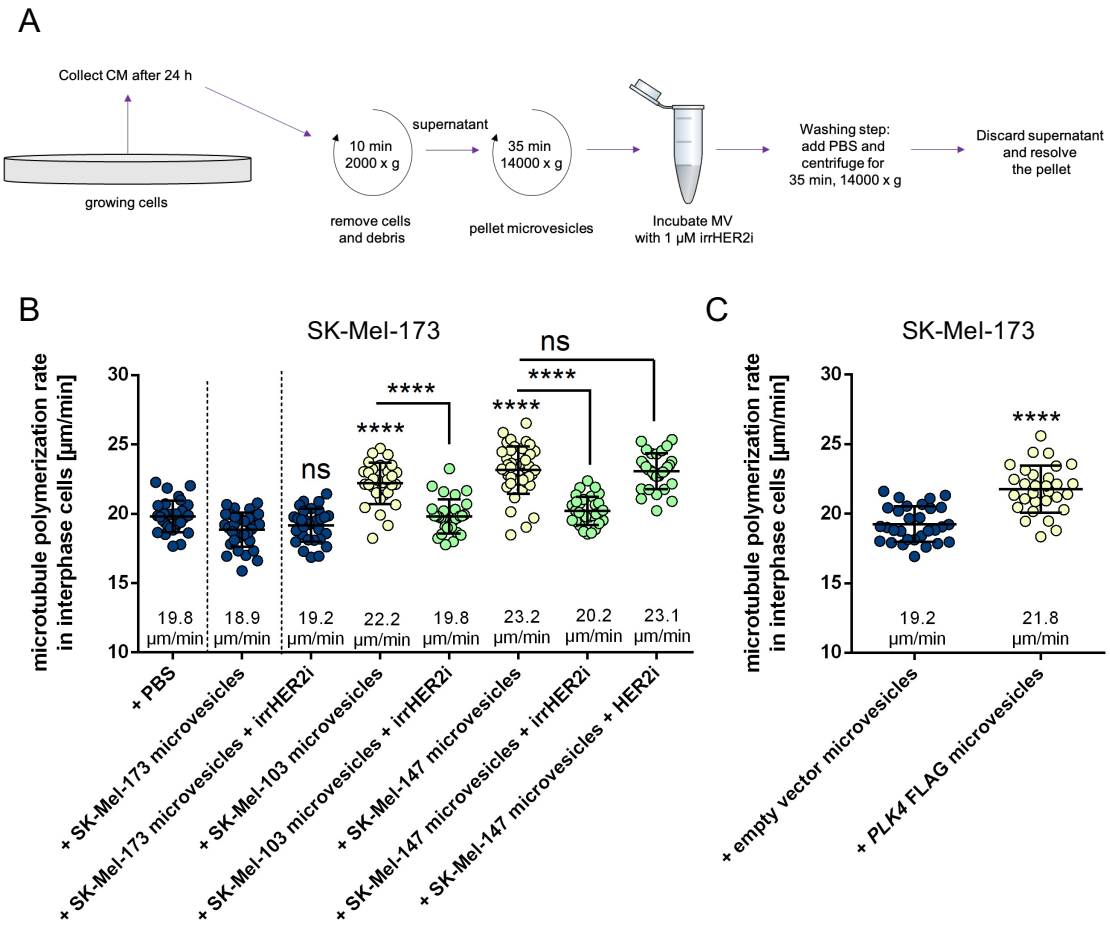

Figure 3.26 Microvesicles from invasive cells or cells overexpressing PLK4 induce microtubule plus end growth rates in non-invasive cells. *A) Scheme depicting the isolation of microvesicles and HER2 inhibitor treatment. B) Measurements of microtubule growth rates in SK-Mel-173 interphase cells treated with microvesicles from invasive cell lines. Microvesicles were incubated with an irreversible (irrHER2i, Canertinib,) EGFR/HER2 or reversible (Trastuzumab) HER2 inhibitor before treatment of SK-Mel-173 cells. Cells treated with PBS served as control cells. C) Measurements of interphase microtubule plus end assembly rates after treatment with microvesicles isolated from cells with an overexpression of PLK4. Scatter dot plots show mean values ± SD, n=30, 20 microtubules were measured per cell, t-test. The indicated p-values are defined as: **** = p ≤ 0.0001 and non-significant (ns) = p > 0.05. The indicated significances refer to corresponding control cells.*

3.2.12. Identification of proteins associated with microvesicles

Since microvesicles derived from cells with an overexpression of *PLK4* contained activities to increase microtubule growth rates, I embarked on identifying proteins that are associated with microvesicles from cells with a transient overexpression of *PLK4* compared to microvesicles from control transfected cells. For this purpose, microvesicles were isolated from the non-invasive cell line SK-Mel-173 that was transfected with a *PLK4* overexpressing plasmid and were analyzed using mass spectrometry. The experiments were performed in cooperation with Dr. Markus Räschle from the Technical University in Kaiserslautern. Microvesicles of three independent experiments derived from cells with an overexpression of *PLK4* exhibited 4.84-fold more HER3 and 1.96-fold more HER2 compared to microvesicles derived from control transfected cells, supporting the hypothesis that members of this receptor family might be more incorporated into the membrane of target cells and might contribute to the increase in microtubule plus end assembly in interphase. However, further validation experiments are necessary. All detected proteins were compared to data from the Open Access database Vesiclepedia (Kalra et al., 2012). The proteins found in microvesicles from my set up were compared to a list of proteins published on Vesiclepedia that are often found in extracellular vesicles based on the literature (Kalra et al., 2012). Intriguingly, 85 proteins out of 100 proteins that are often found in extracellular vesicles were also found in my samples, indicating that the isolation of microvesicles was successful.

Microvesicles derived from invasive melanoma cells were also able to increase microtubule growth rates in interphase, therefore, mass spectrometry analyses were performed to identify the content of these microvesicles. For this purpose, microvesicles were isolated from the non-invasive cell line SK-Mel-173 and the invasive cell line SK-Mel-147 and were analyzed using mass spectrometry. Again, in four independent experiments 83 proteins out of 100 proteins that are often found in extracellular vesicles were also found in my samples (Kalra et al., 2012). The mass spectrometry analyses from microvesicles derived from the non-invasive SK-Mel-173 cells with a transient overexpression of *PLK4* detected in total 4415 proteins, compared to 2534 proteins detected in the second experiment. 2312 proteins were found in both experimental set ups, indicating a high reproducibility. HER2 or HER3 were not among the detected proteins, indicating potentially different ways of induction of increased microtubule plus end assembly rates in target cells. However, EGFR was 3-fold more abundant in microvesicles derived from invasive cells. Proteins, like fibrous sheath interacting protein 1 (Fsip1) and transforming growth factor β induced (TGFβI), were 3623- and 113-fold increased in microvesicles derived from invasive cells. Their overexpression was shown to be directly associated with increased invasiveness

(Zhu et al., 2015) and Fsip1 is a signaling partner of HER2 (Liu et al., 2017), indicating that microvesicles derived from invasive cell lines might mediate HER2 signaling through the transmission of HER2 signaling inducing factors.

3.2.13. HER2 or ERK inhibition reduces cell migration in invasive melanoma cell lines

HER2 and ERK signaling was found to be part of the paracrine signaling of melanoma and colorectal cancer cells involved in the regulation of microtubule plus end growth rates.

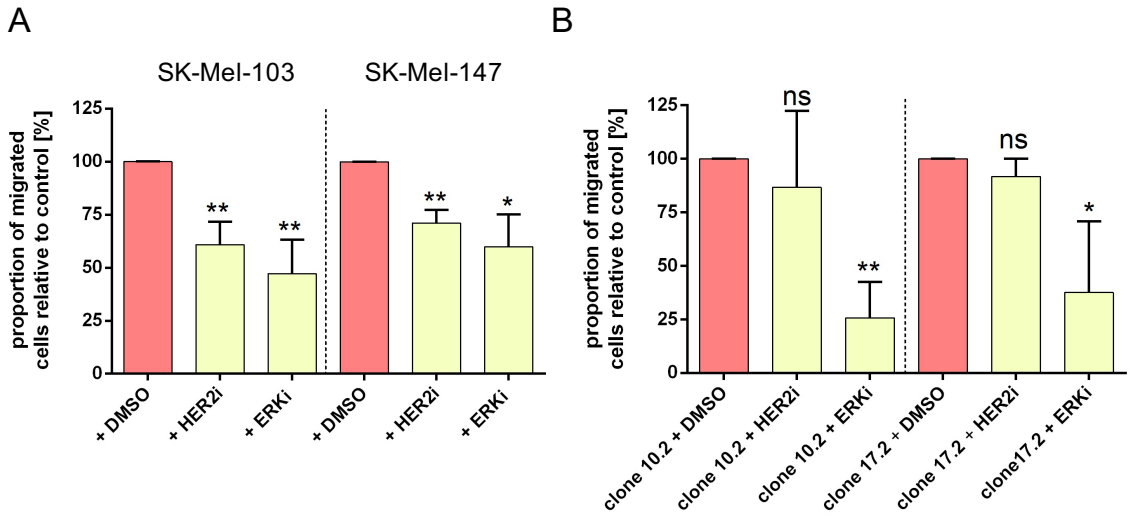

Figure 3.27 Migration of invasive melanoma and colorectal cancer cells is partially dependent on HER2 and ERK. *A) Determination of cell migration of melanoma cell lines after treatment with inhibitors. Cells were treated with 40 µM HER2i (Trastuzumab) or 20 µM ERKi (PD98059). DMSO treated cells served as control cells. B) Determination of cell migration of HCT116 + TP73shRNA/TP53$^{-/-}$ cells after treatment with inhibitors. Cells were treated with 40 µM HER2i (Trastuzumab) or 20 µM ERKi (PD98059). Bar graphs show mean values ± SD, n=3, t-test. Indicated stars are defined as followed: ** = p ≤ 0.01, * = p ≤ 0.05 and non-significant (ns) = p > 0.05. The indicated significances refer to control cells. Different cell lines are separated through dotted lines.*

Therefore, the role of HER2 and ERK in cell migration of invasive donor cells was investigated. SK-Mel-103 and SK-Mel-147 cells were treated with HER2 (Trastuzumab) and ERK (PD98059) inhibitors and cell migration was examined using transwell migration assays. Treatment with HER2 (Trastuzumab) or ERK (PD98059) inhibitors led in both invasive melanoma cell lines to a significant reduction of cell migration of at least 40 % for SK-Mel-103 cells and 30 % for SK-Mel-147 cells (Figure 3.27A).

Interestingly, treatment of HCT116 + TP73shRNA/TP53-/- clone 10.2 and clone 17.2 cells with the ERK inhibitor (PD98059) led also to a reduction of cell migration by 70 % (Figure 3.27B). However, the treatment with the HER2 inhibitor (Trastuzumab) had no significant effect. The effects of HER2 and ERK inhibition on melanoma cells were also examined in 3D spheroid assays. Spheroids derived from invasive SK-Mel-147 cells were

transferred to Matrigel™ and treated with 0.5 nM of Taxol, 20 µM of ERK inhibitor (PD98059), 40 µM of HER2 inhibitor (Trastuzumab) and 1 µM of the irreversible EGFR/HER2 inhibitor (irrHER2i, Canertinib). Representative images of spheroids treated with the inhibitors after 48 h in Matrigel™ are shown in Figure 3.28A. All inhibitor treatments showed a significant reduction of spheroid outgrowth (Figure 3.28B), indicating a dependence of cell invasion in melanoma cells on HER2/ERK signaling.

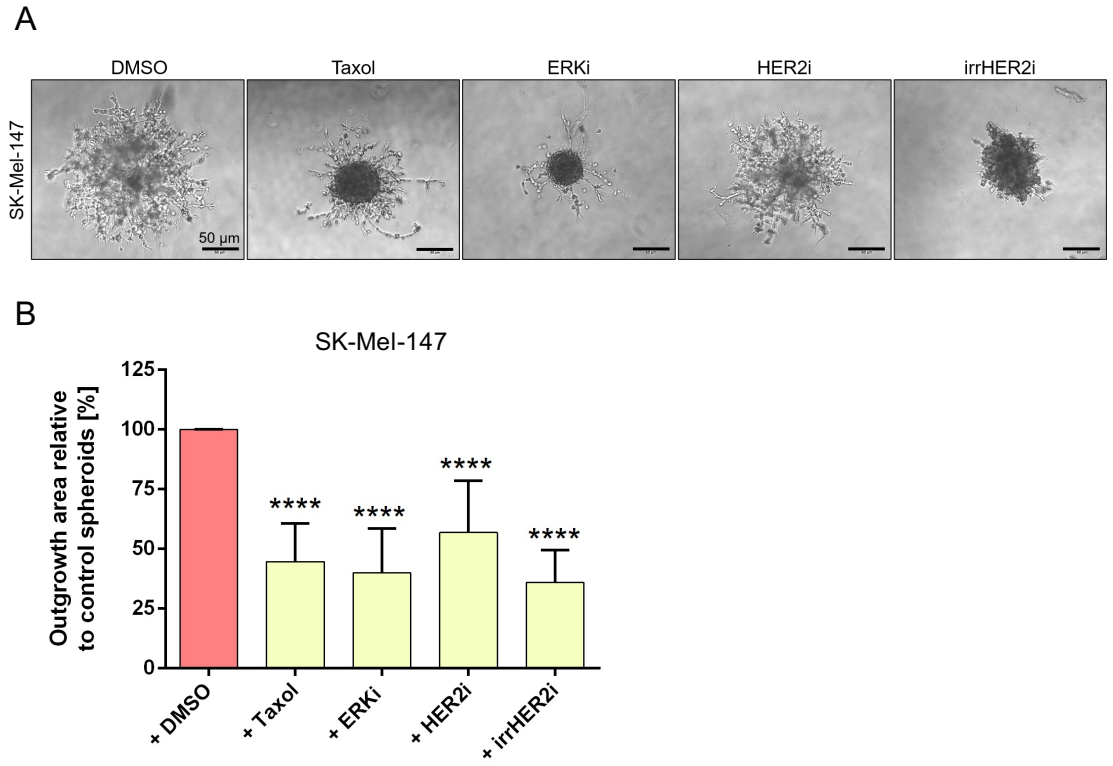

Figure 3.28 HER2 or ERK inhibition suppresses 3D spheroid outgrowth of invasive melanoma cells. *A) Representative images of 3D spheroids derived from SK-Mel-147 cells and treated with DMSO, 0.5 nM of Taxol, 20 µM of ERKi (PD98059), 40 µM of HER2i (Trastuzumab) and 1 µM of the irreversible EGFR/HER2 inhibitor (irrHER2i, Canertinib). 3D spheroids were grown in a 96-well plate for 48 h. 3D spheroids were transferred to Matrigel™. Images were taken after 48 h. Scale bar, 50 µm. B) Quantification of outgrowth area of spheroids derived from SK-Mel-147 cells treated with inhibitors after 48 h. n=26 (Taxol), n=24 (ERKi), n=27 (HER2i) and n=27 (irrHER2i) spheroids were analyzed after 48 h in Matrigel™. The area of outgrowth was calculated relative to control cells. Bar graphs show mean values ± SD, n=3, t-test. Data for Taxol treated spheroids were already shown in Figure 3.7. Indicated stars are defined as followed: **** = p ≤ 0.0001. Significances refer to DMSO treated control cells.*

3.2.14. Conditioned medium treatment on non-invasive spheroids and in transwell cell migration inserts does not increase cell migration or invasiveness

Treatment of non-invasive recipient cells with conditioned medium from invasive cell lines induced microtubule plus end growth rates. The treatment of the non-invasive cell line SK-Mel-173 with invasive conditioned medium from the SK-Mel-147 cell line did not increase cell migration in transwell migration assays (Figure 3.29A). The treatment of spheroids

derived from the non-invasive cell line SK-Mel-173 with conditioned medium from the invasive cell line SK-Mel-103 did not lead to an increase of invasive structures, although the spheroids treated with conditioned medium derived from the invasive cell line showed some invasive structures more compared to the control treated spheroids (Figure 3.29B).

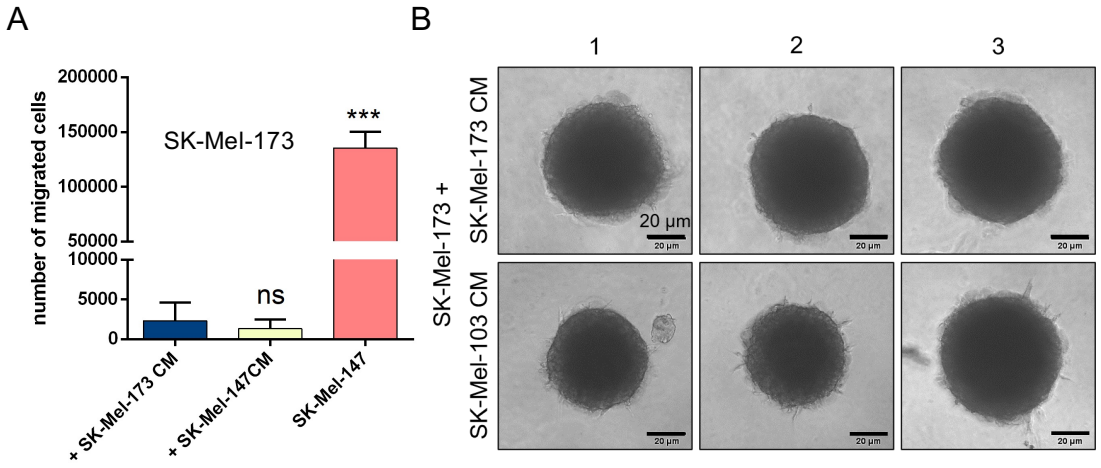

Figure 3.29 Treatment of non-invasive spheroids with conditioned medium from invasive cells does not induce invasion. *A) Determination of cell migration of SK-Mel-173 cells treated with conditioned medium (CM) from an invasive cell line. The data for the migration of SK-Mel-147 were already shown in Figure 3.4. B) Exemplary images of spheroids derived from SK-Mel-173 cells after treatment with conditioned medium from the invasive cell line SK-Mel-103. Spheroids were treated for five days with conditioned medium. Depicted are three spheroids per condition. Scale bar, 20 µm. Bar graphs show mean values ± SD, n=3, t-test. Indicated stars are defined as followed: *** = p ≤ 0.001 and non-significant (ns) = p > 0.05. Significances refer to control cells.*

4. Discussion

The present study demonstrated an intriguing correlation between increased numbers of centrosomes, increased microtubule plus end assembly rates, and enhanced invasiveness in colorectal cancer as well as melanoma cell lines. Most melanoma cell lines are characterized by a hyperactivation of the MAPK signaling pathway mediated through mutations in *BRAF*, *NRAS*, and *NF1 (Neurofibromin1)* (Akbani et al., 2015; Tate et al., 2019). Together with mutations in constituents of the PI3K/AKT signaling pathway these genetic aberrations are implicated in increased cell survival, enhanced tumor cell growth, and high invasiveness seen in cutaneous melanoma (Hodis et al., 2012). Intriguingly, this present study revealed a link between abnormal centrosome amplification as a trigger for increased microtubule plus end assembly rates in interphase possibly connected to enhanced cell migration and invasion in melanoma cell lines. In the proposed model (Figure 4.1), invasive donor cells characterized by supernumerary centrosomes, increased microtubule plus end assembly rates in interphase, and the elevated formation of invasive structures induce a microvesicle dependent paracrine signaling.

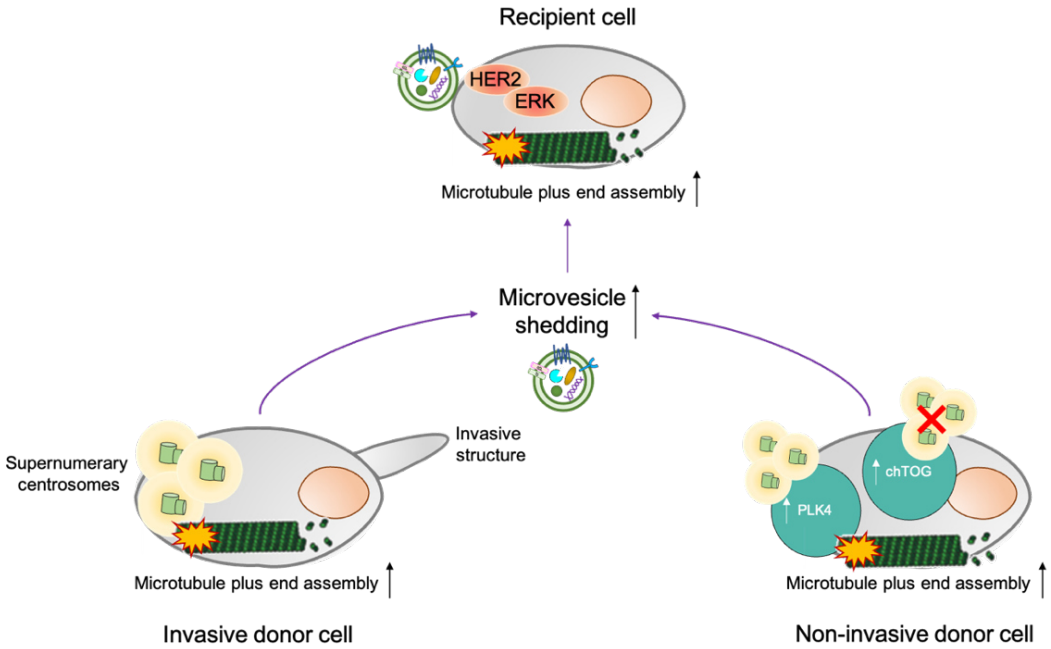

Figure 4.1 Model of the interplay between supernumerary centrosomes, microtubule dynamics in interphase, and cancer cell invasion in melanoma and colorectal cancer cell lines. *Invasive cancer cells are characterized by abnormal centrosome amplification, increased microtubule plus end assembly rates in interphase, and the elevated formation of invasive actin structures. The overexpression of PLK4 in non-invasive donor cells induces supernumerary centrosomes accompanied by increased microtubule plus end assembly rates. The overexpression of chTOG increases microtubule dynamics without affecting the number of centrosomes. Both conditions induce a paracrine signaling through the release of microvesicles that induce increased microtubule plus*

end assembly rates in recipient cells potentially mediated through a HER2 – ERK dependent pathway leading to increased microtubule dynamics, which is required for increased cell migration and invasion.

A *PLK4* or *chTOG* dependent acceleration of microtubule dynamics in non-invasive donor cells leads also to the elevated release of microvesicles, which seems to be independent from the status of centrosome amplification. The microtubule dynamics dependent paracrine signaling induces the increase of microtubule plus end assembly rates in recipient cells possibly through a HER2/ERK dependent pathway.

Supernumerary centrosomes are associated with increased microtubule plus end assembly rates in interphase

Supernumerary centrosomes in mitosis are associated with the formation of lagging chromosomes, chromosome missegregation and chromosomal instability in human cancer (Ganem et al., 2009). However, the effects of supernumerary centrosomes on interphase cells are attracting more and more attention. This present study demonstrated that the induction of supernumerary centrosomes in cancer cells is sufficient to increase microtubule plus end assembly rates in interphase. Surprisingly, measuring microtubule plus end assembly rates in mitotic HCT116 cells after induction of an abnormal number of centrosomes revealed no significant increase of microtubule plus end growth rates. This observation indicates a specificity of the link between supernumerary centrosomes and microtubule dynamics for interphase, however, it is currently unknown how this discrepancy between mitosis and interphase can be explained.

Are increased microtubule plus end assembly rates in interphase a read out for increased microtubule nucleation?

De novo microtubule nucleation activity was shown to be low during interphase (Piehl et al., 2004). Indeed, microtubule nucleation is fivefold increased during mitosis (Salisbury et al., 1999) and the dynamic behavior of mitotic microtubules is approximately 3.5-fold increased compared to interphase microtubules (Rusan et al., 2001). An aberrant number of centrosomes was directly associated with enhanced microtubule nucleation in cells derived from the breast epithelium (Godinho et al., 2014) and led to accelerated interphase microtubule plus end assembly rates in melanoma and colorectal cancer cell lines as shown in this study. The activity of microtubule nucleation is proportional to the amount of pericentriolar material (PCM) surrounding the centrioles, which was shown to be aberrantly increased during interphase in the presence of supernumerary centrosomes (D'assoro et al., 2002; Lingle et al., 2001). The depletion of the PCM proteins γ-tubulin (Thawani et al.,

2018) or Cep192 (O'Rourke et al., 2014) was associated with reduced centrosomal microtubule nucleation. Interestingly, this study showed that the partial depletion of the microtubule nucleators Cep192 or γ-tubulin suppresses increased microtubule plus end assembly rates in invasive melanoma cell lines. Cep192 and γ-tubulin are proteins directly associated with the PCM at the centrosome (Gomez-Ferreria et al., 2007). The processive microtubule polymerase chTOG, whose partial depletion also rescued increased microtubule plus end assembly in interphase cells, is known for its role as a microtubule polymerase (Brouhard et al., 2008). In addition, chTOG was shown to be associated with *de novo* microtubule nucleation at the centrosome (Thawani et al., 2018), indicating that the partial loss of chTOG might be also linked to reduced microtubule nucleation at the centrosome. Even though γ-tubulin is described and known as the main microtubule nucleator, studies in *Drosophila melanogaster* reported about the localization of γ-tubulin along interphase microtubules, thereby fulfilling microtubule stabilizing functions (Bouissou et al., 2009). The microtubule associated protein TPX2 was shown to promote microtubule nucleation (Wieczorek et al., 2015) and stimulate microtubule assembly (Carter et al., 2017). The loss of Survivin was associated with reduced microtubule nucleation and microtubule dynamics in mitotic and interphase cells (Rosa et al., 2006), indicating that changes of microtubule regulators affect both *de novo* microtubule nucleation and dynamics. Furthermore, this study demonstrated that the inductive effect of Plk4-induced supernumerary centrosomes on microtubule dynamics is abolished after depletion of the microtubule polymerase chTOG or the microtubule nucleators γ-tubulin or Cep192, indicating a connection between these processes. Interestingly, a stronger rescue of cell migration and invasion was achieved after the partial loss of *CKAP5* compared to treatment with Taxol. The loss of *CKAP5* is associated with reduced microtubule plus end growth rates and possibly with reduced microtubule nucleation, whereas the function of Taxol is limited to microtubule plus ends. Therefore, it is possible that increased microtubule plus end assembly rates in interphase are a direct consequence and a read out for increased *de novo* microtubule nucleation at the centrosome.

The role of microtubule dynamics for targeting supernumerary centrosomes in cancer cells

Targeting supernumerary centrosomes leading to the aberrant regulation of interphase microtubules in cancer cells is of great interest (Ogden et al., 2014). Cancer cells can overcome negative consequences of aberrant centrosome amplification by clustering centrosomes not only in mitosis to avoid the assembly of a multipolar spindle, but also in interphase to avoid impaired cell polarization and defects in cancer cell invasion (Pannu

et al., 2014). Furthermore, studies performed in the model organism *C. elegans* showed that additional centrosomes can also be inactivated mediated through phosphatase dependent disruption of the inner layer of the pericentriolar material (PCM) accompanied by microtubule dependent cortical forces that will lead to the rupture of the outer layer of the PCM (Magescas et al., 2019). Similar observations of centrosome inactivation were made in the wing disc epithelium of *Drosophila melanogaster* (Sabino et al., 2015). Interestingly, it has been shown that agents targeting clustered supernumerary centrosomes have a higher impact on interphase cells than on mitotic cells, since 95 % of cells in an asynchronously growing cell population are in interphase (Ogden et al., 2014). In a recent study, the loss of centrosomes in interphase was associated with a shift to non-centrosomal microtubule nucleation, which led to the excessive transport of Rac1 to the cell cortex. Aberrant activity of Rac1 was associated with defects in actin cytoskeleton organization, lost cell polarity and consequently with failed directional cell migration (Cheng et al., 2019). The mentioned study highlights the importance of non-centrosomal microtubule organizing centers during interphase, such as the golgi apparatus (Gavilan et al., 2018). Remarkably, microtubules derived from the golgi apparatus have also been implicated in regulating cell polarization and cell invasion in 3D cultures (Wu et al., 2016). However, the centrosome is the main center of microtubule nucleation (Petry & Vale, 2015), therefore, this study focused on γ-tubulin positive centrosomes and their way of microtubule organization.

Interphase cells treated with small molecule inhibitors leading to declustered supernumerary centrosomes were shown to exhibit a defective organization of the golgi complex, lost cell polarization, abnormal formation of cell protrusions, resulting in an overall reduced invasive phenotype (Pannu et al., 2014). Pannu and colleagues tested Reduced-9-bromonoscapine (RedBr-Nos) (Karna et al., 2011), Griseofulvin (Rebacz et al., 2007) and phenanthridines (PJ-34) (Castiel et al., 2011) as declustering agents. RedBr-Nos and Griseofulvin are known to bind to tubulin and interfere with microtubule polymerization, therefore, slowing down microtubule dynamics. The treatment with PJ-34, an inhibitor for the poly ADP-ribose polymerase (PARP), was associated with declustered centrosomes in mitosis, most likely through the post translational modification of centrosome clustering factors, like NuMA and HSET (Visochek et al., 2017). Interestingly, in another study, the authors demonstrated that the enhancement of microtubule nucleation in interphase results in the suppression of centrosome clustering during mitosis (Mariappan et al., 2019). Mariappan and colleagues identified a novel tubulin binding, small molecule inhibitor that interferes with the binding between centrosomal-P4.1-associated protein (CPAP) and tubulin in MCF-10A cells, a complex usually essential for keeping microtubule nucleation activity low during interphase. They proved that inhibitor treatment resulted in increased recruitment

of centrosomal factors to the PCM of interphase centrosomes leading to increased microtubule nucleation prior to mitosis, followed by centrosome declustering during mitosis and the formation of a multipolar spindle. This was accompanied by impaired invasiveness in 3D cultures, however, probably due to increased mitotic arrest. The effects of interphase supernumerary centrosomes on mitosis were not examined within this study. However, the induction of supernumerary centrosomes in the colorectal cancer cell line HCT116 was not linked to increased mitotic microtubule plus end assembly rates, indicating a specificity of the connection between aberrant centrosome amplification and microtubule dynamics for interphase.

Declustering agents target supernumerary centrosomes leading to a reduced invasive phenotype. Agents such as RedBr-Nos and Griseofulvin were shown to function through the suppression of microtubule dynamics to decluster supernumerary centrosomes. The present study demonstrated that enhanced cell migration and invasion is dependent on increased microtubule plus end assembly rates in interphase and the restoration of normal microtubule plus end assembly rates using Taxol treatment partially rescued the invasive phenotype. Since supernumerary centrosomes were found to be a trigger of increased microtubule plus end assembly rates, it might be possible to rescue a supernumerary centrosome associated invasive phenotype by treating cells with low doses of Taxol (Figure 4.2). Further studies could analyze a possible effect of Taxol treatment on supernumerary centrosome organization.

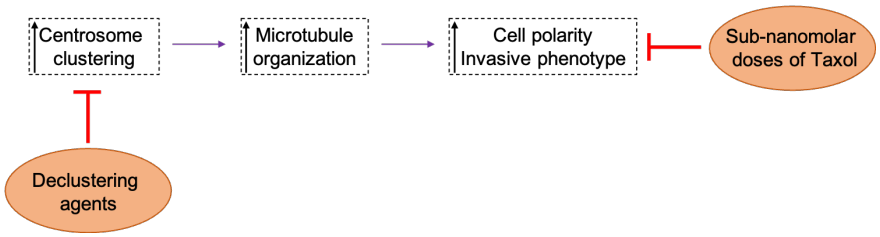

Figure 4.2 Outcome of centrosome clustering in cancer cells. *Cancer cells cluster supernumerary centrosomes to avoid defects in microtubule organization in interphase. Clustered centrosomes establish a functional microtubule network connected to an invasive phenotype. Declustering agents inhibit centrosome clustering resulting in defective organization of microtubules and decreased invasiveness. Sub-nanomolar concentrations of Taxol was shown to suppress a microtubule dynamics dependent invasive phenotype.*

Taken together, correct microtubule organization in interphase is essential for proper cell polarization and cell motility. However, the relationship between supernumerary centrosomes and cell migration and invasion is not exclusively dependent on changes in the microtubule cytoskeleton. A recent publication explained the link between structural centrosome aberrations and increased metastasis (Ganier et al., 2018). A former study established already a link between the induction of structural centrosome aberrations through the overexpression of ninein like protein (Nlp) in breast epithelial cells leading to massive

reorganization of the microtubule cytoskeleton and mislocalization of adhesion proteins (Schnerch & Nigg, 2016). Ganier and colleagues identified that the induction of structural centrosome aberrations triggered the budding of mitotic cells from the epithelium. The group measured the cortical tension of epithelial cells with structural centrosome aberrations and cells exhibiting structural centrosome aberrations were characterized by increased stiffness, which was accompanied by weakened cell junctions. Expansion of mitotic cells within the epithelium was due to the increased stiffness in surrounding interphase cells suppressed, mitotic cells were excluded from the epithelium and were more likely to metastasize. Interestingly, our lab showed that chromosomally instable colorectal cancer cells exhibit reduced cortical tension during mitosis compared to chromosomally stable cells. This was associated with spindle mispositioning and chromosome missegregation (unpublished results, Bastians lab), and indicates that chromosomally instable mitotic cells might be characterized by low cortex tension and are possibly more prone to metastasize.

Increased microtubule dynamics is required but not sufficient to induce cancer cell migration and invasion

Numerical centrosome aberrations were already shown to relate to an invasive phenotype (Arnandis et al., 2018; Godinho et al., 2014; Kazazian et al., 2017; Rivera-Rivera et al., 2021). However, another group reported contrary results, where the overexpression of *PLK4* and the induced amplification of centrosomes was not sufficient to stimulate the formation of invasive protrusions (Schnerch & Nigg, 2016). A further report demonstrated that *PLK4* overexpression alone was not triggering formation of skin tumors, whereas overexpression of *PLK4* accompanied by the loss of *TP53* was associated with increased tumorigenesis in mice (Serçin et al., 2016). The induction of invasive protrusions by the overexpression of *PLK4* or *CKAP5* was also not possible in the present study, which might be explained in different ways. The non-invasive SK-Mel-173 cell line that was primarily used for the studies on the microtubule dependent induction of increased cell invasion exhibits wildtype p53. The cell line is characterized by a single nucleotide polymorphism (SNP) in its wildtype *TP53* gene locus located in codon 72 (P72R) (Alonso-Curbelo et al., 2014). This polymorphism was linked to an increased metastatic behavior of cancer cells, but just in the context with mutant p53 (Basu et al., 2018). Wild type p53 was shown to suppress the activity of the receptor tyrosine kinase c-Met, which is often hyperactivated in cancer and associated with increased invasiveness (Hwang et al., 2011). Restored wild type p53 levels in cancer cells were associated with less cell migration and invasion (Cheng et al., 2019). Interestingly, HCT116 with loss of *TP53* and *TP73* were associated

with increased cell migration and invasion, indicating that p53 and p73 usually contribute to a non-invasive phenotype. However, the induction of a high proportion of cells with supernumerary centrosomes demonstrated that the overexpression of *PLK4* was functional, indicating that the status of p53 might not be critical during this process, but was possibly interfering with cancer cell invasion. Additionally, technical differences in handling extracellular matrix-based 3D models are possible, since the outgrowth of invasive structures is depended on the stiffness, composition, and elasticity of the extracellular matrix (Yamada & Sixt, 2019). Furthermore, it is possible that the definition of invasiveness in 3D assays is different. In the present study, spheroids derived from non-invasive cells were incubated with conditioned medium from invasive cells and exemplary images showed that these spheroids formed more invasive protrusions compared to control spheroids. However, the total amount of invasive protrusions compared to invasive structures formed by the positive controls was remarkably low and quantification of the data was therefore not conducted. It is important to note that a combination of aberrations in different signaling pathways leads to increased invasiveness in melanoma cell lines. It is very likely that the overexpression of a single protein in non-invasive cells while increasing microtubule plus end growth rats, is not sufficient to induce an invasive phenotype to that extended seen in invasive cell lines.

The role of deregulated microtubule dynamics for paracrine signaling

This study showed that centrosome amplifications and the conditioned medium from these cells was a trigger for increased microtubule plus end assembly. Moreover, overexpression of *CKAP5,* which was not affecting centrosome numbers, was sufficient to induce paracrine signaling leading to the induction of microtubule plus end assembly in surrounding cells. Cell type specific effects were excluded, since conditioned medium from invasive melanoma cells was able to increase microtubule plus end assembly rates in interphase in colorectal cancer cells. It is possible that microtubule plus end assembly is the main mediator in inducing paracrine signaling and supernumerary centrosomes are acting as a trigger for the induction of increased microtubule dynamics in interphase.

Microvesicles attract more and more attention in cancer research as they are found in blood and urine samples of cancer patients and function as potential biomarkers (Menck et al., 2017). The number of tumor-associated microvesicles in the blood of cancer patients is remarkably low compared to the abundance of normal microvesicles, however, the amount is sufficient to account for poor prognosis (Menck et al., 2017). Due to this importance, it is of great interest to elucidate the mechanisms leading to the release of microvesicle and finding a way to suppress it. The exact mechanisms of extracellular vesicle shedding, and the contribution of the microtubule cytoskeleton remains poorly understood.

In contrast to exosomes, the formation and release of microvesicles is dependent on the actin cytoskeleton and released vesicles are actin positive (Jeppesen et al., 2019; Wang et al., 2014). It was shown that Ras related in brain (Rab) GTPases are directly associated with the intracellular trafficking and release of extracellular vesicles (Ostrowski et al., 2010; Wang et al., 2014). Signaling initiated through the small GTPase RhoA leading to the downstream activation of the LIM domain containing (LIM) kinase and subsequent inhibition of cofilin and its actin severing activity, was shown to be essential for microvesicle biogenesis (Li et al., 2012). Another study showed that cells can switch between the formation of invadopodia or the release of invasion promoting microvesicles dependent on the substrate they are growing on. Increased activity of Rac1 was associated with invadopodia formation and antagonized the shedding of microvesicles, whereas RhoA signaling led to increased release of microvesicles (Sedgwick et al., 2015).

Microtubules were previously directly connected to actin coats on secretory vesicles and disruption of the microtubule cytoskeleton interfered with actin polymerization and exocytosis (Müller et al., 2019). A recent publication reported about the correlation between the intracellular level of β3-tubulin and the release of microvesicles in malignant melanoma (Altonsy et al., 2020). The levels of β3-tubulin in malignant melanoma were shown to be increased and depletion subsequently led to decreased microtubule dynamics associated with less microvesicle shedding, indicating a direct link between microtubule dynamics and microvesicle shedding as demonstrated in this study with melanoma cell lines. It is important to note that microvesicles are also shed from the tumor microenvironment to enhance tumorigenic features of cancer cells. For instance, cancer-associated fibroblasts were shown to release microvesicles containing cancer cell migration inducing factors (Toti et al., 2021). An increased number of small extracellular vesicles that activate fibroblast like cells of the tumor microenvironment was released in pancreatic cancer cells with supernumerary centrosomes (Adams et al., 2021). The release of exosomes is not mediated through membrane budding, but rather dependent on the fusion of multivesicular bodies (MVB) with the plasma membrane and the subsequent release of the content (Hessvik & Llorente, 2018). Adams and colleagues reported about a reactive oxygen species (ROS) mediated lysosomal dysfunction leading to enhanced fusion of MVB with the plasma membrane (Adams et al., 2021), indicating a process independent of microtubules. This is in line with the finding of this study where extracellular vesicles, active in increasing microtubule plus end assembly rates, were already sedimented at low centrifugation speed, indicating that microvesicles rather than exosomes are involved.

Microtubules are known to interact with actin filaments at the centrosome and at the cell periphery, as also seen during the process of cell migration and invasion. Accordingly,

increased microtubule plus end assembly in interphase might lead to enhanced transport of actin nucleators and polymerization factors to the cell cortex, subsequently leading to elevated actin polymerization resulting in increased microvesicle shedding (Figure 4.3). Furthermore, supernumerary centrosomes are associated with increased *de novo* microtubule nucleation (D'assoro et al., 2002; Lingle et al., 2001), thereby, providing an increased number of microtubules. More microtubules might transport more cargo to the cell cortex and interact more efficiently with the actin cytoskeleton to increase the release of microvesicles. Indeed, our lab found recently that enhanced microtubule plus end assembly during mitosis might influence cortical actin polymerization to deregulate mitotic spindle orientation through a Rac1/Arp2/3 mediated signaling pathway (unpublished results, Bastians lab). Taken together, microtubule plus end assembly might influence the actin cytoskeleton, thereby, favoring the release of microvesicles (Figure 4.3). This study showed that the treatment of cells with sub-nanomolar doses of the microtubule stabilizing drug Taxol is sufficient to restore normal microtubule plus end assembly rates in interphase, which might also reduce the release of cancer-relevant microvesicles, thereby, offering new possibilities for cancer therapy.

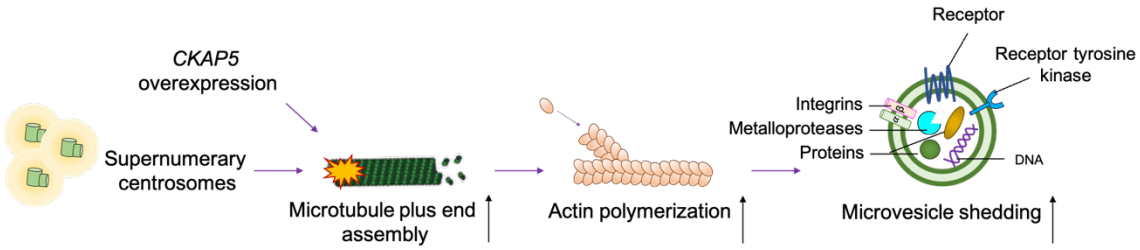

Figure 4.3 Mechanisms of microvesicle shedding in cancer cells. *Triggers upstream of microtubule plus end assembly rates in interphase, such as supernumerary centrosomes or overexpression of CKAP5, lead to increased microtubule growth rates, subsequently affecting actin polymerization in the cell periphery and leading to the increased release of microvesicles containing tumorigenic factors.*

Involvement of HER2 and ERK in paracrine signaling leading to increased microtubule dynamics

This study showed that conditioned media from invasive cell lines or cells with a transient overexpression of *PLK4* contain microvesicles that were active to increase microtubule plus end assembly rates in non-invasive target cells. Moreover, the treatment of recipient cells or of the microvesicles with inhibitors for HER2 or ERK restored normal microtubule plus end assembly rates, suggesting that microvesicles mediated their activity through HER2/ERK signaling (Figure 4.4).

It is established that microvesicles enable the transmission of tumorigenic factors and accelerate tumor proliferation (Arendt et al., 2014) and cell invasion (Menck et al., 2015) in target cells. A recent publication showed data indicating that IL8/HER2/ERK signaling can mediate invasion in response to centrosome amplification induced paracrine signaling (Arnandis et al., 2018). In this setting, the receptor for IL8 might activate HER2 as shown during breast cancer stem cell activation (Singh et al., 2013). However, in my hands, inhibition of IL8 signaling was not affecting microtubule plus end assembly rates in melanoma cell lines. It is possible that transactivation of HER2 via IL8 is breast epithelial cell specific and that HER2 is activated through another mechanism in melanoma cell lines. Interestingly, HER2 was shown to interact at the plasma membrane with TGFβ receptors. HER2 signaling was associated with increased activation of Smad3 and a shift from tumor suppressing TGFβ signaling to EMT promoting signaling (Huang et al., 2018). TGFβ signaling was also shown to induce the clustering of HER2 with integrins at the plasma membrane leading to the increased activation of downstream signaling including the MAPK pathway (Wang et al., 2009). The specific interaction of the TGFβ receptor with HER2 is of great interest, since my work showed that microvesicles of invasive melanoma cell lines contained more ligand for the TGFβ receptor compared to microvesicles derived from non-invasive cells. Furthermore, the intracellular binding partner of HER2, fibrous sheath interacting protein 1 (Fsip1), was more abundant in microvesicles derived from invasive cells compared to microvesicles from non-invasive cells. Fsip1 protein levels and HER2 present in the plasma membrane were shown to correlate positively in breast cancer (Zhang et al., 2015). Overexpression of *FSIP1* is also associated with colorectal cancer (Wu et al., 2020). Interestingly, an increased protein level of Fsip1 accompanied by increased binding of Fsip1 to HER2 was associated with enhanced invasiveness in breast cancer (Liu et al., 2017).

Additionally, it is possible that microvesicles exhibit an elevated number of HER2 or members of the same receptor family anchored in their plasma membranes. The fusion of microvesicles with target cells could lead to an increased incorporation of the receptor and subsequently to enhanced HER2 signaling (Figure 4.4). This would be in line with data from the mass spectrometry analyses of microvesicles derived from cells with a transient overexpression of *PLK4*. These microvesicles exhibited a higher proportion of HER3 and HER2 compared to microvesicles from control transfected cells. Indeed, HER3 was demonstrated to be the critical dimerization partner of HER2 in breast cancer and co-expression was associated with shorter overall survival in breast cancer (Berghoff et al., 2014; Lee-Hoeflich et al., 2008) and colorectal cancer (Beji et al., 2012).

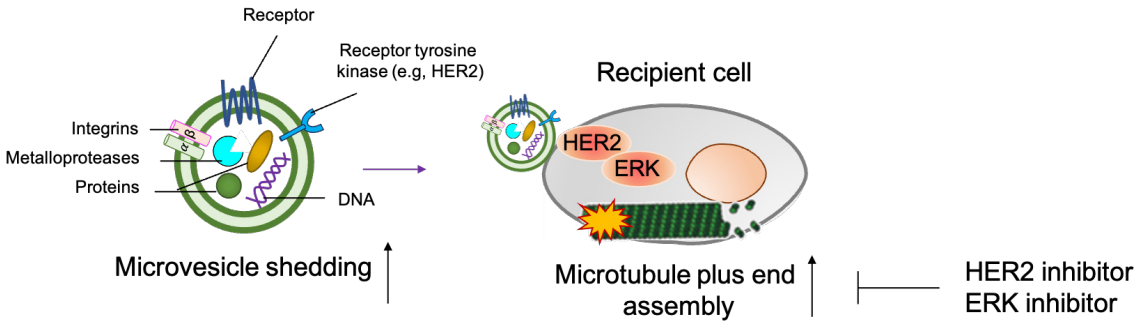

Figure 4.4 Model of microvesicle induced signaling to deregulate microtubule dynamics. *Microvesicles released from invasive melanoma cell lines reach the target cells and activate HER2/ERK signaling leading to increased microtubule plus end assembly rates.*

HER3 inhibition was shown to be effective to induce tumor regression after HER2 positive breast cancer cells acquired resistance to trastuzumab treatment (Gandullo-Sánchez et al., 2020), indicating that HER3 is an essential signaling partner of HER2. The mass spectrometry analyses of microvesicles from invasive cells could not detect HER2 or HER3, and EGFR was slightly increased in microvesicles derived from invasive cells, indicating that a different mechanism possibly including TGFβI or Fsip1 signaling might be involved. However, pre-incubation of microvesicles derived from invasive cells with an irreversible EGFR/HER2 inhibitor before target cells were treated abolished the inductive effect of microvesicles on microtubule plus end assembly rates, indicating that a combination of the transfer of EGFR and HER2 signaling might contribute to the increase of microtubule plus end assembly rates. Validation experiments, such as western blot detection of protein levels of EGFR, HER2, and HER3 in microvesicles derived from invasive cells or cells with a *PLK4* overexpression, are necessary. Furthmore, in depth analyses of the mass spectrometry data might reveal if microvesicles from invasive cells or cells with *PLK4* overexpression exhibit a different composition of proteins compared to control microvesicles or if these microvesicles contain an identical protein composition except some proteins being more abundant.

The transport of receptors via microvesicles was already reported. HER2 was detected on microvesicles released from breast cancer cells (Nanou et al., 2020) and colorectal cancer cells (Zembala et al., 2015). An oncogenic isoform of the EGF receptor (EGFRvIII) was transmitted via oncosomes between glioma cells leading to the hyperactivation of the MAPK pathway in target cells (Al-Nedawi et al., 2008). Receptors of the EGF family are often found to be transmitted via cancer-relevant microvesicles (Menck et al., 2017).

An increased incorporation of HER2 in the plasma membrane of target cells might lead to increased activation of ERK signaling, one of the two main pathways downstream of activated HER2 (Kirouac et al., 2016), and subsequently to increased microtubule plus end

assembly rates in interphase. It remains to be identified if a potential activity of ERK within microvesicles is also contributing to the observed phenotype. For this purpose, cells can be treated with an irreversible ERK inhibitor before microvesicles will be collected and used for further validation experiments.

Interestingly, activated ERK is not only associated with modulating gene transcription, thereby, inducing for instance cancer cell invasion in a variety of human cancers (Chen et al., 2015; Fang et al., 2021; Liu et al., 2018), but was also found to decorate and stimulate interphase microtubules (Harrison & Turley, 2001; Reszka et al., 1995). Proteins of the MAPK signaling pathway were associated with tubulin or microtubule associated proteins (Morishima-Kawashima & Kosik, 1996) and activated MAPK was implicated in the phosphorylation of microtubule associated proteins, like tau (Li et al., 2018), MAP4 (Zhang et al., 2019) and MAP65-1 (Komis et al., 2011). In addition, an integrin dependent activation of ERK was shown to be associated with increased microtubule nucleation in interphase through the accelerated recruitment of γ-tubulin to the centrosome (Colello et al., 2012), supporting the notion that increased microtubule plus end assembly rates might be a read out for increased microtubule nucleation. A very recent publication reported about a positive feedback loop between activated ERK signaling and the microtubule end binding protein 2 (EB2) in hepatocellular carcinoma (Zhong et al., 2021). Another study described a novel, single tubulin binding TOG-domain in MEKK1, the kinase responsible for the downstream activation of ERK. Mutations within the TOG-domain resulted in reduced amounts of microtubules at the leading edge (Filipčík et al., 2020). Increased activity of ERK was also associated with suppressed miRNA nucleus export in liver cancer cells leading to the upregulation of the microtubule affinity regulating kinase 4 (MARK4), which was linked to increased microtubule dynamics (Sun et al., 2016).

The contribution of ERK signaling in cancer cell migration and invasion was already demonstrated in several cancer types, such as breast cancer, renal cell carcinoma, tongue cancer, glioblastoma, and melanoma (Chen et al., 2015; Fang et al., 2021; Liu et al., 2018; Noi et al., 2018). Specifically in melanoma, mutations in genes encoding for either *NRAS* or *BRAF* are found in over 65 % of melanoma patients (Savoia et al., 2019; Sullivan & Flaherty, 2013). Studies showed that melanoma cells with the $BRAF^{V600E}$ mutation exhibit increased invasiveness mediated through the ERK dependent phosphorylation of the actin regulator cortactin (Lu et al., 2016). Hyperactivated ERK mediates its cancer cell invasion promoting function either through regulation of the gene expression of essential EMT mediators or through the direct phosphorylation of constituent of the cell motility machinery, such as WAVE or Rac1 (Mendoza et al., 2011; Tanimura & Takeda, 2017; Tong et al., 2013). Together, all these studies indicate that HER2/ERK signaling be initiated in

response to paracrine signaling leading to increased microtubule dynamics and enhanced cell migration and invasion.

How is microtubule plus end assembly involved in cancer cell invasion regulated?

Our lab currently revealed a mechanistic link between the loss of *TP53*/*TP73* and increased microtubule plus end assembly rates in mitotic cells of the colorectal cancer cell line HCT116 (Schmidt et al., 2021). Furthermore, increased microtubule plus end assembly within mitotic spindles was shown to cause transient spindle mispositioning, which fosters the generation of lagging chromosomes leading to chromosome missegregation and chromosomal instability (Ertych et al., 2014; Schermuly, 2019). Astonishingly, the loss of *TP53*/*TP73* also triggered an increased microtubule polymerization rate in interphase cells, here correlating with an invasive phenotype (Berger, 2016). The misalignment of the spindle axis in mitosis is dependent on the hyperactivation of a signaling pathway mediated through Rac1 – Arp2/3 (unpublished data, Bastians lab). However, signaling pathways upstream of deregulated microtubule plus end assembly especially in interphase of melanoma cells remain unknown.

The present study demonstrated that cell migration and invasion in colorectal cancer and melanoma cell lines is dependent on microtubule plus end assembly rates in interphase. Restoring normal microtubule plus end assembly rates in invasive cells was linked to the reduction of cell migration and invasion (Figure 4.5A). However, the increase of microtubule plus end assembly did not lead to enhanced cell migration and invasion (Figure 4.5B), indicating that increased microtubule plus end assembly rates are required but not sufficient to enhance cell migration and invasion.

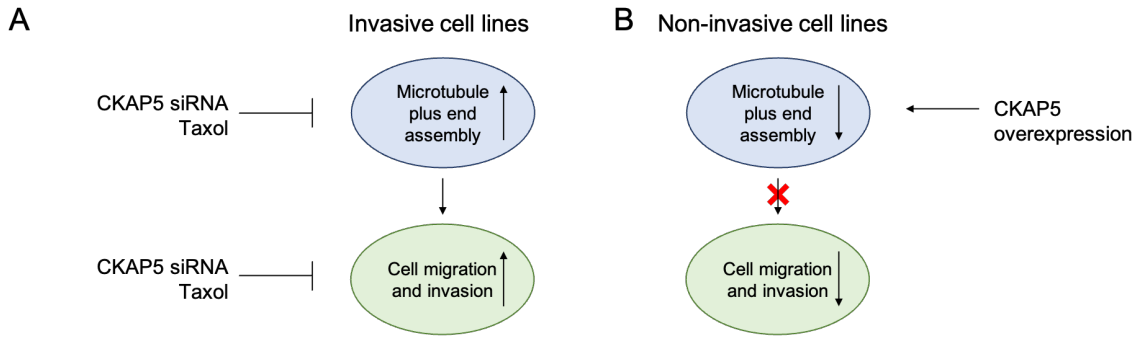

Figure 4.5 Model of the link between microtubule plus end assembly in interphase and enhanced cell migration and invasion in melanoma and colorectal cancer cell lines. *A) Invasive cell lines are characterized by increased microtubule plus end assembly rates during interphase. Both cellular processes seem to be connected, since restoration of proper microtubule plus end assembly through partial depletion of CKAP5 or treatment with sub-nanomolar doses of Taxol was associated with the partial rescue of increased cell migration and invasion. B) The overexpression*

of CKAP5 in non-invasive cells led to increased microtubule growth rates, however, without affecting cell motility.

The contribution of microtubules in processes involved in cell migration and invasion has been studied extensively. Microtubule associated proteins stabilize microtubules at the cell cortex to enable directional cell migration (Zhang et al., 2013), interact with actin regulatory proteins (Adams et al., 2016) and microtubule associated motor proteins transport cargo, like organelles, secretory vesicles, and actin nucleators (Kavallaris, 2010).

The small GTPase Ras related C3 botulinum toxin substrate 1 (Rac1) and its downstream effector Pak are associated with the stabilization of microtubules at the leading edge and thereby enable directional cell migration (Waterman-Storer et al., 1999; Wittmann et al., 2003). Downstream targets of Rac1 implicated in the regulation of microtubule dynamics at the leading edge are for instance Stathmin (Oncoprotein 18), end binding protein 1 (EB1), and microtubule affinity regulating kinase 2 (MARK2) (Nishimura et al., 2012). Loss of MARK2 was associated with enhanced microtubule growth and defective microtubule orientation at the leading edge (Nishimura et al., 2012). Additionally, it has been reported that Rac1 and Cdc42 establish a complex with the microtubule associated proteins CLIP-170 and IQGAP1 to capture microtubules at the leading edge of migrating cells (Fukata et al., 2002). Microtubules were identified to be essential for the delivery of guanosine exchanging factors (GEFs) to the cell cortex to activate Rac1 (Cheng et al., 2019). Previous work from our lab revealed a potential signaling pathway connecting the microtubule and actin cytoskeleton in mitosis and interphase cells. Here, EB1 binds to growing microtubule plus ends and might activate TRIO, a GEF for Rac1 (van Haren et al., 2014). Activation of Rac1 through TRIO might enhance cell migration by supporting actin polymerization through the Arp2/3 complex (Berger, 2016). Increased microtubule plus end assembly rates were shown to induce a hyperactivation of the signaling pathway leading to mitotic chromosome missegregation and enhanced cell migration in a microtubule dependent manner (Berger, 2016).

Cancer-relevant deregulations of the microtubule cytoskeleton are also achieved by the misregulation of microtubule associated proteins controlling and regulating the growth rates of microtubules. Critical factors, like the processive microtubule polymerase chTOG (Charrasse et al., 1995; Yu et al., 2016) and Stathmin (Oncoprotein 18) (Biaoxue et al., 2016), are found to be overexpressed in different cancer types. Previous work from our lab demonstrated the suppression of increased microtubule plus end assembly rates in mitosis through the partial depletion of *CKAP5* in colorectal cancer cell lines (Ertych et al., 2014; Stolz et al., 2015). Intriguingly, the same effect was achieved with mitotic and interphase microtubules of HCT116 cells with a concomitant loss of *TP53* and *TP73* (Berger, 2016). In line with this, the present study showed that the restoration of normal microtubule

plus end assembly rates leads to the partial rescue of enhanced cell migration and invasion in melanoma cells. Thus, the correlation between increased microtubule plus end assembly rates and enhanced cell migration and invasion is not limited to the colorectal cancer cell line but might be a general cancer-relevant mechanism.

The inhibition of HER2/ERK signaling was shown to restore normal microtubule plus end assembly rates in interphase and partially rescued increased cell migration and invasion in invasive melanoma cells (Figure 4.6). The treatment of spheroids derived from invasive donor cells with a reversible or irreversible HER2 inhibitor or with an inhibitor for ERK resulted in reduced spheroid outgrowth, however, the treatment with the irreversible inhibitor showed a stronger reduction of the spheroid outgrowth area compared to the reversible HER2 inhibitor. Spheroids derived from invasive cells embedded in extracellular matrix were incubated with medium containing the inhibitors. Since trastuzumab functions through a monoclonal antibody (Vu & Claret, 2012), it is possible that the antibody was not able to surpass the extracellular matrix as good as the irreversible inhibitor to reach the spheroids. Furthermore, the irreversible inhibitor was shown to inhibit EGFR, HER2 and HER3 receptor phosphorylation (Severinsson et al., 2011), suggesting that a synergistic effect might be responsible for the stronger effect.

Additional factors that were analyzed within this study included E2F1 and upstream regulators of its activity, as well as Cdk1. The knockdown or inhibition of E2F1, cyclin D1, and Cdk1 restored normal microtubule plus end growth rates in interphase and partially rescued increased cell migration and invasion (Figure 4.6).

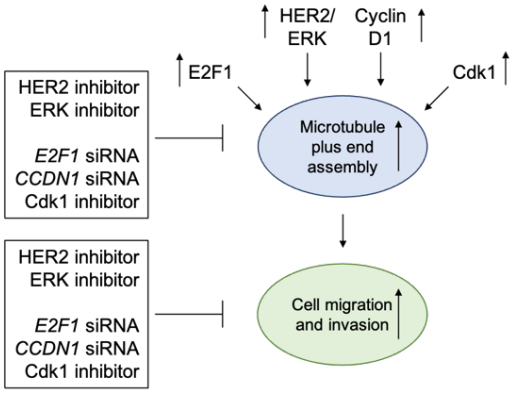

Figure 4.6 Model representing potential upstream signals for increased microtubule dynamics connected to enhanced cell migration and invasion. *A) Potential upstream triggers for increased microtubule plus end assembly rates might be the increased activity of HER2/ERK, E2F1, Cdk1 and cyclin D1. The depletion or inhibition of these regulators rescued increased microtubule plus end growth rates and enhanced cell migration and invasion.*

Upregulation of members of the transcription factor family E2F, especially E2F1, were shown to be linked to enhanced invasiveness and formation of metastases in a variety of human cancers, like prostate cancer (Liang et al., 2016), breast cancer (Hollern et al.,

2014), small cell lung cancer (Wang et al., 2017), and melanoma (Alla et al., 2010). Interestingly, E2F transcription factors were found to manipulate the dynamics of the microtubule cytoskeleton by enhancing the transcription of microtubule stabilizing and destabilizing proteins, like Stathmin (Chen et al., 2013; Lyu et al., 2020) and the fibroblast growth factor 13 (FGF13) (Hollern et al., 2019). Intriguingly, my study demonstrated that increased microtubule plus end growth rates in melanoma cells correlated positively with the amount of E2F1. The regulation of E2F1 dependent transcription mainly relies on the activity of the Retinoblastoma (Rb) protein and cyclin dependent kinases (Cdks), especially Cdk2-cyclin E and Cdk4-cyclin D complexes (Laine & Westermarck, 2014). In fact, the partial loss of the Rb protein, associated with hyperactive E2F1, was sufficient to accelerate microtubule plus end assembly in melanoma cells. Furthermore, the loss of cyclin D1 restored normal microtubule plus end assembly rates and partially rescued cell migration and invasion, which is compatible with unleashed E2F1 activity. The abnormal activity of the interphase kinases Cdk4 and Cdk2 is implicated in the development of human cancer (Goel et al., 2018; Patel et al., 2018; Sherr et al., 2016). Moreover, the overexpression of D-type cyclins is clearly linked to poor prognosis in cancer (Mermelshtein et al., 2005). In fact, *CDK4* and *CCND1* are implicated as oncogenes (Curtin et al., 2005). However, rescue experiments using Cdk2 and Cdk4 inhibitors showed inconsistent effects on microtubule plus end growth rates and cell migration and invasion.

The inhibition of Cdk1 was also associated with a restoration of normal microtubule plus end assembly rates in interphase of melanoma cell lines. The activity of Cdk1 mainly regulates entry and progression through mitosis (Qian et al., 2015) and increased Cdk1 activity causes increased microtubule plus end assembly rates in mitotic HCT116 cells resulting in chromosome instability (Schmidt et al., 2021). Cdk1 is overexpressed in colorectal cancer (Li et al., 2020), lung cancer (Li et al., 2020), and breast cancer (Izadi et al., 2020). In addition to its role in mitosis, Cdk1 can also function in interphase. Jones and colleagues reported about the Cdk1 dependent phosphorylation and activation of the formin like protein 2 (FMNL2), a formin implicated in the stimulation of the actin cytoskeleton leading to an increase in the adhesion complex area in HeLa cells during interphase (Jones et al., 2018). An isoform of FMNL2 was shown to be upregulated in melanoma and colorectal cancer cell lines and was associated with increased invasiveness (Péladeau et al., 2016), suggesting a link between Cdk1 activity and cancer cell invasion.

Interestingly, the loss of the Rb protein was associated with the increased generation of supernumerary centrosomes in mouse embryonic fibroblasts (Iovino et al., 2006). Even more interesting in this new context is the finding of this study that the loss of the Rb protein in non-invasive melanoma cell lines leads to increased microtubule plus end assembly rates in interphase. Therefore, it is possible that centrosome amplification might be a

potential intermediate step in the process leading to increased microtubule growth rates and enhanced cell invasion. However, the outcome of the loss of *RB* on centrosome amplification was not investigated. Intriguingly, also the increased recruitment of Cdk1 to centrosomes by overexpressed Cep63 was associated with overamplified centrosomes (Löffler et al., 2011), possibly explaining the restoration of normal microtubule plus end assembly rates in interphase after inhibition of Cdk1 in melanoma cell lines.

The present study demonstrated a dependence of increased microtubule plus end assembly rates and enhanced cell migration and invasion on HER2/ERK signaling. Indeed, several studies showed that the activation of the MAPK signaling pathway is linked to the activation of E2F1 and the transcription of target genes in melanoma cell lines. The upregulation of ERK1 and ERK2 was associated with the overexpression of cyclin D1 (Lavoie et al., 1996). Melanoma cell lines are characterized by mutations that lead to a hyperactivation of the MAPK signaling pathway, *e.g.,* mutations in *BRAF (V600E), NRAS* or *NF1* (Hodis et al., 2012). These cell lines exhibit hyperactive ERK1 and ERK2 leading to the increased phosphorylation of cyclin D1, resulting in more Cdk4-cyclin D complex that inhibits the Rb protein. Inhibition of Rb results in hyperactivated E2F1 (Riverso et al., 2017), a potential trigger for increased microtubule plus end growth rates in interphase (Figure 4.7). Several genes controlling tumor growth, like *MELK* (Janostiak et al., 2017) and *KLF4* (Riverso et al., 2017), underly the MAPK/E2F1 dependent signaling pathway in melanoma.

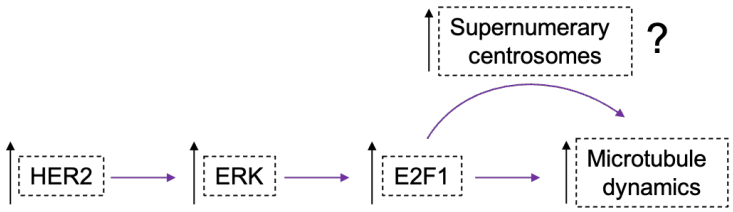

Figure 4.7 Model of potential upstream signaling leading to increased microtubule dynamics in interphase of melanoma cell lines. *Increased HER2 signaling leads to the hyperactivation of ERK and the subsequent activation of E2F1. The loss of the Rb protein and the hyperactivation of E2F1 were shown to be associated with the increased generation of supernumerary centrosomes* (Iovino et al., 2006)*. This Ph.D. thesis identified supernumerary centrosomes as a direct trigger for increased microtubule dynamics in melanoma cell lines. However, the hyperactivation of E2F1 itself was in parts associated with increased microtubule plus end growth rates in interphase.*

Literature

Adams, G., Zhou, J., Wang, W., Wu, H., Quan, J., Liu, Y., Xia, P., Wang, Z., Zhou, S., Jiang, J., Mo, F., Zhuang, X., Thomas, K., Hill, D. L., Aikhionbare, F. O., He, P., Liu, X., Ding, X., & Yao, X. (2016). The microtubule plus end tracking protein TIP150 interacts with cortactin to steer directional cell migration. *Journal of Biological Chemistry*, *291*(39), 20692–20706. https://doi.org/10.1074/jbc.M116.732719

Adams, S. D., Csere, J., D'angelo, G., Carter, E. P., Romao, M., Arnandis, T., Dodel, M., Kocher, H. M., Grose, R., Raposo, G., Mardakheh, F., & Godinho, S. A. (2021). Centrosome amplification mediates small extracellular vesicle secretion via lysosome disruption. *Current Biology*, *31*(7), 1403-1416.e7. https://doi.org/10.1016/j.cub.2021.01.028

Akbani, R., Akdemir, K. C., Aksoy, B. A., Albert, M., Ally, A., Amin, S. B., Arachchi, H., Arora, A., Auman, J. T., Ayala, B., Baboud, J., Balasundaram, M., Balu, S., Barnabas, N., Bartlett, J., Bartlett, P., Bastian, B. C., Baylin, S. B., Behera, M., … Zou, L. (2015). Genomic Classification of Cutaneous Melanoma. *Cell*, *161*(7), 1681–1696. https://doi.org/10.1016/j.cell.2015.05.044

Al-Bassam, J., & Chang, F. (2011). Regulation of microtubule dynamics by TOG-domain proteins XMAP215/Dis1 and CLASP. *Trends in Cell Biology*, *21*(10), 604–614. https://doi.org/10.1016/j.tcb.2011.06.007

Alla, V., Engelmann, D., Niemetz, A., Pahnke, J., Schmidt, A., Kunz, M., Emmrich, S., Steder, M., Koczan, D., & Pützer, B. M. (2010). E2F1 in melanoma progression and metastasis. *Journal of the National Cancer Institute*, *102*(2), 127–133. https://doi.org/10.1093/jnci/djp458

Al-Nedawi, K., Meehan, B., Micallef, J., Lhotak, V., May, L., Guha, A., & Rak, J. (2008). Intercellular transfer of the oncogenic receptor EGFRvIII by microvesicles derived from tumour cells. *Nature Cell Biology*, *10*(5), 619–624. https://doi.org/10.1038/ncb1725

Alonso-Curbelo, D., Riveiro-Falkenbach, E., Pérez-Guijarro, E., Cifdaloz, M., Karras, P., Osterloh, L., Megías, D., Cañón, E., Calvo, T. G., Olmeda, D., Gómez-López, G., Graña, O., Sánchez-ArévaloLobo, V. J., Pisano, D. G., Wang, H. W., Ortiz-Romero, P., Tormo, D., Hoek, K., Rodríguez-Peralto, J., … Soengas, M. S. (2014). RAB7 Controls Melanoma Progression by Exploiting a Lineage-Specific Wiring of the Endolysosomal Pathway. *Cancer Cell*, *26*(1), 61–76. https://doi.org/10.1016/j.ccr.2014.04.030

Altonsy, M. O., Ganguly, A., Amrein, M., Surmanowicz, P., Li, S. S., Lauzon, G. J., & Mydlarski, P. R. (2020). Beta3-tubulin is critical for microtubule dynamics, cell cycle regulation, and spontaneous release of microvesicles in human malignant melanoma cells (A375). *International Journal of Molecular Sciences*, *21*(5), 3–9. https://doi.org/10.3390/ijms21051656

Arendt, B. K., Walters, D. K., Wu, X., Tschumper, R. C., & Jelinek, D. F. (2014). Multiple myeloma cell-derived microvesicles are enriched in CD147 expression and enhance tumor cell proliferation. *Oncotarget*, *5*(14), 5686–5699. https://doi.org/10.18632/oncotarget.2159

Arnandis, T., Monteiro, P., Adams, S. D., Bridgeman, V. L., Rajeeve, V., Gadaleta, E., Marzec, J., Chelala, C., Malanchi, I., Cutillas, P. R., & Godinho, S. A. (2018). Oxidative Stress in Cells with Extra Centrosomes Drives Non-Cell-Autonomous Invasion. *Developmental Cell*, *47*(4), 409-424.e9. https://doi.org/10.1016/j.devcel.2018.10.026

Augoff, K., Hryniewicz-Jankowska, A., & Tabola, R. (2020). Invadopodia: clearing the way for cancer cell invasion. *Annals of Translational Medicine*, *8*(14), 902–902. https://doi.org/10.21037/atm.2020.02.157

Azimzadeh, J., & Marshall, W. F. (2010). Building the centriole. *Current Biology*, *20*(18), 816–825. https://doi.org/10.1016/j.cub.2010.08.010

Bach, D. H., Zhang, W., & Sood, A. K. (2019). Chromosomal instability in tumor initiation and development. *Cancer Research*, *79*(16), 3995–4002. https://doi.org/10.1158/0008-5472.CAN-18-3235

Bakhoum, S. F., & Landau, D. A. (2017). Chromosomal instability as a driver of tumor heterogeneity and evolution. *Cold Spring Harbor Perspectives in Medicine*, *7*(6), 1–13. https://doi.org/10.1101/cshperspect.a029611

Bakhoum, S. F., Ngo, B., Laughney, A. M., Cavallo, J. A., Murphy, C. J., Ly, P., Shah, P., Sriram, R. K., Watkins, T. B. K., Taunk, N. K., Duran, M., Pauli, C., Shaw, C., Chadalavada, K., Rajasekhar, V. K., Genovese, G., Venkatesan, S., Birkbak, N. J., McGranahan, N., … Cantley, L. C. (2018). Chromosomal instability drives metastasis through a cytosolic DNA response. *Nature*, *553*(7689), 467–472. https://doi.org/10.1038/nature25432

Bartolini, F., Moseley, J. B., Schmoranzer, J., Cassimeris, L., Goode, B. L., & Gundersen, G. G. (2008). The formin mDia2 stabilizes microtubules independently of its actin nucleation activity. *Journal of Cell Biology*, *181*(3), 523–536. https://doi.org/10.1083/jcb.200709029

Basu, S., Gnanapradeepan, K., Barnoud, T., Kung, C. P., Tavecchio, M., Scott, J., Watters, A., Chen, Q., Kossenkov, A. v., & Murphy, M. E. (2018). Mutant p53 controls

tumor metabolism and metastasis by regulating PGC-1α. *Genes and Development*, *32*(3–4), 230–243. https://doi.org/10.1101/gad.309062.117

Baugh, E. H., Ke, H., Levine, A. J., Bonneau, R. A., & Chan, C. S. (2018). Why are there hotspot mutations in the TP53 gene in human cancers? *Cell Death and Differentiation*, *25*(1), 154–160. https://doi.org/10.1038/cdd.2017.180

Beji, A., Horst, D., Engel, J., Kirchner, T., & Ullrich, A. (2012). Toward the prognostic significance and therapeutic potential of HER3 receptor tyrosine kinase in human colon cancer. *Clinical Cancer Research*, *18*(4), 956–968. https://doi.org/10.1158/1078-0432.CCR-11-1186

Berger, K. (2016). *A Role For Microtubule Dynamics For The Induction Of Chromosomal Instability And Cell Migration And Invasion In Human Cancer Cells*. http://hdl.handle.net/11858/00-1735-0000-0023-3E82-9

Berghoff, A. S., Bartsch, R., Preusser, M., Ricken, G., Steger, G. G., Bago-Horvath, Z., Rudas, M., Streubel, B., Dubsky, P., Gnant, M., Fitzal, F., Zielinski, C. C., & Birner, P. (2014). Co-overexpression of HER2/HER3 is a predictor of impaired survival in breast cancer patients. *The Breast*, *23*(5), 637–643. https://doi.org/10.1016/j.breast.2014.06.011

Biaoxue, R., Xiguang, C., Hua, L., & Shuanying, Y. (2016). Stathmin-dependent molecular targeting therapy for malignant tumor: The latest 5 years' discoveries and developments. *Journal of Translational Medicine*, *14*(279), 1–18. https://doi.org/10.1186/s12967-016-1000-z

Booth, D. G., Hood, F. E., Prior, I. A., & Royle, S. J. (2011). A TACC3/ch-TOG/clathrin complex stabilises kinetochore fibres by inter-microtubule bridging. *EMBO Journal*, *30*(5), 906–919. https://doi.org/10.1038/emboj.2011.15

Bouissou, A., Vérollet, C., Sousa, A., Sampaio, P., Wright, M., Sunkel, C. E., Merdes, A., & Raynaud-Messina, B. (2009). γ-Tubulin ring complexes regulate microtubule plus end dynamics. *Journal of Cell Biology*, *187*(3), 327–334. https://doi.org/10.1083/jcb.200905060

Bracken, A. P., Ciro, M., Cocito, A., & Helin, K. (2004). E2F target genes: Unraveling the biology. *Trends in Biochemical Sciences*, *29*(8), 409–417. https://doi.org/10.1016/j.tibs.2004.06.006

Braicu, C., Buse, M., Busuioc, C., Drula, R., Gulei, D., Raduly, L., Rusu, A., Irimie, A., Atanasov, A. G., Slaby, O., Ionescu, C., & Berindan-Neagoe, I. (2019). A comprehensive review on MAPK: A promising therapeutic target in cancer. *Cancers*, *11*(1618), 1–25. https://doi.org/10.3390/cancers11101618

Branch, K. M., Hoshino, D., & Weaver, A. M. (2012). Adhesion rings surround invadopodia and promote maturation. *Biology Open*, *1*(8), 711–722. https://doi.org/10.1242/bio.20121867

Bravo-Cordero, J. J., Magalhaes, M. A. O., Eddy, R. J., Hodgson, L., & Condeelis, J. (2013). Functions of cofilin in cell locomotion and invasion. *Nature Reviews Molecular Cell Biology*, *14*(7), 405–417. https://doi.org/10.1038/nrm3609

Brouhard, G. J., Stear, J. H., Noetzel, T. L., Al-Bassam, J., Kinoshita, K., Harrison, S. C., Howard, J., & Hyman, A. A. (2008). XMAP215 is a processive microtubule polymerase. *Cell*, *132*(1), 79–88. https://doi.org/10.1016/j.cell.2007.11.043

Brücher, B. L. D. M., & Jamall, I. S. (2014). Cell-cell communication in the tumor microenvironment, carcinogenesis, and anticancer treatment. *Cellular Physiology and Biochemistry*, *34*(2), 213–243. https://doi.org/10.1159/000362978

Buchwalter, R. A., Chen, J. v, Zheng, Y., & Megraw, T. L. (2016). Centrosome in Cell Division, Development and Disease. In *eLS. John Wiley & Sons, Ltd: Chichester* (pp. 1–12). John Wiley & Sons, Ltd. https://doi.org/10.1002/9780470015902.a0020872

Burkhart, D. L., & Sage, J. (2008). Cellular mechanisms of tumour suppression by the retinoblastoma gene. *Nature Reviews Cancer*, *8*(9), 671–682. https://doi.org/10.1038/nrc2399

Byrnes, A. E., & Slep, K. C. (2017). TOG-tubulin binding specificity promotes microtubule dynamics and mitotic spindle formation. *Journal of Cell Biology*, *216*(6), 1641–1657. https://doi.org/10.1083/jcb.201610090

Carey, T. E., Takahashi, T., Resnick, L. A., Oettgen, H. F., & Old, L. J. (1976). Cell surface antigens of human malignant melanoma: Mixed hemadsorption assays for humoral immunity to cultured autologous melanoma cells. *PNAS*, *73*(9), 3278–3282. https://doi.org/10.1073/pnas.73.9.3278

Carter, A. P., Zhang, R., Roostalu, J., Surrey, T., & Nogales, E. (2017). Structural insight into TPX2-stimulated microtubule assembly. *ELife*, 1–22. https://doi.org/10.7554/eLife.30959.001

Casalou, C., Ferreira, A., & Barral, D. C. (2020). The Role of ARF Family Proteins and Their Regulators and Effectors in Cancer Progression: A Therapeutic Perspective. *Frontiers in Cell and Developmental Biology*, *8*(217), 1–13. https://doi.org/10.3389/fcell.2020.00217

Castiel, A., Visochek, L., Mittelman, L., Dantzer, F., Izraeli, S., & Cohen-Armon, M. (2011). A phenanthrene derived PARP inhibitor is an extra-centrosomes de-clustering agent exclusively eradicating human cancer cells. *BMC Cancer*, *11*(412), 1–14. https://doi.org/10.1186/1471-2407-11-412

Cathcart, J., Pulkoski-Gross, A., & Cao, J. (2015). Targeting matrix metalloproteinases in cancer: Bringing new life to old ideas. *Genes and Diseases*, *2*(1), 26–34. https://doi.org/10.1016/j.gendis.2014.12.002

Chaffer, C. L., & Weinberg, R. A. (2011). A Perspective on Cancer Cell Metastasis. *Science*, *331*(6024), 1559–1564. http://science.sciencemag.org/

Charrasse, S., Maxel, M., Taviaux, S., Berta, P., Chow, T., & Larroqubi, C. (1995). Characterization of the cDNA and pattern of expression of a new gene over-expressed in human hepatomas and colonic tumors. *Eur. J. Biochcm*, *234*(2), 406–413. https://doi.org/10.1111/j.1432-1033.1995.406_b.x

Chen, F., Deng, J., Liu, X., Li, W., & Zheng, J. (2015). HCRP-1 regulates cell migration and invasion via EGFR-ERK mediated up-regulation of MMP-2 with prognostic significance in human renal cell carcinoma. *Scientific Reports*, *5*(13470), 1–14. https://doi.org/10.1038/srep13470

Chen, Y. L., Uen, Y. H., Li, C. F., Horng, K. C., Chen, L. R., Wu, W. R., Tseng, H. Y., Huang, H. Y., Wu, L. C., & Shiue, Y. L. (2013). The E2F transcription factor 1 transactives stathmin 1 in hepatocellular carcinoma. *Annals of Surgical Oncology*, *20*(12), 4041–4054. https://doi.org/10.1245/s10434-012-2519-8

Cheng, H. W., Hsiao, C. te, Chen, Y. Q., Huang, C. M., Chan, S. I., Chiou, A., & Kuo, J. C. (2019). Centrosome guides spatial activation of Rac to control cell polarization and directed cell migration. *Life Science Alliance*, *2*(1), 1–20. https://doi.org/10.26508/LSA.201800135

Cheng, J. C., Chang, H. M., & Leung, P. C. K. (2011). Wild-type p53 attenuates cancer cell motility by inducing growth differentiation factor-15 expression. *Endocrinology*, *152*(8), 2987–2995. https://doi.org/10.1210/en.2011-0059

Colello, D., Mathew, S., Ward, R., Pumiglia, K., & LaFlamme, S. E. (2012). Integrins regulate microtubule nucleating activity of centrosome through mitogen-activated protein kinase/extracellular signal-regulated kinase kinase/extracellular signal-regulated kinase (MEK/ERK) signaling. *Journal of Biological Chemistry*, *287*(4), 2520–2530. https://doi.org/10.1074/jbc.M111.254128

Conduit, P. T., Wainman, A., & Raff, J. W. (2015). Centrosome function and assembly in animal cells. *Nature Reviews Molecular Cell Biology*, *16*(10), 611–624. https://doi.org/10.1038/nrm4062

Conlon, G. A., & Murray, G. I. (2019). Recent advances in understanding the roles of matrix metalloproteinases in tumour invasion and metastasis. *Journal of Pathology*, *247*(5), 629–640. https://doi.org/10.1002/path.5225

Cosenza, M. R., Cazzola, A., Rossberg, A., Schieber, N. L., Konotop, G., Bausch, E., Slynko, A., Holland-Letz, T., Raab, M. S., Dubash, T., Glimm, H., Poppelreuther, S.,

Herold-Mende, C., Schwab, Y., & Krämer, A. (2017). Asymmetric Centriole Numbers at Spindle Poles Cause Chromosome Missegregation in Cancer. *Cell Reports*, *20*(8), 1906–1920. https://doi.org/10.1016/j.celrep.2017.08.005

Courtemanche, N. (2018). Mechanisms of formin-mediated actin assembly and dynamics. *Biophysical Reviews*, *10*(6), 1553–1569. https://doi.org/10.1007/s12551-018-0468-6

Cox, J., & Mann, M. (2008). MaxQuant enables high peptide identification rates, individualized p.p.b.-range mass accuracies and proteome-wide protein quantification. *Nature Biotechnology*, *26*(12), 1367–1372. https://doi.org/10.1038/nbt.1511

Cox, J., Neuhauser, N., Michalski, A., Scheltema, R. A., Olsen, J. v., & Mann, M. (2011). Andromeda: A peptide search engine integrated into the MaxQuant environment. *Journal of Proteome Research*, *10*(4), 1794–1805. https://doi.org/10.1021/pr101065j

Curtin, J. A., Fridlyand, J., Kageshita, T., Patel, H. N., Busam, K. J., Kutzner, H., Cho, K.-H., Aiba, S., Bröcker, E.-B., Leboit, P. E., Pinkel, D., & Bastian, B. C. (2005). Distinct Sets of Genetic Alterations in Melanoma. *The New England Journal of Medicine*, *20*(353), 2135–2182. https://doi.org/10.1056/NEJMoa050092

D'assoro, A. B., Barrett, S. L., Folk, C., Negron, V. C., Boeneman, K., Busby, R., Whitehead, C., Stivala, F., Lingle, W. L., & Salisbury, J. L. (2002). Amplified centrosomes in breast cancer: a potential indicator of tumor aggressiveness. *Breast Cancer Research and Treatment*, *75*, 25–34. https://doi.org/10.1023/a:1016550619925.

Devreotes, P., & Horwitz, A. R. (2015). Signaling networks that regulate cell migration. *Cold Spring Harbor Perspectives in Biology*, *7*(8), 1–17. https://doi.org/10.1101/cshperspect.a005959

Difilippantonio, M. J., Ghadimi, B. M., Howard, T., Camps, J., Nguyen, Q. T., Ferris, D. K., Sackett, D. L., & Ried, T. (2009). Nucleation capacity and presence of centrioles define a distinct category of centrosome abnormalities that induces multipolar mitoses in cancer cells. *Environmental and Molecular Mutagenesis*, *50*(8), 672–696. https://doi.org/10.1002/em.20532

Djerf Severinsson, E. A., Trinks, C., Gréen, H., Abdiu, A., Hallbeck, A. L., Stål, O., & Walz, T. M. (2011). The pan-ErbB receptor tyrosine kinase inhibitor canertinib promotes apoptosis of malignant melanoma in vitro and displays anti-tumor activity in vivo. *Biochemical and Biophysical Research Communications*, *414*(3), 563–568. https://doi.org/10.1016/j.bbrc.2011.09.118

Dongre, A., & Weinberg, R. A. (2019). New insights into the mechanisms of epithelial–mesenchymal transition and implications for cancer. *Nature Reviews Molecular Cell Biology*, *20*(2), 69–84. https://doi.org/10.1038/s41580-018-0080-4

Ertych, N., Stolz, A., Stenzinger, A., Weichert, W., Kaulfuß, S., Burfeind, P., Aigner, A., Wordeman, L., & Bastians, H. (2014). Increased microtubule assembly rates influence chromosomal instability in colorectal cancer cells. *Nature Cell Biology*, *16*(8), 779–791. https://doi.org/10.1038/ncb2994

Ertych, N., Stolz, A., Valerius, O., Braus, G. H., & Bastians, H. (2016). CHK2-BRCA1 tumor-suppressor axis restrains oncogenic Aurora-A kinase to ensure proper mitotic microtubule assembly. *PNAS*, *113*(7), 1817–1822. https://doi.org/10.1073/pnas.1525129113

European Union. (2021, May 5). *ECIS – European Cancer Information System*. Https://Ecis.Jrc.Ec.Europa.Eu.

Fan, G., Sun, L., Meng, L., Hu, C., Wang, X., Shi, Z., Hu, C., Han, Y., Yang, Q., Cao, L., Zhang, X., Zhang, Y., Song, X., Xia, S., He, B., Zhang, S., & Wang, C. (2021). The ATM and ATR kinases regulate centrosome clustering and tumor recurrence by targeting KIFC1 phosphorylation. *Nature Communications*, *12*(20), 1–16. https://doi.org/10.1038/s41467-020-20208-x

Fang, R., Chen, X., Zhang, S., Shi, H., Ye, Y., Shi, H., Zou, Z., Li, P., Guo, Q., Ma, L., He, C., & Huang, S. (2021). EGFR/SRC/ERK-stabilized YTHDF2 promotes cholesterol dysregulation and invasive growth of glioblastoma. *Nature Communications*, *12*(1), 1–17. https://doi.org/10.1038/s41467-020-20379-7

Fares, J., Fares, M. Y., Khachfe, H. H., Salhab, H. A., & Fares, Y. (2020). Molecular principles of metastasis: a hallmark of cancer revisited. *Signal Transduction and Targeted Therapy*, *5*(1), 1–17. https://doi.org/10.1038/s41392-020-0134-x

Farina, F., Gaillard, J., Guérin, C., Couté, Y., Sillibourne, J., Blanchoin, L., & Théry, M. (2016). The centrosome is an actin-organizing centre. *Nature Cell Biology*, *18*(1), 65–75. https://doi.org/10.1038/ncb3285

Farina, F., Ramkumar, N., Brown, L., Samandar Eweis, D., Anstatt, J., Waring, T., Bithell, J., Scita, G., Thery, M., Blanchoin, L., Zech, T., & Baum, B. (2019). Local actin nucleation tunes centrosomal microtubule nucleation during passage through mitosis. *The EMBO Journal*, *38*(11), 1–16. https://doi.org/10.15252/embj.201899843

Filipčík, P., Latham, S. L., Cadell, A. L., Day, C. L., Croucher, D. R., & Mace, P. D. (2020). A cryptic tubulin-binding domain links MEKK1 to curved tubulin protomers. *PNAS*, *117*(35), 21308–21318. https://doi.org/10.1073/pnas.2006429117/-/DCSupplemental

Fischer, M. (2017). Census and evaluation of p53 target genes. *Oncogene*, *36*(28), 3943–3956. https://doi.org/10.1038/onc.2016.502

Friedl, P., & Alexander, S. (2011). Cancer invasion and the microenvironment: Plasticity and reciprocity. *Cell*, *147*(5), 992–1009. https://doi.org/10.1016/j.cell.2011.11.016

Friedl, P., & Wolf, K. (2003). Tumour-cell invasion and migration: Diversity and escape mechanisms. *Nature Reviews Cancer*, *3*(5), 362–374. https://doi.org/10.1038/nrc1075

Fukata, M., Watanabe, T., Noritake, J., Nakagawa, M., Yamaga, M., Kuroda, S., Matsuura, Y., Iwamatsu, A., Perez, F., & Kaibuchi, K. (2002). Rac1 and Cdc42 Capture Microtubules through IQGAP1 and CLIP-170 leading edges. *Cell*, *109*(7), 873–885.

Furey, C., Jovasevic, V., & Walsh, D. (2020). TACC3 Regulates Microtubule Plus-End Dynamics and Cargo Transport in Interphase Cells. *Cell Reports*, *30*(1), 269–283. https://doi.org/10.1016/j.celrep.2019.12.025

Gandullo-Sánchez, L., Capone, E., Ocaña, A., Iacobelli, S., Sala, G., & Pandiella, A. (2020). HER3 targeting with an antibody-drug conjugate bypasses resistance to anti-HER2 therapies. *EMBO Molecular Medicine*, *12*(5), 1–16. https://doi.org/10.15252/emmm.201911498

Ganem, N. J., Godinho, S. A., & Pellman, D. (2009). A mechanism linking extra centrosomes to chromosomal instability. *Nature*, *460*(7252), 278–282. https://doi.org/10.1038/nature08136

Ganier, O., Schnerch, D., Oertle, P., Lim, R. Y., Plodinec, M., & Nigg, E. A. (2018). Structural centrosome aberrations promote non-cell-autonomous invasiveness. *The EMBO Journal*, *37*(9), 1–19. https://doi.org/10.15252/embj.201798576

Gao, C., Su, Y., Koeman, J., Haak, E., Dykema, K., Essenberg, C., Hudson, E., Petillo, D., Khoo, S. K., & vande Woude, G. F. (2016). Chromosome instability drives phenotypic switching to metastasis. *PNAS*, *113*(51), 14793–14798. https://doi.org/10.1073/pnas.1618215113

García-Fernández, M., Karras, P., Checinska, A., Cañón, E., Calvo, G. T., Gómez-López, G., Cifdaloz, M., Colmenar, A., Espinosa-Hevia, L., Olmeda, D., & Soengas, M. S. (2016). Metastatic risk and resistance to BRAF inhibitors in melanoma defined by selective allelic loss of ATG5. *Autophagy*, *12*(10), 1776–1790. https://doi.org/10.1080/15548627.2016.1199301

Garcin, C., & Straube, A. (2019). Microtubules in cell migration. *Essays in Biochemistry*, *63*(5), 509–520. https://doi.org/10.1042/EBC20190016

Gavi, S., Shumay, E., Wang, H. Y., & Malbon, C. C. (2006). G-protein-coupled receptors and tyrosine kinases: Crossroads in cell signaling and regulation. *Trends in Endocrinology and Metabolism*, *17*(2), 48–54. https://doi.org/10.1016/j.tem.2006.01.006

Gavilan, M. P., Gandolfo, P., Balestra, F. R., Arias, F., Bornens, M., & Rios, R. M. (2018). The dual role of the centrosome in organizing the microtubule network in interphase. *EMBO Reports*, *19*(11), 1–21. https://doi.org/10.15252/embr.201845942

Godek, K. M., Kabeche, L., & Compton, D. A. (2015). Regulation of kinetochore-microtubule attachments through homeostatic control during mitosis. *Nature Reviews Molecular Cell Biology*, *16*(1), 57–64. https://doi.org/10.1038/nrm3916

Godinho, S. A., & Pellman, D. (2014). Causes and consequences of centrosome abnormalities in cancer. *Philosophical Transactions of the Royal Society B: Biological Sciences*, *369*(1650), 1–13. https://doi.org/10.1098/rstb.2013.0467

Godinho, Susana A., Picone, R., Burute, M., Dagher, R., Su, Y., Leung, C. T., Polyak, K., Brugge, J. S., Théry, M., & Pellman, D. (2014). Oncogene-like induction of cellular invasion from centrosome amplification. *Nature*, *510*(7503), 167–171. https://doi.org/10.1038/nature13277

Goel, S., DeCristo, M. J., McAllister, S. S., & Zhao, J. J. (2018). CDK4/6 Inhibition in Cancer: Beyond Cell Cycle Arrest. *Trends in Cell Biology*, *28*(11), 911–925. https://doi.org/10.1016/j.tcb.2018.07.002

Gomez-Ferreria, M. A., Rath, U., Buster, D. W., Chanda, S. K., Caldwell, J. S., Rines, D. R., & Sharp, D. J. (2007). Human Cep192 Is Required for Mitotic Centrosome and Spindle Assembly. *Current Biology*, *17*(22), 1960–1966. https://doi.org/10.1016/j.cub.2007.10.019

Gönczy, P. (2015). Centrosomes and cancer: Revisiting a long-standing relationship. *Nature Reviews Cancer*, *15*(11), 639–652. https://doi.org/10.1038/nrc3995

Gruis, N. A., van der Velden, P. A., Sandkuijl, L. A., Prins, D. E., Weaver-Feldhaus, J., Kamb, A., Bergman, W., & Frants, R. R. (1995). Homozygotes for CDKN2 (p16) germline mutation in Dutch familial melanoma kindreds. *Nature Genetics*, *10*(3), 351–353. https://doi.org/10.1038/ng0795-351

Guo, Y., Pan, W., Liu, S., Shen, Z., Xu, Y., & Hu, L. (2020). ERK/MAPK signalling pathway and tumorigenesis (Review). *Experimental and Therapeutic Medicine*, *19*(3), 1997–2007. https://doi.org/10.3892/etm.2020.8454

Gupta, P., & Srivastava, S. K. (2014). HER2 mediated de novo production of TGFβ leads to SNAIL driven epithelial-to-mesenchymal transition and metastasis of breast cancer. *Molecular Oncology*, *8*(8), 1532–1547. https://doi.org/10.1016/j.molonc.2014.06.006

Hanahan, D., & Weinberg, R. A. (2011). Hallmarks of cancer: The next generation. *Cell*, *144*(5), 646–674. https://doi.org/10.1016/j.cell.2011.02.013

Hao, H., Niu, J., Xue, B., Su, Q. P., Liu, M., Yang, J., Qin, J., Zhao, S., Wu, C., & Sun, Y. (2020). Golgi-associated microtubules are fast cargo tracks and required for

persistent cell migration. *EMBO Reports*, *21*(3), 1–16. https://doi.org/10.15252/embr.201948385

Harrison, R. E., & Turley, E. A. (2001). Active Erk Regulates Microtubule Stability in H-ras-Transformed Cells 1. *Neoplasia*, *3*(5), 385–394. www.nature.com/neo

Herman, J. A., Miller, M. P., & Biggins, S. (2020). chTOG is a conserved mitotic error correction factor. *ELife*, *9*, 1–28. https://doi.org/10.7554/eLife.61773

Hessvik, N. P., & Llorente, A. (2018). Current knowledge on exosome biogenesis and release. *Cellular and Molecular Life Sciences*, *75*(2), 193–208. https://doi.org/10.1007/s00018-017-2595-9

Hirokawa, N., Noda, Y., Tanaka, Y., & Niwa, S. (2009). Kinesin superfamily motor proteins and intracellular transport. *Nature Reviews Molecular Cell Biology*, *10*(10), 682–696. https://doi.org/10.1038/nrm2774

Hodis, E., Watson, I. R., Kryukov, G. v., Arold, S. T., Imielinski, M., Theurillat, J. P., Nickerson, E., Auclair, D., Li, L., Place, C., Dicara, D., Ramos, A. H., Lawrence, M. S., Cibulskis, K., Sivachenko, A., Voet, D., Saksena, G., Stransky, N., Onofrio, R. C., … Chin, L. (2012). A landscape of driver mutations in melanoma. *Cell*, *150*(2), 251–263. https://doi.org/10.1016/j.cell.2012.06.024

Hofmann, U., Westphal, J. R., van Muijen, G. N. P., & Ruiter, D. J. (2000). Matrix metalloproteinases in human melanoma. *Journal of Investigative Dermatology*, *115*(3), 337–344. https://doi.org/10.1046/j.1523-1747.2000.00068.x

Hofmann, U., Westphal, J., Waas, E., Zendman, A., Cornelissen, I., Ruiter, D., & van Muijen, G. (1999). Matrix metalloproteinases in human melanoma cell lines and xenografts: increased expression of activated matrix metalloproteinase-2 (MMP-2) correlates with melanoma progression. *British Journal of Cancer*, *81*(5), 774–782.

Hollern, D. P., Honeysett, J., Cardiff, R. D., & Andrechek, E. R. (2014). The E2F Transcription Factors Regulate Tumor Development and Metastasis in a Mouse Model of Metastatic Breast Cancer. *Molecular and Cellular Biology*, *34*(17), 3229–3243. https://doi.org/10.1128/mcb.00737-14

Hollern, D. P., Swiatnicki, M. R., Rennhack, J. P., Misek, S. A., Matson, B. C., McAuliff, A., Gallo, K. A., Caron, K. M., & Andrechek, E. R. (2019). E2F1 Drives Breast Cancer Metastasis by Regulating the Target Gene FGF13 and Altering Cell Migration. *Scientific Reports*, *9*(10718), 1–13. https://doi.org/10.1038/s41598-019-47218-0

Hopfner, K. P., & Hornung, V. (2020). Molecular mechanisms and cellular functions of cGAS–STING signalling. *Nature Reviews Molecular Cell Biology*, *21*(9), 501–521. https://doi.org/10.1038/s41580-020-0244-x

Huang, F., Shi, Q., Li, Y., Xu, L., Xu, C., Chen, F., Wang, H., Liao, H., Chang, Z., Liu, F., Zhang, X. H. F., Feng, X. H., Han, J. D. J., Luo, S., & Chen, Y. G. (2018).

HER2/EGFR–AKT signaling switches TGFb from inhibiting cell proliferation to promoting cell migration in breast cancer. *Cancer Research*, *78*(21), 6073–6085. https://doi.org/10.1158/0008-5472.CAN-18-0136

Hurley, J. H., Boura, E., Carlson, L. A., & Róycki, B. (2010). Membrane budding. *Cell*, *143*(6), 875–887. https://doi.org/10.1016/j.cell.2010.11.030

Hwang, C. il, Matoso, A., Corney, D. C., Flesken-Nikitin, A., Körner, S., Wang, W., Boccaccio, C., Thorgeirsson, S. S., Comoglio, P. M., Hermeking, H., & Nikitin, A. Y. (2011). Wild-type p53 controls cell motility and invasion by dual regulation of MET expression. *PNAS*, *108*(34), 14240–14245. https://doi.org/10.1073/pnas.1017536108

Ingthorsson, S., Andersen, K., Hilmarsdottir, B., Maelandsmo, G. M., Magnusson, M. K., & Gudjonsson, T. (2016). HER2 induced EMT and tumorigenicity in breast epithelial progenitor cells is inhibited by coexpression of EGFR. *Oncogene*, *35*(32), 4244–4255. https://doi.org/10.1038/onc.2015.489

Innocenti, M. (2018). New insights into the formation and the function of lamellipodia and ruffles in mesenchymal cell migration. *Cell Adhesion and Migration*, *12*(5), 401–416. https://doi.org/10.1080/19336918.2018.1448352

Iovino, F., Lentini, L., Amato, A., & di Leonardo, A. (2006). RB acute loss induces centrosome amplification and aneuploidy in murine primary fibroblasts. *Molecular Cancer*, *5*(38), 1–11. https://doi.org/10.1186/1476-4598-5-38

Iqbal, N., & Iqbal, N. (2014). Human Epidermal Growth Factor Receptor 2 (HER2) in Cancers: Overexpression and Therapeutic Implications. *Molecular Biology International*, *2014*(852748), 1–9. https://doi.org/10.1155/2014/852748

Izadi, S., Nikkhoo, A., Hojjat-Farsangi, M., Namdar, A., Azizi, G., Mohammadi, H., Yousefi, M., & Jadidi-Niaragh, F. (2020). CDK1 in Breast Cancer: Implications for Theranostic Potential. *Anti-Cancer Agents in Medicinal Chemistry*, *20*(7), 758–767. https://doi.org/10.2174/1871520620666200203125712

Janostiak, R., Rauniyar, N., Lam, T. K. T., Ou, J., Zhu, L. J., Green, M. R., & Wajapeyee, N. (2017). MELK Promotes Melanoma Growth by Stimulating the NF-κB Pathway. *Cell Reports*, *21*(10), 2829–2841. https://doi.org/10.1016/j.celrep.2017.11.033

Jeong, J., Kim, W., Kim, L. K., van Houten, J., & Wysolmerski, J. J. (2017). HER2 signaling regulates HER2 localization and membrane retention. *PLoS ONE*, *12*(4), 1–16. https://doi.org/10.1371/journal.pone.0174849

Jeppesen, D. K., Fenix, A. M., Franklin, J. L., Higginbotham, J. N., Zhang, Q., Zimmerman, L. J., Liebler, D. C., Ping, J., Liu, Q., Evans, R., Fissell, W. H., Patton, J. G., Rome, L. H., Burnette, D. T., & Coffey, R. J. (2019). Reassessment of Exosome Composition. *Cell*, *177*(2), 428–445. https://doi.org/10.1016/j.cell.2019.02.029

Jones, M. C., Askari, J. A., Humphries, J. D., & Humphries, M. J. (2018). Cell adhesion is regulated by CDK1 during the cell cycle. *Journal of Cell Biology*, *217*(9), 3203–3218. https://doi.org/10.1083/jcb.201802088

Juanes, M. A., Fees, C. P., Hoeprich, G. J., Jaiswal, R., & Goode, B. L. (2020). EB1 Directly Regulates APC-Mediated Actin Nucleation. *Current Biology*, *30*(23), 4763–4772. https://doi.org/10.1016/j.cub.2020.08.094

Kalluri, R., & LeBleu, V. S. (2020). The biology, function, and biomedical applications of exosomes. *Science*, *367*(6478), 1–17. https://doi.org/10.1126/science.aau6977

Kalra, H., Simpson, R. J., Ji, H., Aikawa, E., Altevogt, P., Askenase, P., Bond, V. C., Borràs, F. E., Breakefield, X., Budnik, V., Buzas, E., Camussi, G., Clayton, A., Cocucci, E., Falcon-Perez, J. M., Gabrielsson, S., Gho, Y. S., Gupta, D., Harsha, H. C., … Mathivanan, S. (2012). Vesiclepedia: A Compendium for Extracellular Vesicles with Continuous Community Annotation. *PLoS Biology*, *10*(12), 1–5. https://doi.org/10.1371/journal.pbio.1001450

Karna, P., Rida, P. C. G., Pannu, V., Gupta, K. K., Dalton, W. B., Joshi, H., Yang, V. W., Zhou, J., & Aneja, R. (2011). A novel microtubule-modulating noscapinoid triggers apoptosis by inducing spindle multipolarity via centrosome amplification and declustering. *Cell Death and Differentiation*, *18*(4), 632–644. https://doi.org/10.1038/cdd.2010.133

Kavallaris, M. (2010). Microtubules and resistance to tubulin-binding agents. *Nature Reviews Cancer*, *10*(3), 194–204. https://doi.org/10.1038/nrc2803

Kaverina, I., & Straube, A. (2011). Regulation of cell migration by dynamic microtubules. *Seminars in Cell and Developmental Biology*, *22*(9), 968–974. https://doi.org/10.1016/j.semcdb.2011.09.017

Kazazian, K., Go, C., Wu, H., Brashavitskaya, O., Xu, R., Dennis, J. W., Gingras, A. C., & Swallow, C. J. (2017). Plk4 promotes cancer invasion and metastasis through Arp2/3 complex regulation of the actin cytoskeleton. *Cancer Research*, *77*(2), 434–447. https://doi.org/10.1158/0008-5472.CAN-16-2060

Kelly, A. E., & Funabiki, H. (2009). Correcting aberrant kinetochore microtubule attachments: an Aurora B-centric view. *Current Opinion in Cell Biology*, *21*(1), 51–58. https://doi.org/10.1016/j.ceb.2009.01.004

Kendellen, M. F., Bradford, J. W., Lawrence, C. L., Clark, K. S., & Baldwin, A. S. (2014). Canonical and non-canonical NF-κB signaling promotes breast cancer tumor-initiating cells. *Oncogene*, *33*(10), 1297–1305. https://doi.org/10.1038/onc.2013.64

Khodjakov, A., & Pines, J. (2010). Centromere tension: A divisive issue. *Nature Cell Biology*, *12*(10), 919–923. https://doi.org/10.1038/ncb1010-919

Kirouac, D. C., Du, J., Lahdenranta, J., Onsum, M. D., Nielsen, U. B., Schoeberl, B., & McDonagh, C. F. (2016). HER2+ Cancer Cell Dependence on PI3K vs. MAPK Signaling Axes Is Determined by Expression of EGFR, ERBB3 and CDKN1B. *PLoS Computational Biology*, *12*(4), 1–23. https://doi.org/10.1371/journal.pcbi.1004827

Kojima, S., & Cimini, D. (2019). Aneuploidy and gene expression: Is there dosage compensation? *Epigenomics*, *11*(16), 1827–1837. https://doi.org/10.2217/epi-2019-0135

Komis, G., Illés, P., Beck, M., & Šamaj, J. (2011). Microtubules and mitogen-activated protein kinase signalling. *Current Opinion in Plant Biology*, *14*(6), 650–657. https://doi.org/10.1016/j.pbi.2011.07.008

Krämer, A., Maier, B., & Bartek, J. (2011). Centrosome clustering and chromosomal (in)stability: A matter of life and death. *Molecular Oncology*, *5*(4), 324–335. https://doi.org/10.1016/j.molonc.2011.05.003

Kwon, M. (2016). Using cell culture models of centrosome amplification to study centrosome clustering in cancer. In *Methods in Molecular Biology* (Vol. 1413, pp. 367–392). Humana Press Inc. https://doi.org/10.1007/978-1-4939-3542-0_23

Laine, A., & Westermarck, J. (2014). Molecular pathways: Harnessing E2F1 regulation for prosenescence therapy in p53-defective cancer cells. *Clinical Cancer Research*, *20*(14), 3644–3650. https://doi.org/10.1158/1078-0432.CCR-13-1942

Lara-Gonzalez, P., Westhorpe, F. G., & Taylor, S. S. (2012). The spindle assembly checkpoint. *Current Biology*, *22*(22), 966–980. https://doi.org/10.1016/j.cub.2012.10.006

Lavoie, H., Gagnon, J., & Therrien, M. (2020). ERK signalling: a master regulator of cell behaviour, life and fate. *Nature Reviews Molecular Cell Biology*, *21*(10), 607–632. https://doi.org/10.1038/s41580-020-0255-7

Lavoie, J. N., L'Allemain, G., Brunei, A., Müller, R., & Pouysségur, J. (1996). Cyclin D1 expression is regulated positively by the p42/p44(MAPK) and negatively by the p38/HOG(MAPK) pathway. *Journal of Biological Chemistry*, *271*(34), 20608–20616. https://doi.org/10.1074/jbc.271.34.20608

Lee, D. W., Ramakrishnan, D., Valenta, J., Parney, I. F., Bayless, K. J., & Sitcheran, R. (2013). The NF-κB RelB Protein Is an Oncogenic Driver of Mesenchymal Glioma. *PLoS ONE*, *8*(2), 1–11. https://doi.org/10.1371/journal.pone.0057489

Lee-Hoeflich, S. T., Crocker, L., Yao, E., Pham, T., Munroe, X., Hoeflich, K. P., Sliwkowski, M. X., & Stern, H. M. (2008). A central role for HER3 in HER2-amplified breast cancer: Implications for targeted therapy. *Cancer Research*, *68*(14), 5878–5887. https://doi.org/10.1158/0008-5472.CAN-08-0380

Levine, M. S., Bakker, B., Boeckx, B., Moyett, J., Lu, J., Vitre, B., Spierings, D. C., Lansdorp, P. M., Cleveland, D. W., Lambrechts, D., Foijer, F., & Holland, A. J. (2017).

Centrosome Amplification Is Sufficient to Promote Spontaneous Tumorigenesis in Mammals. *Developmental Cell*, *40*(3), 313–322. https://doi.org/10.1016/j.devcel.2016.12.022

Li, B., Antonyak, M. A., Zhang, J., & Cerione, R. A. (2012). RhoA triggers a specific signaling pathway that generates transforming microvesicles in cancer cells. *Oncogene*, *31*(45), 4740–4749. https://doi.org/10.1038/onc.2011.636

Li, J., Wang, Y., Wang, X., & Yang, Q. (2020). CDK1 and CDC20 overexpression in patients with colorectal cancer are associated with poor prognosis: Evidence from integrated bioinformatics analysis. *World Journal of Surgical Oncology*, *18*(50), 1–11. https://doi.org/10.1186/s12957-020-01817-8

Li, M., He, F., Zhang, Z., Xiang, Z., & Hu, D. (2020). CDK1 serves as a potential prognostic biomarker and target for lung cancer. *Journal of International Medical Research*, *48*(2), 1–12. https://doi.org/10.1177/0300060519897508

Li, T., Shi, H., & Zhao, Y. (2018). Phosphorylation of microtubule-associated protein tau by mitogen-activated protein kinase in Alzheimer's disease. *IOP Conference Series: Materials Science and Engineering*, *394*(2), 1–5. https://doi.org/10.1088/1757-899X/394/2/022023

Liang, Y. X., Lu, J. M., Mo, R. J., He, H. C., Xie, J., Jiang, F. N., Lin, Z. Y., Chen, Y. R., Wu, Y. D., Luo, H. W., Luo, Z., & Zhong, W. de. (2016). E2F1 promotes tumor cell invasion and migration through regulating CD147 in prostate cancer. *International Journal of Oncology*, *48*(4), 1650–1658. https://doi.org/10.3892/ijo.2016.3364

Liao, G., Nagaski, T., & Gundersen, G. G. (1995). Liao 1995 MT cell migration. *Journal of Cell Science*, *108*, 3473–3483.

Liao, Z., Zhang, H., Fan, P., Huang, Q., Dong, K., Qi, Y., Song, J., Chen, L., Liang, H., Chen, X., Zhang, Z., & Zhang, B. (2019). High PLK4 expression promotes tumor progression and induces epithelial-mesenchymal transition by regulating the Wnt/β-catenin signaling pathway in colorectal cancer. *International Journal of Oncology*, *54*(2), 479–490. https://doi.org/10.3892/ijo.2018.4659

Lim, S., Kawamura, E., Fielding, A. B., Maydan, M., & Dedhar, S. (2013). Integrin-Linked Kinase Regulates Interphase and Mitotic Microtubule Dynamics. *PLoS ONE*, *8*(1), 1–11. https://doi.org/10.1371/journal.pone.0053702

Lingle, W. L., Barrett, S. L., Negron, V. C., D'assoro, A. B., Boeneman, K., Liu, W., Whitehead, C. M., Carol, R., & Salisbury, J. L. (2001). Centrosome amplification drives chromosomal instability in breast tumor development. *PNAS*, *99*(4), 1978–1983. https://doi.org/10.1073/pnas.032479999

Liu, B., Xing, X., Li, X., Guo, Q., Xu, T., & Xu, K. (2018). ZNF259 promotes breast cancer cells invasion and migration via ERK/GSK3β/snail signaling. *Cancer Management and Research*, *10*, 3159–3168. https://doi.org/10.2147/CMAR.S174745

Liu, T., Zhang, H., Sun, L., Zhao, D., Liu, P., Yan, M., Zaidi, N., Izadmehr, S., Gupta, A., Abu-Amer, W., Luo, M., Yang, J., Ou, X., Wang, Y., Bai, X., Wang, Y., New, M. I., Zaidi, M., Yuen, T., & Liu, C. (2017). FSIP1 binds HER2 directly to regulate breast cancer growth and invasiveness. *Proceedings of the National Academy of Sciences of the United States of America*, *114*(29), 7683–7688. https://doi.org/10.1073/pnas.1621486114

Liu, Y., Kim, J., Philip, R., Sridhar, V., Chandrashekhar, M., Moffat, J., van Breugel, M., & Pelletier, L. (2020). Direct interaction between CEP85 and STIL mediates PLK4-driven directed cell migration. *Journal of Cell Science*, *133*(8), 1–9. https://doi.org/10.1242/jcs.238352

Löffler, H., Fechter, A., Matuszewska, M., Saffrich, R., Mistrik, M., Marhold, J., Hornung, C., Westermann, F., Bartek, J., & Krämer, A. (2011). Cep63 recruits Cdk1 to the centrosome: Implications for regulation of mitotic entry, centrosome amplification, and genome maintenance. *Cancer Research*, *71*(6), 2129–2139. https://doi.org/10.1158/0008-5472.CAN-10-2684

LoMastro, G. M., & Holland, A. J. (2019). The Emerging Link between Centrosome Aberrations and Metastasis. *Developmental Cell*, *49*(3), 325–331. https://doi.org/10.1016/j.devcel.2019.04.002

Lu, H., Liu, S., Zhang, G., Kwong, L. N., Zhu, Y., Miller, J. P., Hu, Y., Zhong, W., Zeng, J., Wu, L., Krepler, C., Sproesser, K., Xiao, M., Xu, W., Karakousis, G. C., Schuchter, L. M., Field, J., Zhang, P. J., Herlyn, M., … Guo, W. (2016). Oncogenic BRAF-Mediated Melanoma Cell Invasion. *Cell Reports*, *15*(9), 2012–2024. https://doi.org/10.1016/j.celrep.2016.04.073

Lyu, J., Yang, E. J., Zhang, B., Wu, C., Pardeshi, L., Shi, C., Mou, P. K., Liu, Y., Tan, K., & Shim, J. S. (2020). Synthetic lethality of RB1 and aurora A is driven by stathmin-mediated disruption of microtubule dynamics. *Nature Communications*, *11*(1), 1–16. https://doi.org/10.1038/s41467-020-18872-0

Magescas, J., Zonka, J. C., & Feldman, J. L. (2019). A two-step mechanism for the inactivation of microtubule organizing center function at the centrosome. *ELife*, *8*(47867), 1–28. https://doi.org/10.7554/eLife.47867.001

Maiti, S., Kolkata, I., & Bamburg, I. J. R. (2013). Actin-Capping and-Severing Proteins. In *Cell Architecture and Function* (Vol. 4, pp. 18–26).

Malumbres, M., & Barbacid, M. (2009). Cell cycle, CDKs and cancer: A changing paradigm. *Nature Reviews Cancer*, *9*(3), 153–166. https://doi.org/10.1038/nrc2602

Mannavola, F., D'oronzo, S., Cives, M., Stucci, L. S., Ranieri, G., Silvestris, F., & Tucci, M. (2020). Extracellular vesicles and epigenetic modifications are hallmarks of melanoma progression. *International Journal of Molecular Sciences*, *21*(52), 1–16. https://doi.org/10.3390/ijms21010052

Mariappan, A., Soni, K., Schorpp, K., Zhao, F., Minakar, A., Zheng, X., Mandad, S., Macheleidt, I., Ramani, A., Kubelka, T., Dawidowski, M., Golfmann, K., Wason, A., Yang, C., Simons, J., Schmalz, H., Hyman, A. A., Aneja, R., Ullrich, R., … Gopalakrishnan, J. (2019). Inhibition of CPAP –tubulin interaction prevents proliferation of centrosome-amplified cancer cells. *The EMBO Journal*, *38*(2), 1–24. https://doi.org/10.15252/embj.201899876

Marteil, G., Guerrero, A., Vieira, A. F., de Almeida, B. P., Machado, P., Mendonça, S., Mesquita, M., Villarreal, B., Fonseca, I., Francia, M. E., Dores, K., Martins, N. P., Jana, S. C., Tranfield, E. M., Barbosa-Morais, N. L., Paredes, J., Pellman, D., Godinho, S. A., & Bettencourt-Dias, M. (2018). Over-elongation of centrioles in cancer promotes centriole amplification and chromosome missegregation. *Nature Communications*, *9*(1258), 1–17. https://doi.org/10.1038/s41467-018-03641-x

Martínez-Alonso, D., & Malumbres, M. (2020). Mammalian cell cycle cyclins. *Seminars in Cell and Developmental Biology*, *107*, 28–35. https://doi.org/10.1016/j.semcdb.2020.03.009

Mattila, P. K., & Lappalainen, P. (2008). Filopodia: Molecular architecture and cellular functions. *Nature Reviews Molecular Cell Biology*, *9*(6), 446–454. https://doi.org/10.1038/nrm2406

Mayor, R., & Etienne-Manneville, S. (2016). The front and rear of collective cell migration. *Nature Reviews Molecular Cell Biology*, *17*(2), 97–109. https://doi.org/10.1038/nrm.2015.14

Meiring, J. C. M., Shneyer, B. I., & Akhmanova, A. (2020). Generation and regulation of microtubule network asymmetry to drive cell polarity. *Current Opinion in Cell Biology*, *62*, 86–95. https://doi.org/10.1016/j.ceb.2019.10.004

Menck, K., Bleckmann, A., Wachter, A., Hennies, B., Ries, L., Schulz, M., Balkenhol, M., Pukrop, T., Schatlo, B., Rost, U., Wenzel, D., Klemm, F., & Binder, C. (2017). Characterisation of tumour-derived microvesicles in cancer patients' blood and correlation with clinical outcome. *Journal of Extracellular Vesicles*, *6*(1), 1–17. https://doi.org/10.1080/20013078.2017.1340745

Menck, K., Scharf, C., Bleckmann, A., Dyck, L., Rost, U., Wenzel, D., Dhople, V. M., Siam, L., Pukrop, T., Binder, C., & Klemm, F. (2015). Tumor-derived microvesicles mediate human breast cancer invasion through differentially glycosylated

EMMPRIN. *Journal of Molecular Cell Biology*, *7*(2), 143–153. https://doi.org/10.1093/jmcb/mju047

Menck, K., Sivaloganathan, S., Bleckmann, A., & Binder, C. (2020). Microvesicles in cancer: Small size, large potential. *International Journal of Molecular Sciences*, *21*(15), 1–30. https://doi.org/10.3390/ijms21155373

Mendoza, M. C., Er, E. E., Zhang, W., Ballif, B. A., Elliott, H. L., Danuser, G., & Blenis, J. (2011). ERK-MAPK Drives Lamellipodia Protrusion by Activating the WAVE2 Regulatory Complex. *Molecular Cell*, *41*(6), 661–671. https://doi.org/10.1016/j.molcel.2011.02.031

Mennella, V., Agard, D. A., Huang, B., & Pelletier, L. (2014). Amorphous no more: Subdiffraction view of the pericentriolar material architecture. *Trends in Cell Biology*, *24*(3), 188–197. https://doi.org/10.1016/j.tcb.2013.10.001

Mermelshtein, A., Gerson, A., Walfisch, S., Delgado, B., Shechter-Maor, G., Delgado, J., Fich, A., & Gheber, L. (2005). Expression of D-type cyclins in colon cancer and in cell lines from colon carcinomas. *British Journal of Cancer*, *93*(3), 338–345. https://doi.org/10.1038/sj.bjc.6602709

Meunier, S., & Vernos, I. (2012). Microtubule assembly during mitosis - from distinct origins to distinct functions? *Journal of Cell Science*, *125*(12), 2805–2814. https://doi.org/10.1242/jcs.092429

Miller, M., Shirole, N., Tian, R., Pal, D., & Sordella, R. (2016). The Evolution of TP53 Mutations: From Loss-of-Function to Separation-of-Function Mutants. *J Cancer Biol Res*, *4*(4), 1–13.

Mittal, K., Choi, D. H., Ogden, A., Donthamsetty, S., Melton, B. D., Gupta, M. v., Pannu, V., Cantuaria, G., Varambally, S., Reid, M. D., Jonsdottir, K., Janssen, E. A. M., Aleskandarany, M. A., Ellis, I. O., Rakha, E. A., Rida, P. C. G., & Aneja, R. (2017). Amplified centrosomes and mitotic index display poor concordance between patient tumors and cultured cancer cells. *Scientific Reports*, *7*(43984), 1–16. https://doi.org/10.1038/srep43984

Mittal, K., Kaur, J., Jaczko, M., Wei, G., Toss, M. S., Rakha, E. A., Janssen, E. A. M., Søiland, H., Kucuk, O., Reid, M. D., Gupta, M. v., & Aneja, R. (2020). Centrosome amplification: a quantifiable cancer cell trait with prognostic value in solid malignancies. *Cancer and Metastasis Reviews*, *40*(1), 319–339. https://doi.org/10.1007/s10555-020-09937-z

Moasser, M. M. (2007). The oncogene HER2: Its signaling and transforming functions and its role in human cancer pathogenesis. *Oncogene*, *26*(45), 6469–6487. https://doi.org/10.1038/sj.onc.1210477

Molinie, N., & Gautreau, A. (2018). The Arp2/3 Regulatory System and Its Deregulation in Cancer. *Physiol Rev*, *98*, 215–238. https://doi.org/10.1152/physrev.00006.2017

Møller, L. L. V., Klip, A., & Sylow, L. (2019). Rho GTPases—Emerging Regulators of Glucose Homeostasis and Metabolic Health. *Cells*, *8*(434), 1–21. https://doi.org/10.3390/cells8050434

Morishima-Kawashima, M., & Kosik, K. S. (1996). The Pool of MAP Kinase Associated with Microtubules Is Small but Constitutively Active. *Molecular Biology of the Cell*, *7*, 893–905. https://doi.org/10.1091/mbc.7.6.893

Morris, E. J., Kawamura, E., Gillespie, J. A., Balgi, A., Kannan, N., Muller, W. J., Roberge, M., & Dedhar, S. (2017). Stat3 regulates centrosome clustering in cancer cells via Stathmin/PLK1. *Nature Communications*, *8*(15289), 1–15. https://doi.org/10.1038/ncomms15289

Moyer, T. C., & Holland, A. J. (2019). PLK4 promotes centriole duplication by phosphorylating STIL to link the procentriole cartwheel to the microtubule wall. *ELife*, *8*(46054), 1–26. https://doi.org/10.7554/eLife.46054.001

Müller, M. T., Schempp, R., Lutz, A., Felder, T., Felder, E., & Miklavc, P. (2019). Interaction of microtubules and actin during the post-fusion phase of exocytosis. *Scientific Reports*, *9*(1), 1–15. https://doi.org/10.1038/s41598-019-47741-0

Muralidharan-Chari, V., Clancy, J. W., Sedgwick, A., & D'Souza-Schorey, C. (2010). Microvesicles: Mediators of extracellular communication during cancer progression. *Journal of Cell Science*, *123*(10), 1603–1611. https://doi.org/10.1242/jcs.064386

Muroyama, A., & Lechler, T. (2017). Microtubule organization, dynamics and functions in differentiated cells. *Development (Cambridge)*, *144*(17), 3012–3021. https://doi.org/10.1242/dev.153171

Murphy, D. A., & Courtneidge, S. A. (2011). The "ins" and "outs" of podosomes and invadopodia: Characteristics, formation and function. *Nature Reviews Molecular Cell Biology*, *12*(7), 413–426. https://doi.org/10.1038/nrm3141

Nanou, A., Zeune, L. L., Bidard, F. C., Pierga, J. Y., & Terstappen, L. W. M. M. (2020). HER2 expression on tumor-derived extracellular vesicles and circulating tumor cells in metastatic breast cancer. *Breast Cancer Research*, *22*(1), 1–11. https://doi.org/10.1186/s13058-020-01323-5

Nejedlá, M., Klebanovych, A., Sulimenko, V., Sulimenko, T., Dráberová, E., Dráber, P., & Karlsson, R. (2020). The actin regulator profilin 1 is functionally associated with the mammalian centrosome. *Life Science Alliance*, *4*(1), 1–8. https://doi.org/10.26508/LSA.202000655

Nigg, E. A. (2002). Centrosome Aberrations: Cause or consequence of cancer progression? *Nature Reviews Genetics*, *2*(11), 1–11. https://doi.org/10.1038/nrg924

Nishimura, Y., Applegate, K., Davidson, M. W., Danuser, G., & Waterman, C. M. (2012). Automated screening of microtubule growth dynamics identifies MARK2 as a regulator of leading edge microtubules downstream of RAC1 in migrating cells. *PLoS ONE*, *7*(7), 1–15. https://doi.org/10.1371/journal.pone.0041413

Noi, M., Mukaisho, K. I., Yoshida, S., Murakami, S., Koshinuma, S., Adachi, T., Machida, Y., Yamori, M., Nakayama, T., Yamamoto, G., & Sugihara, H. (2018). ERK phosphorylation functions in invadopodia formation in tongue cancer cells in a novel silicate fibre-based 3D cell culture system. *International Journal of Oral Science*, *10*(4), 1–10. https://doi.org/10.1038/s41368-018-0033-y

Novikov, N. M., Zolotaryova, S. Y., Gautreau, A. M., & Denisov, E. v. (2021). Mutational drivers of cancer cell migration and invasion. *British Journal of Cancer*, *124*(1), 102–114. https://doi.org/10.1038/s41416-020-01149-0

O'Brien, K., Breyne, K., Ughetto, S., Laurent, L. C., & Breakefield, X. O. (2020). RNA delivery by extracellular vesicles in mammalian cells and its applications. *Nature Reviews Molecular Cell Biology*, *21*(10), 585–606. https://doi.org/10.1038/s41580-020-0251-y

Ogden, A., Rida, P. C. G., Reid, M. D., & Aneja, R. (2014). Interphase microtubules: Chief casualties in the war on cancer? *Drug Discovery Today*, *19*(7), 824–829. https://doi.org/10.1016/j.drudis.2013.10.022

Oh, D. Y., & Bang, Y. J. (2020). HER2-targeted therapies — a role beyond breast cancer. *Nature Reviews Clinical Oncology*, *17*(1), 33–48. https://doi.org/10.1038/s41571-019-0268-3

O'Rourke, B. P., Gomez-Ferreria, M. A., Berk, R. H., Hackl, A. M. U., Nicholas, M. P., O'Rourke, S. C., Pelletier, L., & Sharp, D. J. (2014). Cep192 controls the balance of centrosome and non-centrosomal microtubules during interphase. *PLoS ONE*, *9*(6), 1–13. https://doi.org/10.1371/journal.pone.0101001

Ostrowski, M., Carmo, N. B., Krumeich, S., Fanget, I., Raposo, G., Savina, A., Moita, C. F., Schauer, K., Hume, A. N., Freitas, R. P., Goud, B., Benaroch, P., Hacohen, N., Fukuda, M., Desnos, C., Seabra, M. C., Darchen, F., Amigorena, S., Moita, L. F., & Thery, C. (2010). Rab27a and Rab27b control different steps of the exosome secretion pathway. *Nature Cell Biology*, *12*(1), 19–30. https://doi.org/10.1038/ncb2000

Pannu, V., Rida, P. C. G., Celik, B., Turaga, R. C., Ogden, A., Cantuaria, G., Gopalakrishnan, J., & Aneja, R. (2014). Centrosome-declustering drugs mediate a two-pronged attack on interphase and mitosis in supercentrosomal cancer cells. *Cell Death and Disease*, *5*(11), 1–10. https://doi.org/10.1038/cddis.2014.505

Pannu, Vaishali, Mittal, K., Cantuaria, G., Reid, M. D., Li, X., Donthamsetty, S., Mcbride, M., Klimov, S., Osan, R., Gupta, M. v, Rida, P. C. G., & Aneja, R. (2015). Rampant

centrosome amplification underlies more aggressive disease course of triple negative breast cancers. *Oncotarget*, *6*(12), 10487–10497. https://doi.org/10.18632/oncotarget.3402

Patel, P., Tsiperson, V., Gottesman, S. R. S., Somma, J., & Blain, S. W. (2018). Dual inhibition of CDK4 and CDK2 via targeting p27 tyrosine phosphorylation induces a potent and durable response in breast cancer cells. *Molecular Cancer Research*, *16*(3), 361–377. https://doi.org/10.1158/1541-7786.MCR-17-0602

Péladeau, C., Heibein, A., Maltez, M. T., Copeland, S. J., & Copeland, J. W. (2016). A specific FMNL2 isoform is up-regulated in invasive cells. *BMC Cell Biology*, *17*(1), 1–12. https://doi.org/10.1186/s12860-016-0110-z

Petry, S., & Vale, R. D. (2015). Microtubule nucleation at the centrosome and beyond. *Nature Cell Biology*, *17*(9), 1089–1093. https://doi.org/10.1038/ncb3220

Piehl, M., Serdar Tulu, U., Wadsworth, P., & Cassimeris, L. (2004). Centrosome maturation: Measurement of microtubule nucleation throughout the cell cycle by using GFP-tagged EB1. *PNAS*, *101*(6), 1584–1588. www.pnas.orgcgi-doi10.1073pnas.0308205100

Pollard, T. D. (2016). Actin and actin-binding proteins. *Cold Spring Harbor Perspectives in Biology*, *8*(8), 1–17. https://doi.org/10.1101/cshperspect.a018226

Poppy Roworth, A., Ghari, F., & la Thangue, N. B. (2015). To live or let die–complexity within the E2F1 pathway. *Molecular and Cellular Oncology*, *2*(1), 1–12. https://doi.org/10.4161/23723548.2014.970480

Qian, J., Beullens, M., Huang, J., de Munter, S., Lesage, B., & Bollen, M. (2015). Cdk1 orders mitotic events through coordination of a chromosome-associated phosphatase switch. *Nature Communications*, *6*(10215), 1–13. https://doi.org/10.1038/ncomms10215

Rappsilber, J., Mann, M., & Ishihama, Y. (2007). Protocol for micro-purification, enrichment, pre-fractionation and storage of peptides for proteomics using StageTips. *Nature Protocols*, *2*(8), 1896–1906. https://doi.org/10.1038/nprot.2007.261

Rashed, M. H., Bayraktar, E., Helal, G. K., Abd-Ellah, M. F., Amero, P., Chavez-Reyes, A., & Rodriguez-Aguayo, C. (2017). Exosomes: From garbage bins to promising therapeutic targets. *International Journal of Molecular Sciences*, *18*(538), 1–25. https://doi.org/10.3390/ijms18030538

Real, F. X., Houghton, A. N., Albino, A. P., Cordon-Cardo, C., Melamed, M. R., Oettgen, H. F., & Old, L. J. (1985). Surface Antigens of Melanomas and Melanocytes Defined by Mouse Monoclonal Antibodies: Specificity Analysis and Comparison of Antigen Expression in Cultured Cells and Tissues. *Cancer Research*, *45*(9), 4401–4411.

Rebacz, B., Larsen, T. O., Clausen, M. H., Rønnest, M. H., Löffler, H., Ho, A. D., & Krämer, A. (2007). Identification of griseofulvin as an inhibitor of centrosomal clustering in a phenotype-based screen. *Cancer Research*, *67*(13), 6342–6350. https://doi.org/10.1158/0008-5472.CAN-07-0663

Rebecca, V. W., Somasundaram, R., & Herlyn, M. (2020). Pre-clinical modeling of cutaneous melanoma. *Nature Communications*, *11*(2858), 1–9. https://doi.org/10.1038/s41467-020-15546-9

Reszka, A. A., Segert, R., Diltz, C. D., Krebs, E. G., & Fischer, E. H. (1995). Association of mitogen-activated protein kinase with the microtubule cytoskeleton. *Cell Biology*, *92*, 8881–8885. https://doi.org/10.1073/pnas.92.19.8881

Rivera-Rivera, Y., Marina, M., Jusino, S., Lee, M., Velázquez, J. V., Chardón-Colón, C., Vargas, G., Padmanabhan, J., Chellappan, S. P., & Saavedra, H. I. (2021). The Nek2 centrosome-mitotic kinase contributes to the mesenchymal state, cell invasion, and migration of triple-negative breast cancer cells. *Scientific Reports*, *11*(1), 9016. https://doi.org/10.1038/s41598-021-88512-0

Riverso, M., Montagnani, V., & Stecca, B. (2017). KLF4 is regulated by RAS/RAF/MEK/ERK signaling through E2F1 and promotes melanoma cell growth. *Oncogene*, *36*(23), 3322–3333. https://doi.org/10.1038/onc.2016.481

Roostalu, J., & Surrey, T. (2017). Microtubule nucleation: Beyond the template. *Nature Reviews Molecular Cell Biology*, *18*(11), 702–710. https://doi.org/10.1038/nrm.2017.75

Rosa, J., Canovas, P., Islam, A., Altieri, D. C., & Doxsey, S. J. (2006). Survivin Modulates Microtubule Dynamics and Nucleation throughout the Cell Cycle. *Molecular Biology of the Cell*, *17*, 1483–1493. https://doi.org/10.1091/mbc.E05-08

Rusan, N. M., Fagerstrom, C. J., Yvon, A.-M. C., & Wadsworth, P. (2001). Cell Cycle-Dependent Changes in Microtubule Dynamics in Living Cells Expressing Green Fluorescent Protein-Tubulin. *Molecular Biology of the Cell*, *12*(4), 971–980. https://doi.org/10.1091/mbc.12.4.971

Sabino, D., Gogendeau, D., Gambarotto, D., Nano, M., Pennetier, C., Dingli, F., Arras, G., Loew, D., & Basto, R. (2015). Moesin is a major regulator of centrosome behavior in epithelial cells with extra centrosomes. *Current Biology*, *25*(7), 879–889. https://doi.org/10.1016/j.cub.2015.01.066

Salisbury, J. L., Lingle, W. L., White, R. A., Cordes, L. E. M., & Barrett, S. (1999). Microtubule Nucleating Capacity of Centrosomes in Tissue Sections. *The Journal of Histochemistry & Cytochemistry*, *47*(10), 1265–1273. http://www.jhc.org

Sansregret, L., & Swanton, C. (2017). The role of aneuploidy in cancer evolution. *Cold Spring Harbor Perspectives in Medicine*, *7*, 1–18. https://doi.org/10.1101/cshperspect.a028373

Satyanarayana, A., & Kaldis, P. (2009). Mammalian cell-cycle regulation: Several cdks, numerous cyclins and diverse compensatory mechanisms. *Oncogene*, *28*(33), 2925–2939. https://doi.org/10.1038/onc.2009.170

Savoia, P., Fava, P., Casoni, F., & Cremona, O. (2019). Targeting the ERK signaling pathway in melanoma. *International Journal of Molecular Sciences*, *20*(6), 1–37. https://doi.org/10.3390/ijms20061483

Schermuly, N. (2019). *Regulation Of Spindle Orientation By A Mitotic Actin Pathway In Chromosomally Unstable Cancer Cells*. http://hdl.handle.net/21.11130/00-1735-0000-0005-14F2-3

Schiera, G., di Liegro, C. M., Puleo, V., Colletta, O., Fricano, A., Cancemi, P., di Cara, G., & di Liegro, I. (2016). Extracellular vesicles shed by melanoma cells contain a modified form of H1.0 linker histone and H1.0 mRNA-binding proteins. *International Journal of Oncology*, *49*(5), 1807–1814. https://doi.org/10.3892/ijo.2016.3692

Schmidt, A. K., Pudelko, K., Boekenkamp, J. E., Berger, K., Kschischo, M., & Bastians, H. (2021). The p53/p73 - p21CIP1 tumor suppressor axis guards against chromosomal instability by restraining CDK1 in human cancer cells. *Oncogene*, *40*(2), 436–451. https://doi.org/10.1038/s41388-020-01524-4

Schnerch, D., & Nigg, E. A. (2016). Structural centrosome aberrations favor proliferation by abrogating microtubule-dependent tissue integrity of breast epithelial mammospheres. *Oncogene*, *35*(21), 2711–2722. https://doi.org/10.1038/onc.2015.332

Seals, D. F., Azucena, E. F., Pass, I., Tesfay, L., Gordon, R., Woodrow, M., Resau, J. H., & Courtneidge, S. A. (2005). The adaptor protein Tks5/Fish is required for podosome formation and function, and for the protease-driven invasion of cancer cells. *Cancer Cell*, *7*(2), 155–165. https://doi.org/10.1016/j.ccr.2005.01.006

Sedgwick, A. E., Clancy, J. W., Olivia Balmert, M., & D'Souza-Schorey, C. (2015). Extracellular microvesicles and invadopodia mediate non-overlapping modes of tumor cell invasion. *Scientific Reports*, *5*(14748), 1–14. https://doi.org/10.1038/srep14748

Serçin, Ö., Larsimont, J. C., Karambelas, A. E., Marthiens, V., Moers, V., Boeckx, B., le Mercier, M., Lambrechts, D., Basto, R., & Blanpain, C. (2016). Transient PLK4 overexpression accelerates tumorigenesis in p53-deficient epidermis. *Nature Cell Biology*, *18*(1), 100–110. https://doi.org/10.1038/ncb3270

Sherr, C. J., Beach, D., & Shapiro, G. I. (2016). Targeting CDK4 and CDK6: From discovery to therapy. *Cancer Discovery*, *6*(4), 353–367. https://doi.org/10.1158/2159-8290.CD-15-0894

Shi, W., Zhang, G., Ma, Z., Li, L., Liu, M., Qin, L., Yu, Z., Zhao, L., Liu, Y., Zhang, X., Qin, J., Ye, H., Jiang, X., Zhou, H., Sun, H., & Jiao, Z. (2021). Hyperactivation of HER2-SHCBP1-PLK1 axis promotes tumor cell mitosis and impairs trastuzumab sensitivity to gastric cancer. *Nature Communications*, *12*(2812), 1–19. https://doi.org/10.1038/s41467-021-23053-8

Shinmura, K., Kurabe, N., Goto, M., Yamada, H., Natsume, H., Konno, H., & Sugimura, H. (2014). PLK4 overexpression and its effect on centrosome regulation and chromosome stability in human gastric cancer. *Molecular Biology Reports*, *41*(10), 6635–6644. https://doi.org/10.1007/s11033-014-3546-2

Singh, J. K., Farnie, G., Bundred, N. J., Simões, B. M., Shergill, A., Landberg, G., Howell, S. J., & Clarke, R. B. (2013). Targeting CXCR1/2 significantly reduces breast cancer stem cell activity and increases the efficacy of inhibiting HER2 via HER2-dependent and -independent mechanisms. *Clinical Cancer Research*, *19*(3), 643–656. https://doi.org/10.1158/1078-0432.CCR-12-1063

Stolz, A., Ertych, N., & Bastians, H. (2015). A phenotypic screen identifies microtubule plus end assembly regulators that can function in mitotic spindle orientation. *Cell Cycle*, *14*(6), 827–837. https://doi.org/10.1080/15384101.2014.1000693

Stolz, A., Ertych, N., Kienitz, A., Vogel, C., Schneider, V., Fritz, B., Jacob, R., Dittmar, G., Weichert, W., Petersen, I., & Bastians, H. (2010). The CHK2-BRCA1 tumour suppressor pathway ensures chromosomal stability in human somatic cells. *Nature Cell Biology*, *12*(5), 492–499. https://doi.org/10.1038/ncb2051

Sullivan, R. J., & Flaherty, K. (2013). MAP kinase signaling and inhibition in melanoma. *Oncogene*, *32*(19), 2373–2379. https://doi.org/10.1038/onc.2012.345

Sun, H. L., Cui, R., Zhou, J. K., Teng, K. yu, Hsiao, Y. H., Nakanishi, K., Fassan, M., Luo, Z., Shi, G., Tili, E., Kutay, H., Lovat, F., Vicentini, C., Huang, H. L., Wang, S. W., Kim, T., Zanesi, N., Jeon, Y. J., Lee, T. J., … Croce, C. M. (2016). ERK Activation Globally Downregulates miRNAs through Phosphorylating Exportin-5. *Cancer Cell*, *30*(5), 723–736. https://doi.org/10.1016/j.ccell.2016.10.001

Svitkina, T. (2018). The actin cytoskeleton and actin-based motility. *Cold Spring Harbor Perspectives in Biology*, *10*(1), 1–22. https://doi.org/10.1101/cshperspect.a018267

Tanaka, K., Takeda, S., Mitsuoka, K., Oda, T., Kimura-Sakiyama, C., Maéda, Y., & Narita, A. (2018). Structural basis for cofilin binding and actin filament disassembly. *Nature Communications*, *9*(1), 1–12. https://doi.org/10.1038/s41467-018-04290-w

Tanimura, S., & Takeda, K. (2017). ERK signalling as a regulator of cell motility. *Journal of Biochemistry*, *162*(3), 145–154. https://doi.org/10.1093/jb/mvx048

Tate, J. G., Bamford, S., Jubb, H. C., Sondka, Z., Beare, D. M., Bindal, N., Boutselakis, H., Cole, C. G., Creatore, C., Dawson, E., Fish, P., Harsha, B., Hathaway, C., Jupe,

S. C., Kok, C. Y., Noble, K., Ponting, L., Ramshaw, C. C., Rye, C. E., … Forbes, S. A. (2019). COSMIC: The Catalogue Of Somatic Mutations In Cancer. *Nucleic Acids Research*, *47*, 941–947. https://doi.org/10.1093/nar/gky1015

Thawani, A., Kadzik, R. S., & Petry, S. (2018). XMAP215 is a microtubule nucleation factor that functions synergistically with the γ-tubulin ring complex. *Nature Cell Biology*, *20*(5), 575–585. https://doi.org/10.1038/s41556-018-0091-6

Thompson, S. L., & Compton, D. A. (2011). Chromosome missegregation in human cells arises through specific types of kinetochore-microtubule attachment errors. *PNAS*, *108*(44), 17974–17978. https://doi.org/10.1073/pnas.1109720108

Tijhuis, A. E., Johnson, S. C., & McClelland, S. E. (2019). The emerging links between chromosomal instability (CIN), metastasis, inflammation and tumour immunity. *Molecular Cytogenetics*, *12*(17), 1–21. https://doi.org/10.1186/s13039-019-0429-1

Tong, J., Li, L., Ballermann, B., & Wang, Z. (2013). Phosphorylation of Rac1 T108 by Extracellular Signal-Regulated Kinase in Response to Epidermal Growth Factor: a Novel Mechanism To Regulate Rac1 Function. *Molecular and Cellular Biology*, *33*(22), 4538–4551. https://doi.org/10.1128/mcb.00822-13

Tong, J., Li, L., Ballermann, B., & Wang, Z. (2016). Phosphorylation and activation of RhoA by ERK in response to epidermal growth factor stimulation. *PLoS ONE*, *11*(1), 1–26. https://doi.org/10.1371/journal.pone.0147103

Toti, A., Santi, A., Pardella, E., Nesi, I., Tomasini, R., Mello, T., Paoli, P., Caselli, A., & Cirri, P. (2021). Activated fibroblasts enhance cancer cell migration by microvesicles-mediated transfer of Galectin-1. *Journal of Cell Communication and Signaling*, 1–15. https://doi.org/10.1007/s12079-021-00624-4

Tricarico, C., Clancy, J., & D'Souza-Schorey, C. (2017). Biology and biogenesis of shed microvesicles. *Small GTPases*, *8*(4), 220–232. https://doi.org/10.1080/21541248.2016.1215283

Trogden, K. P., & Rogers, S. L. (2015). TOG proteins are spatially regulated by rac-GSK3β to control interphase microtubule dynamics. *PLoS ONE*, *10*(9), 1–25. https://doi.org/10.1371/journal.pone.0138966

Tyanova, S., Temu, T., Sinitcyn, P., Carlson, A., Hein, M. Y., Geiger, T., Mann, M., & Cox, J. (2016). The Perseus computational platform for comprehensive analysis of (prote)omics data. *Nature Methods*, *13*(9), 731–740. https://doi.org/10.1038/nmeth.3901

van Haren, J., Boudeau, J., Schmidt, S., Basu, S., Liu, Z., Lammers, D., Demmers, J., Benhari, J., Grosveld, F., Debant, A., & Galjart, N. (2014). Dynamic microtubules catalyze formation of navigator-TRIO complexes to regulate neurite extension. *Current Biology*, *24*(15), 1778–1785. https://doi.org/10.1016/j.cub.2014.06.037

Vasudevan, A., Baruah, P. S., Smith, J. C., Wang, Z., Sayles, N. M., Andrews, P., Kendall, J., Leu, J., Chunduri, N. K., Levy, D., Wigler, M., Storchová, Z., & Sheltzer, J. M. (2020). Single-Chromosomal Gains Can Function as Metastasis Suppressors and Promoters in Colon Cancer. *Developmental Cell*, *52*(4), 413–428. https://doi.org/10.1016/j.devcel.2020.01.034

Venuto, S., Monteonofrio, L., Cozzolino, F., Monti, M., Appolloni, I., Mazza, T., Canetti, D., Giambra, V., Panelli, P., Fusco, C., Squeo, G. M., Croce, A. I., Pucci, P., Malatesta, P., Soddu, S., Merla, G., & Micale, L. (2020). TRIM8 interacts with KIF11 and KIFC1 and controls bipolar spindle formation and chromosomal stability. *Cancer Letters*, *473*, 98–106. https://doi.org/10.1016/j.canlet.2019.12.042

Visochek, L., Castiel, A., Mittelman, L., Elkin, M., Atias, D., Golan, T., Izraeli, S., Peretz, T., & Cohen-Armon, M. (2017). Exclusive destruction of mitotic spindles in human cancer cells. *Oncotarget*, *8*(13), 20813–20824. www.impactjournals.com/oncotarget/

Vu, T., & Claret, F. X. (2012). Trastuzumab: Updated mechanisms of action and resistance in breast cancer. *Frontiers in Oncology*, *2*(62), 1–6. https://doi.org/10.3389/fonc.2012.00062

Vulprecht, J., David, A., Tibelius, A., Castiel, A., Konotop, G., Liu, F., Bestvater, F., Raab, M. S., Zentgraf, H., Izraeli, S., & Krämer, A. (2012). STIL is required for centriole duplication in human cells. *Journal of Cell Science*, *125*(5), 1353–1362. https://doi.org/10.1242/jcs.104109

Wang, S. E., Xiang, B., Zent, R., Quaranta, V., Pozzi, A., & Arteaga, C. L. (2009). Transforming growth factor β induces clustering of HER2 and integrins by activating Src-focal adhesion kinase and receptor association to the cytoskeleton. *Cancer Research*, *69*(2), 475–482. https://doi.org/10.1158/0008-5472.CAN-08-2649

Wang, T., Gilkes, D. M., Takano, N., Xiang, L., Luo, W., Bishop, C. J., Chaturvedi, P., Green, J. J., & Semenza, G. L. (2014). Hypoxia-inducible factors and RAB22A mediate formation of microvesicles that stimulate breast cancer invasion and metastasis. *PNAS*, *111*(31), 3234–3242. https://doi.org/10.1073/pnas.1410041111

Wang, Tingting, Chen, X., Qiao, W., Kong, L., Sun, D., & Li, Z. (2017). Transcription factor E2F1 promotes emt by regulating ZEB2 in small cell lung cancer. *BMC Cancer*, *17*(719), 1–12. https://doi.org/10.1186/s12885-017-3701-y

Watanabe, T., Noritake, J., & Kaibuchi, K. (2005). Regulation of microtubules in cell migration. *Trends in Cell Biology*, *15*(2), 76–83. https://doi.org/10.1016/j.tcb.2004.12.006

Waterman-Storer, C. M., Worthylake, R. A., Liu, B. P., Burridge, K., & Salmon, E. D. (1999). Microtubule growth activates Rac1 to promote lamellipodial protrusion in fibroblasts. *Nature Cell Biology*, *1*, 45–50. https://doi.org/10.1038/9018

Wieczorek, M., Bechstedt, S., Chaaban, S., & Brouhard, G. J. (2015). Microtubule-associated proteins control the kinetics of microtubule nucleation. *Nature Cell Biology*, *17*(7), 907–916. https://doi.org/10.1038/ncb3188

Wittmann, T., Bokoch, G. M., & Waterman-Storer, C. M. (2003). Regulation of leading edge microtubule and actin dynamics downstream of Rac1. *Journal of Cell Biology*, *161*(5), 845–851. https://doi.org/10.1083/jcb.200303082

Wordeman, L. (2010). How kinesin motor proteins drive mitotic spindle function: Lessons from molecular assays. *Seminars in Cell and Developmental Biology*, *21*(3), 260–268. https://doi.org/10.1016/j.semcdb.2010.01.018

Wu, H. Y., Yang, B., & Geng, D. H. (2020). Clinical significance of expression of fibrous sheath interacting protein 1 in colon cancer. *World Journal of Gastrointestinal Oncology*, *12*(6), 677–686. https://doi.org/10.4251/WJGO.V12.I6.677

Wu, J., de Heus, C., Liu, Q., Bouchet, B. P., Noordstra, I., Jiang, K., Hua, S., Martin, M., Yang, C., Grigoriev, I., Katrukha, E. A., Altelaar, A. F. M., Hoogenraad, C. C., Qi, R. Z., Klumperman, J., & Akhmanova, A. (2016). Molecular Pathway of Microtubule Organization at the Golgi Apparatus. *Developmental Cell*, *39*(1), 44–60. https://doi.org/10.1016/j.devcel.2016.08.009

Yamada, K. M., & Sixt, M. (2019). Mechanisms of 3D cell migration. *Nature Reviews Molecular Cell Biology*, *20*, 738–752. https://doi.org/10.1038/s41580

Yang, J., Antin, P., Berx, G., Blanpain, C., Brabletz, T., Bronner, M., Campbell, K., Cano, A., Casanova, J., Christofori, G., Dedhar, S., Derynck, R., Ford, H. L., Fuxe, J., García de Herreros, A., Goodall, G. J., Hadjantonakis, A. K., Huang, R. J. Y., Kalcheim, C., … Sheng, G. (2020). Guidelines and definitions for research on epithelial–mesenchymal transition. *Nature Reviews Molecular Cell Biology*, *21*(6), 341–352. https://doi.org/10.1038/s41580-020-0237-9

Yarden, Y., & Sliwkowski, M. (2001). Untangling the ErbB signalling network. *Molecular Cell Biology Nature Review*, *2*(2), 127–137. www.nature.com/reviews/molcellbio

Yongsheng Chan, J. (2011). A Clinical Overview of Centrosome Amplification in Human Cancers. *Int. J. Biol. Sci*, *7*(8), 1122–1144. https://doi.org/10.7150/ijbs.7.1122

Yu, J.-X., Chen, Q., Yu, Y.-Q., Li, S.-Y., & Song, J.-F. (2016). Upregulation of colonic and hepatic tumor overexpressed gene is significantly associated with the unfavorable prognosis marker of human hepatocellular carcinoma. *American Journal of Cancer Research*, *6*(3), 690–700.

Zembala, M., Stec, M., Baj-Krzyworzeka, M., Baran, J., Węglarczyk, K., Zembala, M., Barbasz, J., & Szczepanik, A. (2015). Isolation and characterization of circulating micro(nano)vesicles in the plasma of colorectal cancer patients and their interactions with tumor cells. *Oncology Reports*, *34*(5), 2768–2775. https://doi.org/10.3892/or.2015.4228

Zhang, B., Kirov, S., & Snoddy, J. (2005). WebGestalt: An integrated system for exploring gene sets in various biological contexts. *Nucleic Acids Research*, *33*, 741–748. https://doi.org/10.1093/nar/gki475

Zhang, C., Liu, J., Xu, D., Zhang, T., Hu, W., & Feng, Z. (2020). Gain-of-function mutant p53 in cancer progression and therapy. *Journal of Molecular Cell Biology*, *12*(9), 674–687. https://doi.org/10.1093/jmcb/mjaa040

Zhang, H., Luo, M., Jin, Z., Wang, D., Sun, M., Zhao, X., Zhao, Z., Lei, H., Li, M., & Liu, C. (2015). Expression and clinicopathological significance of fsip1 in breast cancer. *Oncotarget*, *6*(12), 10658–10666. https://doi.org/10.18632/oncotarget.3381

Zhang, J., Li, L., Zhang, Q., Yang, X., Zhang, C., Zhang, X., Zhang, D., Lv, Y., Song, H., Chen, B., Liu, Y., Hu, J., & Huang, Y. (2019). Phosphorylation of microtubule-associated protein 4 promotes hypoxic endothelial cell migration and proliferation. *Frontiers in Pharmacology*, *10*(368), 1–13. https://doi.org/10.3389/fphar.2019.00368

Zhang, L., Shao, H., Zhu, T., Xia, P., Wang, Z., Liu, L., Yan, M., Hill, D. L., Fang, G., Chen, Z., Wang, D., & Yao, X. (2013). DDA3 associates with microtubule plus ends and orchestrates microtubule dynamics and directional cell migration. *Scientific Reports*, *3*(1681), 1–12. https://doi.org/10.1038/srep01681

Zhang, X., Wei, C., Liang, H., & Han, L. (2021). Polo-Like Kinase 4's Critical Role in Cancer Development and Strategies for Plk4-Targeted Therapy. *Frontiers in Oncology*, *11*(587554), 1–24. https://doi.org/10.3389/fonc.2021.587554

Zhong, F.-J., Li, Y.-M., Xu, C., Sun, B., Wang, J.-L., & Yang, L.-Y. (2021). EB2 promotes hepatocellular carcinoma proliferation and metastasis via MAPK/ERK pathway by modulating microtubule dynamics Running title: The role of EB2 in HCC progression. *Clinical Science*, *135*(7), 847–864. https://doi.org/10.1042/CS20201500/906202/cs-2020-1500.pdf

Zhu, J., Chen, H., Liao, Z., He, C., & Hu, X. (2015). TGFBI protein high expression predicts poor prognosis in colorectal cancer patients. *International Journal of Clinical and Experimental Pathology*, *8*(1), 702–710.

Zhuyan, J., Chen, M., Zhu, T., Bao, X., Zhen, T., Xing, K., Wang, Q., & Zhu, S. (2020). Critical steps to tumor metastasis: Alterations of tumor microenvironment and extracellular matrix in the formation of pre-metastatic and metastatic niche. *Cell and Bioscience*, *10*(89), 1–9. https://doi.org/10.1186/s13578-020-00453-9

Zwetsloot, A. J., Tut, G., & Straube, A. (2018). Measuring microtubule dynamics. *Essays in Biochemistry*, *62*(6), 725–735. https://doi.org/10.1042/EBC20180035

Acknowledgments

At the end of my thesis, I would like to say thank you …

… primarily to my PhD supervisor Prof. Dr. Holger Bastians for giving me the opportunity to work on this topic in his lab. Without his guidance, constant helpful input, and new hypothesis, it would have been not possible for me to make it through the four years of research.

I want to thank all of the members of my examination board. Especially, I would like to thank my thesis committee members Prof. Dr. Matthias Dobbelstein and Prof. Dr. Claudia Binder for the helpful comments and vivid discussions concerning my project.

Furthermore, I would like to thank Prof. Dr. Heike Krebber for allowing me to use her laboratory working materials. I also would like to thank Dr. Oliver Hahn for allowing me to use the Incucyte system and Dr. Markus Räschle for the mass spectrometry analyses and the informative discussions of the results.

Of course, I am extremely grateful for all current and former members of the Bastians lab. I want to especially thank Nadine Schermuly, Elina Glaubke, Ann-Kathrin Schmidt, Magdalena Hennecke, Simranjeet Kaur and Alexander Haas for introducing me to the lab, for helpful comments on my project, for coffee breaks when they were much needed and for all activities outside of the lab. I would like to thank Benjamin Slusarenko for the vivid discussions, encouraging words, the proofreading of parts of my thesis and the many laughter. I want to thank Nicolas Böhly for making every day in the lab an exciting, diversified, and happy day. Thank you for always cheering me up.

My deepest appreciation belongs to my family for supporting me on every level. The continuous love carried me through the four years. The motivational speeches from my little sister prompted me to never stop. The moral (and technical) support from my boyfriend at the end of my thesis pushed me to finish it.
I could not have done it without you.
Thank you!